4. History matching

4.1 Calibration approach

This section details the approach used for history matching the historical groundwater flow regime, UCG activities, and contaminant transport migration within Lot 40 DY85, PL253 and the model domain.

In this study, "history matching" refers to the process of assimilating observed transient groundwater data into the model, its calibration and its outputs. The purpose of history-matching in this context is to constrain model parameters and allowable ranges, based on what we know from field testing, conceptual ideas and observed system behaviour (ideally of direct relevance to the model predictions of interest), using a range of observation data.

This in turn constrains the suite of parameter fields that are used to make model predictions and to assess their uncertainty. This approach provides a sound basis for enhanced use and understanding of model outputs, including their limitations, in decision-making.

PEST, the tool providing the basis for calibration, represents a family of optimisation and uncertainty analysis tools. PEST also represents a suite of workflows for highly parameterised environmental model optimisation (inversion), uncertainty analysis and associated tasks.

ENSI (Ensemble Space Inversion) is a relatively new method for fast history-matching. It attains its speed through estimation of "super parameters" instead of parameters themselves. These super parameters are factors applied to random parameter vectors which, ideally, should be samples of the prior parameter probability distribution. The number of realisations required for achieving a high level of model-to-measurement fit can be far fewer than the number of parameters that are used by a model (Doherty, 2024).

In contrast to other calibration methods such as SVD-assist (which also estimates super parameters), it is not necessary to calculate a Jacobian matrix in order to formulate super parameters prior to implementing ENSI inversion. What it gets is an ensemble of random samples of the prior parameter probability distribution.

The combined steady-state and history-matching transient model is calibrated by adjusting aquifer parameters and other boundary condition parameters for the groundwater flow and transport models to develop a suitable match between the observed and simulated groundwater levels and concentrations across the model domain.

4.2 Parameterisation

This section discusses additional details with respect to the PESTPP-ENSI model parameterisation. Once a good model-to-measurement fit was achieved using PESTPP-ENSI, the model parameterisation was used to inform the PESTPP-IES workflow of uncertainty quantification.

Use of PEST-ENSI for history-matching suggests that its model run efficiency is greater than that of PEST_HP in highly parameterised cases, and its model-to-measurement fit is better than that of PESTPP-IES (Doherty, 2024). However, PEST-ENSI associates no uncertainty with the parameter field that it calculates, and with model predictions that are calculated using this field. The complementary PESTPP-IES methodology is therefore deployed for predictive uncertainty analysis.

Both PEST-ENSI and PESTPP-IES PPP-IES approaches allow for large numbers of pilot points as in practice they sample a subset of pilot points (ensemble) during each iteration. This does not charge parameterisation approach with any further computational penalties.

The parameterisation scheme uses pilot points in the proximity of monitoring sites, acknowledging the need for spatial interpolation and extraction of information from observed data. All pilot points are assigned spatial covariance structures to encourage the history matching process to honour the initial (prior) parameters and their spatial differences as closely as possible. Departures from this would occur where necessary to significantly improve the simulation of historical system behaviour as measured by PESTPP-ENSI against the strategically weighted observation data.

These covariances are computed using PEST utilities MKPPSTAT and PPCOV_SVA. Covariances are computed using a variogram with the range based on the mean distance from each pilot point and its ten nearest neighbours. No nugget is applied.

For parameters that are not spatially correlated, standard deviations are defined in the same way (one quarter of the allowable parameter range). These standard deviations and covariance matrices are provided to PESTPP-IES via a PEST parameter uncertainty file.

The parameterisation scheme was reviewed and revised during history matching with learnings from each iteration feeding to the next round. A total of seven rounds of history matching (each running for several iterations) were conducted.

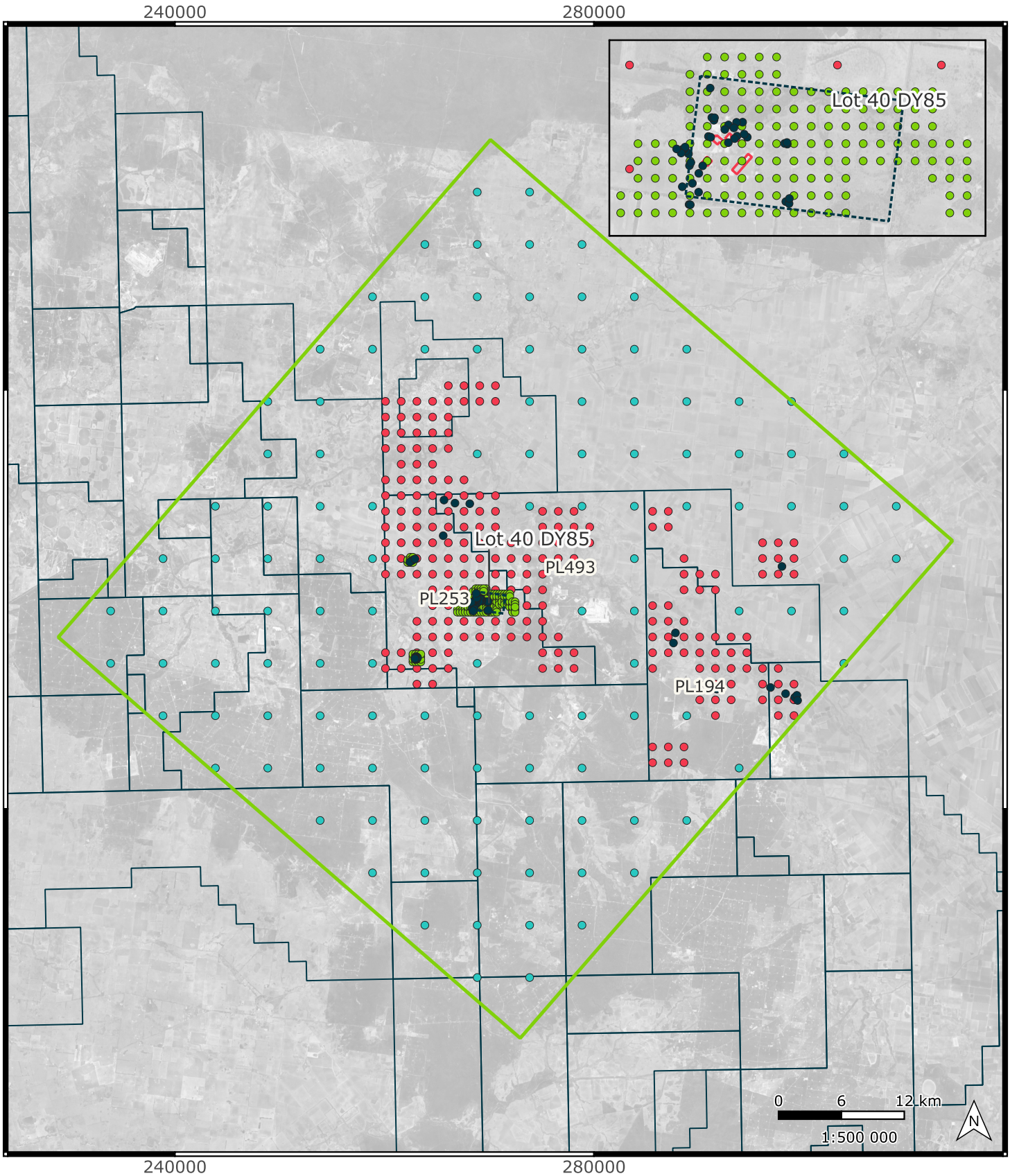
Pilot point interpolation across the model zones using the PLPROC kriging and Python scripting were applied to parameterise successive model runs and adjust model boundary conditions discussed in section 3.1.3.

Overall, the numerical groundwater model has 26,032 adjustable parameters. PEST-ENSI/PESTPP-IES randomly samples parameter fields based on prior parameter ranges where each parameter field is referred to as a “realisation”. An initial ensemble size of 800 realisations was defined for PEST-ENSI/PESTPP-IES automated history matching which was reduced to 364 realisations after seven rounds of calibration iterations removing realisations that did not converge for all the time steps or did not satisfy history matching metrics for the groundwater flow and contaminant transport model. The prior and posterior ranges of parameters were compared ensuring that the posterior parameters fields are not over-constrained.

Pilot point application is described below:

- A total of 578 pilot points is used across the model domain as shown in Figure 4-1.
- Pilot points allow for perturbations in:
  - hydraulic conductivity (horizontal and vertical),
  - specific storage, and
  - specific yield.
- Pilot points are spread out based on their proximity to monitoring sites and potential parameterisation of structures and geological zones within each layer with the following spacings:
  - 250 m within Lot 40 DY85,
  - 1,500 m within areas with groundwater level records, and
  - 5,000 m in areas with no groundwater level data.

A pilot point is placed between each pair of monitoring sites to allow for capturing different groundwater trends in bores caused by heterogeneity in hydraulic properties of HSUs.



Legend

- Groundwater model extent
- Lot 40 DY85

Pilot points with:

- 250 m
- 1500 m
- 5000 m
- Additional PP near monitoring sites

Pilot point locations

Project No.	Client	Figure No.
411001-00917	Arrow	4-1

Notes:
Project CRS: GDA94 / MGA zone 56
Last Saved: 14:49 16/04/2026
Filename: Figure_4-1_pilot_points
Exported by User: Mohsen.Azadi
Project Exported: 15:11 16/04/2026

References:
N/A

File Path: C:\modelling\Arrow\deliverables\Figures_REP-HG-002\Figure_4-1_pilot_points.qgz

© Worley Pty Ltd While every care is taken to ensure the accuracy of this data, Worley makes no representations or warranties aboutits accuracy, reliability, completeness or suitability for any particular purpose and disclaims all responsibility and all liability (including without limitation liability in negligence) for all expenses, losses, damages (including indirect or consequential damage) and costs which might be incurred as a result of the data being inaccurate or incomplete in any way and for any reason.

worley consulting

4.3 Observation data assimilation

PEST is designed to progressively minimise its objective function (phi) by adjusting model parameters in an iterative fashion within prescribed bounds. Phi is calculated internally by PEST as the sum of squared weighted residuals between observations and their modelled counterparts.

PEST allows the user to group different observation data types and apply different weights (and individual observations within each group). This facilitates strategic weighing of different observation types and locations according to the objectives of the modelling and accuracy of various data sources.

For example, strategic weighting may be used to account for the fact that some bores can have far more data than others; those with fewer observation data may be less "visible" to PEST during inversion, unless their weighting is increased relative to those sites with more data.

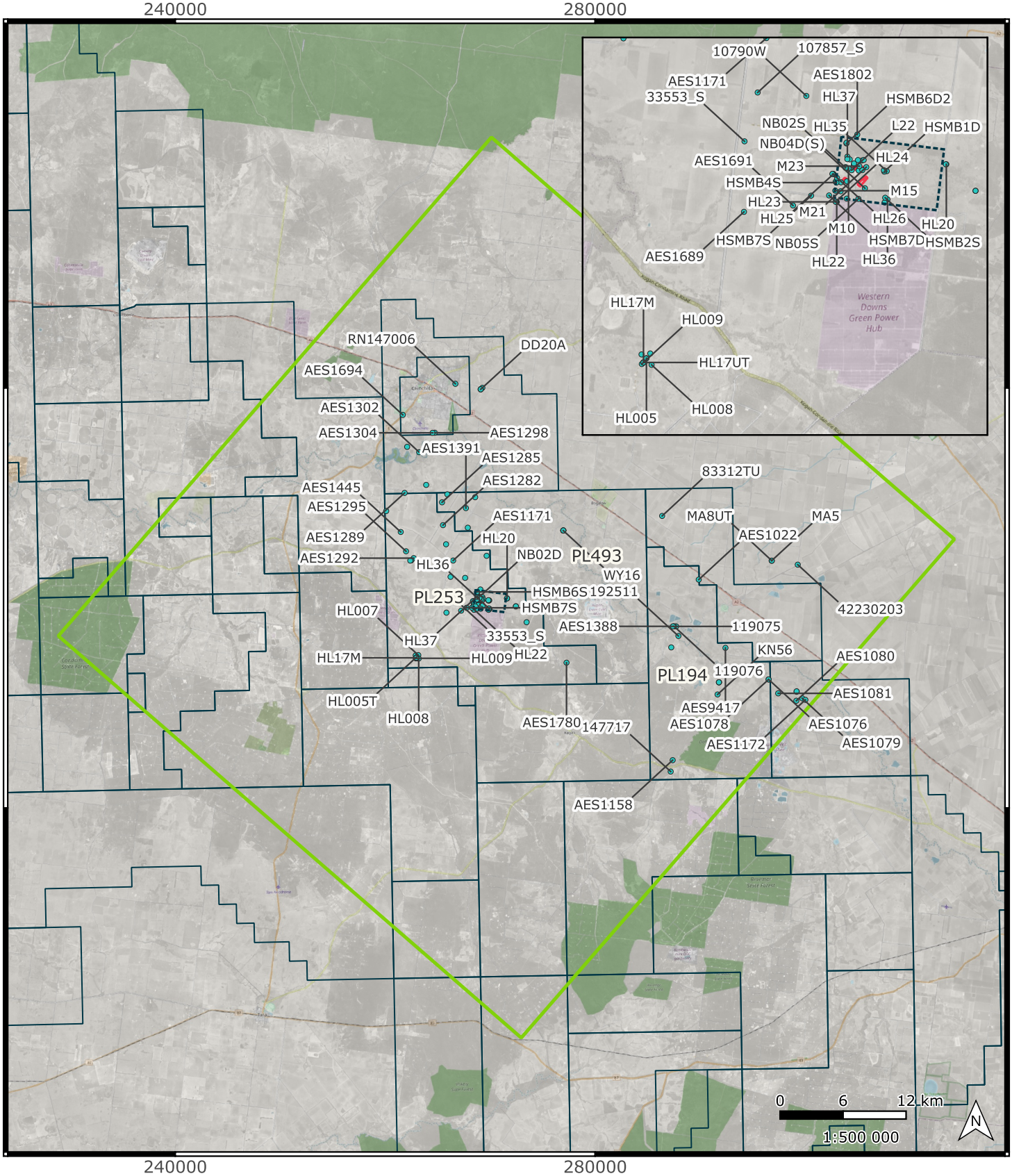
Other reasons for different weightings may include less reliable versus more reliable data. Or bores in a particular area are more important to the project objectives than those in other areas. In the current model, weight adjustment is focused on monitoring bores within PL253 and Lot 40 DY85.

The performance of the model is tested against the measured groundwater levels and concentrations (for benzene and naphthalene) as well as pumping data for Hopeland pilot wells. Observation data used for history matching of the groundwater flow model and the weights assigned to them are defined so that the total calculated phi is distributed among various calibration targets (shown in Figure 4-2):

- Starting water levels in 115 monitoring sites - representing background (pre-abstraction) groundwater level in each monitoring site (10%),
- Transient water levels recorded between 2008 and 2025 in 115 monitoring sites (30%),
- Temporal changes in the transient water levels for 115 monitoring sites (5%),
- Vertical head differences in 18 pairs of monitoring sites (10%),
- Inferred water levels based on Q3 2025 contours in Macalister coal seam shown in Figure 2-2 to replicate current hydraulic gradients within Lot 40 DY85 – water levels in 1,683 model cells across the contoured areas were sampled for a refined per cell history matching (15%),
- Monitoring bores within Springbok sandstone for Q3 2025 (5%), and
- Transient water levels, recorded in the Hopeland pilot wells and HL17 (25%).

For the contaminant transport model, the total calculated phi is distributed among various calibration targets:

- Benzene concentration in 18 monitoring sites located in the Springbok sandstone (50%),
- Benzene concentration in 12 monitoring sites located in the Macalister coal seam (30%),
- Naphthalene concentration in 19 monitoring sites located in the Springbok sandstone (15%), and
- Naphthalene concentration in 12 monitoring sites located in the Macalister coal seam (5%).



Legend

- Groundwater model extent
- Lot 40 DY85
- Monitoring bores

Bore locations with transient groundwater level data

Project No.	Client	Figure No.
411001-00917	Arrow	4-2

Notes:
Project CRS: GDA94 / MGA zone 56
Last Saved: 17:17 16/04/2026
Filename: Figure_4-3_bore_loc
Exported by User: Mohsen.Azadi
Project Exported: 17:22 16/04/2026

References:
N/A

File Path: C:\modelling\Arrow\deliverables\Figures_REP-HG-002\Figure_4-3_bore_loc.qgz

© Worley Pty Ltd While every care is taken to ensure the accuracy of this data, Worley makes no representations or warranties aboutits accuracy, reliability, completeness or suitability for any particular purpose and disclaims all responsibility and all liability (including without limitation liability in negligence) for all expenses, losses, damages (including indirect or consequential damage) and costs which might be incurred as a result of the data being inaccurate or incomplete in any way and for any reason.

4.4 Groundwater flow model

4.4.1 History matching metrics

Model performance acceptance is evaluated based on Australian Groundwater Modelling Guidelines (Barnett et al., 2012) using a number of measures that are not necessarily related to model history matching. The following aspects of the model performance are considered:

- Model convergence: the head change tolerance of 0.001 m between iterations is set in the solver setting,
- Water balance: A value of less than 1% should be achieved at any time step and cumulatively,
- Qualitative measures: robustness/plausibility of model parameters, groundwater flow directions, and temporal groundwater level trends must be consistent with the conceptual model, and
- Quantitative measures such as root mean square error (RMS) and scaled root mean square error (SRMS).

The performance of the 364 model realisations was analysed to ensure the models used during predictive uncertainty analysis are calibrated. A maximum SRMS of 10% was considered as the criterion to assess the model calibration with all 364 models deemed calibrated as shown in Figure 4-3.

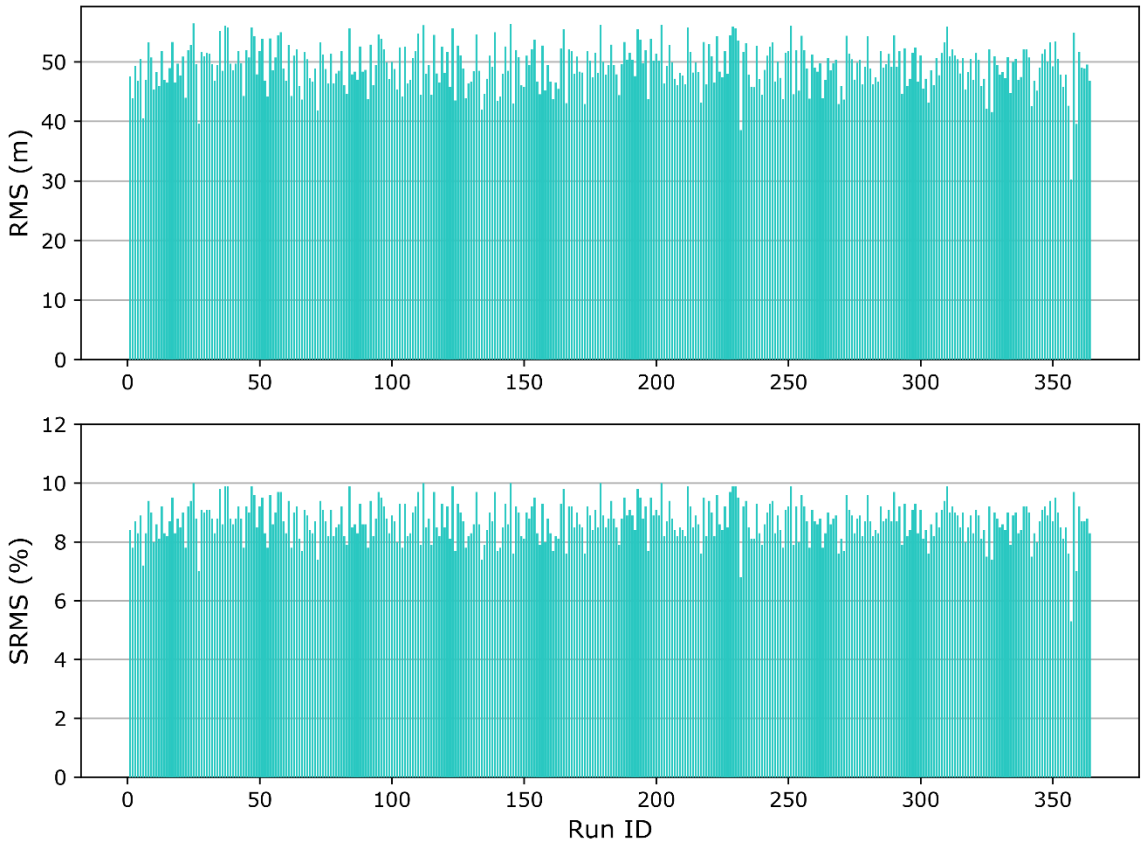


Figure 4-3 Calculated RMS and SRMS for converged model realisations

The results presented in the remainder of this section are extracted from the realisation that yields the best statistical fit with the observed groundwater levels, referred to as reference case.

The matches between individual water level measurements are presented as a scatter plot in Figure 4-4. The calibration statistics are expressed by RMS and the scaled RMS values of 30.2 m and 5.4%, respectively. Barnett et al. (2012) propose that groundwater models should aim to minimise the SRMS (RMS divided by the range of observed data) error to below 10%. Therefore, a value of 5.4% is deemed a satisfactory level of calibration.

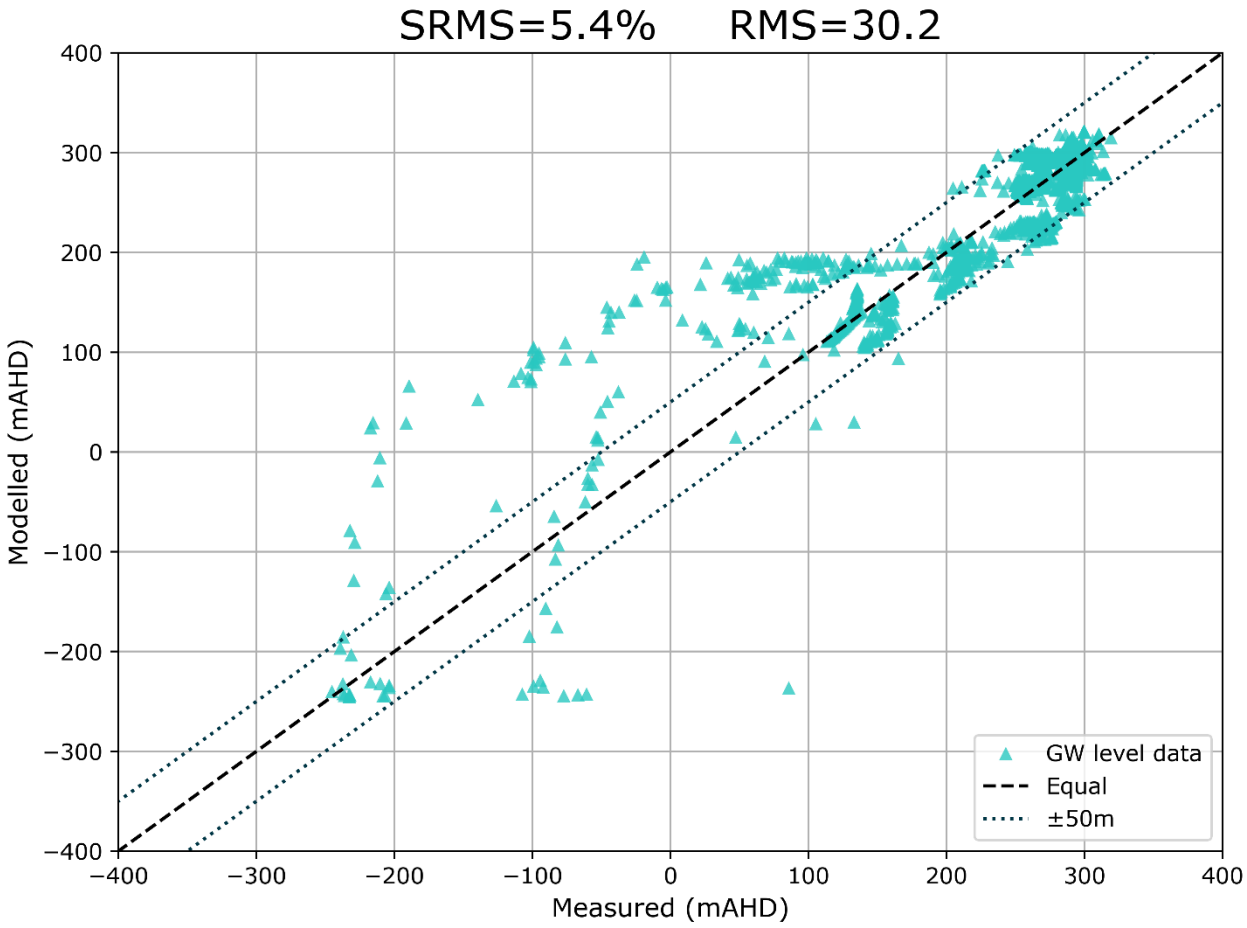
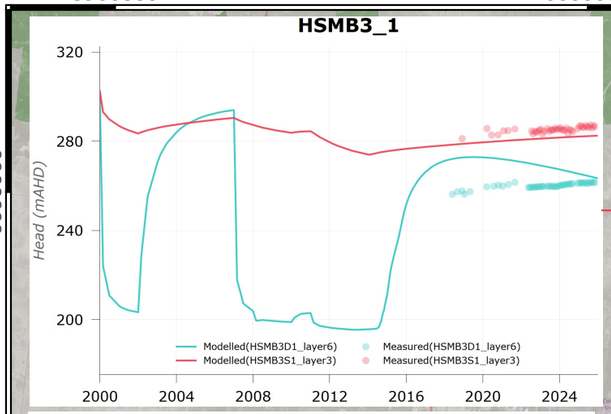


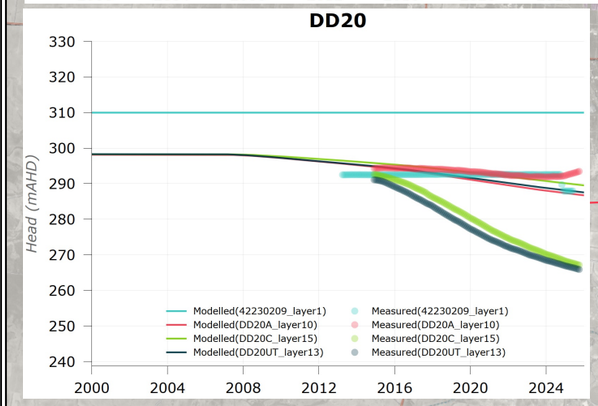
Figure 4-4 Calibration fit of reference case

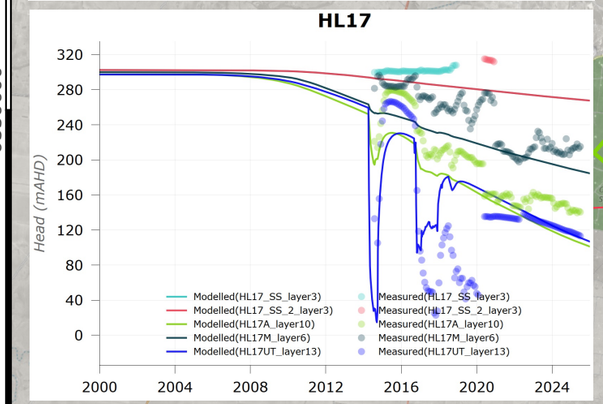
One of the metrics to evaluate groundwater model performance is by quantifying the match between the observed and modelled groundwater levels and by assessing the consistency of their trends.

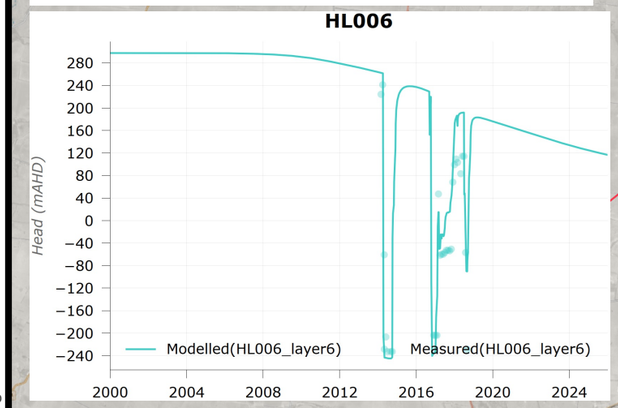
A reasonable match for groundwater level trends was achieved (shown in Figure 4-5) as noted in the observed groundwater levels showing recovering trends or declining trends due to groundwater abstraction.

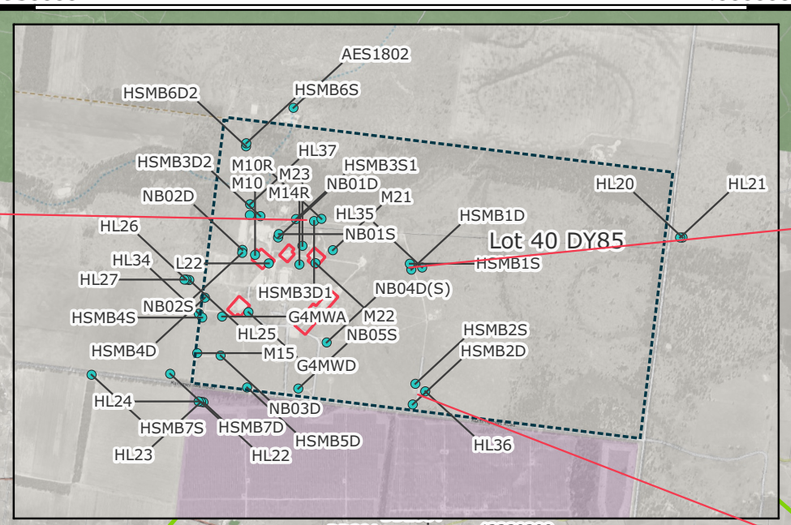
All hydrographs for simulated groundwater levels are presented in Appendix A.

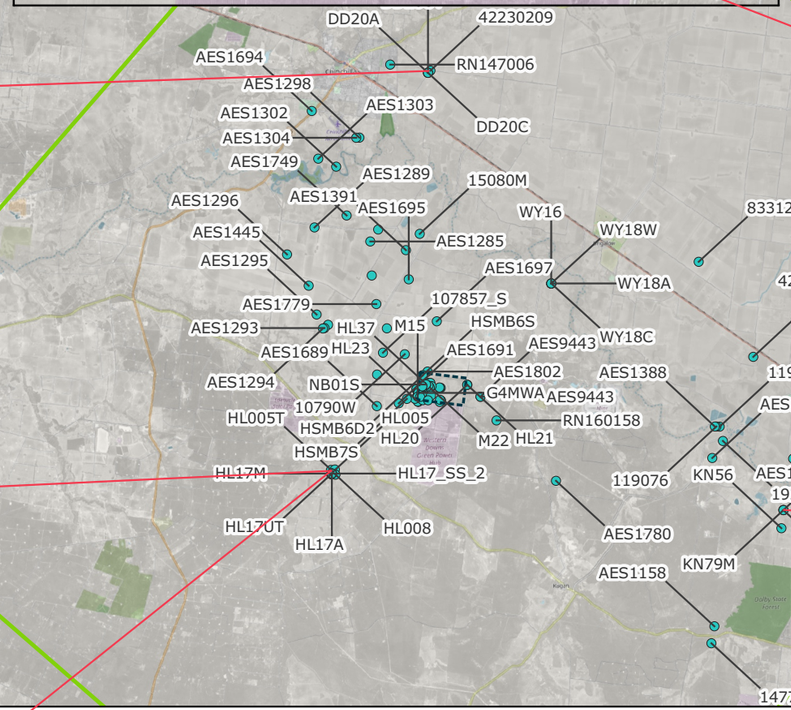


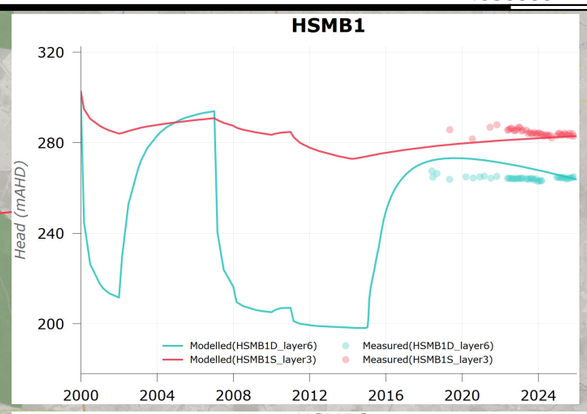


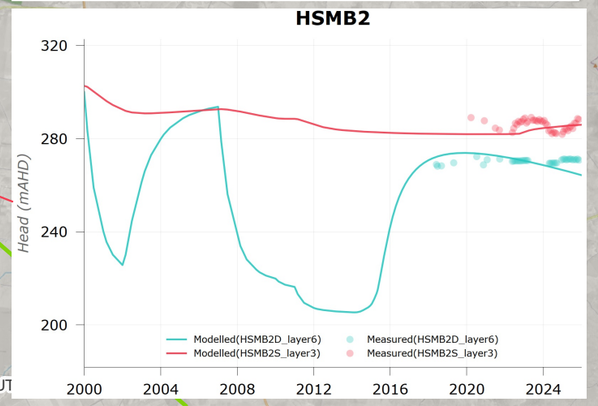


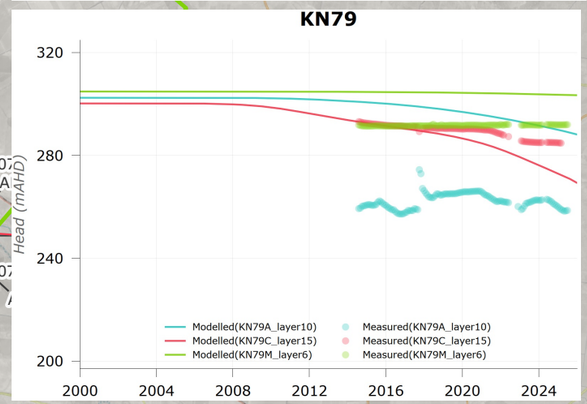












Legend

- Groundwater model extent
- Gasifiers
- Monitoring bores
- Lot 40 DY85

Observed vs modelled groundwater levels in monitoring bores

Project No.	Client	Figure No.
411001-00917	Arrow	4-5

Notes:
Project CRS: GDA94 / MGA zone 56
Last Saved: 20:27 16/04/2026
Exported by User: Mohsen.Azadi
Project Exported: 21:59 16/04/2026

References:
N/A

File Path: C:\modelling\Arrow\deliverables\Figures_REP-HG-002\Figure_4-5_GW_trends.qgz

© Worley Pty Ltd While every care is taken to ensure the accuracy of this data, Worley makes no representations or warranties aboutits accuracy, reliability, completeness or suitability for any particular purpose and disclaims all responsibility and all liability (including without limitation liability in negligence) for all expenses, losses, damages (including indirect or consequential damage) and costs which might be incurred as a result of the data being inaccurate or incomplete in any way and for any reason.

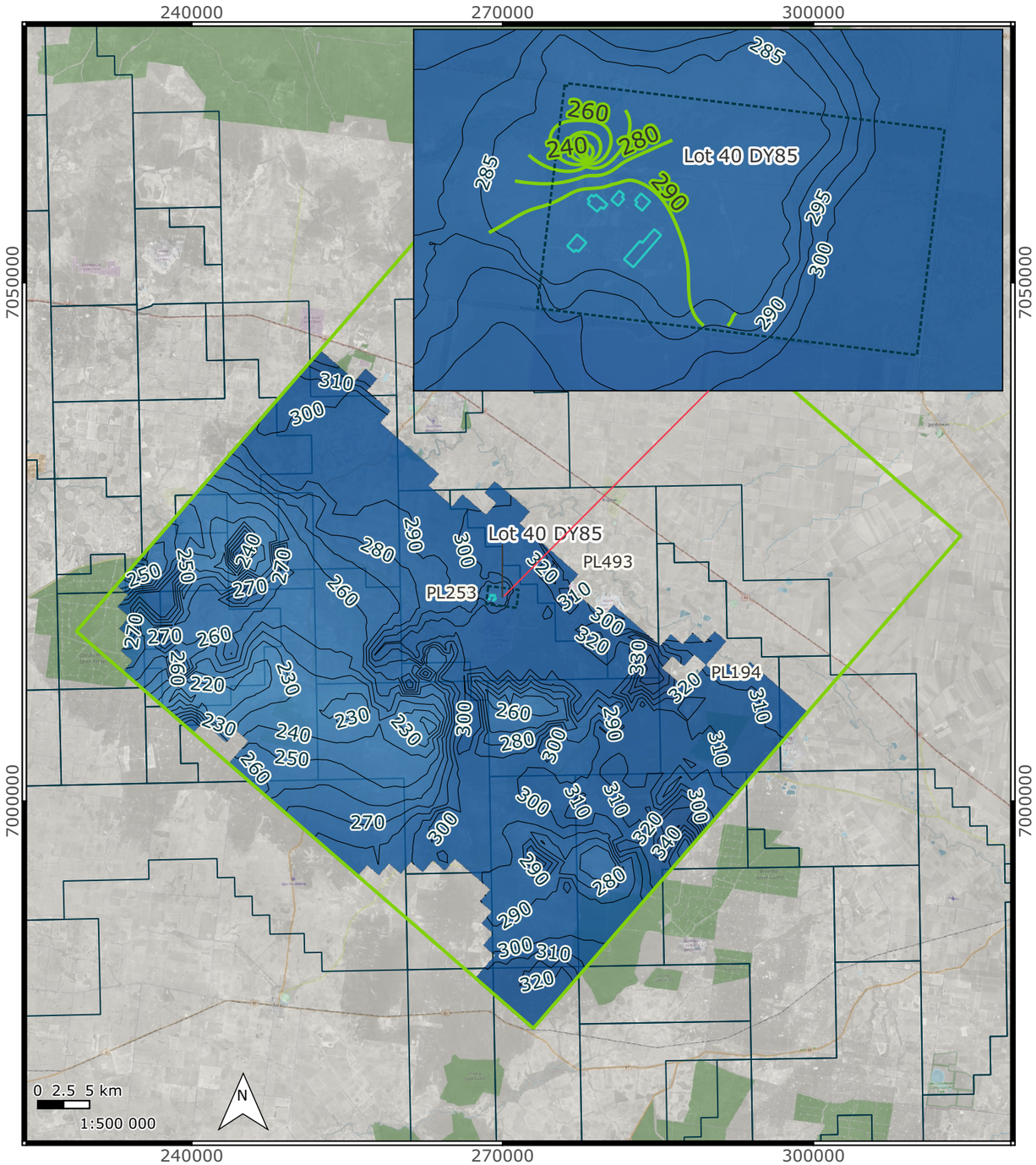
0 4 8 12 16 km
1:391,516
N

4.4.2 Groundwater levels and flow directions

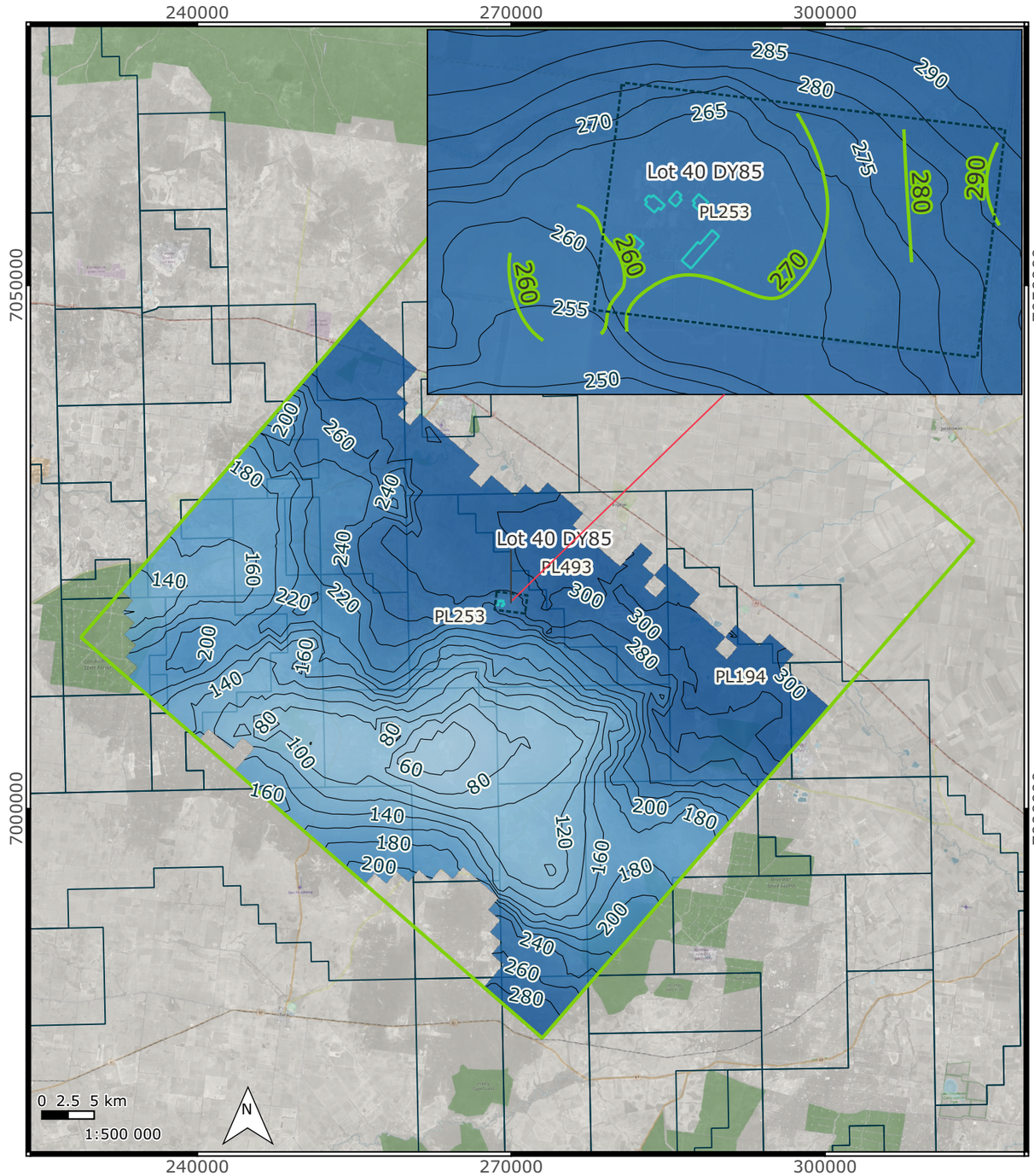
Figure 4-6 shows the simulated groundwater levels (reference case) at the end of the history matching period. As discussed in section 4.3, Q3 2025 groundwater levels were used as a calibration target to ensure the current simulated groundwater flow directions are largely aligned with the interpreted groundwater contours within Lot 40 DY85 (discussed in section 2.4.1). The calibration results indicate this approach achieves a reasonable spatial match between simulated and inferred (from bore measurements) groundwater levels and flow directions.

Modelled groundwater flow gradients within the Springbok sandstone indicate inward flow towards Lot 40 DY85. In the Macalister coal seam, hydraulic gradients are directed towards the gasifiers from the east, north, and parts of the west boundary, with groundwater continuing to flow towards the southwest corner of Lot 40 DY85. This flow direction potentially reflects partial groundwater recovery near the gasifiers and regional south to southwest groundwater flow associated with the current CSG abstraction beyond the PL253 area.

Springbok sandstone



Macalister coal seam



Legend

- Groundwater model extent
- Lot 40 DY85
- Petroleum leases
- Groundwater contours - Q3 2025

Groundwater level (mAHD)

- -200
- -100
- 0
- 100
- 200
- 300
- 400

Simulated groundwater levels in Springbok sandstone and Macalister coal seam (end of December 2025)

Project No.	Client	Figure No.
411001-00917	Arrow	4-6

Notes:
Project CRS: GDA94 / MGA zone 56
Last Saved: 11:48 17/04/2026
Filename: Figure_4-6_GW_cal_end

Exported by User: Mohsen.Azadi
Project Exported: 11:15 28/04/2026

References:
N/A

File Path: C:\modelling\Arrow\deliverables\Figures_REP-HG-002\Figure_4-6_GW_cal_end.qgz

© Worley Pty Ltd While every care is taken to ensure the accuracy of this data, Worley makes no representations or warranties aboutits accuracy, reliability, completeness or suitability for any particular purpose and disclaims all responsibility and all liability (including without limitation liability in negligence) for all expenses, losses, damages (including indirect or consequential damage) and costs which might be incurred as a result of the data being inaccurate or incomplete in any way and for any reason.

4.4.3 Calibrated hydraulic parameters

The ranges of calibrated hydraulic properties derived from the calibration ensemble (reference case realisation) are summarised by respective box and whiskers (BAW) plots shown in Figure 4-7. The BAW plot characterises:

- a median value with the line inside the box
- the range between the 25th and 75th percentiles - box extent
- the minimum and maximum values as whiskers
- an area-averaged value for the cells in each zone (the red line shows) which is discussed below for comparison of hydraulic properties across different zones.

The calibrated hydraulic property ranges indicate that:

- Condamine alluvium has the highest horizontal conductivity with a median value of 14.9 m/day.
- The remaining mode layers are calibrated to a median range of horizontal conductivity between 0.001 m/day and 0.1 m/day with the following exceptions:
  - Kogan interburden, Macalister interburden, and Eurombah formation are calibrated to median values between 0.001 m/day to 0.00001 m/day, and
  - Koan coal seam and Condamine coal seam is calibrated to median values slightly over 0.1 m/day.
- Vertical hydraulic conductivity is calibrated to lower values compared to horizontal hydraulic properties with similar trend among various layers with Condamine alluvium and Eurombah formation having the highest and lowest values, respectively.
- The specific storage and specific yield values are calibrated within the plausible bounds, with a general trend of higher storage values for coal seams and lower values for interburden units and deeper HSUs as the storativity values reduce with depth.

Prior and posterior distribution of median value for each HSU across the full ensemble is presented in Appendix B.



Figure 4-7 Calibrated hydraulic property ranges

4.5 Contaminant transport model

Contaminant transport history matching was undertaken to replicate observed groundwater quality trends for benzene and naphthalene and to provide confidence in subsequent predictive uncertainty analysis. The process focused on assessing whether the combined representation of groundwater flow fluxes, source term characterisation, transport parameters, and natural attenuation processes could reasonably replicate the magnitude, spatial extent, and temporal evolution of measured concentrations.

4.5.1 History-matching metrics

The performance of the 364 model realisations was analysed to ensure the transport models used during predictive uncertainty analysis are calibrated. A maximum SRMS of 10% was adopted as the criterion to assess history matching fit for benzene and naphthalene, with all 364 realisations meeting the history matching criterion, as shown in Figure 4-8 and Figure 4-9.

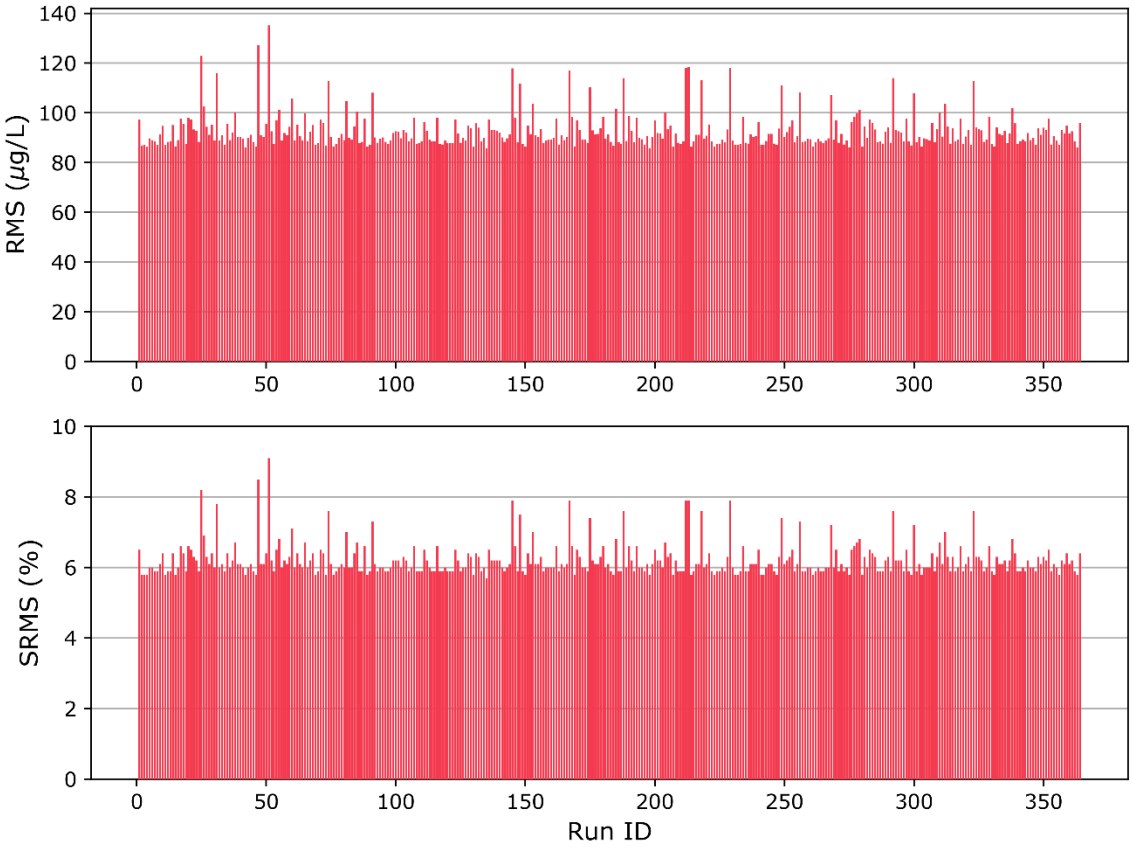


Figure 4-8 Calculated RMS and SRSM for benzene concentration across the posterior ensemble

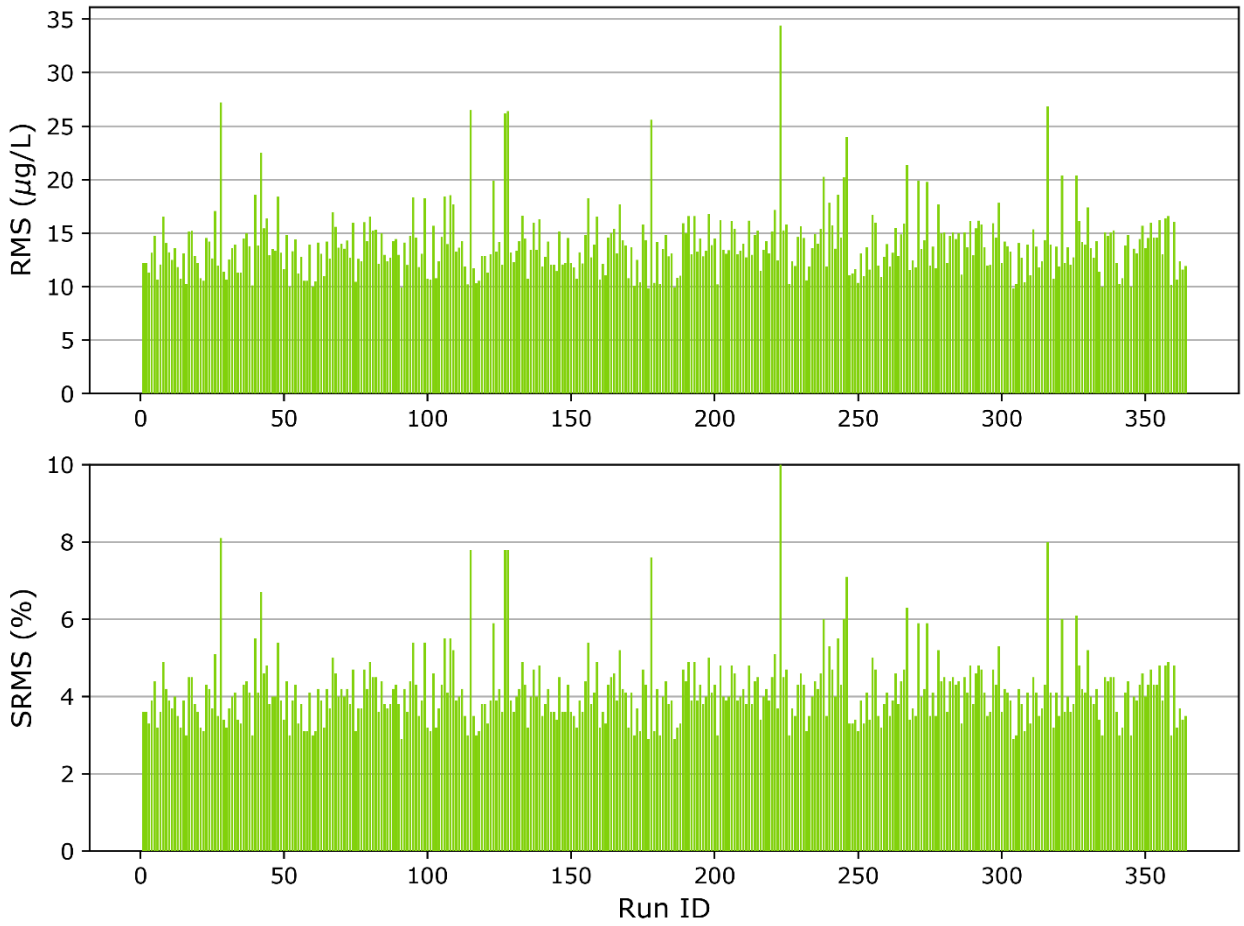


Figure 4-9 Calculated RMS and SRSM for naphthalene concentration across the posterior ensemble

The results presented in the remainder of this section are extracted from the realisation that yields the best statistical fit with the observed groundwater concentrations, referred to as reference case.

The matches between individual water concentration measurements are presented as a scatter plot in Figure 4-10 and Figure 4-11. The history matching results indicate that a good calibration fit is achieved for the magnitude of benzene and naphthalene concentrations in the contaminant transport model.

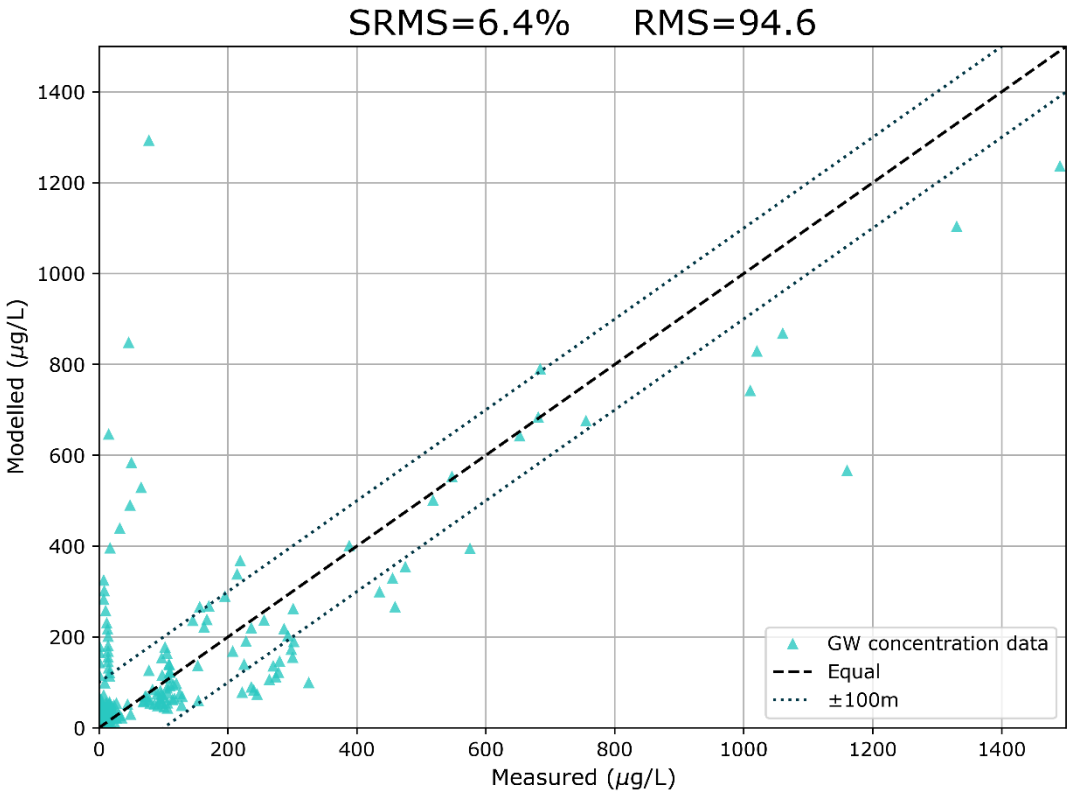


Figure 4-10 Benzene history matching fit for the reference case

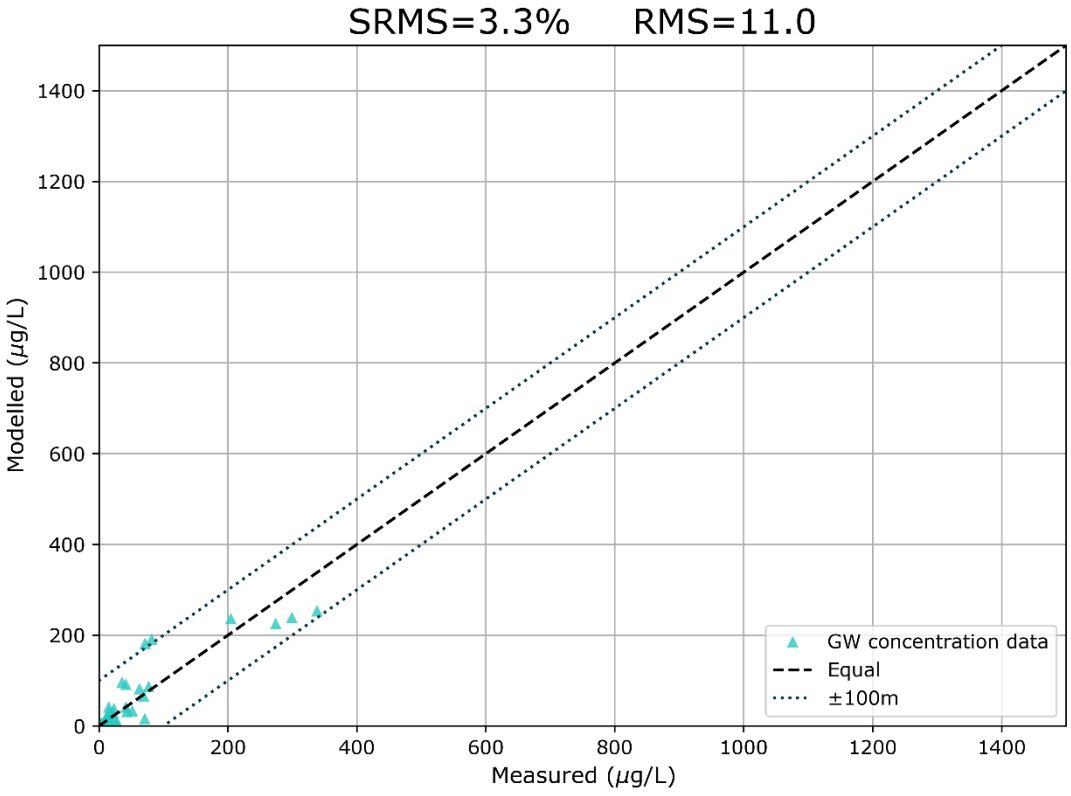


Figure 4-11 Naphthalene history matching fit for the reference case

One of the metrics used to evaluate the transport model performance is by quantifying the match between the observed and modelled groundwater concentrations and by assessing the consistency of their trends.

A reasonable match for groundwater concentration trends was achieved for both benzene and naphthalene (example shown in Figure 4-12) as noted in the observed groundwater concentrations showing below LOR values or declining trends due to groundwater dilution and natural attenuation.

The simulated benzene and naphthalene concentration trends for remaining monitoring bores are presented in Appendix C and D, respectively.

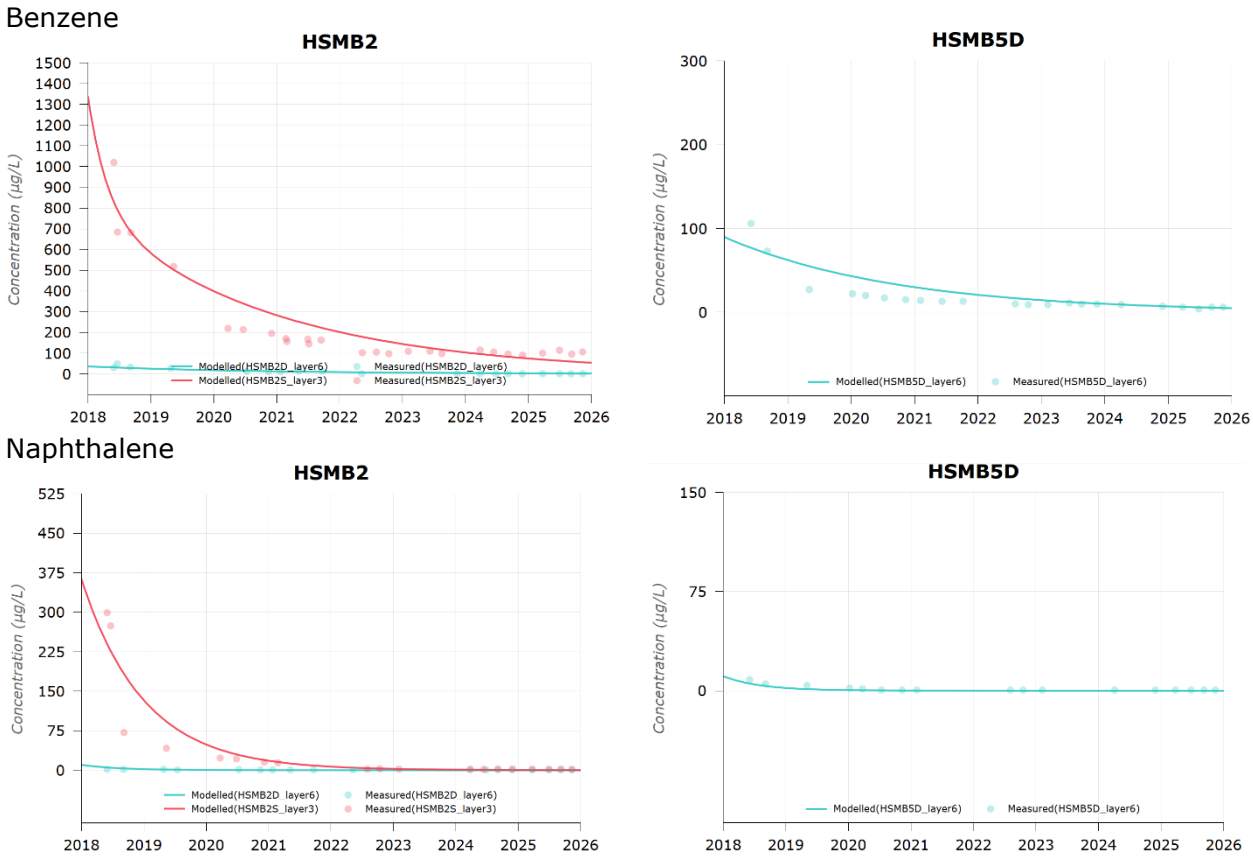


Figure 4-12 Simulated benzene and naphthalene concentration trends for representative monitoring bores screened in the Springbok sandstone and Macalister coal seam

4.5.2 Simulated benzene and naphthalene concentrations

Figure 4-13 shows the simulated benzene concentration (reference case) at the end of the history matching period in the Springbok sandstone and Macalister coal seam. The simulation results indicate that, for both formations, the benzene plume with concentrations exceeding 10 µg/L is largely contained within Lot 40 DY85. This is consistent with groundwater quality monitoring data from bores located outside the Lot 40 DY85 boundary (HL22, HL23, HL25, HL26, HSMB7D, and HL34), where benzene concentrations have remained below the LOR.

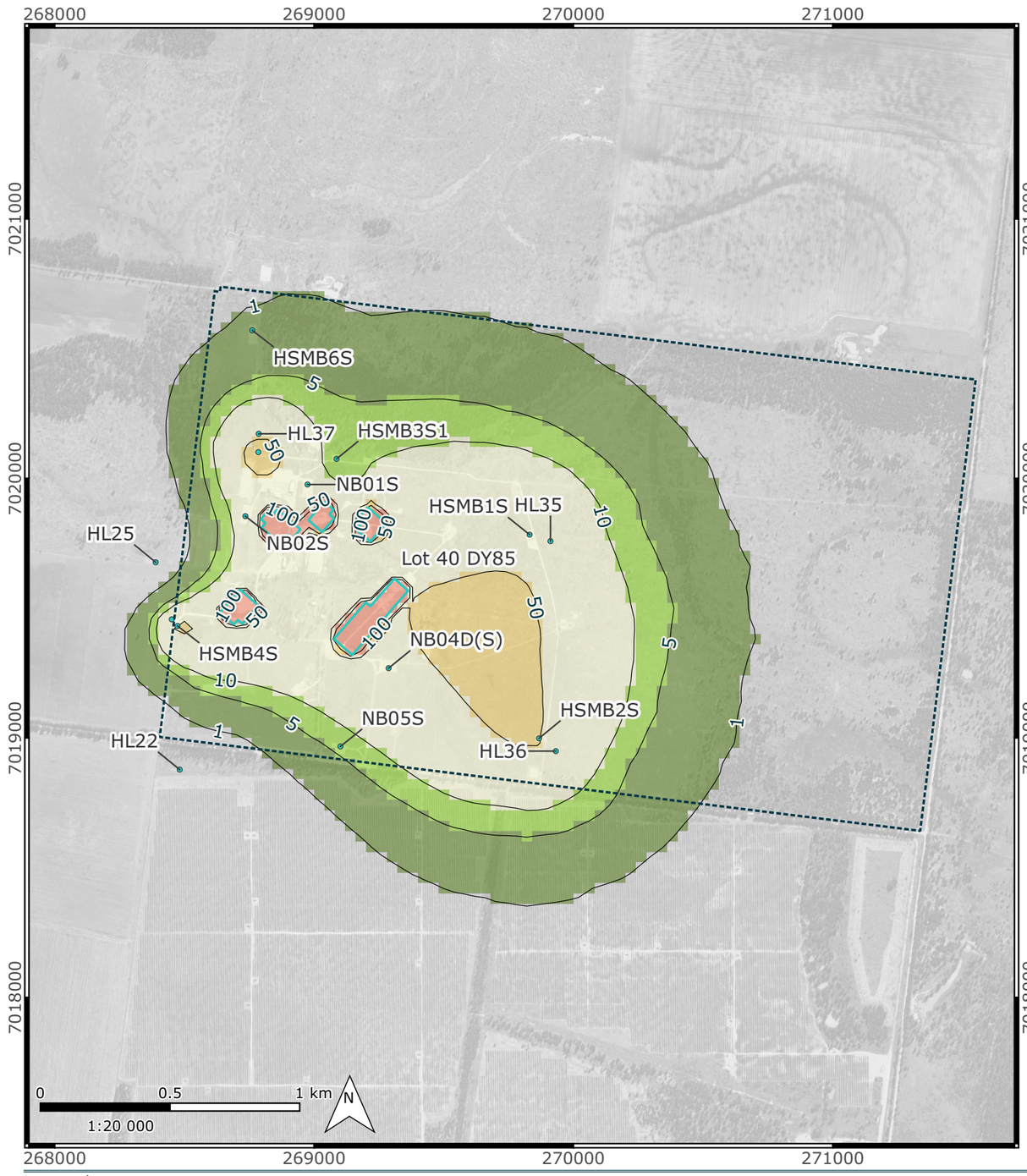
While monitoring bore HSMB4S is located within the Lot 40 DY85 boundary and indicates the potential for limited migration of benzene at concentrations above 10 µg/L beyond the boundary, monitoring results from downstream bores HSMB7S and HL22 have consistently reported below LOR concentrations for several years. This indicates that elevated benzene concentrations observed at HSMB4S are localised, with limited plume migration beyond the Lot 40 DY85 boundary.

The simulated benzene plume shows a zone of elevated concentrations (approximately 50–100 µg/L) within the central part of Lot 40 DY85, extending east of gasifier 5. This zone reflects history matching of the coupled groundwater flow and contaminant transport model to monitoring data that include both below LOR and elevated concentrations, spanning several orders of magnitude. Monitoring data from bores NB04D(S), HL36, HSMB1S, and HL35 (with concentrations below LOR), together with data from bore HSMB2S, define the extent, magnitude, and orientation of the simulated plume in this area.

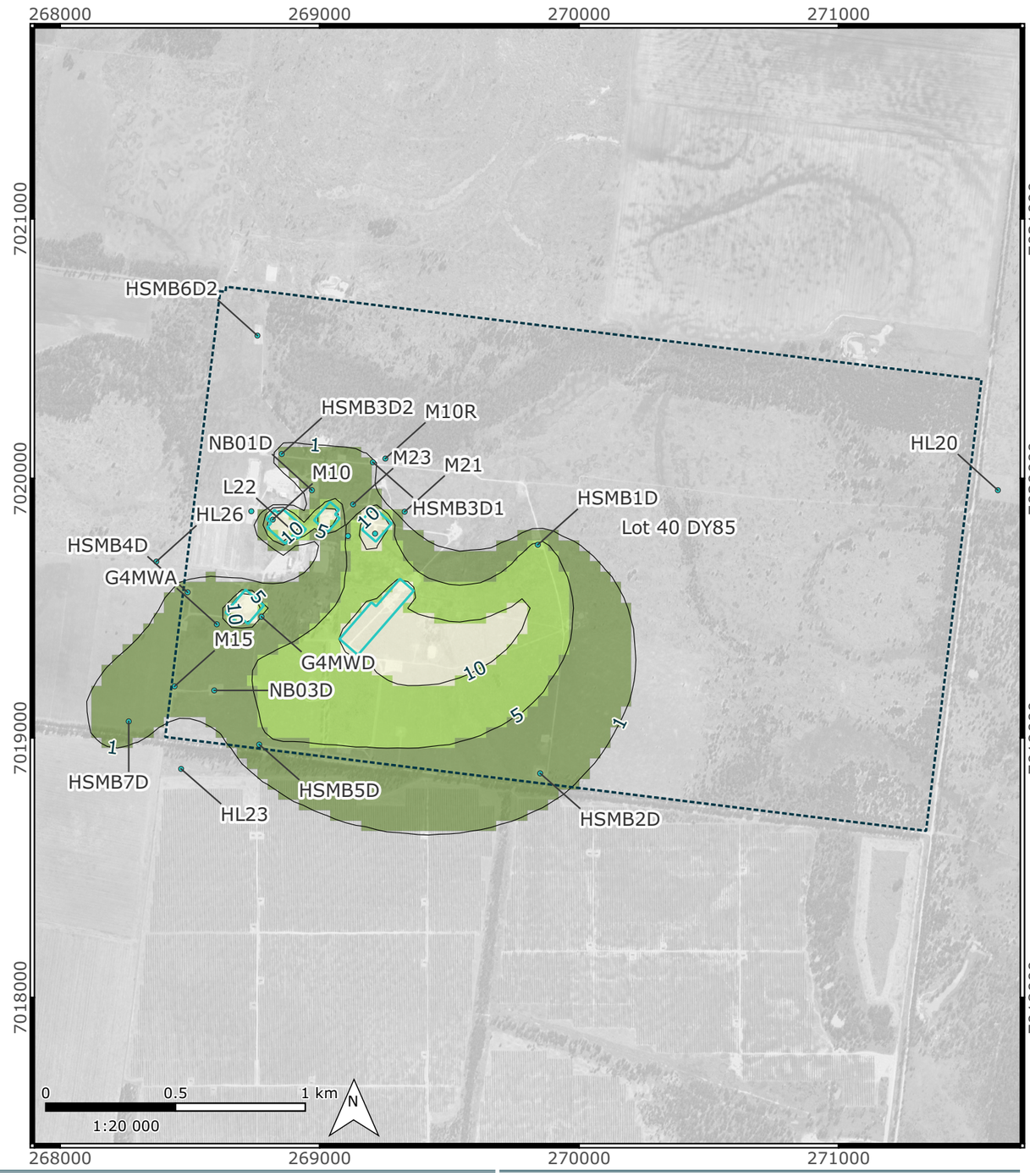
These monitoring data are reflected with spatial variations in calibrated hydraulic conductivity, which indicate the potential presence of a locally enhanced permeability zone near gasifier 5. This feature is interpreted to reflect hydrogeological alteration associated with historical UCG activities, including fracturing of the formation in this direction.

Simulation results at the end of history matching period for naphthalene indicate concentrations below the LOR within the Macalister coal seam across the model domain. In the Springbok sandstone, simulated naphthalene concentrations remain spatially confined within the former gasifier locations. These results reflect the conservative source depletion formulation adopted in the transport model, where the maximum source concentration was defined as 2.2 µg/Lat the end of 2025. The results indicate limited migration potential for naphthalene beyond localised source zones, consistent with groundwater monitoring data.

Springbok sandstone



Macalister coal seam



Legend

- Lot 40 DY85
- Gasifier
- Monitoring bores

Concentration (ug/L)

- 1 - 5
- 5 - 10
- 10 - 50
- 50 - 100
- 100 - 500
- 500 - 1000
- 1000 - 5000

Simulated benzene concentrations in Springbok sandstone and Macalister coal seam (end of December 2025)

Project No.	Client	Figure No.
411001-00917	Arrow	4-13

Notes:
Project CRS: GDA94 / MGA zone 56
Last Saved: 16:48 17/04/2026
Filename: Figure_4-13_benzene_cal_end

Exported by User: Mohsen.Azadi
Project Exported: 17:49 21/04/2026

References:
N/A

File Path: C:\modelling\Arrow\deliverables\Figures_REP-HG-002\Figure_4-13_benzene_cal_end.qgz

© Worley Pty Ltd While every care is taken to ensure the accuracy of this data, Worley makes no representations or warranties aboutits accuracy, reliability, completeness or suitability for any particular purpose and disclaims all responsibility and all liability (including without limitation liability in negligence) for all expenses, losses, damages (including indirect or consequential damage) and costs which might be incurred as a result of the data being inaccurate or incomplete in any way and for any reason.

5. Predictive groundwater flow modelling

5.1 Predictive model setup

Predictive groundwater modelling was undertaken to assess the potential impacts of current and proposed CSG FDP scenarios on groundwater flow and contaminant transport and fate within the Springbok sandstone and the Macalister coal seam. The predictive assessment was based on an ensemble of 364 calibrated realisations, generated through history matching and uncertainty analysis, to quantify the range of potential future outcomes and provide a basis for risk-based impact assessment and decision-making. Model predictions are presented using the P5, P50, and P95 percentiles, representing different likelihoods of predictive outcomes.

Predictive simulations were completed for scenario 2 (existing approved development, including Hopeland pilot wells and authorised Arrow CSG wells) and scenario 3 (maximum proposed development incorporating additional Clynes Road wells). For each scenario, predicted impacts were evaluated separately for the Springbok sandstone and Macalister coal seam. Comparison of percentile-based outcomes between scenarios enabled assessment of incremental impacts attributable to proposed development while explicitly accounting for uncertainty in model parameters and boundary conditions.

All simulations incorporated the full simulation period starting from year 2000, with predictive model starting in 2026, groundwater abstraction ceasing in 2061, and followed by extended recovery simulations through to the end of year 2225. This long-term simulation period allowed assessment of post-abstraction recovery trajectories, potential long-term drawdown or concentration changes.The results of the uncertainty are presented using the risk-based terminology outlined in Peeters & Middlemis (2023) as presented in Table 5-1.

Table 5-1 Probabilistic terminology used (from Peeters & Middlemis, 2023)

Percentile	Probability	Description
<10%	>90%	It is **very likely** that the outcome is **larger** than this value
10–33%	67–90%	It is **likely** that the outcome is **larger** than this value
33–67%	33–67%	It is **as likely as not** that the outcome is **larger** than this value
67–90%	10–33%	It is **unlikely** that the outcome is **larger** than this value
>90%	<10%	It is **very unlikely** that the outcome is **larger** than this value

5.2 Groundwater level and flow directions

Cumulative groundwater abstraction progressively lowers groundwater levels. The extent of the zone affected by abstraction is dependent on the properties of the hydrogeologic units, pumping rates and locations, cumulative production rates, schedule and target aquifer(s) relative to the water table.

Predicted median groundwater levels in the Springbok sandstone and Macalister coal seam at the end of the abstraction period (December 2061), and at the end of the recovery period (December 2225), for non-Arrow wells and Arrow wells in scenario 3, are shown in Figure 5-1 to Figure 5-2.

Model results indicate the development of a cone of depression around abstraction wells because of cumulative groundwater extraction, with regional groundwater flow directed predominantly toward the south and southwest of the model domain.

Within Lot 40 DY85, simulated groundwater flow directions vary by formation. In the Springbok sandstone, predicted groundwater flow is directed toward the gasifiers, with inflow from the north, east, and south boundaries of Lot 40 DY85 and a relatively flat hydraulic gradient along the western boundary. Groundwater flow in the Macalister coal seam is directed toward the southwest. Comparison with groundwater level contours at the end of 2025 (Figure 4-6), indicates partial groundwater recovery in the Springbok sandstone, while groundwater levels in the Macalister coal seam is lowered due to ongoing CSG abstraction from the WCM.

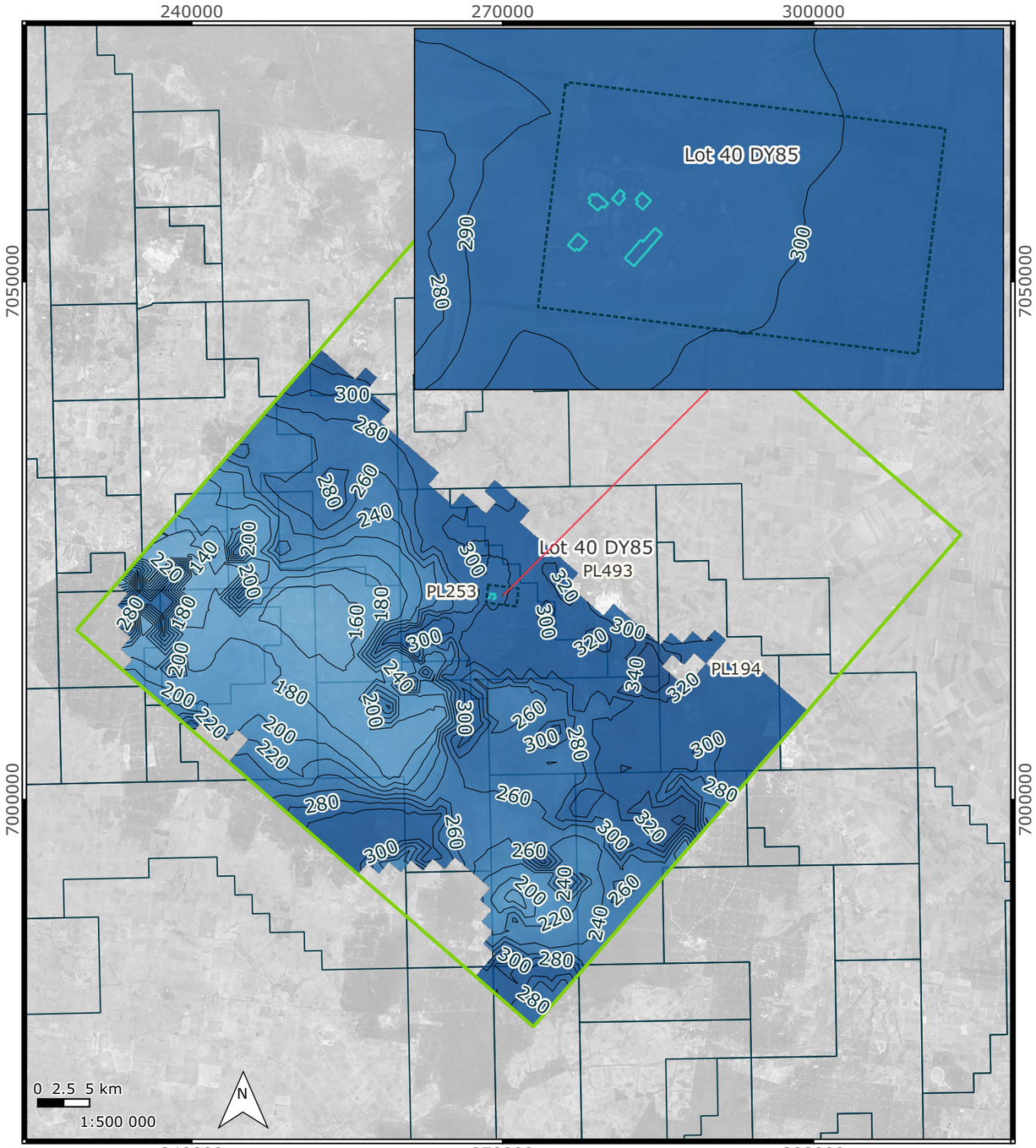
By the end of the recovery period, simulated regional groundwater levels increase relative to those at the end of abstraction period. However, groundwater levels are not predicted to fully return to pre-abstraction conditions. Long-term water balance recovery simulations indicate that total groundwater outflows, including evaporative losses and boundary fluxes, continue to exceed rainfall recharge, limiting full recovery to pre-development groundwater levels.

Differences between the predicted median groundwater levels at the end of abstraction period for scenarios 2 and 3 were evaluated across the ensemble for both the Springbok sandstone and the Macalister coal seam, as shown in Figure 5-3. The predictions indicate a limited area of difference, with up to 1 m change in median groundwater levels occurring at the southwest corner of PL253 within the Springbok sandstone. In the Macalister coal seam, a localised zone with predicted differences of approximately 1–2 m occurs in the vicinity of the proposed Clynes Road wells. These results indicate that the additional abstraction associated with the proposed Clynes Road development results in only minor incremental changes to groundwater levels when compared with the approved development scenario.

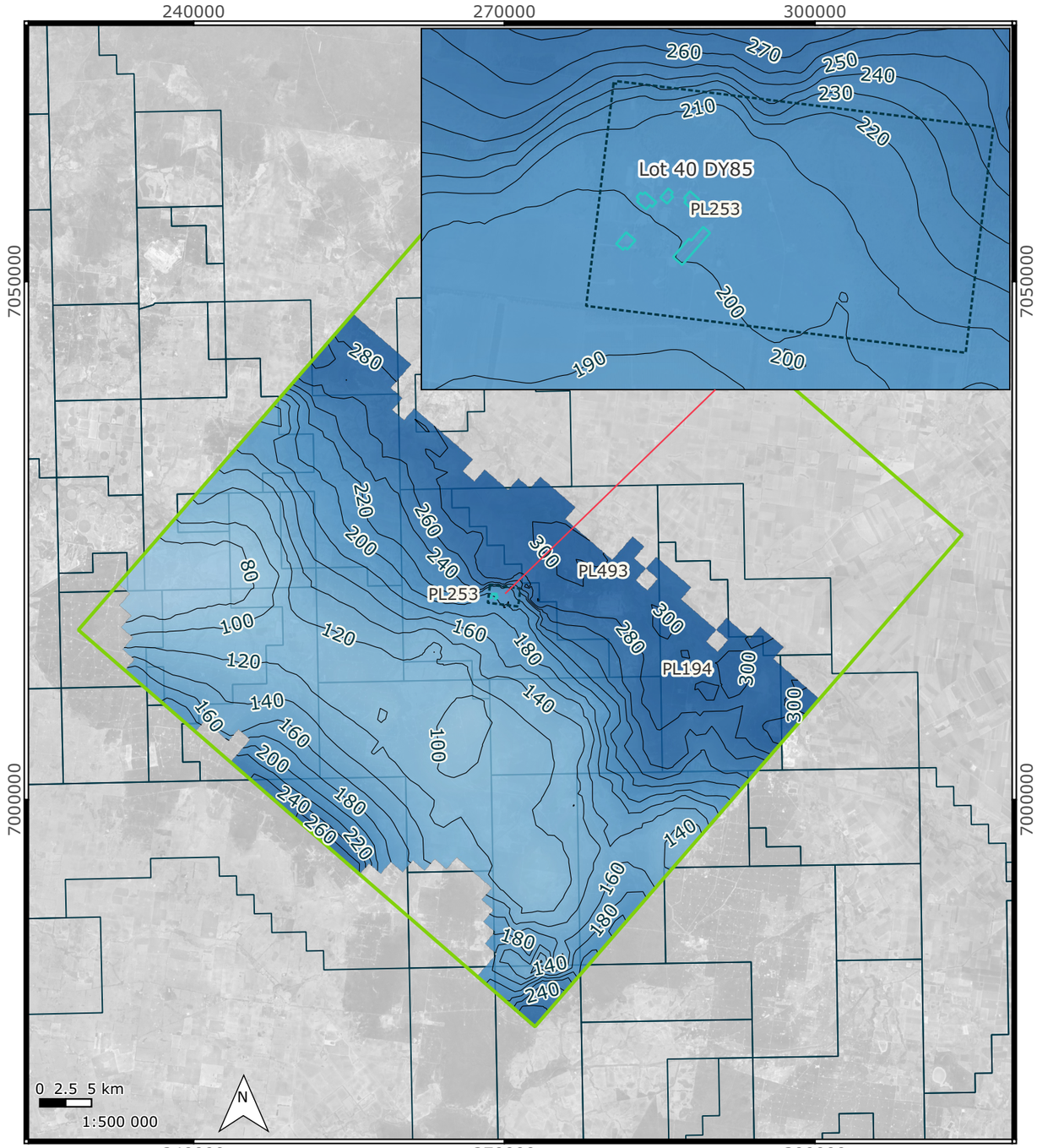
Predicted differences in median groundwater levels at the end of the recovery period between scenarios 2 and 3 are less than 1 m, indicating that inclusion of the proposed Clynes Road wells is not expected to result in a material change to groundwater level recovery relative to the currently approved development.

Predicted groundwater level trends at monitoring bores across the ensemble, showing declining trend during the abstraction period and subsequent recovery following the end of abstraction, are presented in Appendix E.

Springbok sandstone



Macalister coal seam



Legend

- Groundwater model extent
- Lot 40 DY85
- Petroleum leases
- Gasifiers

Groundwater level (mAHD)

- -200
- -100
- 0
- 100
- 200
- 300
- 400

Predicted median groundwater levels in Springbok sandstone and Macalister coal seam for scenario 3 (end of December 2061)

Project No.	Client	Figure No.
411001-00917	Arrow	5-1

Notes:
Project CRS: GDA94 / MGA zone 56
Last Saved: 17:08 17/04/2026
Filename: Figure_5-1_GW_abs_end

Exported by User: Mohsen.Azadi
Project Exported: 18:28 17/04/2026

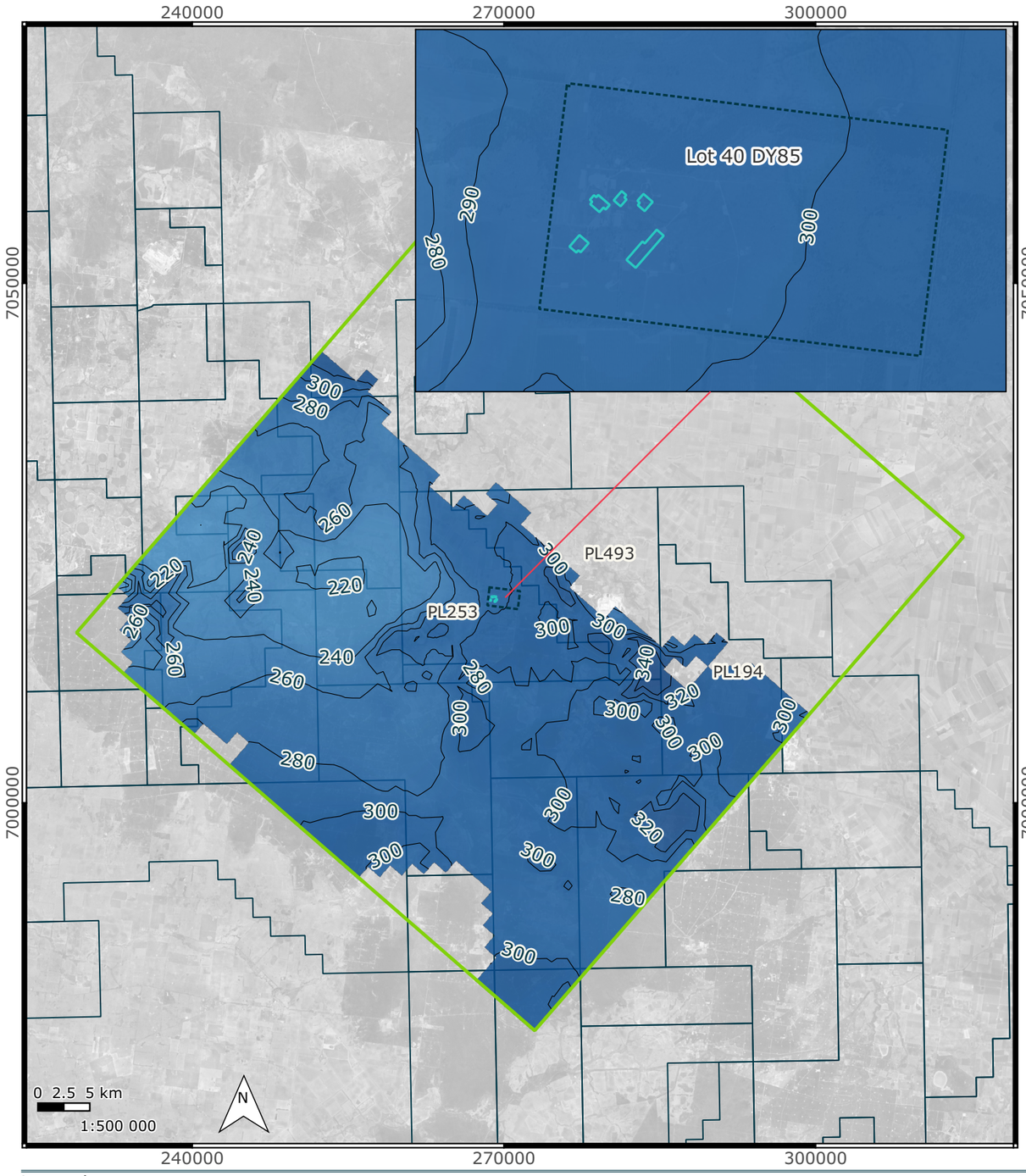
References:
N/A

File Path: C:\modelling\Arrow\deliverables\Figures_REP-HG-002\Figure_5-1_GW_abs_end.qgz

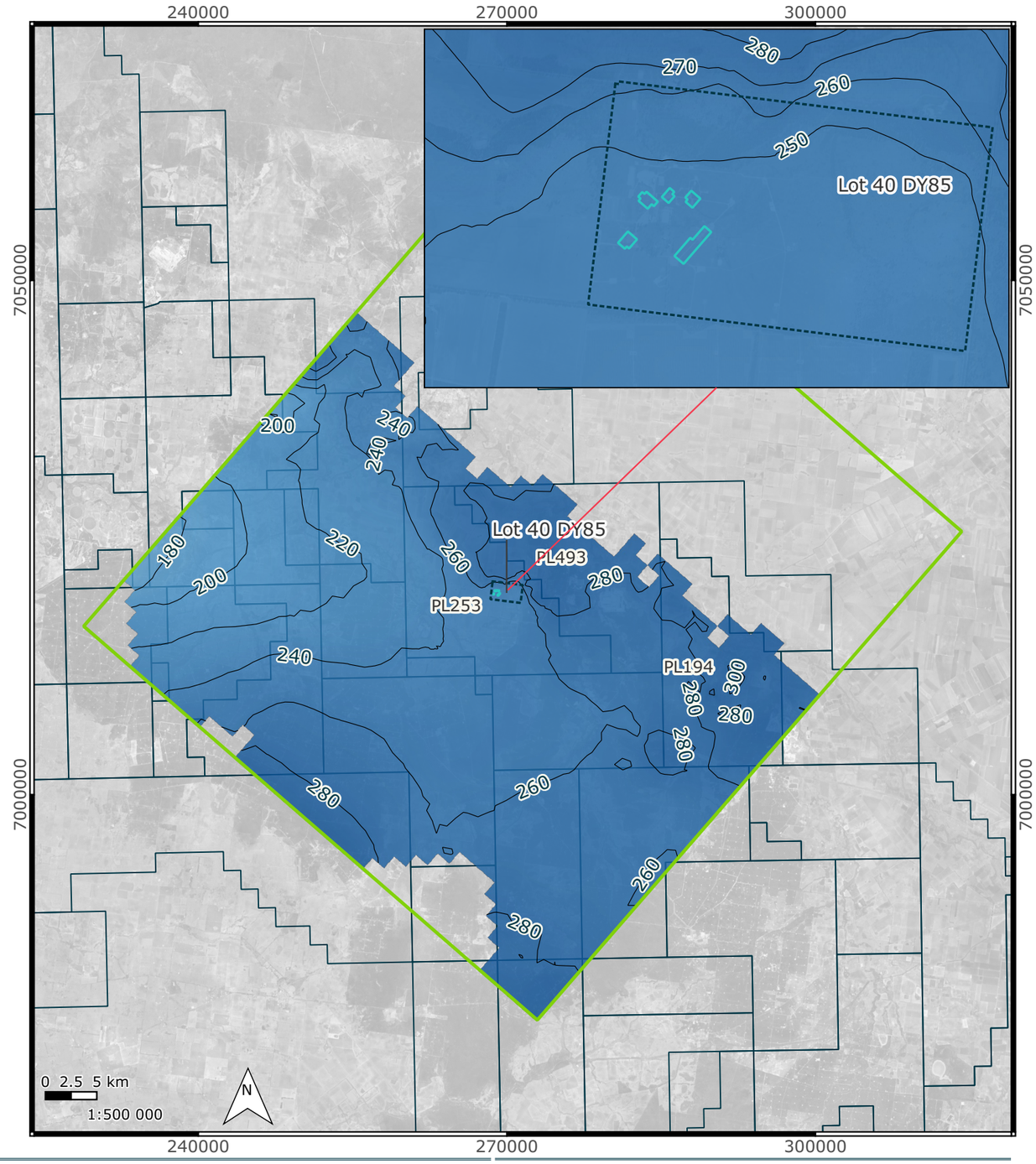
© Worley Pty Ltd While every care is taken to ensure the accuracy of this data, Worley makes no representations or warranties aboutits accuracy, reliability, completeness or suitability for any particular purpose and disclaims all responsibility and all liability (including without limitation liability in negligence) for all expenses, losses, damages (including indirect or consequential damage) and costs which might be incurred as a result of the data being inaccurate or incomplete in any way and for any reason.

worley consulting

Springbok sandstone



Macalister coal seam



Legend

- Groundwater model extent
- Lot 40 DY85
- Petroleum leases
- Gasifiers

Groundwater level (mAHD)

- -200
- -100
- 0
- 100
- 200
- 300
- 400

Predicted median groundwater levels in Springbok sandstone and Macalister coal seam for scenario 3 (end of December 2225)

Project No.	Client	Figure No.
411001-00917	Arrow	5-2

Notes:
Project CRS: GDA94 / MGA zone 56
Last Saved: 18:37 17/04/2026
Filename: Figure_5-2_GW_rec_end

Exported by User: Mohsen.Azadi
Project Exported: 18:38 17/04/2026

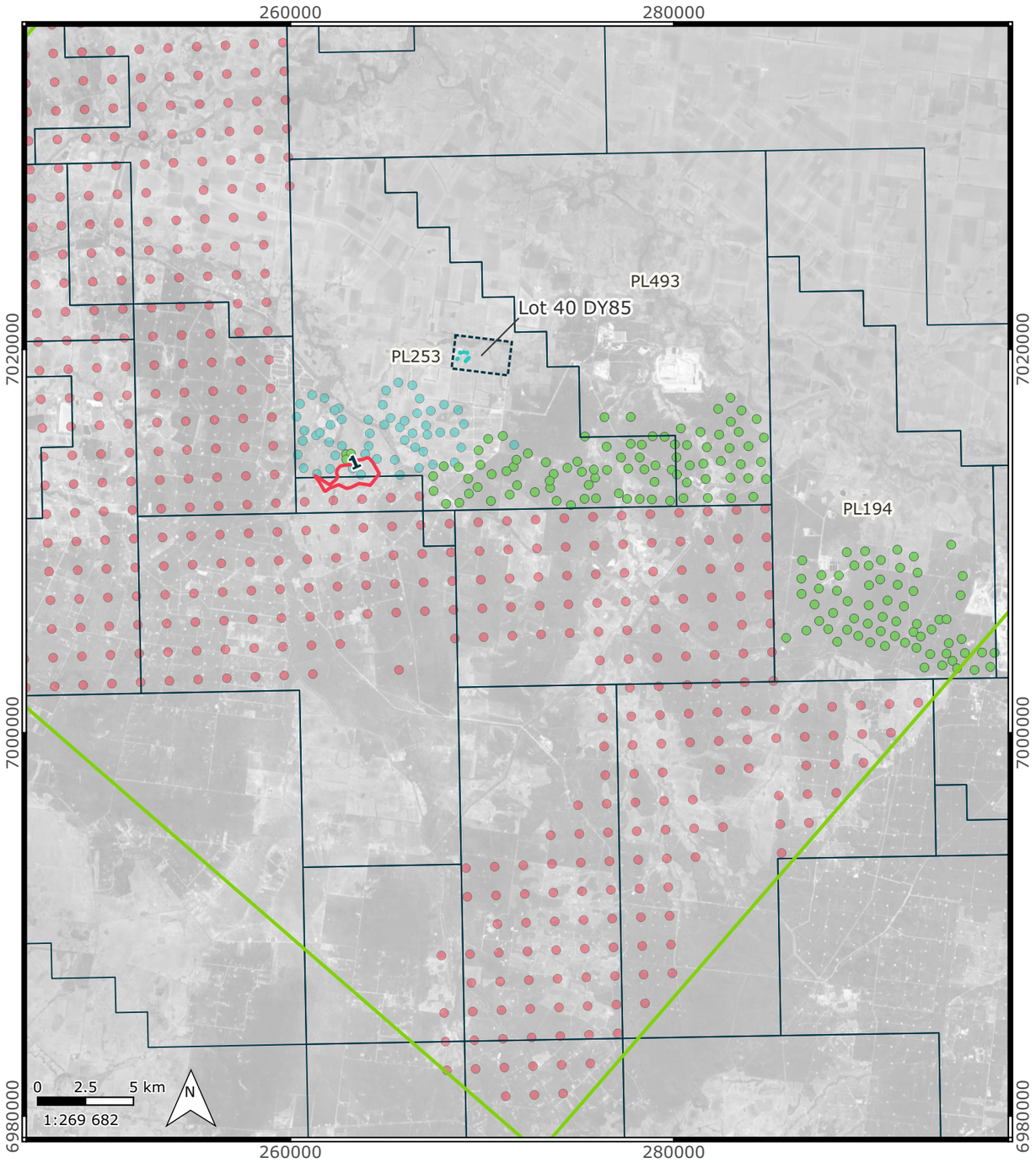
References:
N/A

File Path: C:\modelling\Arrow\deliverables\Figures_REP-HG-002\Figure_5-2_GW_rec_end.qgz

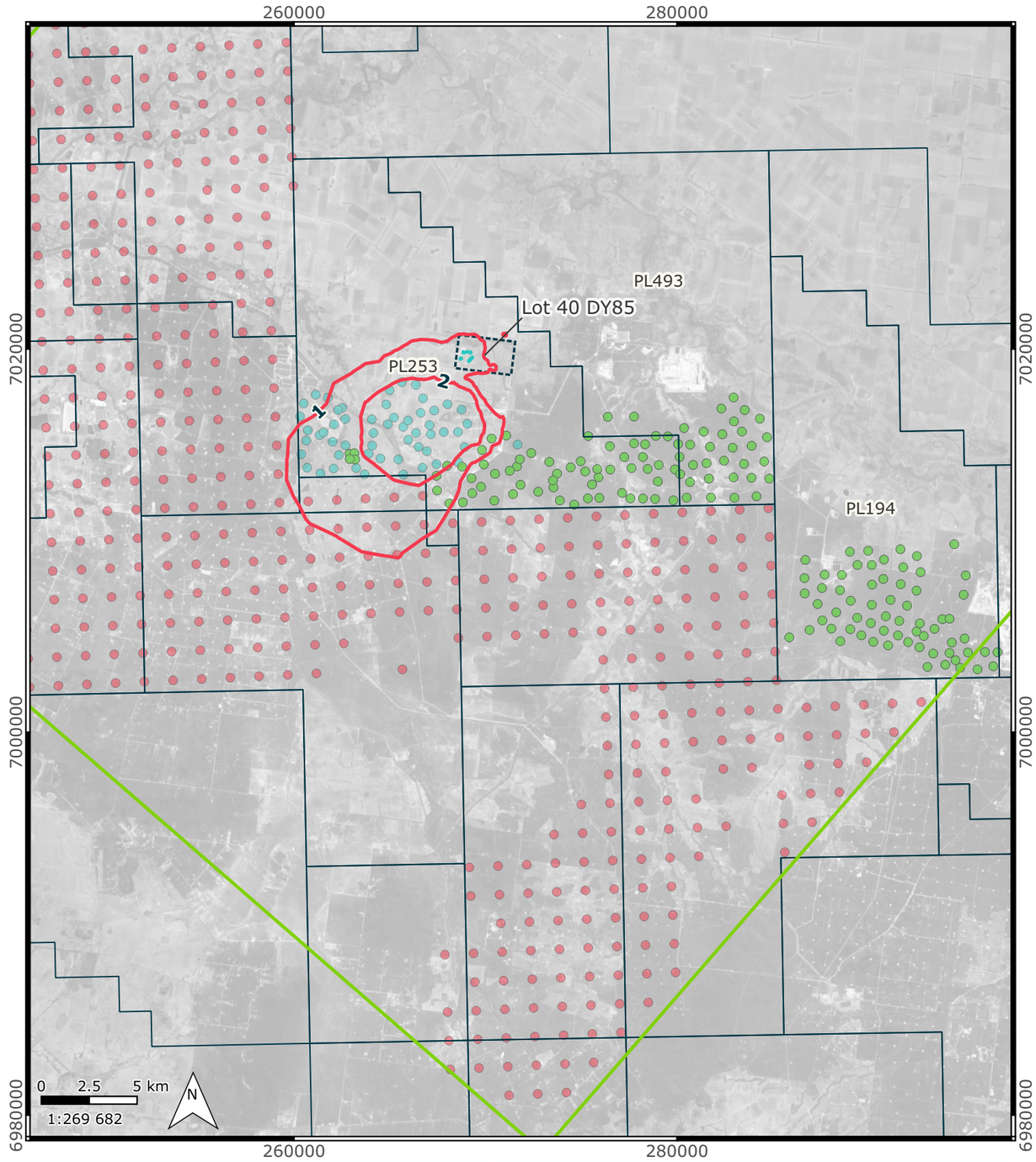
© Worley Pty Ltd While every care is taken to ensure the accuracy of this data, Worley makes no representations or warranties aboutits accuracy, reliability, completeness or suitability for any particular purpose and disclaims all responsibility and all liability (including without limitation liability in negligence) for all expenses, losses, damages (including indirect or consequential damage) and costs which might be incurred as a result of the data being inaccurate or incomplete in any way and for any reason.

worley consulting

Springbok sandstone



Macalister coal seam



Legend

- Groundwater model extent
- Lot 40 DY85
- Gasifiers
- Petroleum Leases

Well groups

- Approved Arrow wells
- Arrow Clynes Rd wells
- Non-Arrow abstraction points (from UWIR 2021)
- Contours of groundwater level difference (m)

Predicted median difference in groundwater levels between scenario 2 and 3 in Springbok sandstone and Macalister coal seam (end of December 2061)

Project No.	Client	Figure No.
411001-00917	Arrow	5-3

Notes:
Project CRS: GDA94 / MGA zone 56
Last Saved: 10:02 20/04/2026
Filename: Figure_5-3_GW_Sc2m3

Exported by User: Mohsen.Azadi
Project Exported: 10:52 20/04/2026

References:
N/A

File Path: C:\modelling\Arrow\deliverables\Figures_REP-HG-002\Figure_5-3_GW_Sc2m3.qgz

© Worley Pty Ltd While every care is taken to ensure the accuracy of this data, Worley makes no representations or warranties aboutits accuracy, reliability, completeness or suitability for any particular purpose and disclaims all responsibility and all liability (including without limitation liability in negligence) for all expenses, losses, damages (including indirect or consequential damage) and costs which might be incurred as a result of the data being inaccurate or incomplete in any way and for any reason.

worley consulting

As discussed in section 2.4.1, historical UCG activities altered local hydraulic gradients within Lot 40 DY85. One of the key QOIs assessed in this study is the incremental change in horizontal hydraulic gradients across the site under the two FDP scenarios. Intera (2025), previously assessed hydraulic gradients using the full extent of Lot 40 DY85.

In the current impact assessment, and in consideration of gasifier locations, regional flow directions, and the need to evaluate the potential for contaminant migration beyond the site boundary, the analysis focused on 1,500 m sections along the southern and western boundaries of Lot 40 DY85 (shown in Figure 5-4). Groundwater level differences were calculated between model cells along these boundary sections and corresponding cells located within a 100 m buffer inside the site boundary. The proportion of boundary cells with higher groundwater levels than interior cells was used as an indicator of groundwater flow direction from locations beyond Lot 40 DY85 toward zones within Lot 40 DY85 (in the vicinity of gasifiers). Comparison of results between scenarios 2 and 3 provides a quantitative basis for assessing the extent to which the proposed Clynes Road wells may influence these hydraulic gradients and associated flow directions.

Summary statistics of predicted horizontal hydraulic gradients toward Lot 40 DY85 along 1,500 m sections of the southern and western boundaries are presented in Table 5-2. The simulation results indicate stronger inward hydraulic gradients in the Springbok sandstone compared to the Macalister coal seam, consistent with the groundwater contour patterns discussed previously. This is considered to reflect potential vertical hydraulic connectivity (near historical UCG activities) between the Springbok sandstone and the underlying Macalister coal seam, together with a downward vertical gradient driven by CSG abstraction within the WCM.

Comparison of summary statistics between the two FDP scenarios indicates that incremental changes in hydraulic gradients across these boundary sections are negligible, with differences generally within 1%. These results suggest that it is unlikely that the proposed Clynes Road wells materially alter regional groundwater flow directions or hydraulic gradients at the boundaries of Lot 40 DY85.

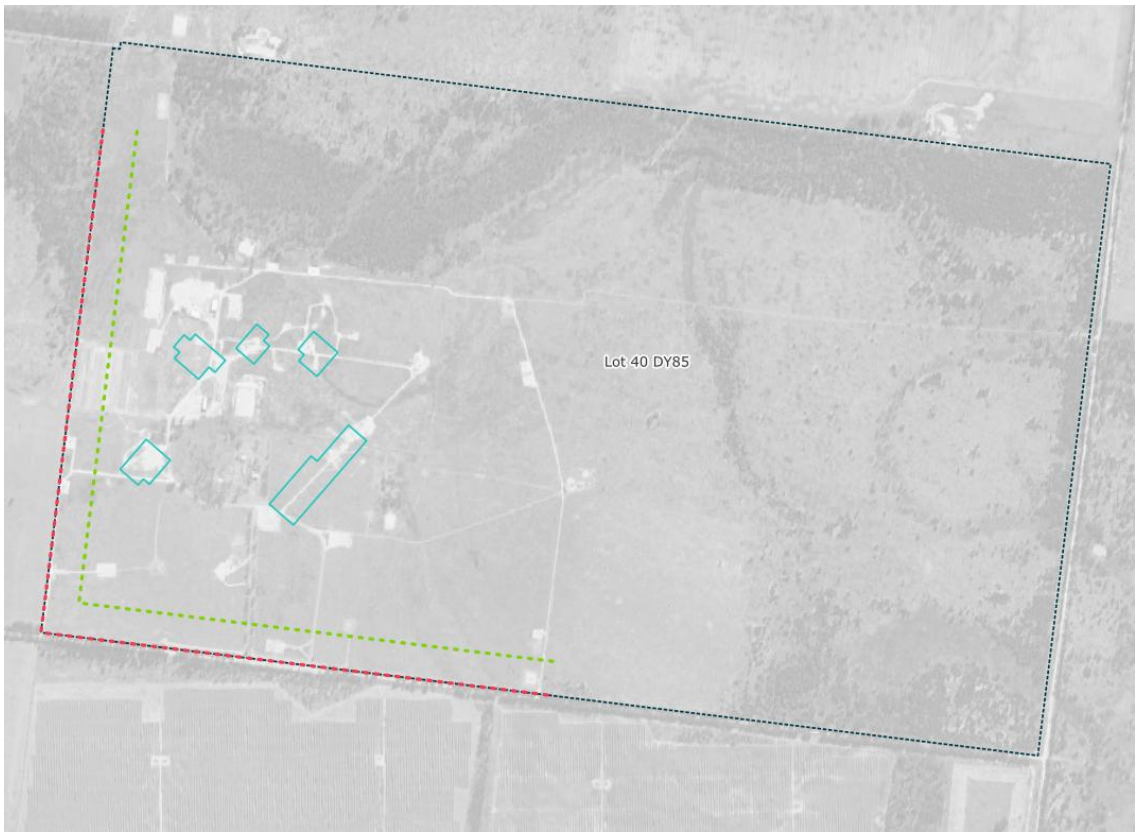


Figure 5-4 Lot 40 DY85 boundary sections (red dashed lines, 1500 m each) and 100 m buffer lines within the boundary (green dashed lines) used for calculation of horizontal hydraulic gradient

Table 5-2 Summary statistics of predicted percentage of cells along 1,500 m sections of the southern and western boundaries with horizontal hydraulic gradients toward Lot 40 DY85

Modelling scenario	Percentile	Springbok sandstone			Macalister coal		
		2025	2040	2061	2025	2040	2061
Scenario 2 (approved)	P5	45%	52%	53%	9%	6%	5%
	P50	74%	75%	78%	20%	13%	13%
	P95	92%	92%	92%	44%	23%	22%
Scenario 3 (Clynes Rd)	P5	45%	52%	52%	9%	5%	6%
	P50	74%	76%	78%	20%	13%	13%
	P95	92%	91%	92%	44%	22%	22%
Predicted impact	P5	<1%	<1%	1%	<1%	1%	-1%
	P50	<1%	-1%	1%	<1%	<1%	<1%
	P95	<1%	1%	<1%	<1%	1%	<1%

5.3 Vertical hydraulic gradient

Assessment of the vertical hydraulic gradient between the Springbok sandstone and the underlying Macalister coal seam was undertaken to confirm the direction of vertical groundwater flow under scenario 3, representing the maximum proposed development. This assessment was intended to evaluate whether vertical gradients are upward or downward under abstraction and recovery conditions. Understanding the direction of vertical flow is important for interpreting potential vertical migration pathways under a conservative development scenario.

The assessment was carried out using 10 pairs of monitoring locations where groundwater level monitoring data was available in both the Springbok sandstone and the Macalister coal seam. For each pair, the groundwater level difference between the two formations was calculated across the ensemble of model realisations. Positive and negative values indicate the direction of the vertical hydraulic gradient, to evaluate whether groundwater flow is directed downward from the Springbok sandstone to the Macalister coal seam (for positive values), or upward in the opposite direction (for negative values).

As shown in Figure 5-5, the predicted groundwater level differences under scenario 3 are positive from 2026 through to 2226, indicating a continuous downward vertical hydraulic gradient from the Springbok sandstone to the Macalister coal seam. This is consistent across all realisations and through both the abstraction and recovery periods.

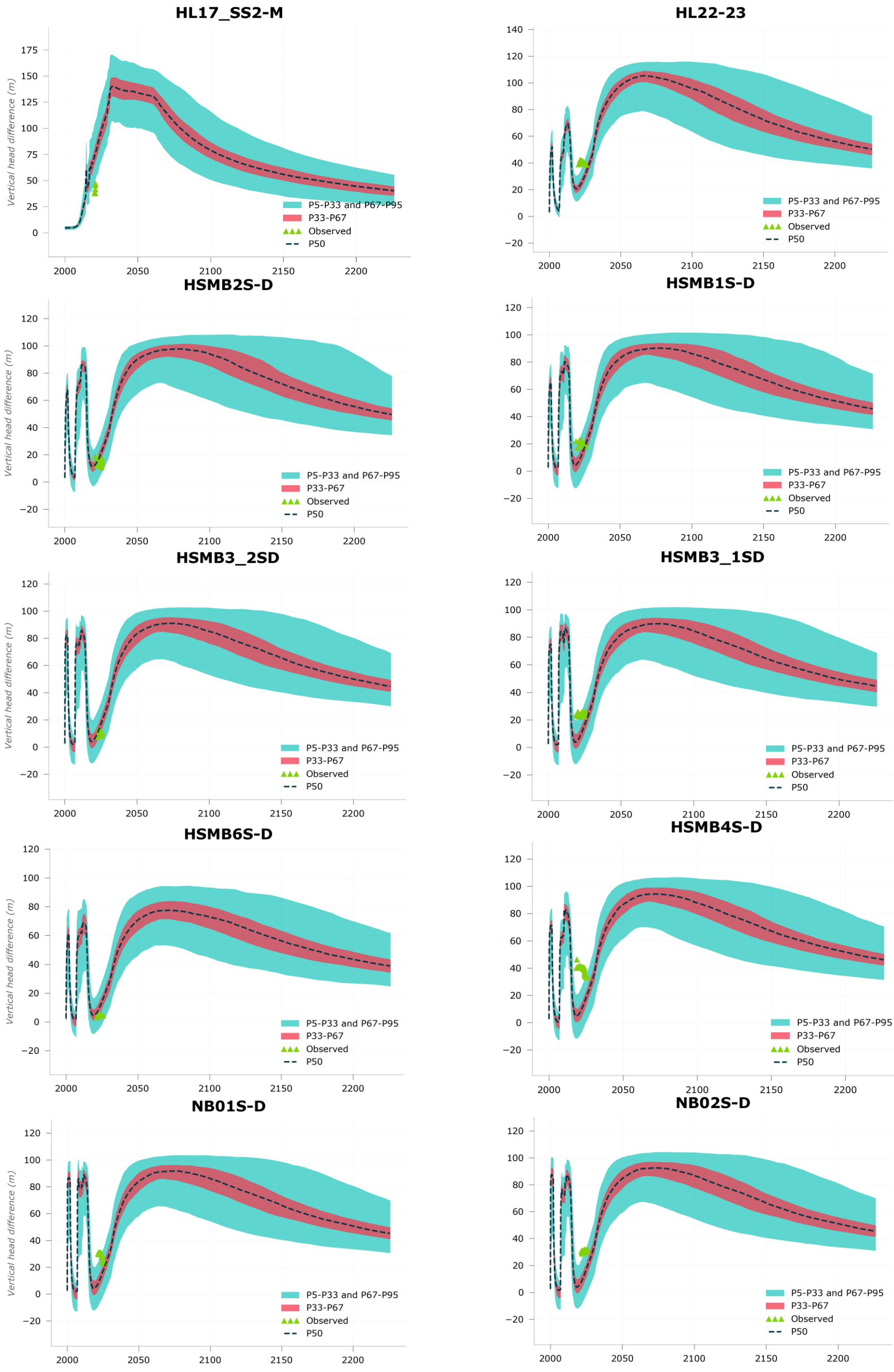


Figure 5-5 Predicted vertical hydraulic gradient between the Springbok sandstone and Macalister coal seam at paired monitoring locations

5.4 Particle tracking

Particle tracking was undertaken as a conservative approach to assess the maximum potential extent of contaminant movement under simulated groundwater flow conditions. Unlike solute transport modelling, particle tracking does not account for attenuation processes such as sorption, degradation, or dilution, and therefore represents an upper-bound estimate of advective contaminant migration. Particles were released in 2019 from the following locations:

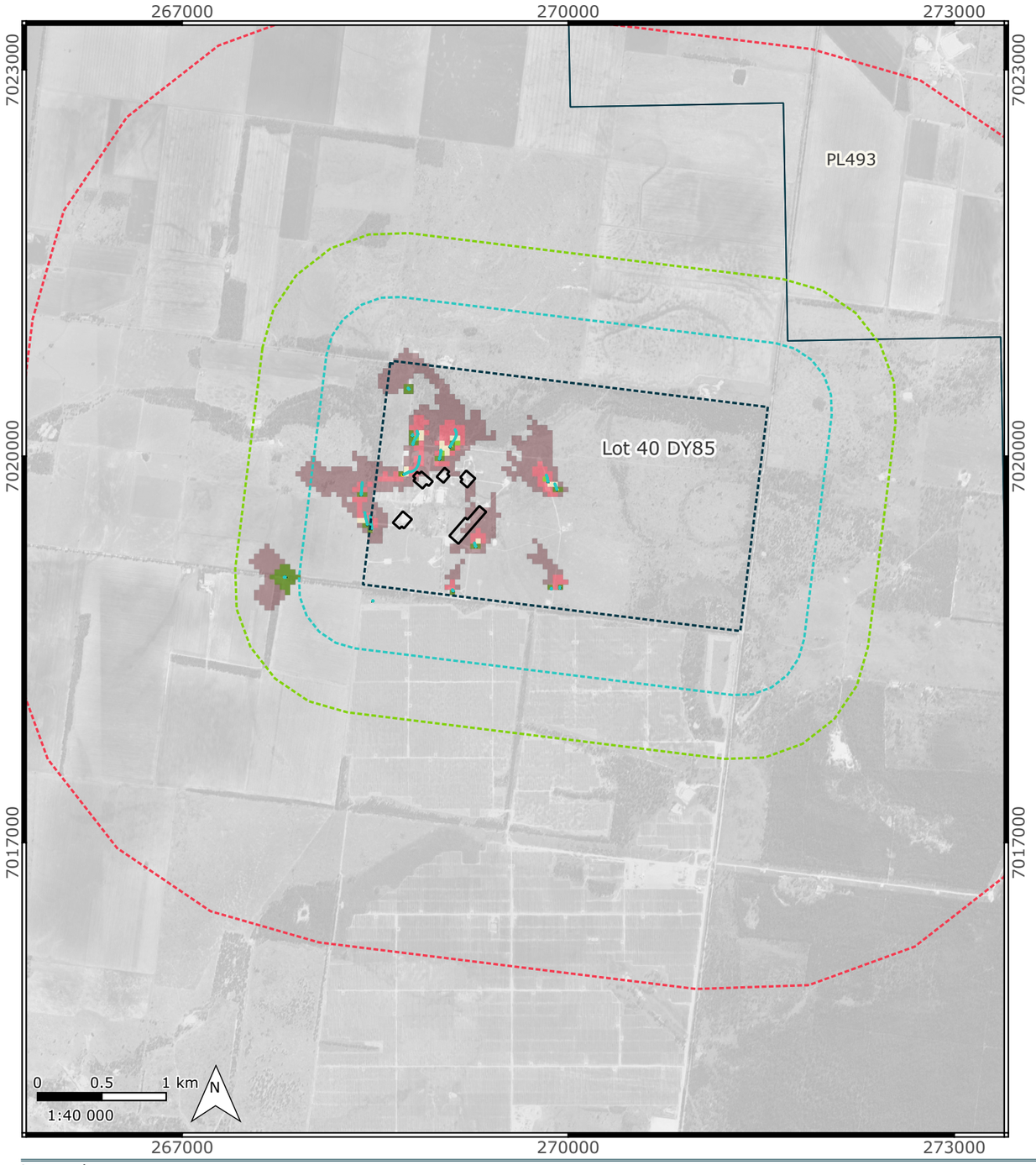
- Monitoring bores,
- Gasifier locations, and
- Lot 40 DY85 boundaries.

Particle movement was simulated under transient conditions from January 2019 through to the end of December 2225 for both scenario 2 and scenario 3.

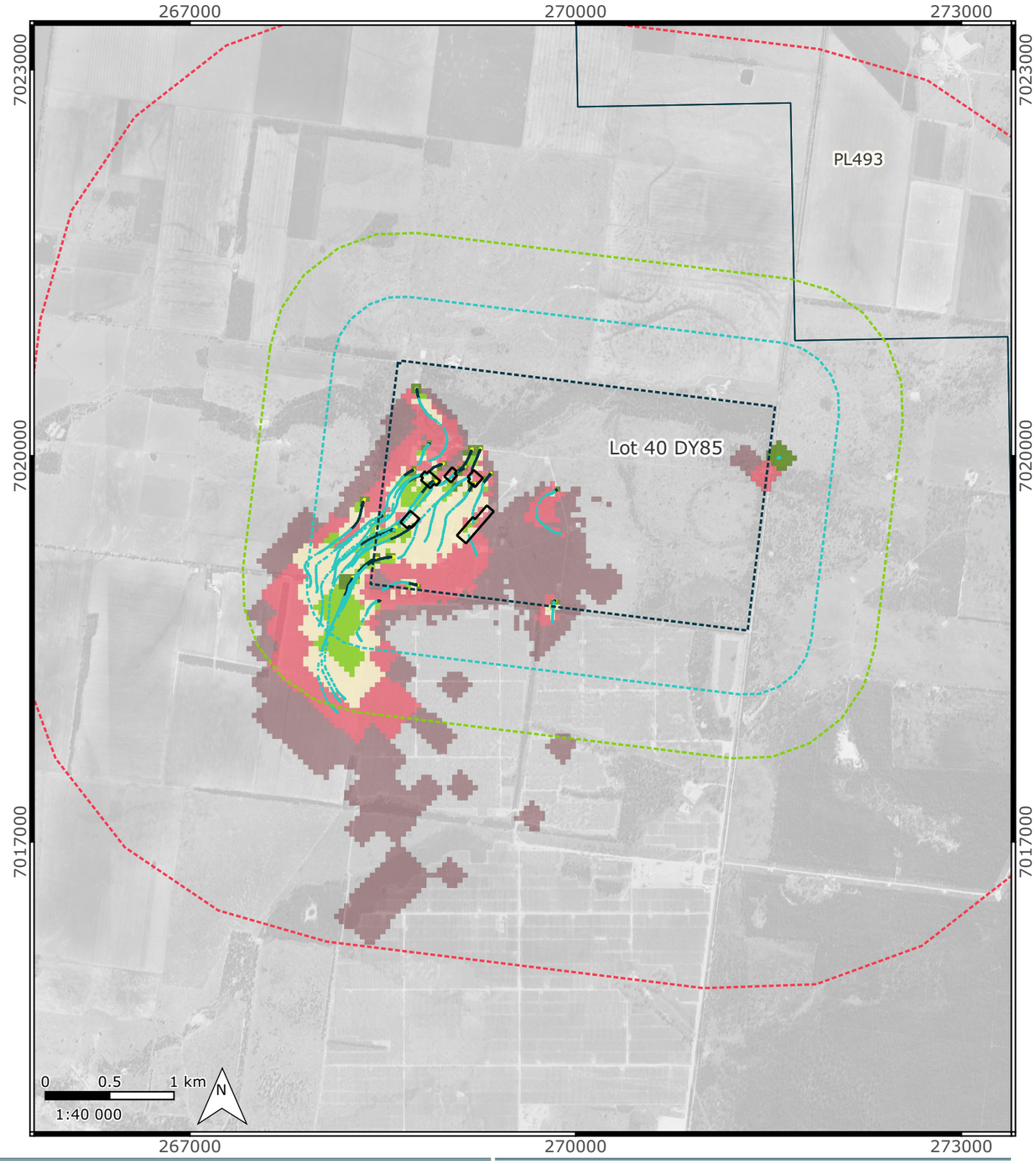
For scenario 3, the probability of particle pathlines intersecting each model cell within the Springbok sandstone and Macalister coal seam is presented in Figure 5-6 to Figure 5-8, for particles released from monitoring bores, gasifier locations, and the Lot 40 DY85 boundaries. These figures also show representative particle pathlines extracted from the realisation simulating the maximum particle displacement for particles released at gasifier locations within the Springbok sandstone. The results indicate that:

- Particles released in the Springbok sandstone generally travel shorter distances than those released in the Macalister coal seam, reflecting lower hydraulic conductivity, reduced transmissivity, and weaker advective flow conditions in the Springbok Sandstone compared to the more transmissive and regionally depressurised Macalister coal seam.
- Groundwater flow within the Macalister coal seam is predominantly directed toward the south-southwest, consistent with regional groundwater flow patterns, whereas flow directions within the Springbok sandstone vary at a more localised scale and are mostly directed inward toward Lot 40 DY85, reflecting the influence of historical depressurisation associated with former UCG activities.
- It is very unlikely (probability of less than 5%) that, by the end of the recovery period in 2225, particles released at or near the gasifier locations will travel beyond:
  - Lot 40 DY85 boundary within the Springbok sandstone, and
  - Approximately 1,250 m beyond the Lot 40 DY85 boundary within the Macalister coal seam.
- Most particle movement occurs during the post-abstraction recovery period (year 2062 to 2225), reflecting longer travel times associated with this phase of the simulation. Given the considerable natural attenuation of contaminants observed in groundwater monitoring data (discussed in section 2.4.2), by the year 2062 these predictions represent a conservative estimate of the likelihood and extent of contaminant movement from Lot 40 DY85.

Springbok sandstone



Macalister coal seam



Legend

- Groundwater model extent
- Lot 40 DY85
- Gasifiers
- Petroleum Leases

Lot 40 DY85 buffer zones:

- 500 m
- 1000 m
- 2800 m

Particle travel period:

- 2019-2025
- 2026-2061
- 2062-2225

Pathline probability

- Very unlikely (<5%)
- Unlikely (5-33%)
- As likely as not (33-67%)
- Likely (67-95%)
- Very likely (>95%)

Probability of particle tracking pathlines in Springbok sandstone and Macalister coal seam for scenario 3 (particles released at monitoring bores)

Project No.	Client	Figure No.
411001-00917	Arrow	5-6

Notes:
Project CRS: GDA94 / MGA zone 56
Last Saved: 16:53 28/04/2026
Filename: Figure_5-6_PT_probability_bores

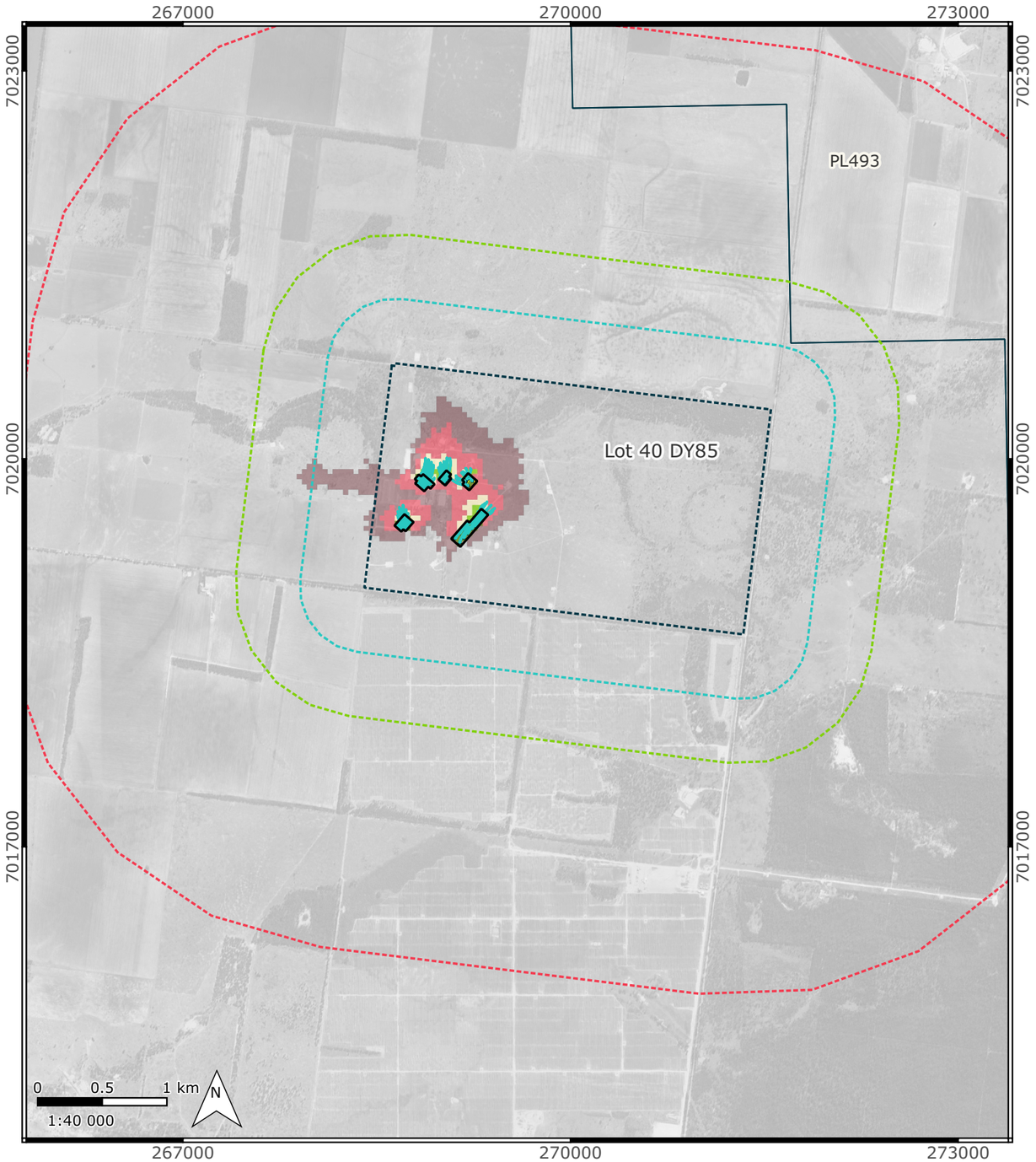
Exported by User: Mohsen.Azadi
Project Exported: 16:54 28/04/2026

References:
N/A

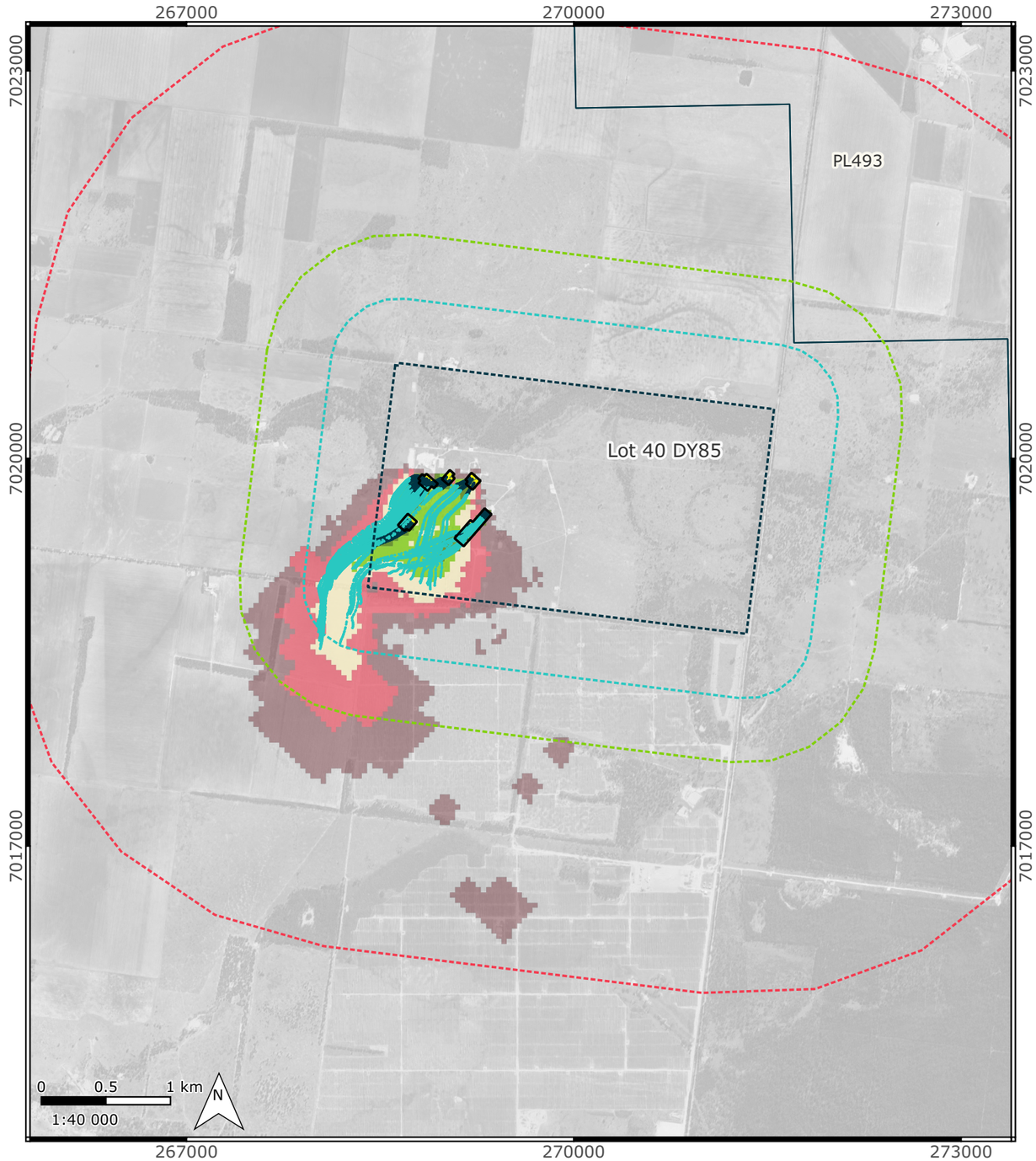
File Path: C:\modelling\Arrow\deliverables\Figures_REP-HG-002\Figure_5-6_PT_probability_bores.qgz

© Worley Pty Ltd While every care is taken to ensure the accuracy of this data, Worley makes no representations or warranties aboutits accuracy, reliability, completeness or suitability for any particular purpose and disclaims all responsibility and all liability (including without limitation liability in negligence) for all expenses, losses, damages (including indirect or consequential damage) and costs which might be incurred as a result of the data being inaccurate or incomplete in any way and for any reason.

Springbok sandstone



Macalister coal seam



Legend

- Groundwater model extent
- Lot 40 DY85
- Gasifiers
- Petroleum Leases

Lot 40 DY85 buffer zones:

- 500 m
- 1000 m
- 2800 m

Particle travel period:

- 2019-2025
- 2026-2061
- 2062-2225

Pathline probability

- Very unlikely (<5%)
- Unlikely (5-33%)
- As likely as not (33-67%)
- Likely (67-95%)
- Very likely (>95%)

Probability of particle tracking pathlines in Springbok sandstone and Macalister coal seam for scenario 3 (particles released at gasifiers)

Project No.	Client	Figure No.
411001-00917	Arrow	5-7

Notes:
Project CRS: GDA94 / MGA zone 56
Last Saved: 16:55 28/04/2026
Filename: Figure_5-6_PT_probability_bores

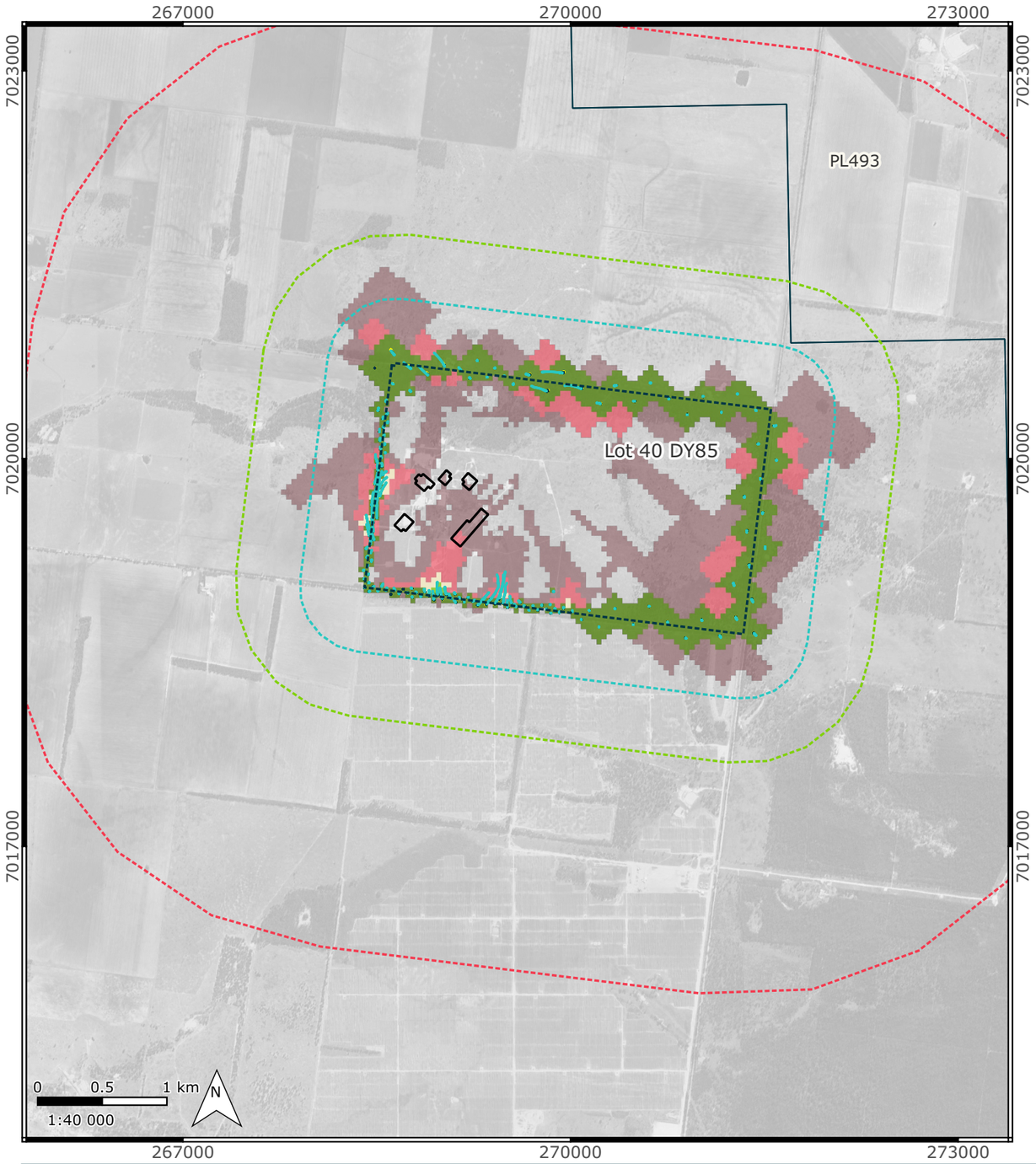
Exported by User: Mohsen.Azadi
Project Exported: 17:04 28/04/2026

References:
N/A

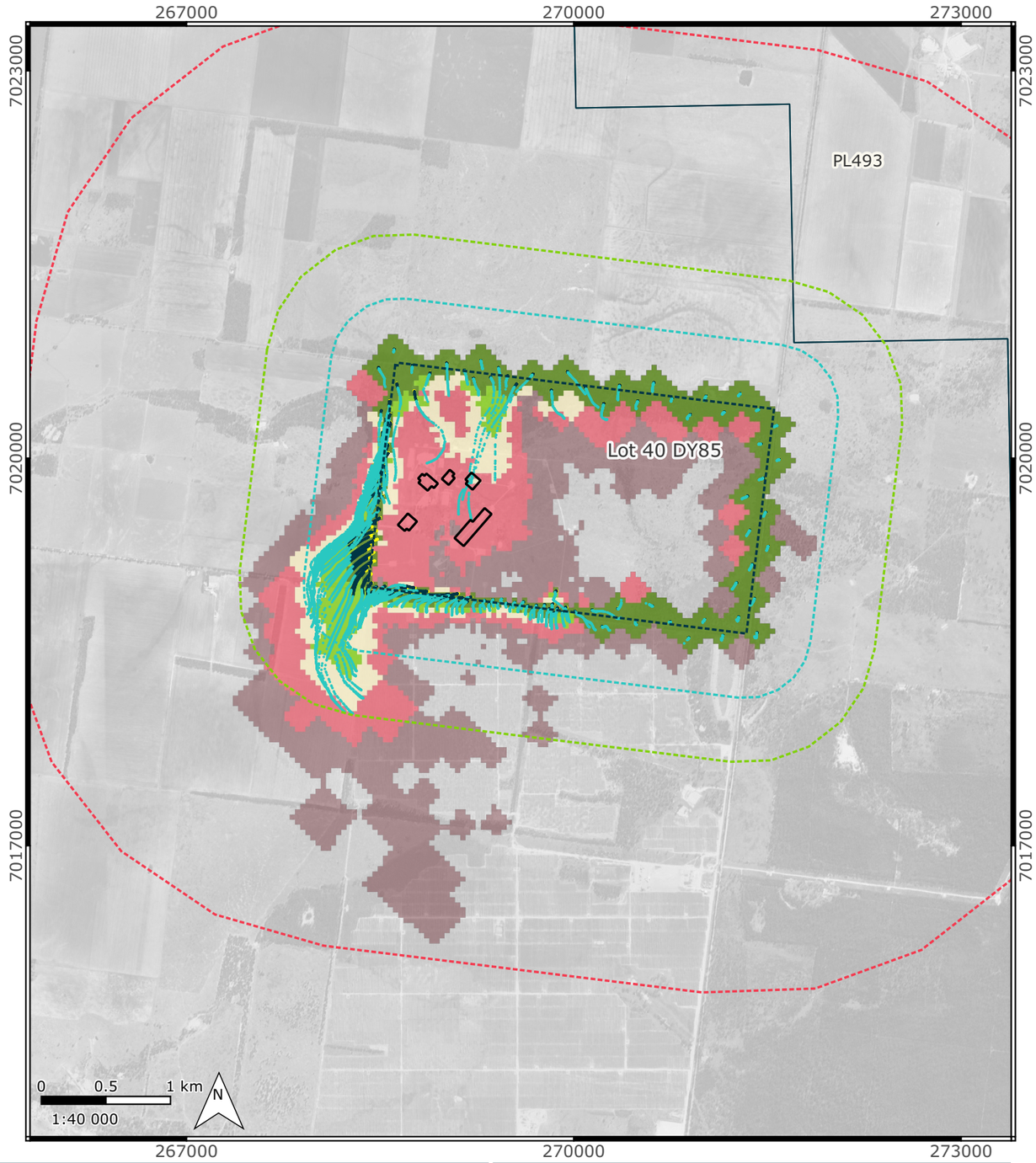
File Path: C:\modelling\Arrow\deliverables\Figures_REP-HG-002\Figure_5-6_PT_probability_bores.qgz

© Worley Pty Ltd While every care is taken to ensure the accuracy of this data, Worley makes no representations or warranties aboutits accuracy, reliability, completeness or suitability for any particular purpose and disclaims all responsibility and all liability (including without limitation liability in negligence) for all expenses, losses, damages (including indirect or consequential damage) and costs which might be incurred as a result of the data being inaccurate or incomplete in any way and for any reason.

Springbok sandstone



Macalister coal seam



Legend

- Groundwater model extent
- Lot 40 DY85
- Gasifiers
- Petroleum Leases

Lot 40 DY85 buffer zones:
- 500 m
- 1000 m
- 2800 m

Particle travel period:
- 2019-2025
- 2026-2061
- 2062-2225

Pathline probability
- Very unlikely (<5%)
- Unlikely (5-33%)
- As likely as not (33-67%)
- Likely (67-95%)
- Very likely (>95%)

Probability of particle tracking pathlines in Springbok sandstone and Macalister coal seam for scenario 3 (particles released at Lot 40 DY85 boundaries)

Project No.	Client	Figure No.
411001-00917	Arrow	5-8

Notes:
Project CRS: GDA94 / MGA zone 56
Last Saved: 17:05 28/04/2026
Filename: Figure_5-6_PT_probability_bores

Exported by User: Mohsen.Azadi
Project Exported: 17:12 28/04/2026

References:
N/A

File Path: C:\modelling\Arrow\deliverables\Figures_REP-HG-002\Figure_5-6_PT_probability_bores.qgz

© Worley Pty Ltd While every care is taken to ensure the accuracy of this data, Worley makes no representations or warranties aboutits accuracy, reliability, completeness or suitability for any particular purpose and disclaims all responsibility and all liability (including without limitation liability in negligence) for all expenses, losses, damages (including indirect or consequential damage) and costs which might be incurred as a result of the data being inaccurate or incomplete in any way and for any reason.

worley consulting

To assess the potential influence of the proposed Clynes Road wells, particle travel distances were compared across the ensemble of model realisations for scenario 2 (approved development) and scenario 3 (approved plus proposed wells). The assessment focused on differences in particle travel distances (simulated to the end of the recovery period) to evaluate whether abstraction from the proposed wells materially modifies advective transport behaviour of the residual contaminants in Lot 40 DY85. This scenario-based comparison allows the potential effect of the Clynes Road wells on maximum contaminant migration to be evaluated independently of attenuation processes, while accounting for parameter uncertainty.

Summary statistics of particle travel distances (from 2019 to 2225) for particles released within the Springbok sandstone and Macalister coal seam under scenario 2, scenario 3, and their incremental differences are presented in Table 5-3. The particle tracking predictions indicate that, by the end of the recovery period in 2225:

- Particle travel distances are consistently greater within the Macalister coal seam than within the Springbok Sandstone, as discussed previously.
- For the ensemble median results:
  - A maximum particle travel distance of approximately 139 m was predicted within the Springbok sandstone,
  - A maximum particle travel distance of approximately 1,092 m was predicted within the Macalister coal seam,
  - A maximum incremental particle travel distance increase of approximately 2 m was predicted in the Springbok sandstone associated with the proposed Clynes Road wells, and
  - A maximum incremental particle travel distance increase of approximately 55 m was predicted in the Macalister coal seam associated with the proposed Clynes Road wells.
- It is very unlikely (based on P95 percentile results) that addition of the proposed Clynes Road wells would result in an increase in particle travel distance exceeding of approximately 24 m in the Springbok sandstone and 92 m in the Macalister coal seam.

Table 5-3 Summary statistics of particle travel distances (from 2019 and 2225) for particles released within Springbok sandstone and Macalister coal seam

Modelling scenario	Layer	Particle location	P5			P50			P95		
			Min	Mean	Max	Min	Mean	Max	Min	Mean	Max
Scenario 2 (approved)	Springbok	Bores	<1	6	24	1	38	103	7	191	910
		Gasifiers	4	15	28	27	80	138	132	280	407
		Boundaries	<1	3	42	<1	18	112	7	114	676
	Macalister	Bores	7	216	526	41	625	963	125	1369	1862
		Gasifiers	99	313	500	516	718	848	1000	1531	1826
		Boundaries	2	72	302	10	288	1038	40	760	1797
Scenario 3 (Clynes Rd)	Springbok	Bores	<1	6	24	1	39	105	7	194	934
		Gasifiers	4	15	28	27	81	139	134	282	409
		Boundaries	<1	3	42	<1	18	112	7	115	682
	Macalister	Bores	8	224	523	41	652	973	126	1419	1943
		Gasifiers	132	321	504	544	749	892	1092	1606	1876
		Boundaries	3	76	336	11	304	1092	46	783	1834
Predicted impacted	Springbok	Bores	<1	<1	<1	<1	<1	2	<1	3	24
		Gasifiers	<1	<1	<1	<1	1	1	2	3	2
		Boundaries	<1	<1	1	<1	<1	1	<1	1	5
	Macalister	Bores	1	8	-3	<1	27	9	1	50	81
		Gasifiers	33	9	4	28	31	45	92	76	50
		Boundaries	<1	4	35	<1	16	55	6	22	37

5.5 Contaminant transport and fate

The contaminant transport and fate were evaluated based on long-term evolution of benzene and naphthalene concentrations under simulated groundwater flow, source depletion, and natural attenuation processes (discussed in section 3.3). Predictions are based on the ensemble of calibrated model realisations and are interpreted using percentile statistics (P5, P50, and P95) to characterise uncertainty and provide a risk-based assessment of contaminant attenuation and migration within the Springbok sandstone and Macalister coal seam. The assessment focuses on concentration trends at monitoring locations, the timing of concentration depletion below LOR, and the spatial distribution of residual concentrations.

Ensemble predictions indicate a consistent decline in benzene and naphthalene concentrations at monitoring locations across both formations, reflecting the combined effects of source dilution and natural attenuation (shown in Appendices F and G). For benzene, concentration trends show progressive reductions over time, with variability between monitoring locations diminishing as source contributions decrease. Naphthalene concentrations decline more rapidly across the ensemble, consistent with its lower source strength and stronger attenuation characteristics. Overall, the ensemble results demonstrate convergence toward declining concentrations at monitoring bores.

The year in which contaminant concentrations are predicted to decline below the LOR was evaluated across the ensemble of model realisations for both HSUs and contaminants, as summarised in in Table 5-4. Ensemble results indicate that the median (P50) predictions are as follows:

- Benzene concentrations are predicted to fall below the LOR in:
  - 2049 for the Springbok sandstone, and
  - 2035 for the Macalister coal seam.
- Naphthalene concentrations are predicted to fall below the LOR in:
  - January 2027 for the Springbok sandstone, and
  - April 2024 for the Macalister coal seam.

Upper-bound ensemble predictions (P95) further indicate that it is very unlikely that the year of depletion below the LOR will exceed the following:

- For benzene:
  - 2053 for the Springbok sandstone, and
  - 2042 for the Macalister coal seam.
- For naphthalene:
  - 2037 for the Springbok sandstone, and
  - June 2024 for the Macalister coal seam, consistent with current groundwater monitoring observations.

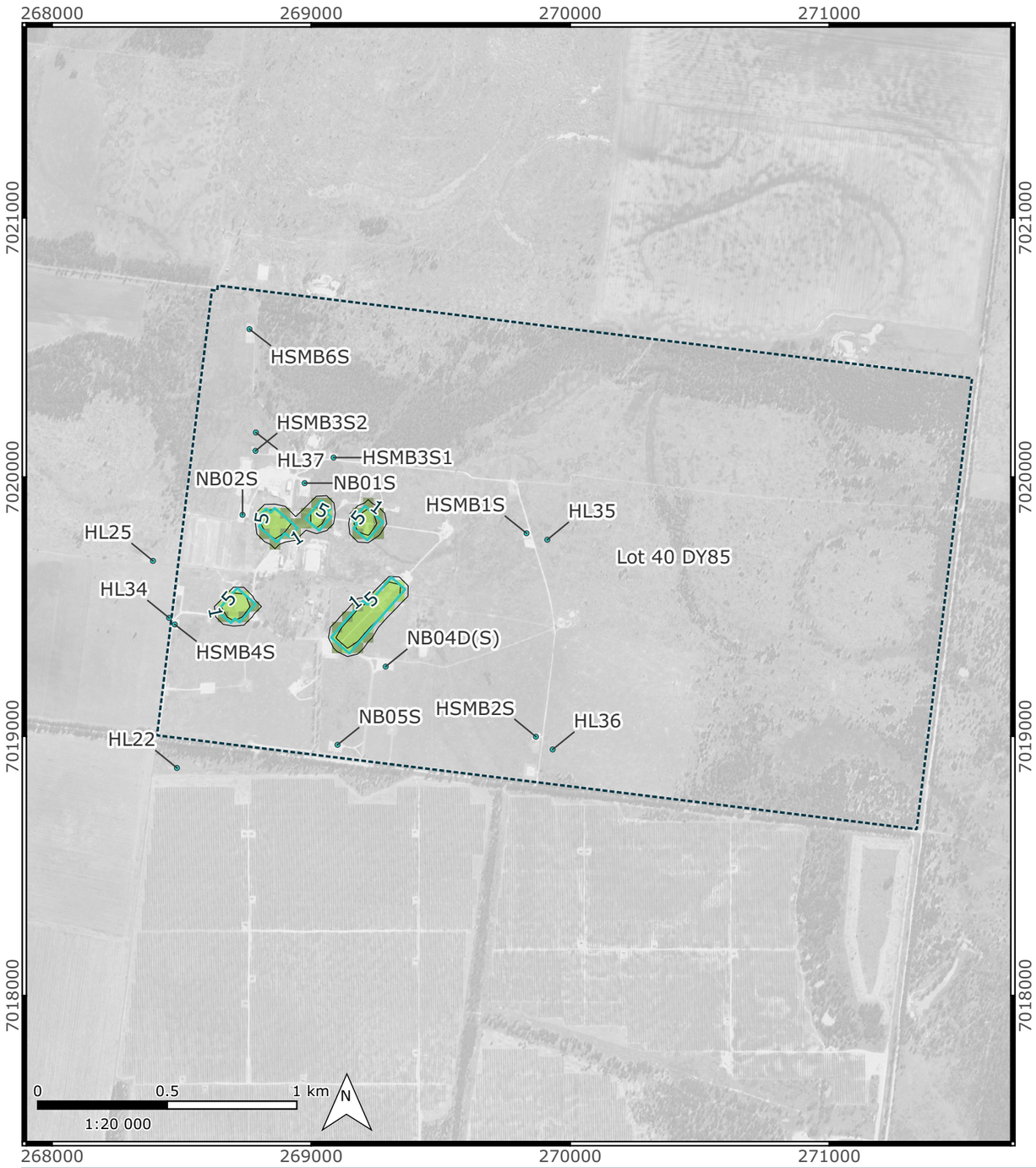
Comparison of predicted depletion timing between scenarios 2 and 3 indicates no change in the year at which concentrations are predicted to fall below the LOR for either contaminant or formation. This outcome indicates that inclusion of the proposed Clynes Road wells is not expected to materially influence natural attenuation or long-term depletion of benzene or naphthalene concentrations.

Based on the ensemble depletion timing, median (P50) benzene concentration distributions were examined for future years, including year 2030 in the Macalister coal seam and year 2040 in the Springbok sandstone (Figure 5-9). These years were chosen based on the median years discussed above to better understand the plume distribution before reaching below LOR. The benzene distribution in the final years before reaching below the LOR are predominantly present within or near gasifier releasing source depletion term. This also indicates that removal of the source terms will likely result in earlier timing when the contaminants concentrations reach below the LOR.

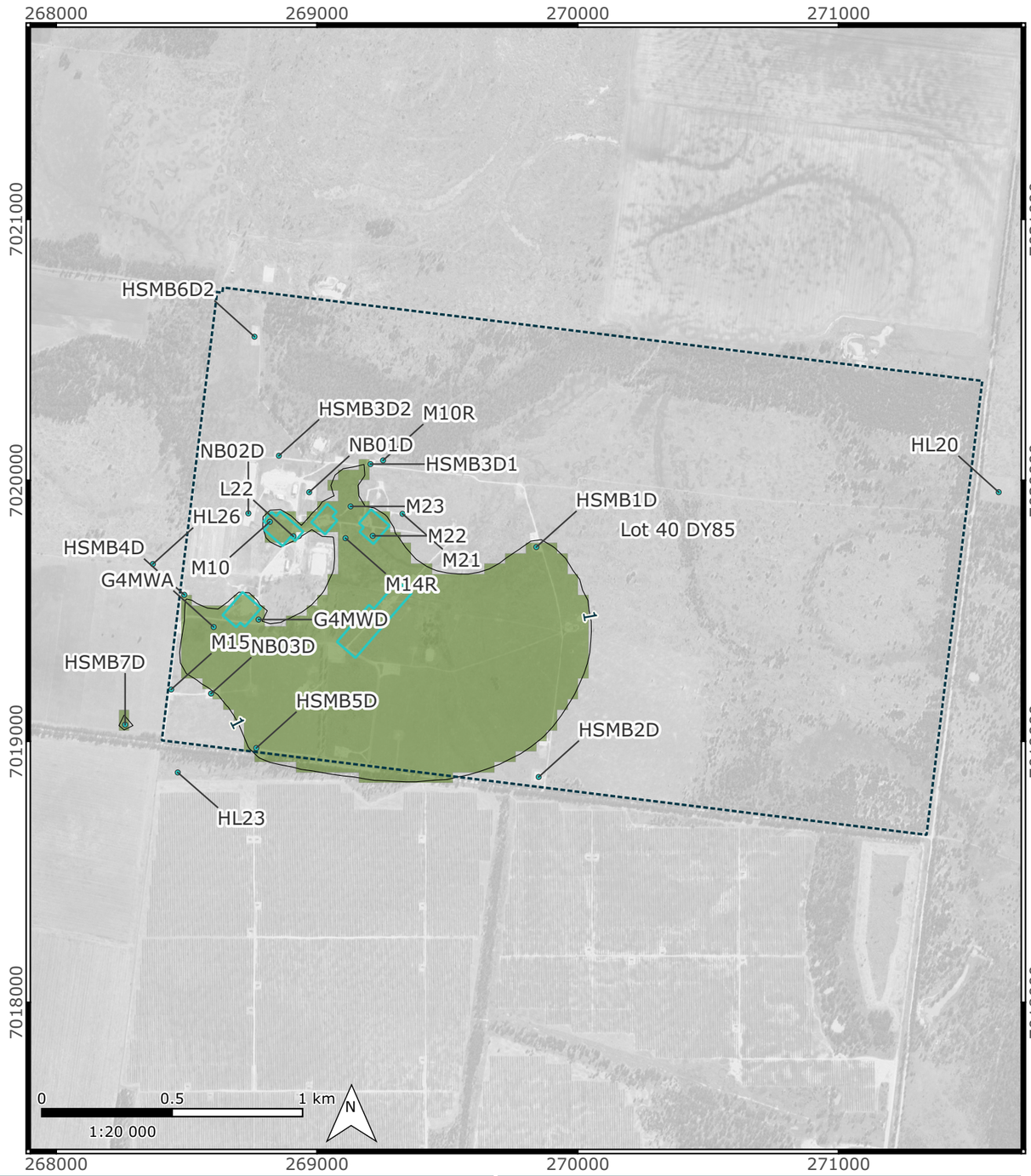
Table 5-4 Predicted year of contaminant concentration reaching below the LOR

Modelling scenario	Compound	Springbok sandstone			Macalister coal		
		P5	P50	P95	P5	P50	P95
Scenario 2 (approved)	Benzene	Jan 2049	Jan 2049	Jan 2053	Jan 2033	Jan 2035	Jan 2042
	Naphthalene	Jan 2026	Jan 2027	Jan 2037	Jan 2024	Apr 2024	Jun 2024
Scenario 3 (Clynes Rd)	Benzene	Jan 2049	Jan 2049	Jan 2053	Jan 2033	Jan 2035	Jan 2042
	Naphthalene	Jan 2026	Jan 2027	Jan 2037	Jan 2024	Apr 2024	Jun 2024

Springbok sandstone (end of 2040)



Macalister coal seam (end of 2030)



Legend

- Lot 40 DY85
- Gasifier
- Monitoring bores

Concentration (ug/L)

- 1 - 5
- 5 - 10
- 10 - 50
- 50 - 100
- 100 - 500
- 500 - 1000
- 1000 - 5000

Predicted median benzene concentrations in the Springbok sandstone (end of December 2040) and Macalister coal seam (end of December 2030)

Project No.	Client	Figure No.
411001-00917	Arrow	5-9

Notes:
Project CRS: GDA94 / MGA zone 56
Last Saved: 17:36 21/04/2026
Filename: Figure_5-9_benzene_pred

Exported by User: Mohsen.Azadi
Project Exported: 17:48 21/04/2026

References:
N/A

File Path: C:\modelling\Arrow\deliverables\Figures_REP-HG-002\Figure_5-9_benzene_pred.qgz

© Worley Pty Ltd While every care is taken to ensure the accuracy of this data, Worley makes no representations or warranties aboutits accuracy, reliability, completeness or suitability for any particular purpose and disclaims all responsibility and all liability (including without limitation liability in negligence) for all expenses, losses, damages (including indirect or consequential damage) and costs which might be incurred as a result of the data being inaccurate or incomplete in any way and for any reason.

5.6 Impact assessment

This impact assessment evaluates the incremental effects of the proposed Clynes Road wells (scenario 3) relative to the currently approved FDP (scenario 2) on groundwater flow, hydraulic gradients, contaminant transport and fate within the Springbok sandstone and Macalister coal seam. The assessment is based on the predictive ensemble modelling results presented in sections 5.2 to 5.5, using uncertainty analysis results (for P5, P50, and P95 percentiles) to provide a conservative, risk-based assessment.

Groundwater levels and flow directions

Predictive groundwater level simulations indicate that cumulative abstraction under both scenarios results in drawdown centered on abstraction areas, with groundwater flow directed predominantly toward the south to southwest at the regional scale. At the end of 2025, groundwater flow shows inward gradients toward Lot 40 DY85 in the Springbok sandstone, while flow in the Macalister coal seam converges toward the gasifiers and continues toward the southwest of the site.

Comparison of median groundwater levels between scenarios 2 and 3 demonstrates that the incremental drawdown attributable to the proposed Clynes Road wells is small and spatially limited. At the end of the abstraction period (2061), predicted median differences are generally less than 1 m, with a localised zone of approximately 1–2 m difference in the Macalister coal seam near the proposed wells. By the end of the recovery period (2225), differences in median groundwater levels between scenarios are less than 1 m across both formations, indicating that inclusion of the Clynes Road wells is not expected to result in a material change to long-term groundwater level recovery relative to the approved development.

Assessment of horizontal hydraulic gradients across 1,500 m sections of the southern and western boundaries of Lot 40 DY85 shows stronger inward gradients in the Springbok sandstone compared to partially-inward gradients in the Macalister coal seam. Comparison between scenarios indicates that incremental changes in these gradients are negligible, with differences generally within ±1% across all percentiles. These results demonstrate that it is unlikely that the proposed Clynes Road wells will materially alter regional or site-scale groundwater flow directions relevant to contaminant migration beyond Lot 40 DY85.

Vertical hydraulic gradient

Evaluation of vertical hydraulic gradients between the Springbok sandstone and the Macalister coal seam was undertaken under scenario 3 to confirm the direction of vertical groundwater flow under the maximum proposed development. Analysis of groundwater level differences at 10 pairs of monitoring locations indicates continuous positive head differences from 2026 through to 2225, corresponding to a constant downward vertical gradient from the Springbok sandstone into the Macalister coal seam.

This outcome is consistent across the ensemble and throughout both abstraction and recovery phases, indicating that vertical groundwater flow remains directed downward under scenario 3. These results predict that the proposed Clynes Road wells do not cause upward vertical flow from the Macalister coal seam into the overlying Springbok sandstone, supporting a very low likelihood of upward contaminant migration under the maximum development scenario.

Particle tracking – conservative assessment of contaminants

Particle tracking was undertaken as a conservative assessment of maximum potential contaminant movement, independent of attenuation processes such as sorption, degradation, and dilution. Comparison of ensemble particle travel distances between scenarios 2 and 3 provides a measure of the incremental impact of the proposed Clynes Road wells on potential migration pathways.

Results indicate that particle travel distances are consistently greater in the Macalister coal seam than in the Springbok sandstone, reflecting higher formation transmissivity and CSG abstraction within WCM. For ensemble median (P50) results, maximum particle travel distances of approximately 139 m were predicted in the Springbok sandstone and approximately 1,092 m in the Macalister coal seam. The incremental impact associated with the proposed Clynes Road wells is small, with maximum increases in median particle travel distance of approximately 2 m in the Springbok sandstone and approximately 55 m in the Macalister coal seam.

Upper-bound (P95) results further indicate that it is very unlikely that inclusion of the proposed Clynes Road wells would result in an increase in particle travel distance exceeding of approximately 24 m in the Springbok sandstone or approximately 92 m in the Macalister coal seam. These incremental changes are small relative to overall travel distances (between 2019 and 2225) and do not materially change particle migration pathways beyond those predicted under the approved scenario.

Contaminant transport and fate

Contaminant transport modelling indicates continued long-term decline in benzene and naphthalene concentrations across both formations due to dilution and natural attenuation. Ensemble results show consistent depletion trends at monitoring locations, with naphthalene attenuating more rapidly than benzene and reaching below the laboratory limit of reporting (LOR) earlier across all percentiles.

Predicted depletion timing indicates that, at the ensemble median (P50), benzene concentrations fall below the LOR by approximately 2049 in the Springbok sandstone and approximately 2035 in the Macalister coal seam, while naphthalene concentrations fall below the LOR by approximately January 2027 and April 2024, respectively. Upper-bound (P95) predictions indicate that it is very unlikely for benzene depletion to extend beyond approximately 2053 for Springbok sandstone or 2042 for Macalister coal seam, and for naphthalene beyond approximately 2037 and mid-2024, respectively.

Comparison of depletion timing between scenarios 2 and 3 indicates no change in predicted years at which concentrations fall below the LOR for either contaminant or formation. This outcome indicates that inclusion of the proposed Clynes Road wells is not expected to materially influence natural attenuation or long-term depletion of benzene or naphthalene concentrations.

Overall impact assessment

Collectively, results from groundwater level predictions, hydraulic gradient assessments, particle tracking, and contaminant transport modelling demonstrate that the proposed Clynes

Road wells (scenario 3) result in minor localised incremental changes relative to the approved development (scenario 2). No material changes are predicted in groundwater flow directions, vertical gradients, contaminant migration, or contaminant depletion timing. The assessment indicates that the proposed development is unlikely to increase the risk of off-site contaminant migration or compromise long-term groundwater recovery and containment of residual contamination associated with the former Hopeland UCG site.

6. Conclusions and recommendations

This groundwater impact assessment presents the results of an updated numerical groundwater flow and contaminant transport modelling study undertaken to support Arrow Energy's proposed Field Development Plan (FDP) for Clynes Road (scenario 3) within PL253. The study builds on a sequence of previous investigations and modelling studies (AGE, 2021; AGE, 2023; Intera, 2024; Intera, 2025), incorporating updated monitoring data, revised conceptual model and hydrostratigraphic interpretation, and improved representation of boundary conditions and modelling assumptions The modelling has been undertaken in accordance with Environmental Authority EA0001401, OGIA (2021a) regional groundwater modelling approach, Australian Groundwater Modelling Guidelines (Barnett et al., 2012), and using the risk-based terminology outlined in Peeters & Middlemis (2023) with a focus on groundwater flow behaviour, contaminant migration, uncertainty analysis, and long term recovery associated with the former Hopeland UCG site on Lot 40 DY85.

Hydrogeological conceptualisation of the PL253 area and the former Hopeland UCG site was updated building upon, and refining, the conceptual understanding established in earlier studies (including AGE and Intera investigations). The updated conceptualisation incorporates the latest groundwater level and groundwater quality monitoring data, revised hydrostratigraphic interpretation, and updated regional groundwater incorporation to better represent current groundwater conditions. The Springbok sandstone and the Walloon Coal Measures (WCM), particularly the Macalister coal seam, remain the key hydrostratigraphic units governing groundwater flow and contaminant behaviour, with monitoring data confirming persistent downward vertical hydraulic gradients from the Springbok sandstone toward the WCM. Updated groundwater level and quality datasets indicate that residual effects of historical UCG activities remain localised within Lot 40 DY85, with declining benzene and naphthalene concentrations. Regionally, groundwater flow is expected to be directed predominantly toward the south to southwest, consistent with OGIA (2021) conceptualisation, while local scale variability reflects historical UCG depressurisation and formation heterogeneity near gasifier locations.

The groundwater flow and contaminant transport model, consistent with recent studies (Intera, 2024 and 2025), were developed in MODFLOW 6 to better replicate the groundwater flow regime and contaminant transport processes, while targeted refinements were introduced to improve representation of hydrostratigraphic units, boundary conditions, and historical UCG related activities. Key improvements include alignment of General Head Boundary (GHB) and drain boundary conditions with OGIA (2021) regional model datasets for non-Arrow CSG extraction, updated boundary condition for simulation of Arrow CSG extraction, adjusted simulation of Hopeland pilot wells using the Multi Aquifer Well package, and incorporation of time varying hydraulic properties to represent UCG related fracturing and material alteration. For contaminant transport, the model implements data driven source depletion terms, dual domain porosity, mechanical dispersion, molecular diffusion, sorption, and degradation processes using MODFLOW 6 transport packages and aligned with the conceptual understanding of concentration distributions.

The updated groundwater flow and contaminant transport models achieved a good history matching fit with the observed groundwater levels and contaminant concentrations. A total of

364 model realisations satisfied convergence and history matching performance criteria, with scaled root mean square errors less than 10% consistent with Australian Groundwater Modelling Guidelines threshold. History matching successfully reproduced observed temporal trends, spatial groundwater level patterns, vertical hydraulic gradients, and benzene and naphthalene concentration behaviour in both the Springbok sandstone and the Macalister coal seam. History matching also reasonably replicated the current groundwater flow regimes and contaminant transport processes aligned with the conceptual understanding of the study area utilised as history matching targets.

Predictive modelling indicates that inclusion of the proposed Clynes Road wells results in minor and localised incremental impacts relative to the approved development (scenario 2). Differences in predicted median groundwater levels between scenarios 2 and 3 are generally less than 1 m at the end of abstraction and recovery, with localised differences (of approximately 1–2 m) confined to areas near the proposed wells in the Macalister coal seam. Horizontal hydraulic gradient assessments along the southern and western boundaries of Lot 40 DY85 show incremental changes generally within ±1%, indicating no material alteration to Lot 40 DY85 flow directions relevant to contaminant migration beyond the site boundary.

Predictive modelling indicates that inclusion of the proposed Clynes Road wells results in minor and localised incremental impacts relative to the approved development (scenario 2). Differences in predicted median groundwater levels between scenarios 2 and 3 are generally less than 1 m at the end of abstraction and recovery, with localised differences of up to approximately 1-2 m confined to areas near the proposed wells in the Macalister coal seam. Assessment of horizontal hydraulic gradients along the southern and western boundaries of Lot 40 DY85 indicates incremental changes generally within ±1%, demonstrating no material alteration to site-scale flow directions relevant to contaminant migration beyond the site boundary. In addition, predictive results indicate that a downward vertical hydraulic gradient from the Springbok sandstone to the Macalister coal seam is maintained throughout both the abstraction and recovery periods.

Particle tracking and contaminant transport simulations further demonstrate that the proposed Clynes Road wells is unlikely to materially alter contaminant transport pathways, travel distances or contaminant depletion timing. Incremental increases in particle travel distance are small relative to total travel distances and remain spatially limited for the simulation period between 2019 and 2225. Ensemble contaminant transport predictions indicate continued decline in benzene and naphthalene concentrations across both formations, with no change in the predicted year of depletion below the laboratory limit of reporting between scenarios 2 and 3. Residual concentrations predicted during the abstraction period remain confined to areas proximal to former gasifier locations, consistent with the observed monitoring data.

While the current modelling reasonably replicates the magnitude and trends in the observed groundwater level and contaminants' concentrations, continued model update is recommended to further reduce prediction uncertainty over time. Ongoing groundwater level and groundwater quality monitoring should be maintained within the Springbok sandstone and Macalister coal seam, with particular focus on groundwater flow directions, vertical gradients, and any areas of persistent elevated concentrations near former gasifier locations or beyond Lot 40 DY 85. Periodic review and incorporation of new monitoring data into the numerical model would allow reassessment of predictions and confirmation of long-term trends.

It is also recommended that future updates to the groundwater model consider refinement of source representation as additional data becomes available regarding the persistence or removal of residual contamination zones. Should any site-scale alterations occur to the current declining trends across monitoring bores within and around Lot 40 DY85, updated groundwater flow and contaminant transport modelling is recommended to be undertaken to reassess contaminant movement and depletion timing. Continued alignment with OGIA regional model updates is recommended to ensure future modelling remains consistent with updated basin-scale conceptualisation and regional flow directions.

7. References

AGE, (2021). Production Licensing Modelling Support prepared for Arrow Energy by Australasian Groundwater and Environmental Consultants Pty Ltd. June 2021.

AGE, (2023). PL 253 Environmental Approval Amendment Support – Contaminant transport validation – Addendum to AGE (2022) by Australasian Groundwater and Environmental Consultants Pty Ltd. 19th January 2023.

Ahangar, A.G. (2010). Sorption of PAHs in the soil environment with emphasis on the role of soil organic matter: A review. World Applied Sciences Journal, 11(7), 759–765.

Aguilera, R. (2004). A triple porosity model for petrophysical analysis of naturally fractured reservoirs. Petrophysics (SPWLA Journal), 45(2).

Anderson, R.T., Rooney-Varga, J.N., Gaw, C.V. & Lovley, D.R. (1998). Anaerobic benzene oxidation in the Fe(III) reduction zone of petroleum-contaminated aquifers. Environmental Science & Technology, 32(9), 1222–1229.

American Petroleum Institute (API). (1998). Delineation and characterization of the Borden MTBE plume: An evaluation of eight years of natural attenuation processes. Health and Environmental Sciences Department, Publication No. 4668.

Agency for Toxic Substances and Disease Registry (ATSDR). (2024). Toxicological profile for benzene (Draft for public comment). Atlanta, GA: U.S. Department of Health and Human Services, Public Health Service.

Barnett, B., Townley, L., Post, V., Evans, R., Hunt, R., Peeters, L., Richardson, S., Werner, A., Knapton, A., & Boronkay, A. (2012). Australian groundwater modelling guidelines. National Water Commission.

Bayard, R., Barna, L., Mahjoub, B., and Gourdon, R., (2020). Influence of the presence of PAHs and coal tar on naphthalene sorption in soils. Journal of Contaminant Hydrology, Volume 46, Issues 1–2, pp. 61-80. https://doi.org/10.1016/S0169-7722(00)00125-X.

Bjerg, P.L., Rügge, K., Cortsen, J., Nielsen, P.H. & Christensen, T.H. (1999). Degradation of aromatic and chlorinated aliphatic hydrocarbons in the anaerobic part of the Grindsted landfill leachate plume: In situ microcosm and laboratory batch experiments. Ground Water, 37, 113–121.

Bjerg, P.L., Bøllingtoft, A. & Mosthaf, K. (2025). Lecture Note: Dispersion in Aquifers. DTU Sustain.

Doherty, J., (2024). Tutorial: Ensemble Space Inversion. GMDSI. https://gmdsi.org/blog/ensemble-space-inversion/.

Dong, S., Dai, Z., Li, J. & Zhou, W. (2018). The scale dependence of dispersivity in multi-facies heterogeneous formations. Carbonates and Evaporites, 33, 161–165.

ECETOC (European Centre for Ecotoxicology and Toxicology of Chemicals). (2013). Environmental Exposure Assessment of Ionisable Organic Compounds. Technical Report No. 123, Brussels: ECETOC.

Epic, (2020). Former Underground Coal Gasification Plant, Hopeland - Updated Conceptual Site Model. 17 December 2020.

Gelhar, L.W., Welty, C. & Rehfeldt, K.R. (1992). A critical review of data on field-scale dispersion in aquifers. Water Resources Research, 28(7), 1955–1974.

GHD, (2019). Arrow Hopeland Groundwater Study Groundwater Modelling Report – PL253.

Grathwohl, P., Eberhardt, C., Klenk, I., Rügner, H. & Maier, U. (2000). Transverse vertical dispersivity in aquifer materials: Implications on mass transfer across the capillary fringe and the length of steady state plumes. In: Bjerg, P.L. (ed.), Groundwater 2000: Proceedings of the International Conference on Groundwater Research, Copenhagen, Denmark, 6–8 June 2000. Rotterdam: A.A. Balkema.

Gustafson, K.E. & Dickhut, R.M. (1994). Molecular diffusivity of polycyclic aromatic hydrocarbons in air. Journal of Chemical & Engineering Data, 39(2), 286–289.

Intera (2024). PL253 –Site Conceptual Model, and Groundwater Flow, Contaminant Transport and Predictive Modelling.

Intera (2025). PL253 Groundwater Flow and Contaminant Transport Modelling Report. Prepared for Arrow Energy Pty Ltd.

King, G.R., Ertekin, T. & Schwerer, F.C. (1986). Numerical simulation of the transient behavior of coal-seam degasification wells. SPE Formation Evaluation, 1(2), 165–183.

Langevin, C.D., Provost, A.M., Panday, S. & Hughes, J.D. (2022). Documentation for the MODFLOW 6 Groundwater Transport Model. U.S. Geological Survey, Techniques and Methods, Book 6, Chap. A61.

Musat, F., Galushko, A., Jacob, J., Widdel, F., Kube, M., Reinhardt, R., Wilkes, H., Schink, B. & Rabus, R. (2009). Anaerobic degradation of naphthalene and 2-methylnaphthalene by strains of marine sulfate-reducing bacteria. Environmental Microbiology, 11(1), 209–219.

Newell, C.J., Rifai, H.S., Wilson, J.T., Connor, J.A., Aziz, J.A. & Suarez, M.P. (2002). Calculation and use of first-order rate constants for monitored natural attenuation studies. U.S. Environmental Protection Agency, Ground Water Issue.

Odermatt, J.R., (1994). Natural chromatographic separation of benzene, toluene, ethylbenzene and xylenes (BTEX compounds) in a gasoline contaminated ground water aquifer. Organic Chemistry v. 21, 10-11; p 1141-1150.

OGIA, (2021a). Modelling of Cumulative Groundwater Impacts in the Surat CMA: Approach and Methods. Version 1.0.

OGIA, (2021b). Regional Flow Systems and Potentiometry in Queensland's Surat and Southern Bowen Basins. Version 1.0.

Osagie, E.I. & Owabor, C.N. (2015a). Adsorption of benzene in batch system in natural clay and sandy soil. Advances in Chemical Engineering and Science, 5, 352–361.

Osagie, E.I. & Owabor, C.N. (2015b). Adsorption of naphthalene on clay and sandy soil from aqueous solution. Advances in Chemical Engineering and Science, 5, 345–351.

Peeters, L.J.M. and Middlemis, H. (2023). Information Guidelines Explanatory Note: Uncertainty analysis for groundwater modelling. Independent Expert Scientific Committee on Coal Seam Gas and Large Coal Mining Development, Commonwealth of Australia.

Prommer, H., Davis G.B., Barry D.A., Miller C.T., (2003). Modelling the Fate of Petroleum Hydrocarbons in Groundwater. Proceedings of the Fifth National Workshop on the Assessment of Site Contamination.

Pruess, K. & Narasimhan, T.N. (1985). A practical method for modeling fluid and heat flow in fractured porous media. Society of Petroleum Engineers Journal, 25(1), 14–26.

Schulze-Makuch, D. (2005). Longitudinal dispersivity data and implications for scaling behavior. Ground Water, 43(3), 443–456.

Shi, B., Ngueleu, S.K., Rezanezhad, F., Slowinski, S., Pronk, G.J., Smeaton, C.M., Stevenson, K., Al-Raoush, R.I. & Van Cappellen, P. (2020). Sorption and desorption of the model aromatic hydrocarbons naphthalene and benzene: Effects of temperature and soil composition. Frontiers in Environmental Chemistry, 1, 581103.

Ukalska-Jaruga, A. & Smreczak, B. (2020). The impact of organic matter on polycyclic aromatic hydrocarbon (PAH) availability and persistence in soils. Molecules, 25(11), 2470.

U.S. Environmental Protection Agency (U.S. EPA). (1996). A citizen's guide to natural attenuation. EPA 542-F-96-015, Office of Solid Waste and Emergency Response.

U.S. Environmental Protection Agency (US EPA). (1999). Monitored natural attenuation of petroleum hydrocarbons. EPA 600/F-98/021.

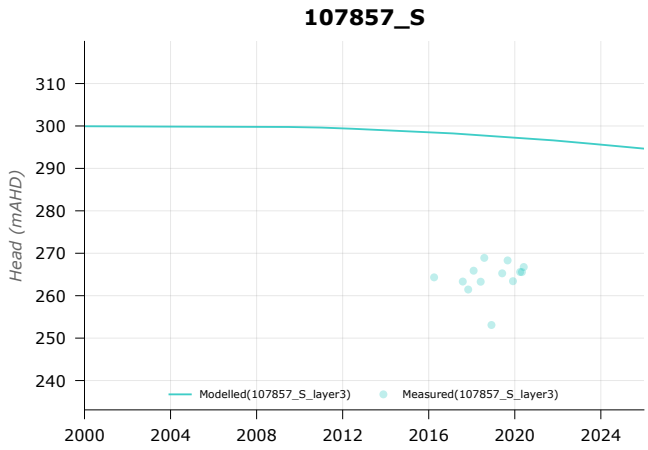
Warren, J.E. & Root, P.J. (1963). The behavior of naturally fractured reservoirs. Society of Petroleum Engineers Journal, 3(3), 245–255.

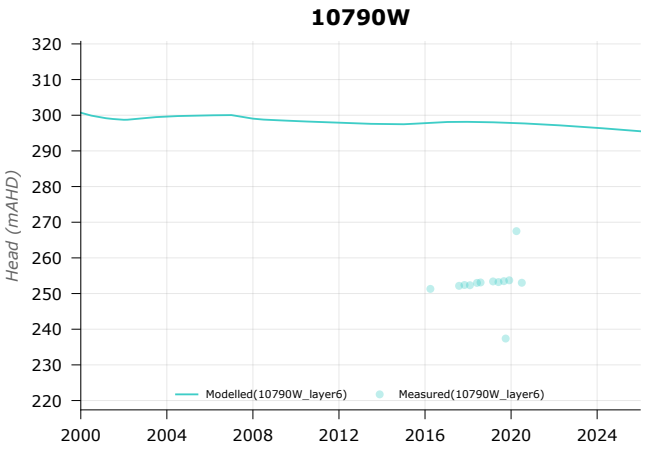
White, J.T., (2018). A model-independent iterative ensemble smoother for efficient history-matching and uncertainty quantification in very high dimensions. Environmental Modelling & Software, vol. 109.

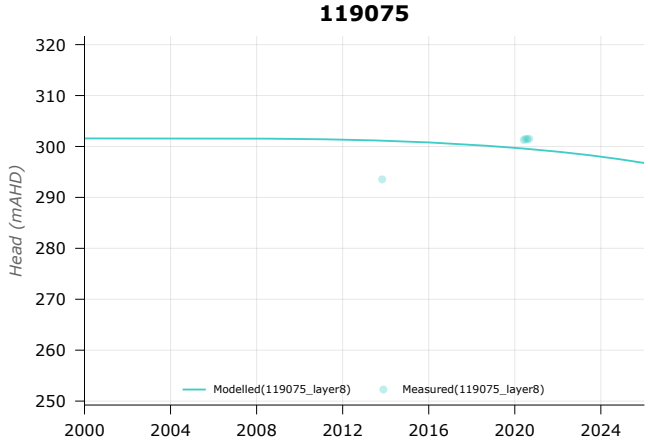
Wiedemeier, T.H., Rifai, H.S., Newell, C.J., and Wilson, J.T. (1999). Natural Attenuation of Fuels and Chlorinated Solvents in the Subsurface. John Wiley & Sons, New York, 617 pp.

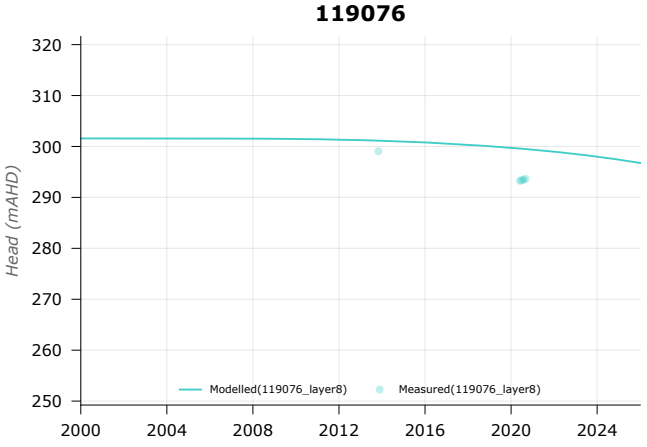
Zhang, T., [et al.] (2005). Hydroxylation and carboxylation—two crucial steps of anaerobic benzene degradation by Dechloromonas strain RCB. Applied and Environmental Microbiology, 71(9), 5427–5432.

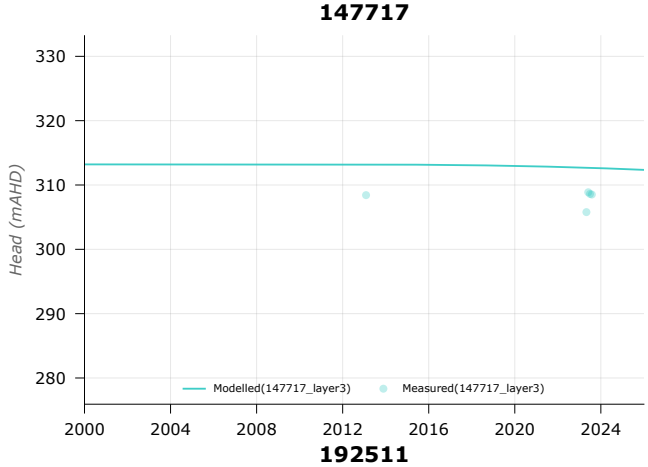
Appendix A. Modelled versus observed hydrographs

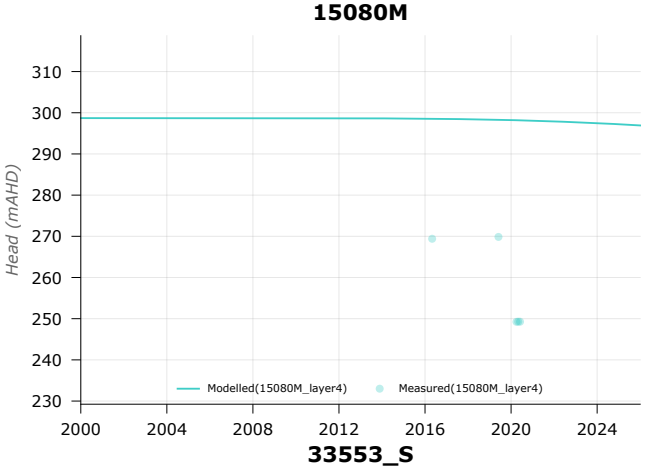

107857_S
Head (mAHD)
Modelled(107857_S_layer3)
Measured(107857_S_layer3)

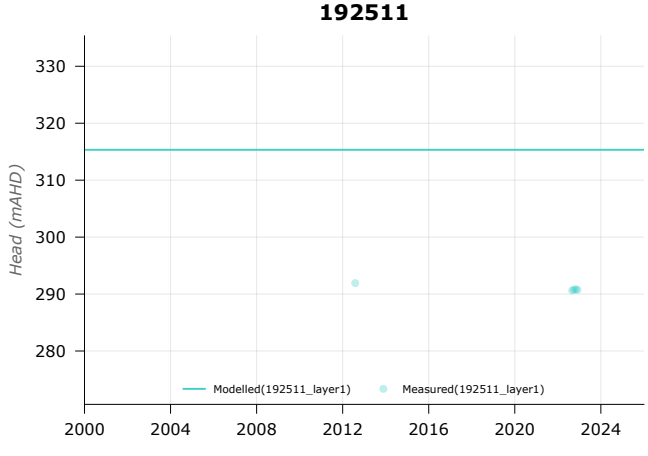

10790W
Head (mAHD)
Modelled(10790W_layer6)
Measured(10790W_layer6)

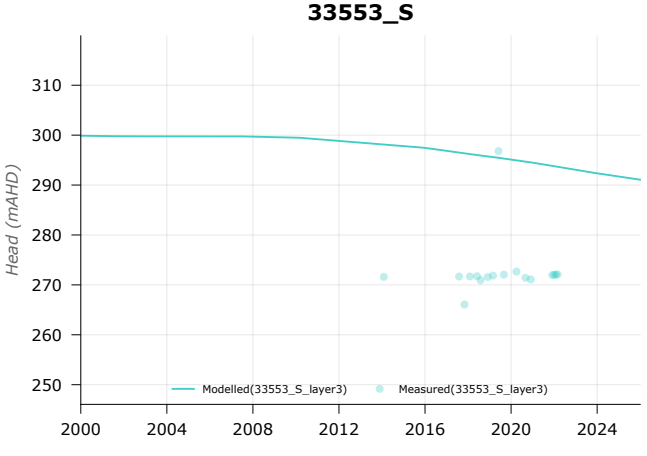

119075
Head (mAHD)
Modelled(119075_layer8)
Measured(119075_layer8)

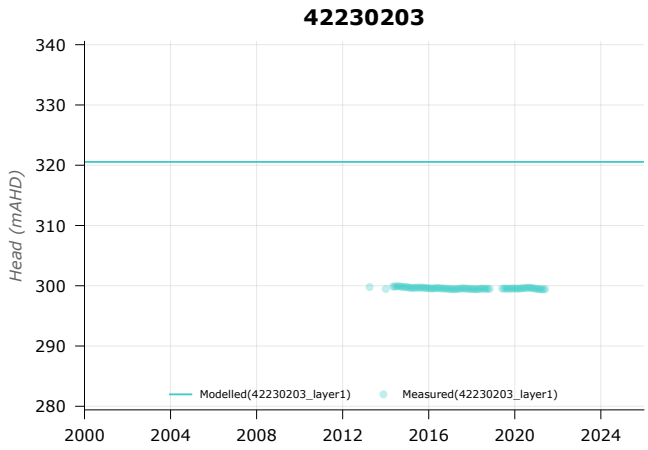

119076
Head (mAHD)
Modelled(119076_layer8)
Measured(119076_layer8)

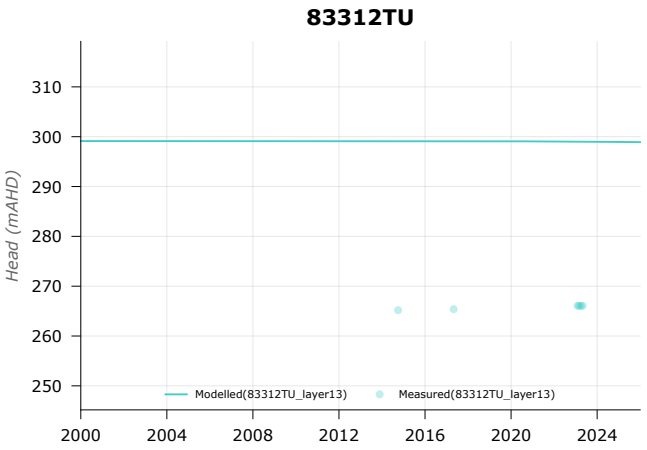

147717
Head (mAHD)
Modelled(147717_layer3)
Measured(147717_layer3)

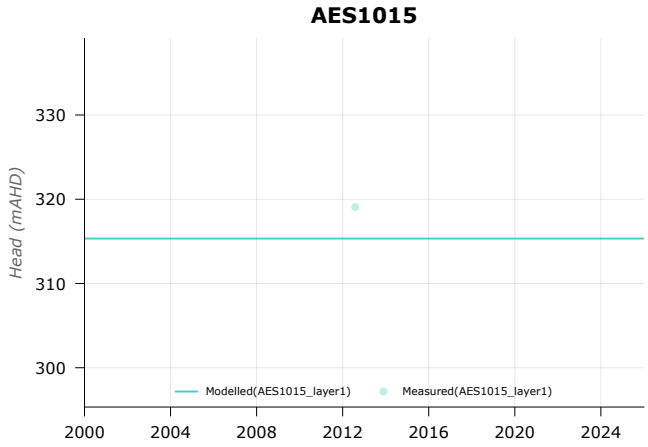

15080M
Head (mAHD)
Modelled(15080M_layer4)
Measured(15080M_layer4)

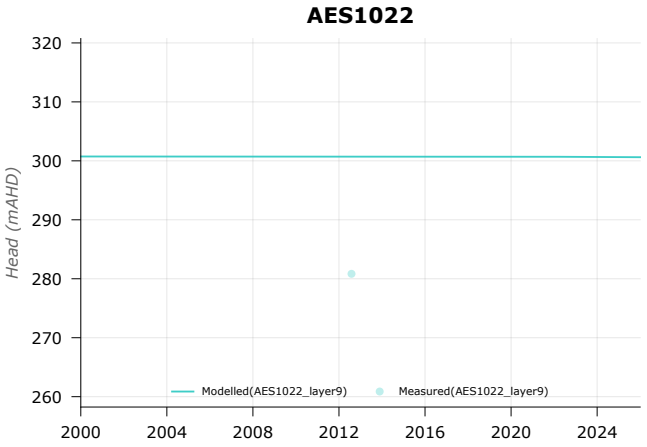

192511
Head (mAHD)
Modelled(192511_layer1)
Measured(192511_layer1)

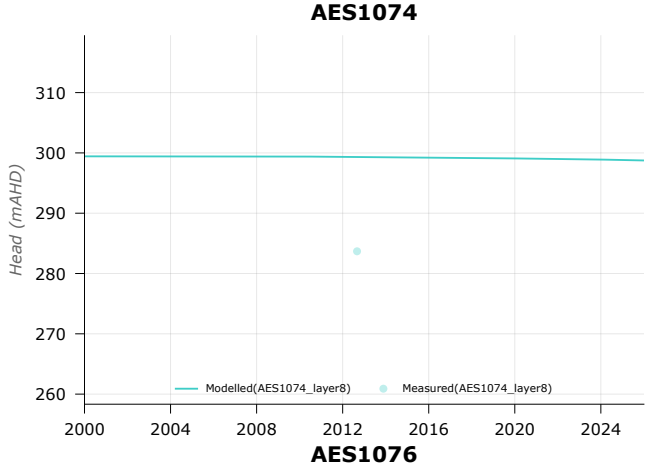

33553_S
Head (mAHD)
Modelled(33553_S_layer3)
Measured(33553_S_layer3)

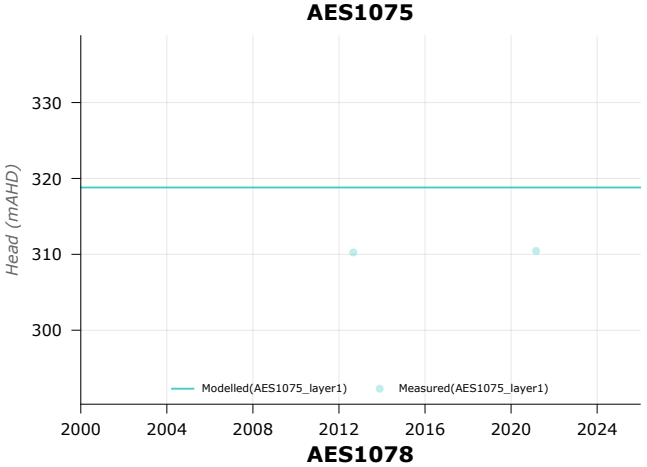

42230203
Head (mAHD)
340
330
320
310
300
290
280
2000
2004
2008
2012
2016
2020
2024
Modelled(42230203_layer1)
Measured(42230203_layer1)

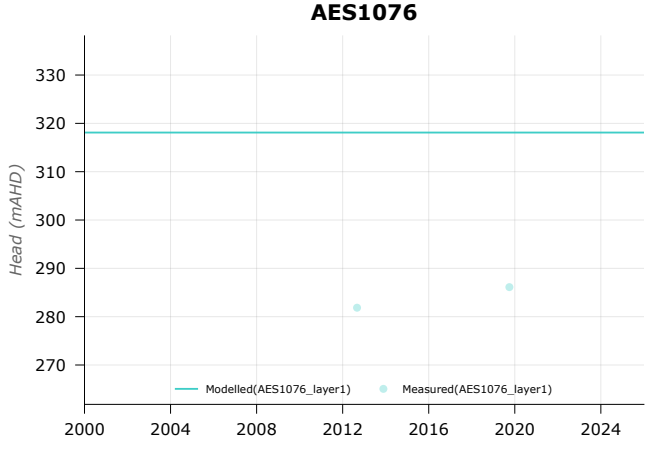

83312TU
Head (mAHD)
310
300
290
280
270
260
250
2000
2004
2008
2012
2016
2020
2024
Modelled(83312TU_layer13)
Measured(83312TU_layer13)

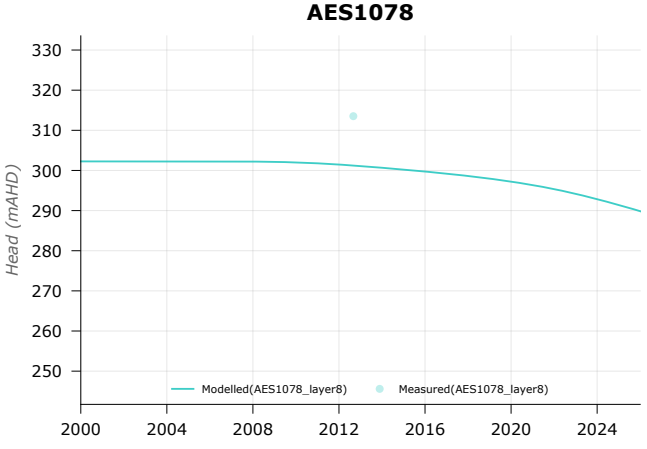

AES1015
Head (mAHD)
330
320
310
300
2000
2004
2008
2012
2016
2020
2024
Modelled(AES1015_layer1)
Measured(AES1015_layer1)

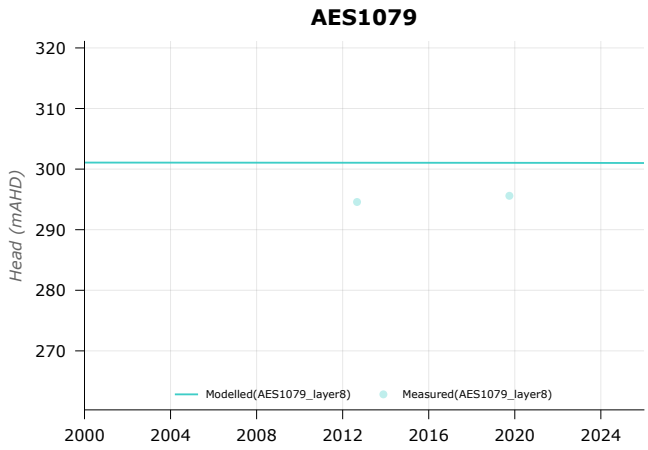

AES1022
Head (mAHD)
320
310
300
290
280
270
260
2000
2004
2008
2012
2016
2020
2024
Modelled(AES1022_layer9)
Measured(AES1022_layer9)

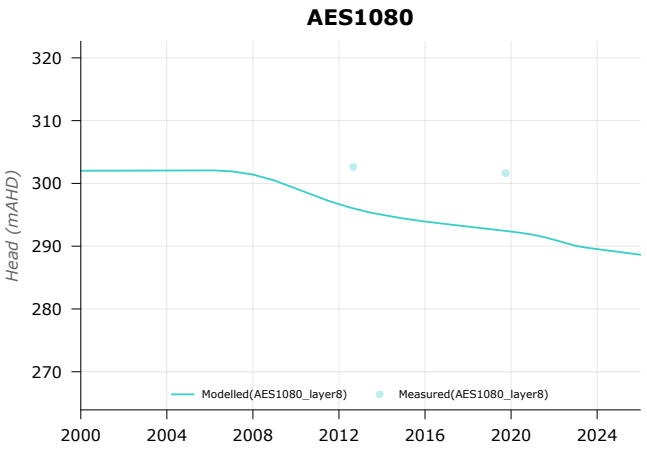

AES1074
Head (mAHD)
310
300
290
280
270
260
2000
2004
2008
2012
2016
2020
2024
Modelled(AES1074_layer8)
Measured(AES1074_layer8)

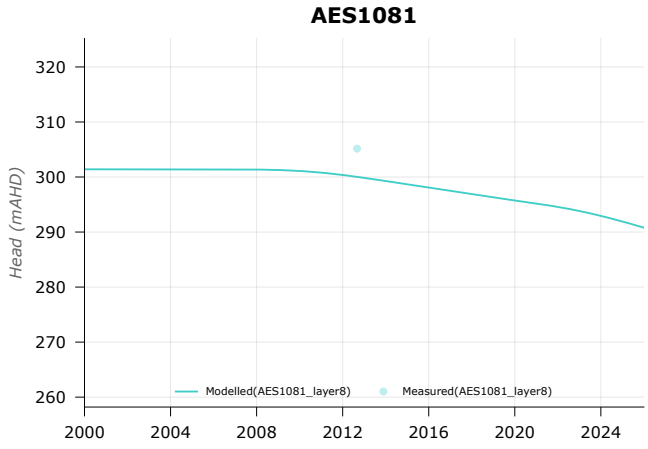

AES1075
Head (mAHD)
330
320
310
300
2000
2004
2008
2012
2016
2020
2024
Modelled(AES1075_layer1)
Measured(AES1075_layer1)

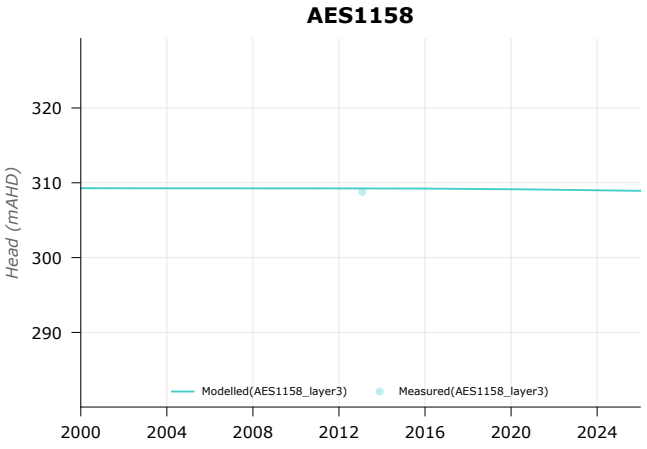

AES1076
Head (mAHD)
330
320
310
300
290
280
270
2000
2004
2008
2012
2016
2020
2024
Modelled(AES1076_layer1)
Measured(AES1076_layer1)

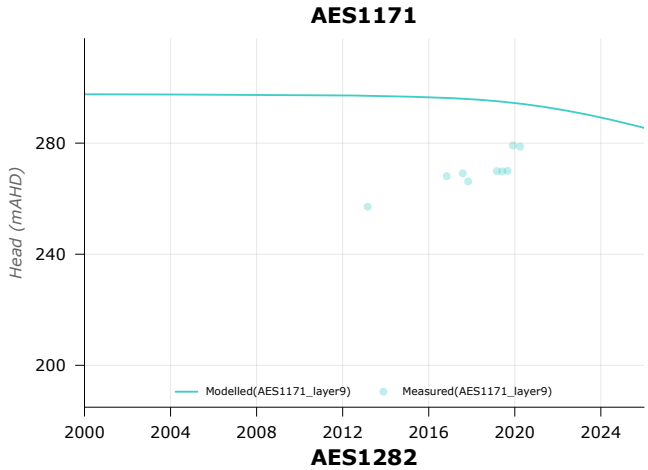

AES1078
Head (mAHD)
330
320
310
300
290
280
270
260
250
2000
2004
2008
2012
2016
2020
2024
Modelled(AES1078_layer8)
Measured(AES1078_layer8)

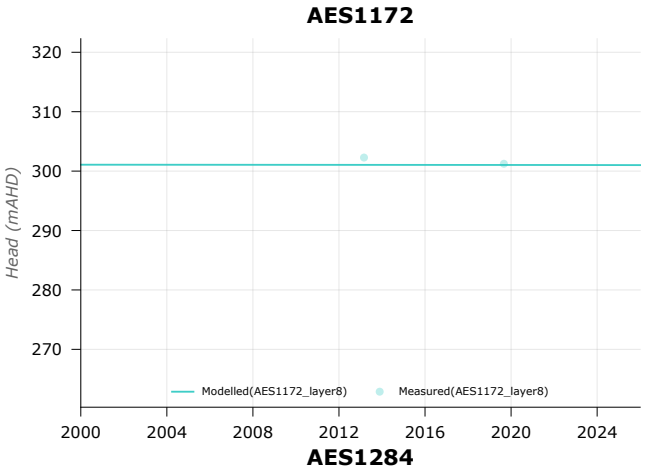

AES1079
Head (mAHD)
320
310
300
290
280
270
2000
2004
2008
2012
2016
2020
2024
Modelled(AES1079_layer8)
Measured(AES1079_layer8)

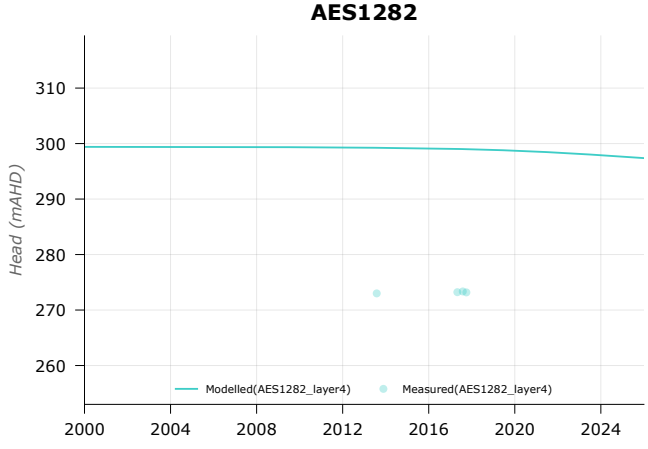

AES1080
Head (mAHD)
320
310
300
290
280
270
2000
2004
2008
2012
2016
2020
2024
Modelled(AES1080_layer8)
Measured(AES1080_layer8)

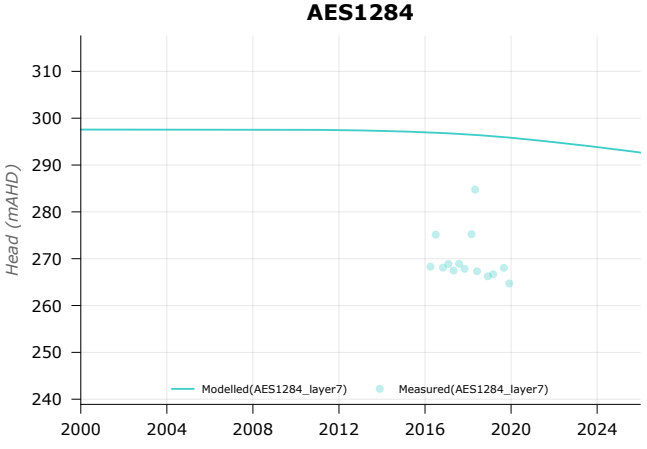

AES1081
Head (mAHD)
320
310
300
290
280
270
260
2000
2004
2008
2012
2016
2020
2024
Modelled(AES1081_layer8)
Measured(AES1081_layer8)

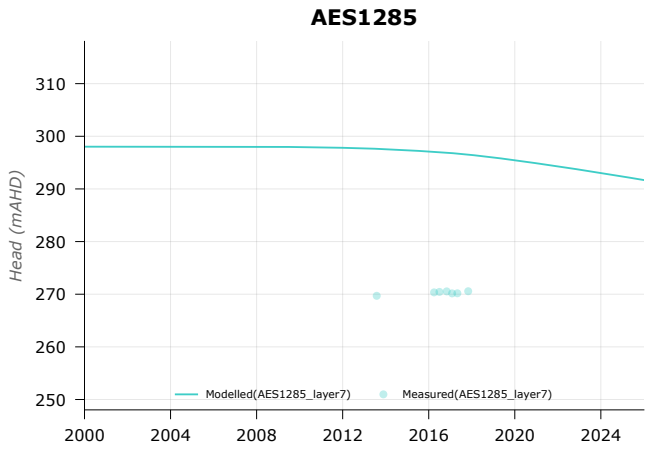

AES1158
Head (mAHD)
320
310
300
290
2000
2004
2008
2012
2016
2020
2024
Modelled(AES1158_layer3)
Measured(AES1158_layer3)

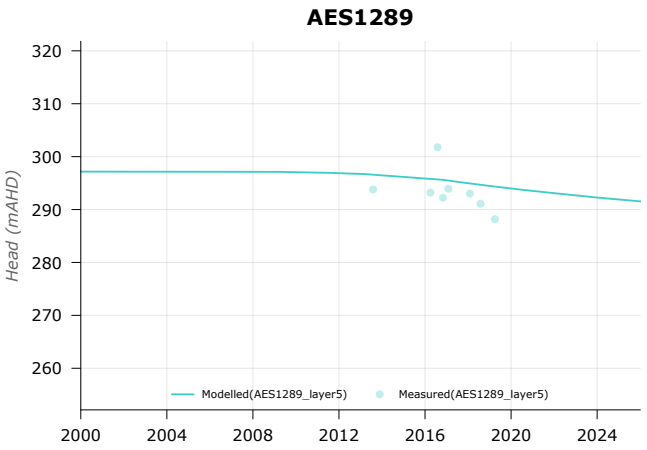

AES1171
Head (mAHD)
280
240
200
2000
2004
2008
2012
2016
2020
2024
Modelled(AES1171_layer9)
Measured(AES1171_layer9)

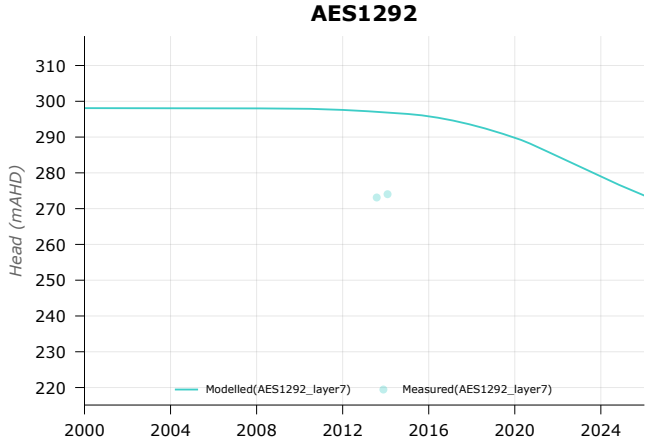

AES1172
Head (mAHD)
320
310
300
290
280
270
2000
2004
2008
2012
2016
2020
2024
Modelled(AES1172_layer8)
Measured(AES1172_layer8)

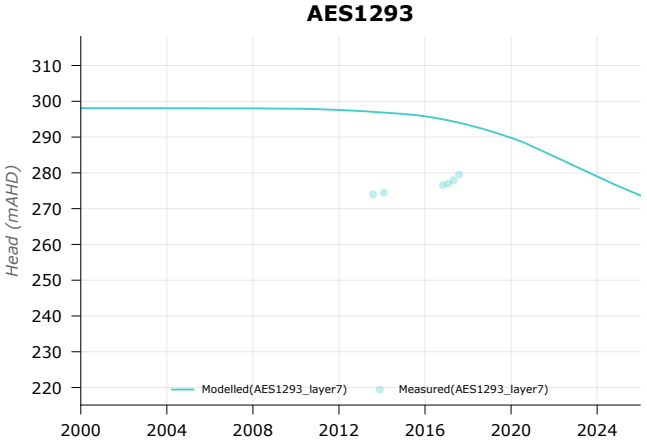

AES1282
Head (mAHD)
310
300
290
280
270
260
2000
2004
2008
2012
2016
2020
2024
Modelled(AES1282_layer4)
Measured(AES1282_layer4)

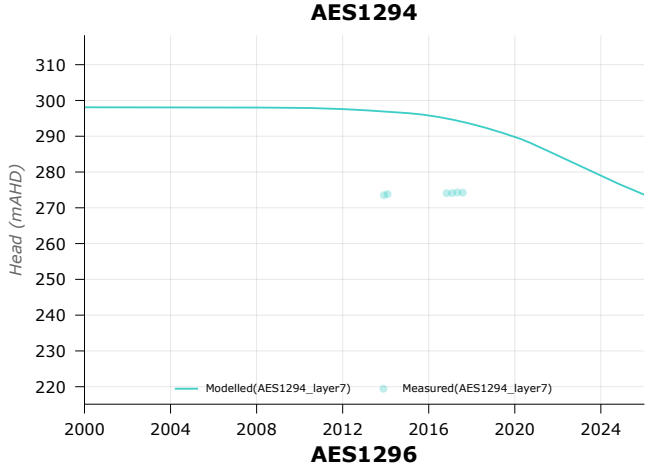

AES1284
Head (mAHD)
310
300
290
280
270
260
250
240
2000
2004
2008
2012
2016
2020
2024
Modelled(AES1284_layer7)
Measured(AES1284_layer7)

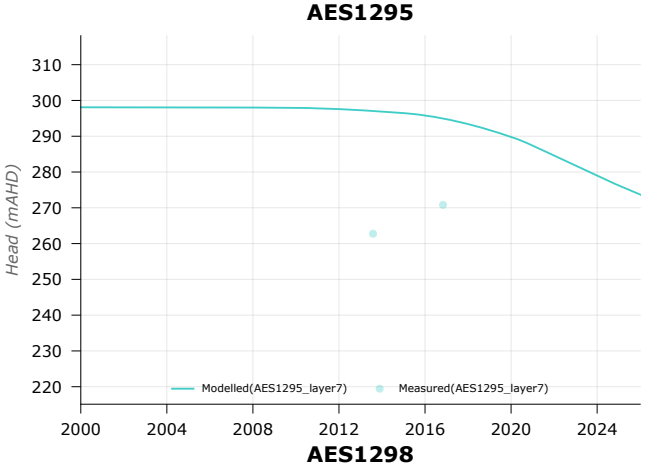

AES1285
Head (mAHD)
Modelled(AES1285_layer7)
Measured(AES1285_layer7)

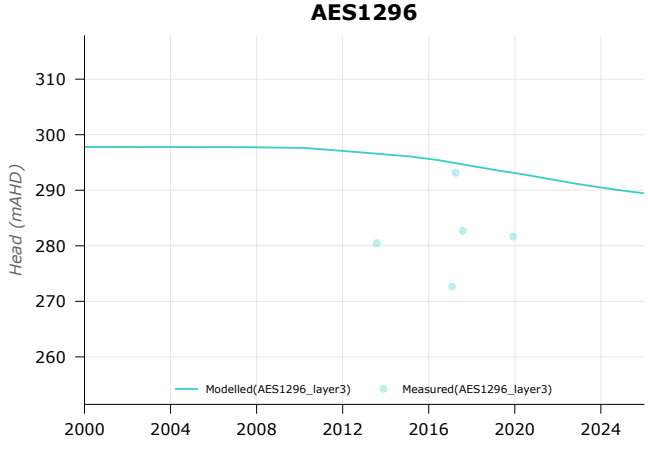

AES1289
Head (mAHD)
Modelled(AES1289_layer5)
Measured(AES1289_layer5)

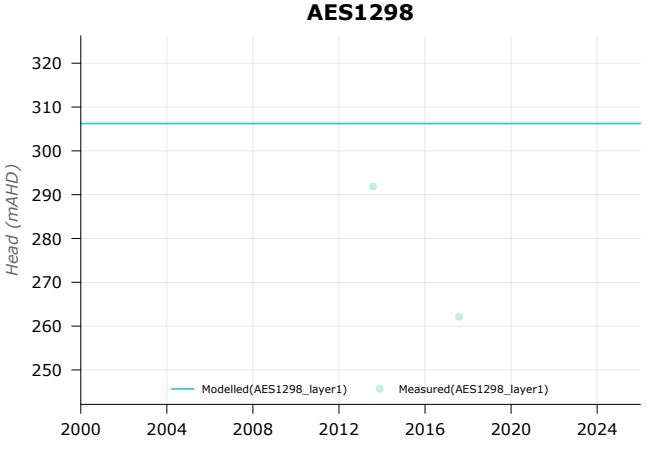

AES1292
Head (mAHD)
Modelled(AES1292_layer7)
Measured(AES1292_layer7)

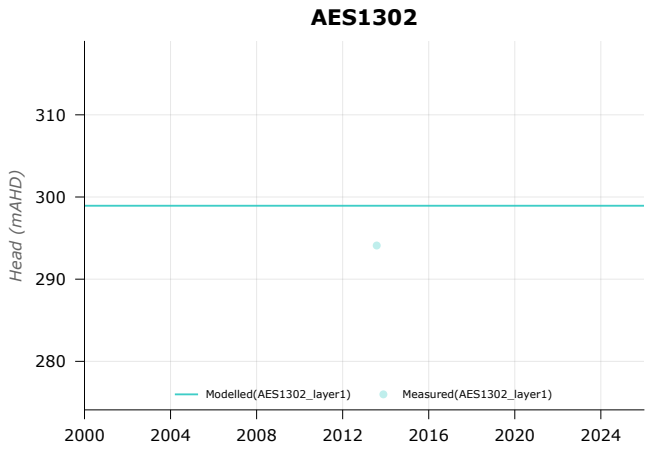

AES1293
Head (mAHD)
Modelled(AES1293_layer7)
Measured(AES1293_layer7)

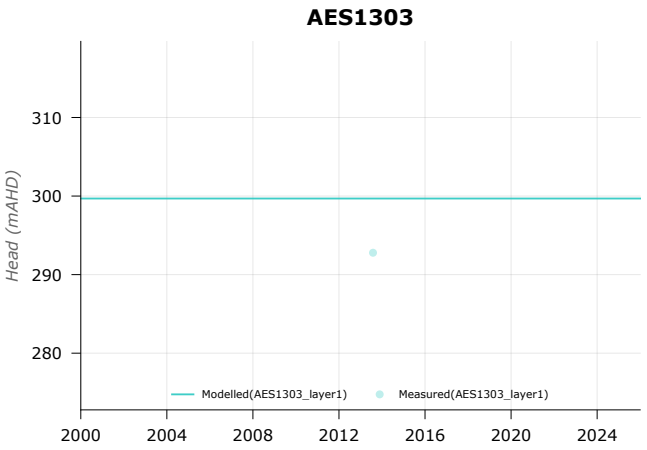

AES1294
Head (mAHD)
Modelled(AES1294_layer7)
Measured(AES1294_layer7)

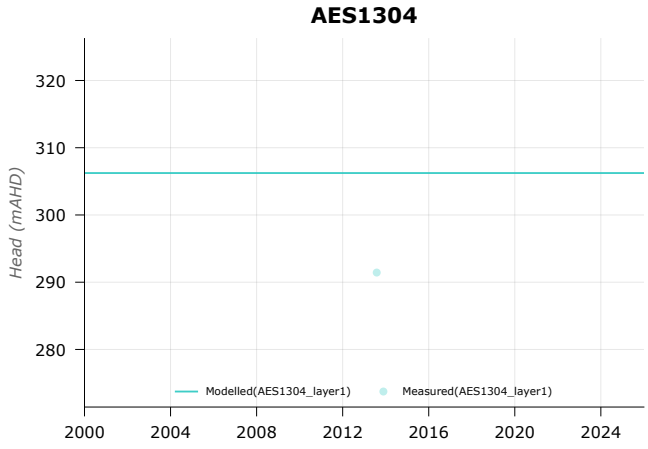

AES1295
Head (mAHD)
Modelled(AES1295_layer7)
Measured(AES1295_layer7)

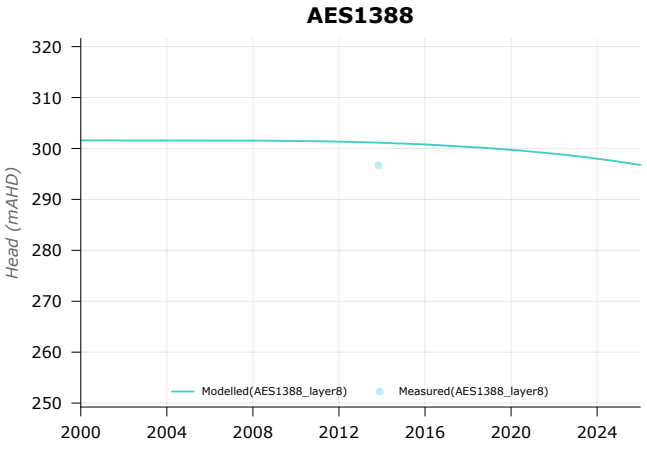

AES1296
Head (mAHD)
Modelled(AES1296_layer3)
Measured(AES1296_layer3)

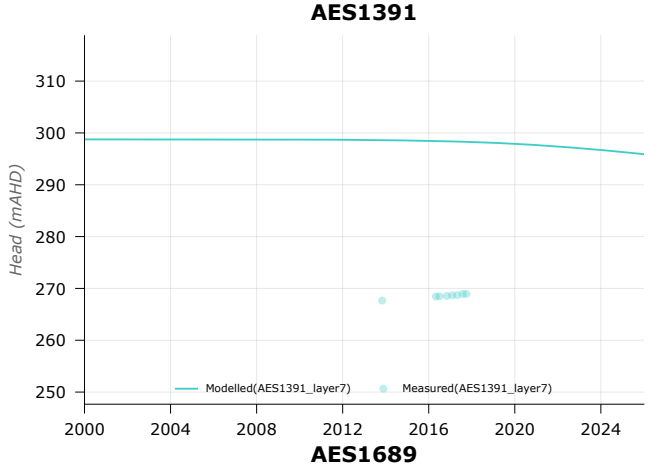

AES1298
Head (mAHD)
Modelled(AES1298_layer1)
Measured(AES1298_layer1)

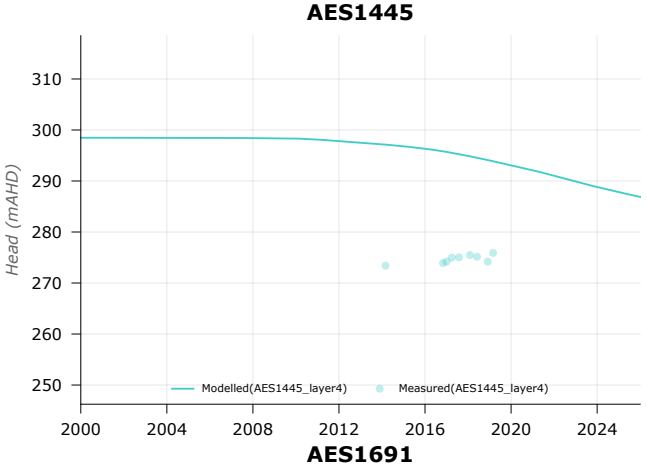

AES1302
Head (mAHD)
310
300
290
280
2000
2004
2008
2012
2016
2020
2024
Modelled(AES1302_layer1)
Measured(AES1302_layer1)

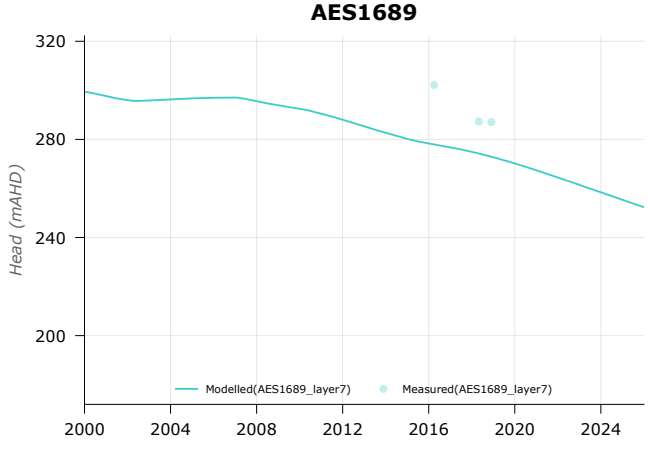

AES1303
Head (mAHD)
310
300
290
280
2000
2004
2008
2012
2016
2020
2024
Modelled(AES1303_layer1)
Measured(AES1303_layer1)

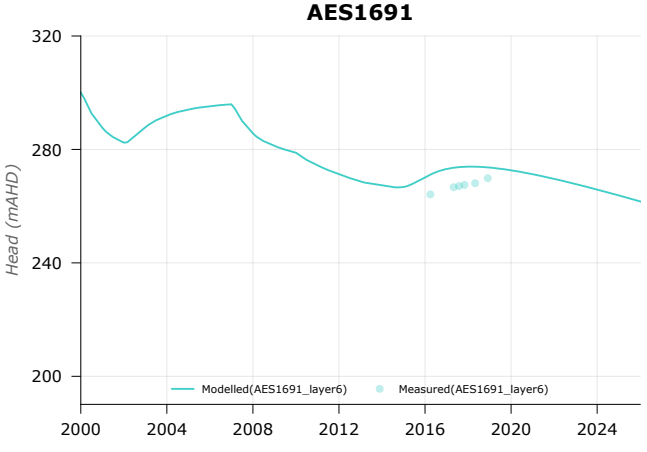

AES1304
Head (mAHD)
320
310
300
290
280
2000
2004
2008
2012
2016
2020
2024
Modelled(AES1304_layer1)
Measured(AES1304_layer1)

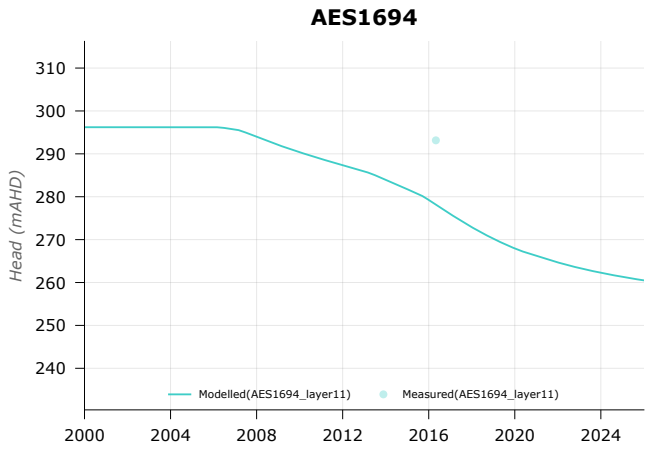

AES1388
Head (mAHD)
320
310
300
290
280
270
260
250
2000
2004
2008
2012
2016
2020
2024
Modelled(AES1388_layer8)
Measured(AES1388_layer8)

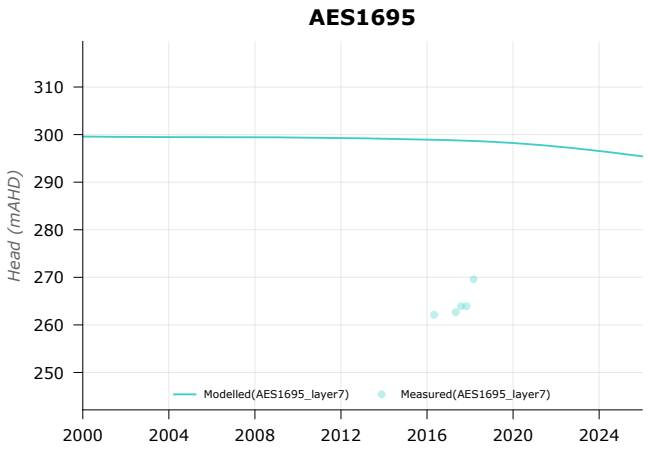

AES1391
Head (mAHD)
310
300
290
280
270
260
250
2000
2004
2008
2012
2016
2020
2024
Modelled(AES1391_layer7)
Measured(AES1391_layer7)

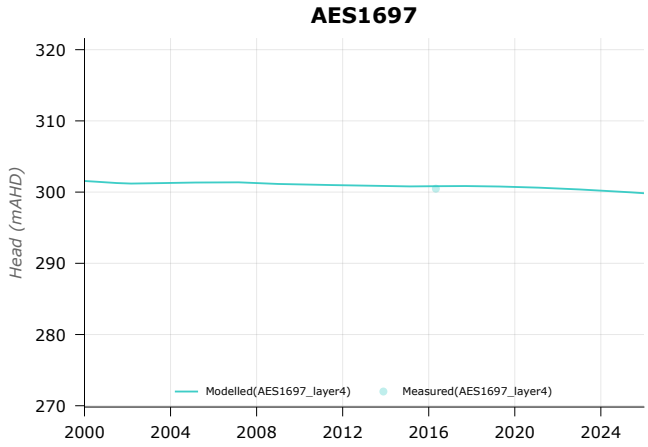

AES1445
Head (mAHD)
310
300
290
280
270
260
250
2000
2004
2008
2012
2016
2020
2024
Modelled(AES1445_layer4)
Measured(AES1445_layer4)

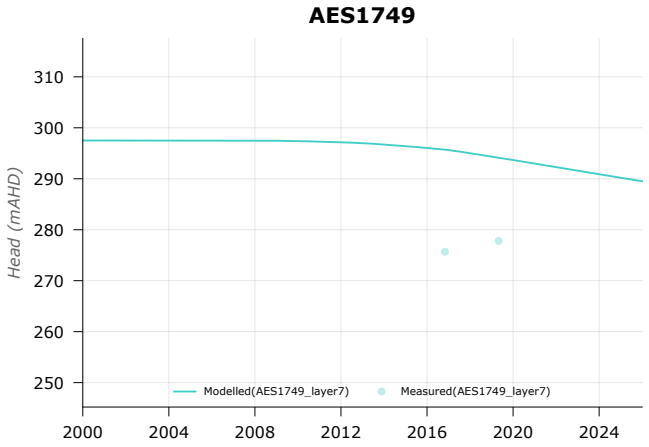

AES1689
Head (mAHD)
320
280
240
200
2000
2004
2008
2012
2016
2020
2024
Modelled(AES1689_layer7)
Measured(AES1689_layer7)

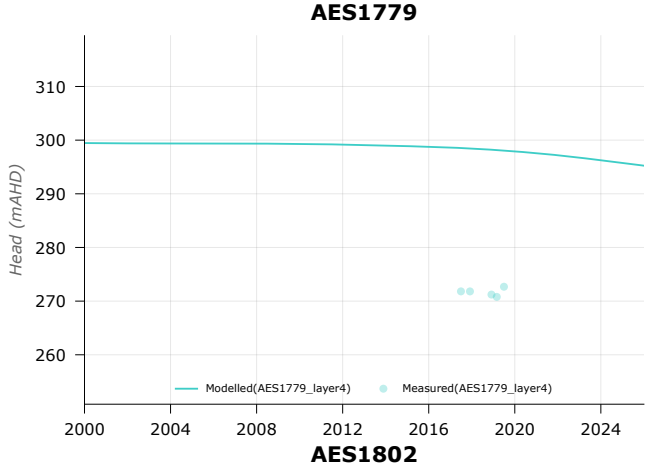

AES1691
Head (mAHD)
320
280
240
200
2000
2004
2008
2012
2016
2020
2024
Modelled(AES1691_layer6)
Measured(AES1691_layer6)

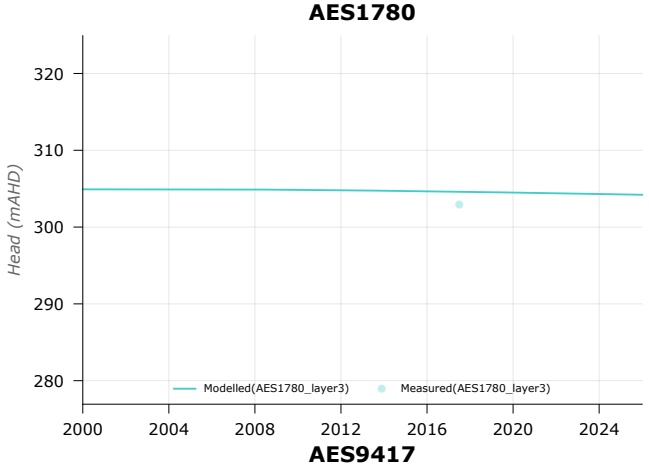

AES1694
Head (mAHD)
Modelled(AES1694_layer11)
Measured(AES1694_layer11)

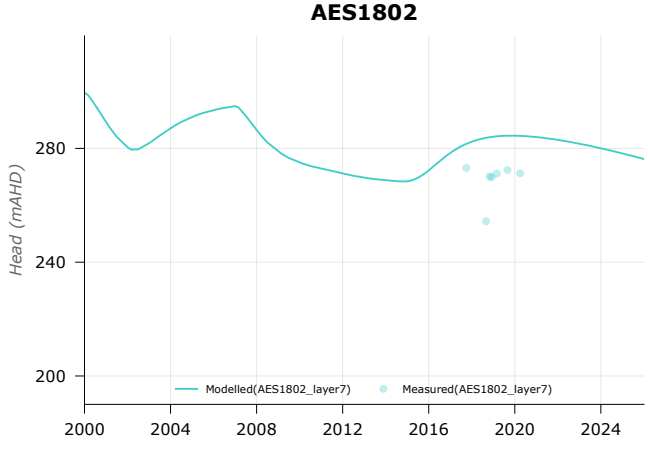

AES1695
Head (mAHD)
Modelled(AES1695_layer7)
Measured(AES1695_layer7)

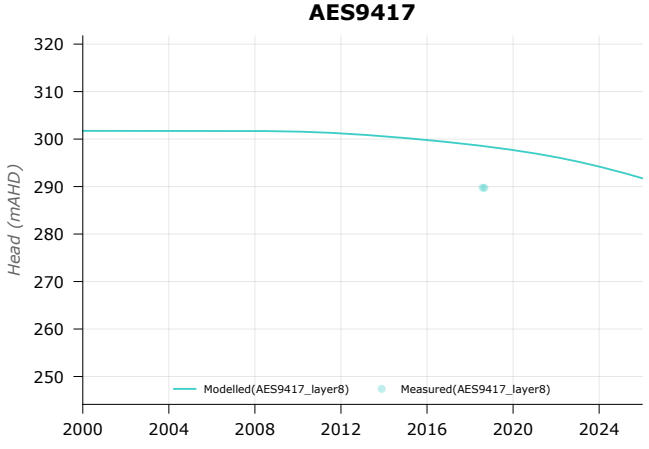

AES1697
Head (mAHD)
Modelled(AES1697_layer4)
Measured(AES1697_layer4)

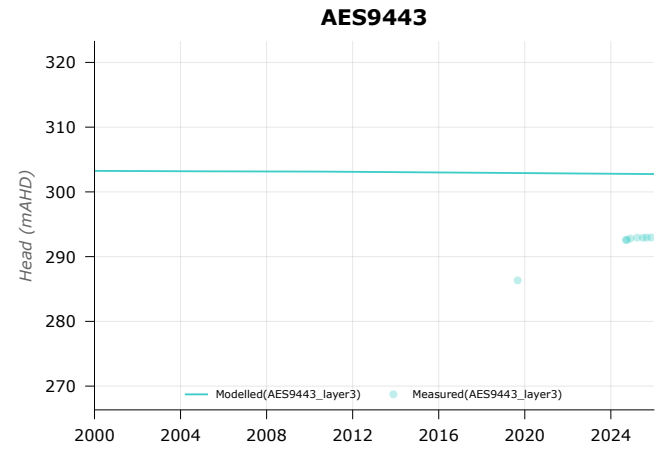

AES1749
Head (mAHD)
Modelled(AES1749_layer7)
Measured(AES1749_layer7)

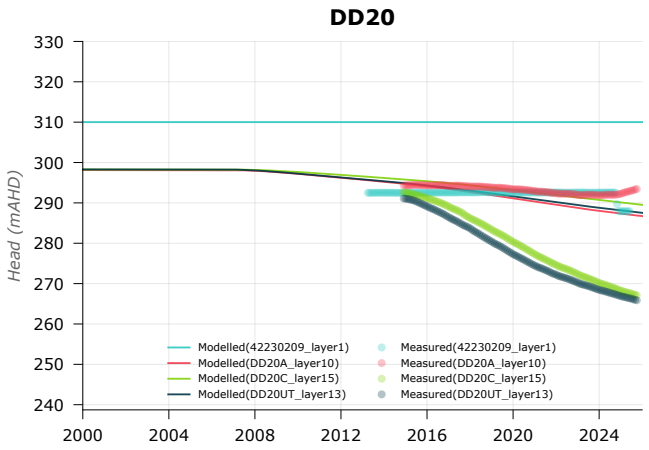

AES1779
Head (mAHD)
Modelled(AES1779_layer4)
Measured(AES1779_layer4)

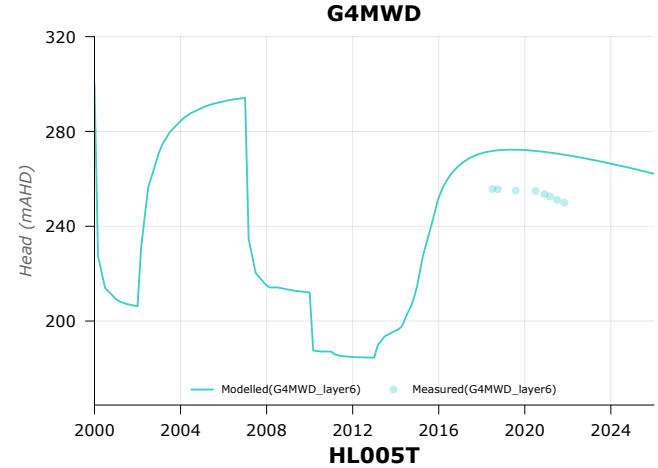

AES1780
Head (mAHD)
Modelled(AES1780_layer3)
Measured(AES1780_layer3)

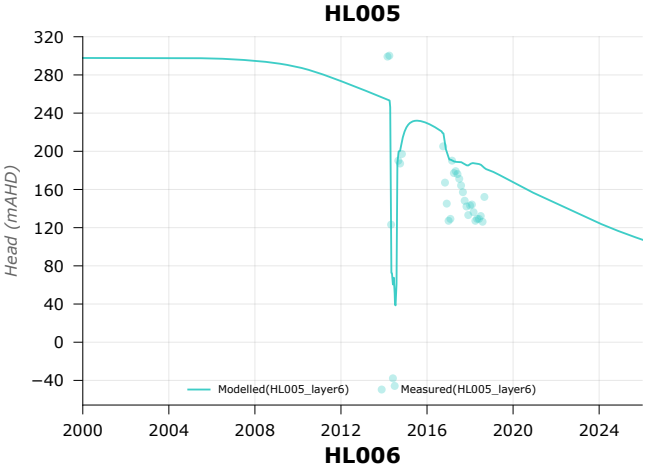

AES1802
Head (mAHD)
Modelled(AES1802_layer7)
Measured(AES1802_layer7)

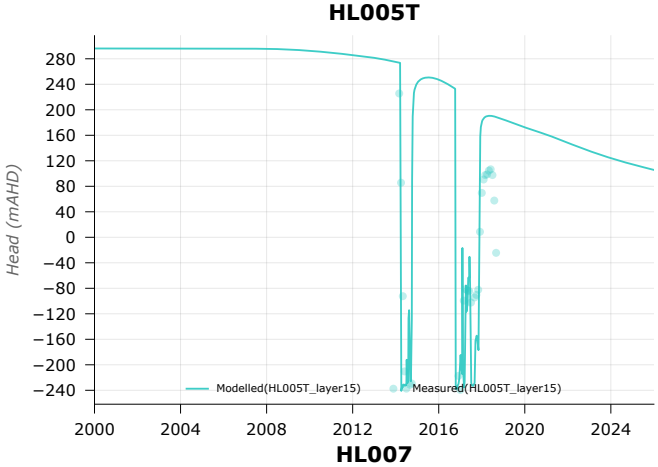

AES9417
Head (mAHD)
Modelled(AES9417_layer8)
Measured(AES9417_layer8)

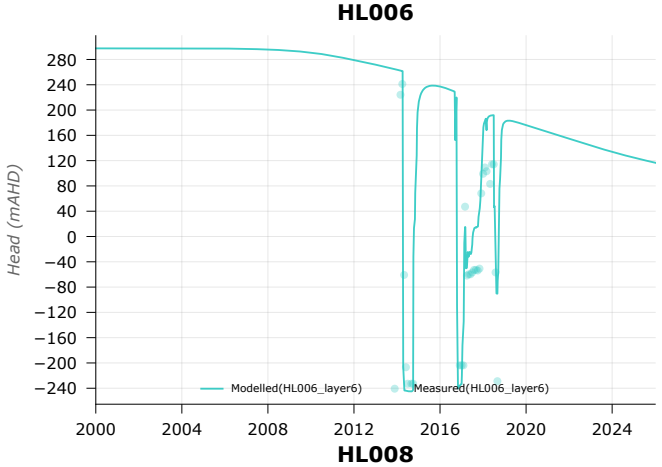

AES9443
Head (mAHD)
Modelled(AES9443_layer3)
Measured(AES9443_layer3)

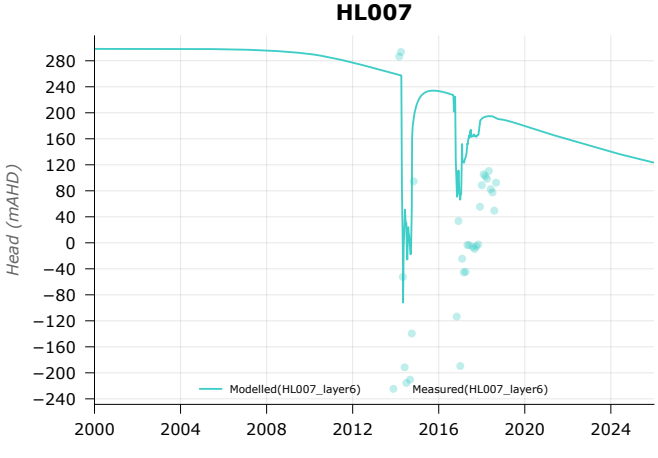

DD20
Head (mAHD)
Modelled(42230209_layer1)
Measured(42230209_layer1)
Modelled(DD20A_layer10)
Measured(DD20A_layer10)
Modelled(DD20C_layer15)
Measured(DD20C_layer15)
Modelled(DD20UT_layer13)
Measured(DD20UT_layer13)

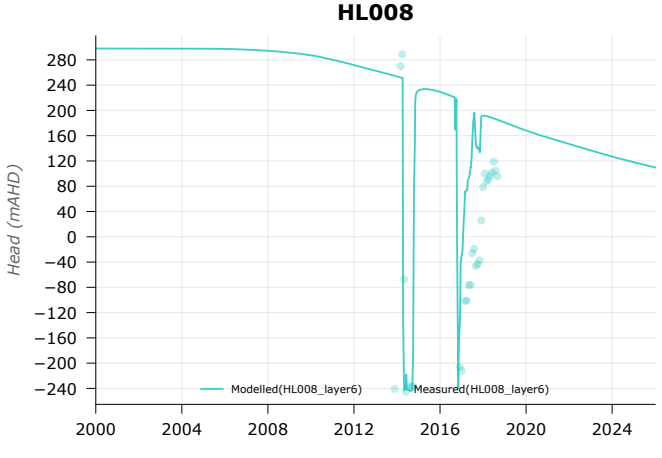

G4MWD
Head (mAHD)
Modelled(G4MWD_layer6)
Measured(G4MWD_layer6)


HL005
Head (mAHD)
Modelled(HL005_layer6)
Measured(HL005_layer6)

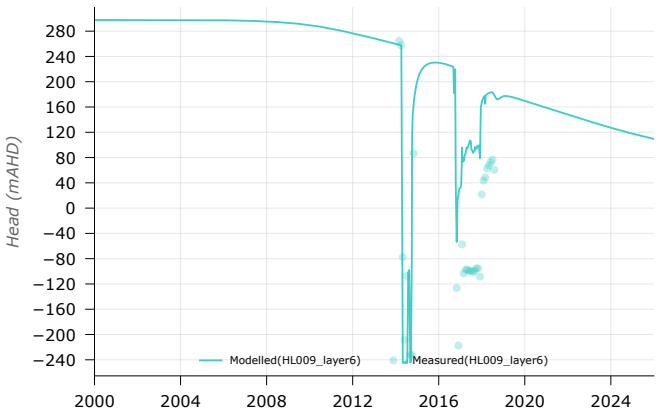

HL005T
Head (mAHD)
Modelled(HL005T_layer15)
Measured(HL005T_layer15)


HL006
Head (mAHD)
Modelled(HL006_layer6)
Measured(HL006_layer6)

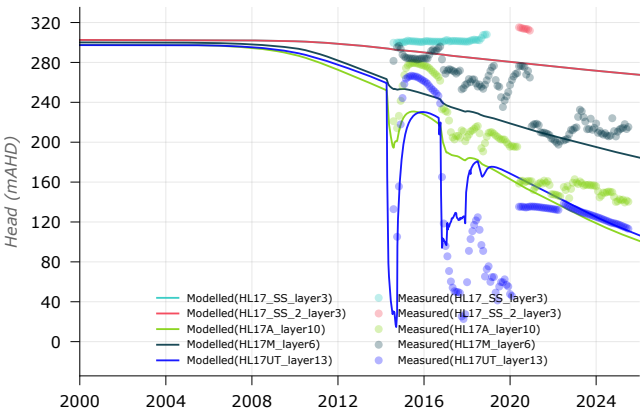

HL007
Head (mAHD)
Modelled(HL007_layer6)
Measured(HL007_layer6)


HL008
Head (mAHD)
Modelled(HL008_layer6)
Measured(HL008_layer6)

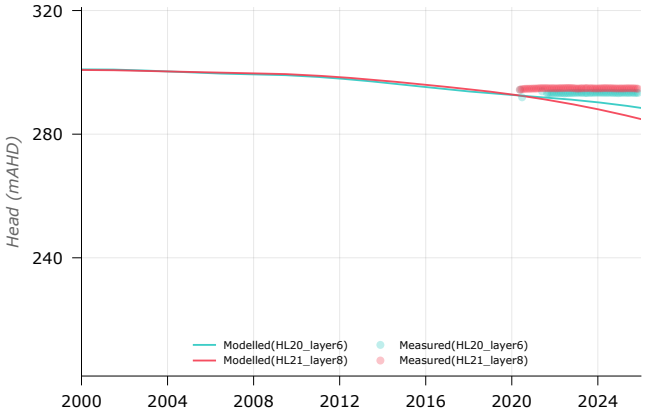
HL009



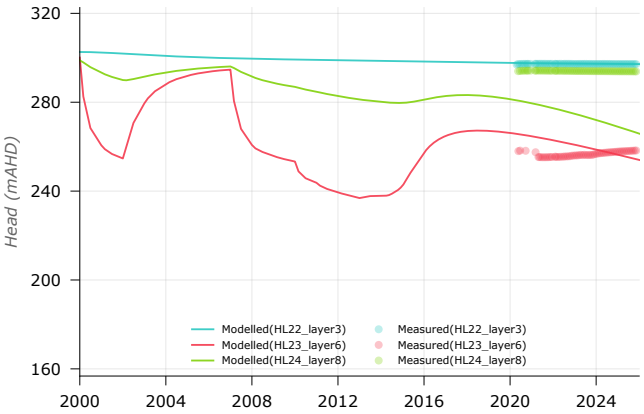
HL17



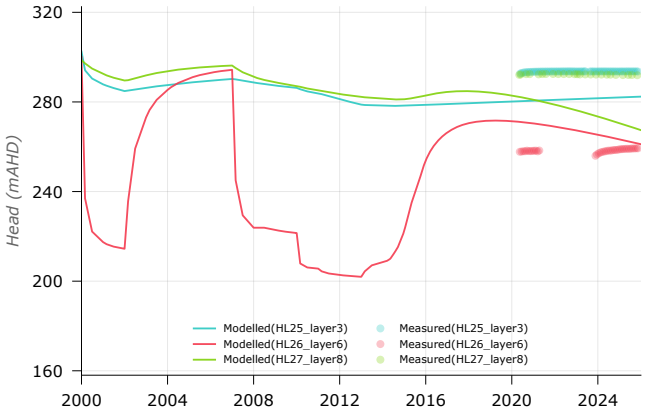
HL20-21



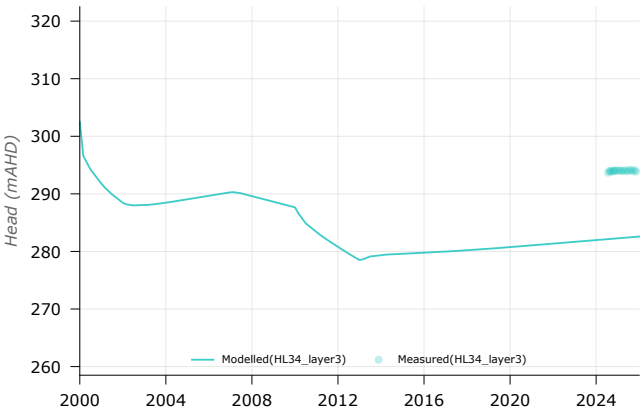
HL22-24



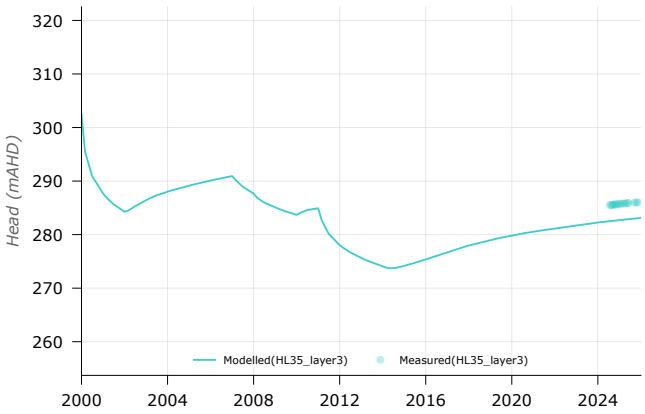
HL25-27



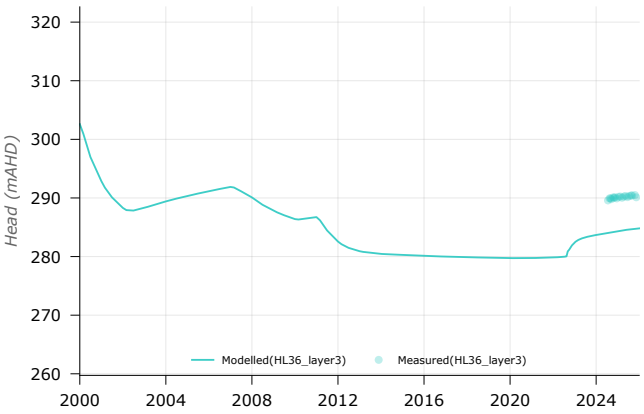
HL34

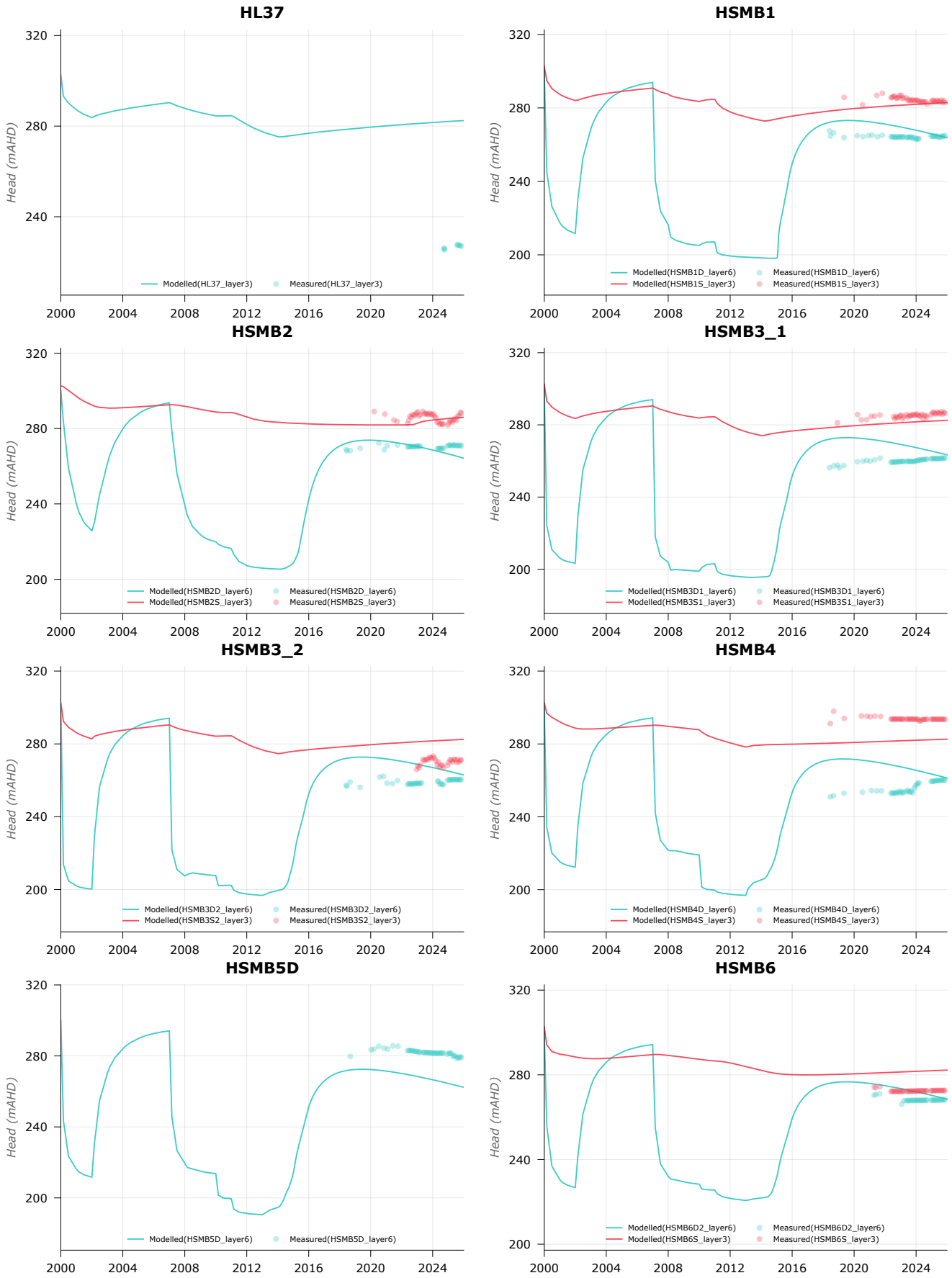


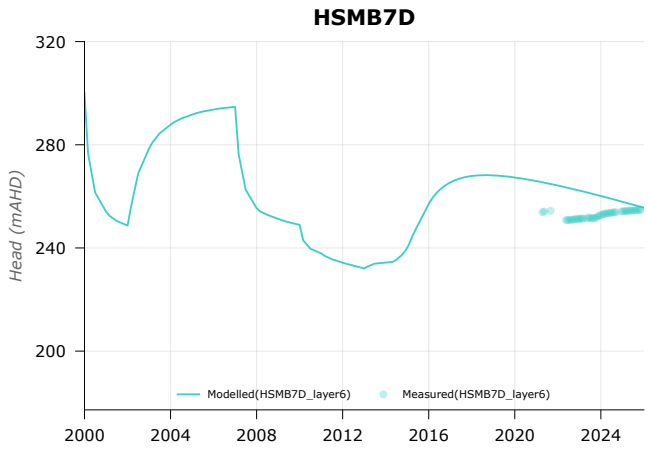
HL35

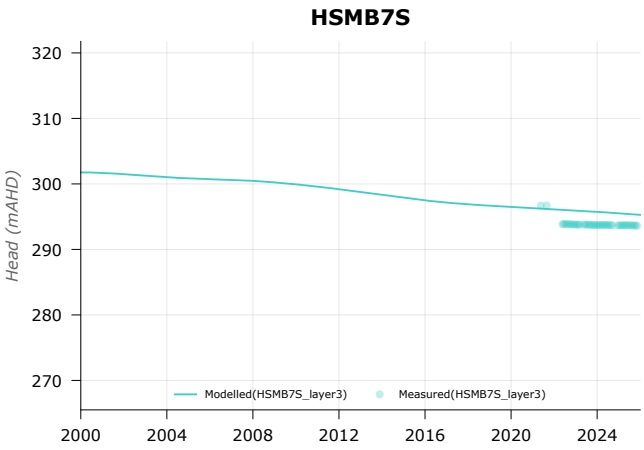


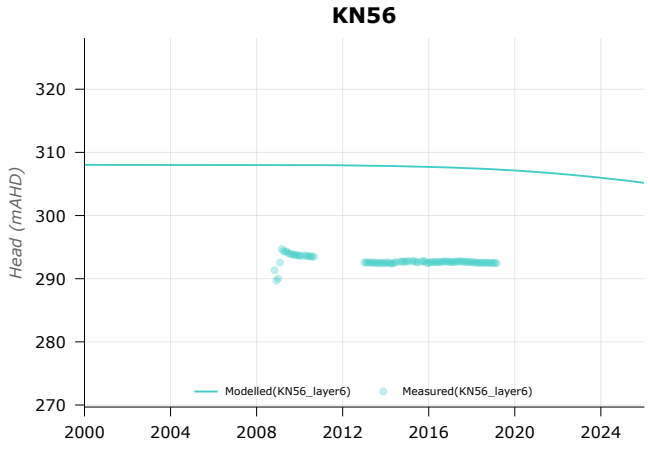
HL36

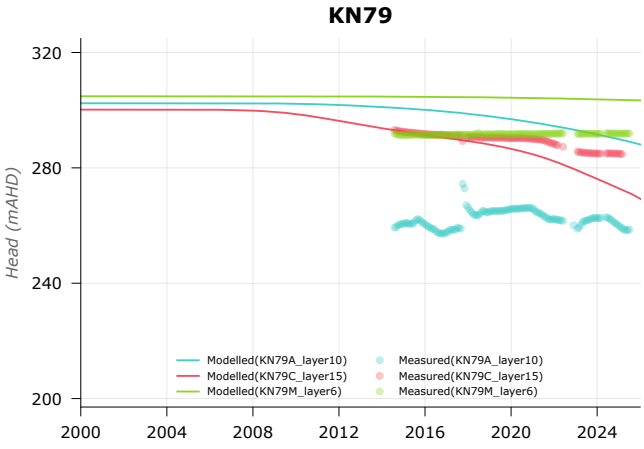


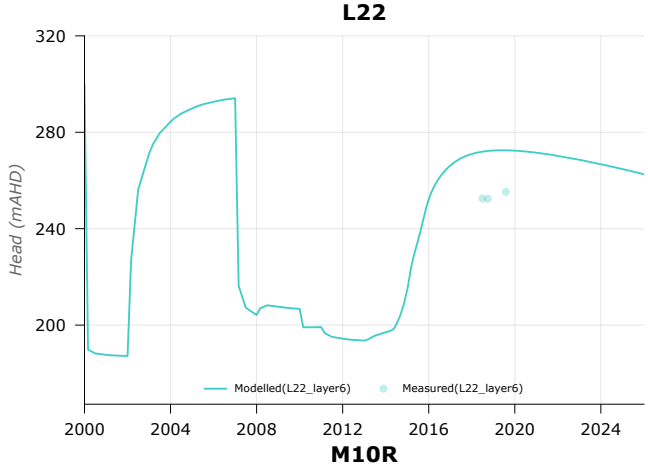

HL37
Head (mAHD)
320
280
240
2000
2004
2008
2012
2016
2020
2024
Modelled(HL37_layer3)
Measured(HL37_layer3)
HSMB1
200
Modelled(HSMB1D_layer6)
Measured(HSMB1D_layer6)
Modelled(HSMB1S_layer3)
Measured(HSMB1S_layer3)
HSMB2
Modelled(HSMB2D_layer6)
Measured(HSMB2D_layer6)
Modelled(HSMB2S_layer3)
Measured(HSMB2S_layer3)
HSMB3_1
Modelled(HSMB3D1_layer6)
Measured(HSMB3D1_layer6)
Modelled(HSMB3S1_layer3)
Measured(HSMB3S1_layer3)
HSMB3_2
Modelled(HSMB3D2_layer6)
Measured(HSMB3D2_layer6)
Modelled(HSMB3S2_layer3)
Measured(HSMB3S2_layer3)
HSMB4
Modelled(HSMB4D_layer6)
Measured(HSMB4D_layer6)
Modelled(HSMB4S_layer3)
Measured(HSMB4S_layer3)
HSMB5D
Modelled(HSMB5D_layer6)
Measured(HSMB5D_layer6)
HSMB6
Modelled(HSMB6D2_layer6)
Measured(HSMB6D2_layer6)
Modelled(HSMB6S_layer3)
Measured(HSMB6S_layer3)

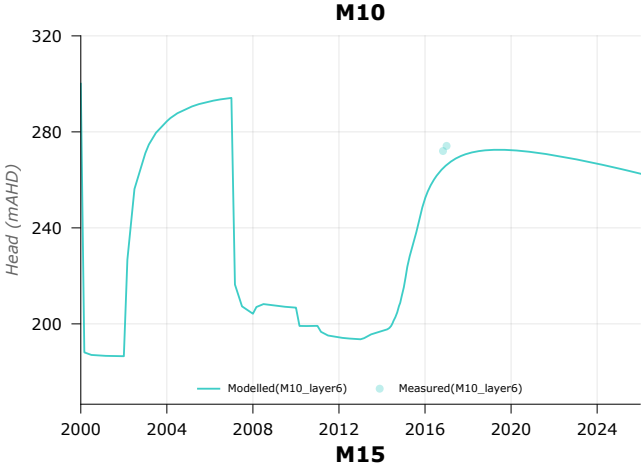

HSMB7D
Head (mAHD)
320
280
240
200
2000
2004
2008
2012
2016
2020
2024
Modelled(HSMB7D_layer6)
Measured(HSMB7D_layer6)

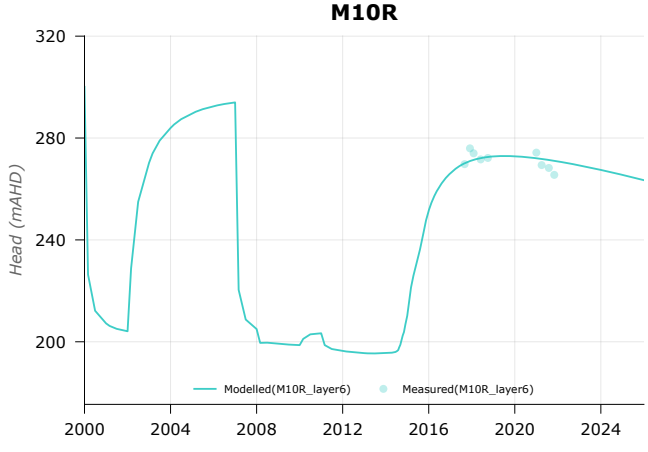

HSMB7S
Head (mAHD)
320
310
300
290
280
270
2000
2004
2008
2012
2016
2020
2024
Modelled(HSMB7S_layer3)
Measured(HSMB7S_layer3)

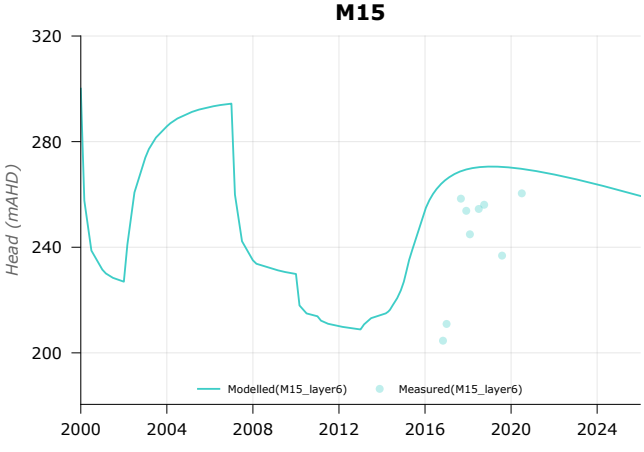

KN56
Head (mAHD)
320
310
300
290
280
270
2000
2004
2008
2012
2016
2020
2024
Modelled(KN56_layer6)
Measured(KN56_layer6)

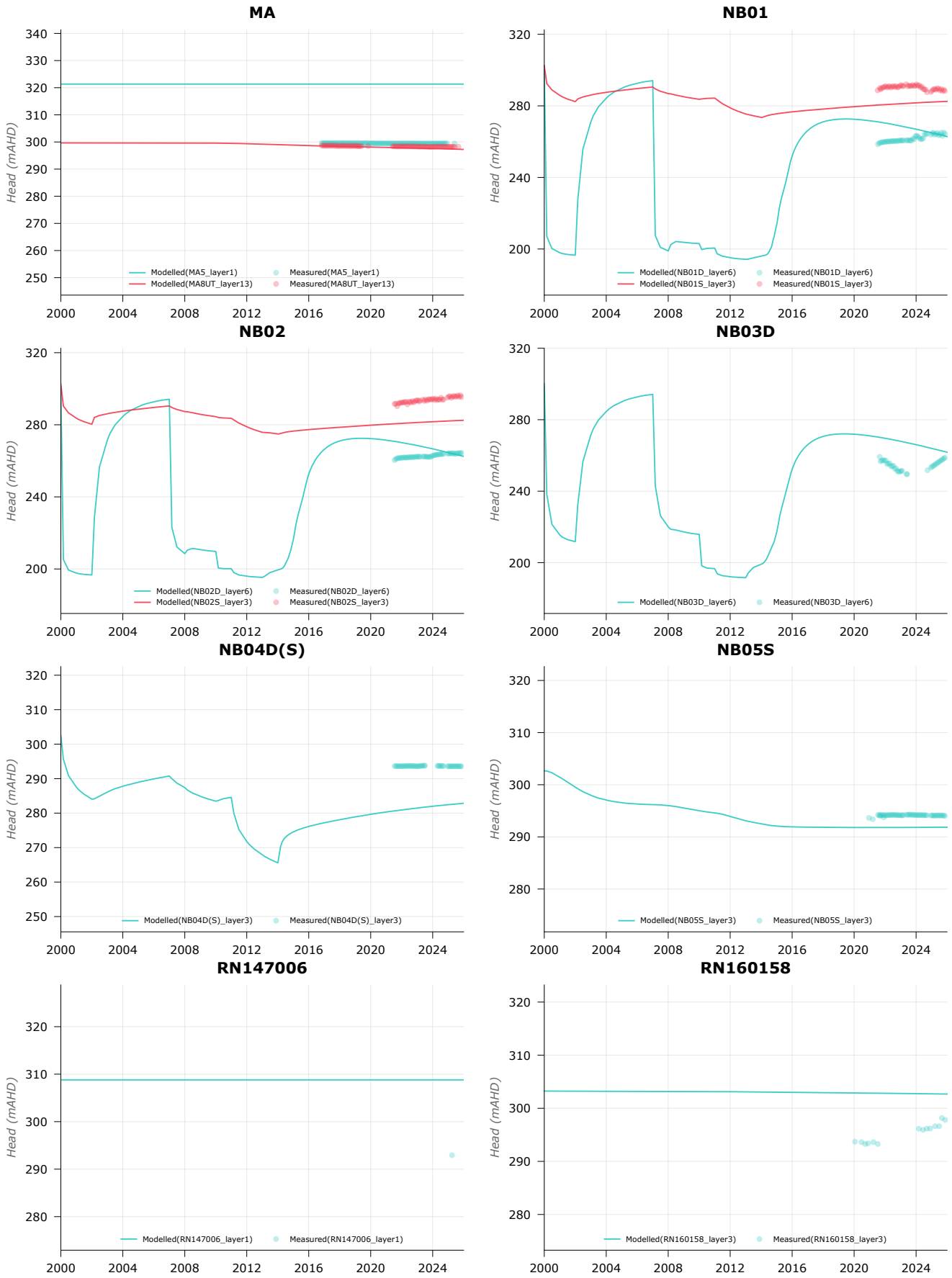

KN79
Head (mAHD)
320
280
240
200
2000
2004
2008
2012
2016
2020
2024
Modelled(KN79A_layer10)
Measured(KN79A_layer10)
Modelled(KN79C_layer15)
Measured(KN79C_layer15)
Modelled(KN79M_layer6)
Measured(KN79M_layer6)

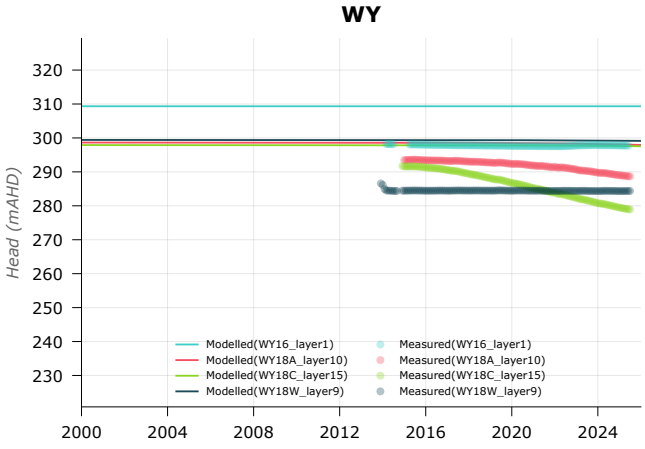

L22
Head (mAHD)
320
280
240
200
2000
2004
2008
2012
2016
2020
2024
Modelled(L22_layer6)
Measured(L22_layer6)


M10
Head (mAHD)
320
280
240
200
2000
2004
2008
2012
2016
2020
2024
Modelled(M10_layer6)
Measured(M10_layer6)


M10R
Head (mAHD)
320
280
240
200
2000
2004
2008
2012
2016
2020
2024
Modelled(M10R_layer6)
Measured(M10R_layer6)

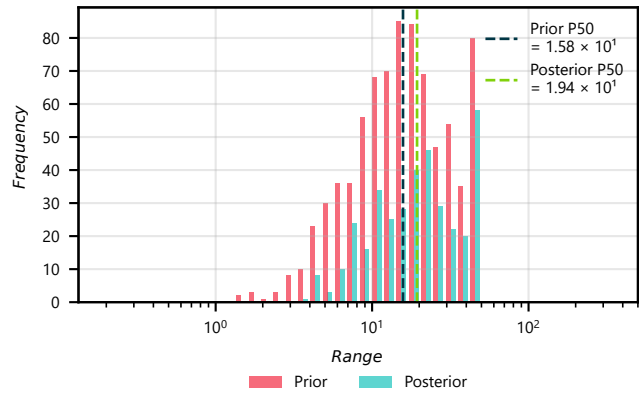

M15
Head (mAHD)
320
280
240
200
2000
2004
2008
2012
2016
2020
2024
Modelled(M15_layer6)
Measured(M15_layer6)


MA
Head (mAHD)
Modelled(MA5_layer1)
Measured(MA5_layer1)
Modelled(MA8UT_layer13)
Measured(MA8UT_layer13)
NB01
Modelled(NB01D_layer6)
Measured(NB01D_layer6)
Modelled(NB01S_layer3)
Measured(NB01S_layer3)
NB02
Modelled(NB02D_layer6)
Measured(NB02D_layer6)
Modelled(NB02S_layer3)
Measured(NB02S_layer3)
NB03D
Modelled(NB03D_layer6)
Measured(NB03D_layer6)
NB04D(S)
Modelled(NB04D(S)_layer3)
Measured(NB04D(S)_layer3)
NB05S
Modelled(NB05S_layer3)
Measured(NB05S_layer3)
RN147006
Modelled(RN147006_layer1)
Measured(RN147006_layer1)
RN160158
Modelled(RN160158_layer3)
Measured(RN160158_layer3)

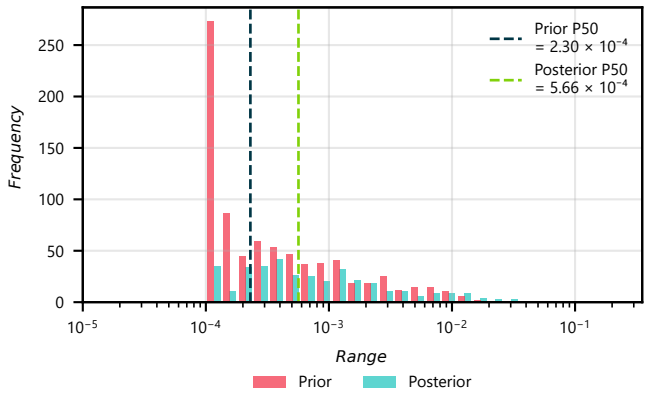

WY
Head (mAHD)
320
310
300
290
280
270
260
250
240
230
2000
2004
2008
2012
2016
2020
2024
Modelled(WY16_layer1)
Modelled(WY18A_layer10)
Modelled(WY18C_layer15)
Modelled(WY18W_layer9)
Measured(WY16_layer1)
Measured(WY18A_layer10)
Measured(WY18C_layer15)
Measured(WY18W_layer9)

Appendix B. Median prior and posterior parameter distributions

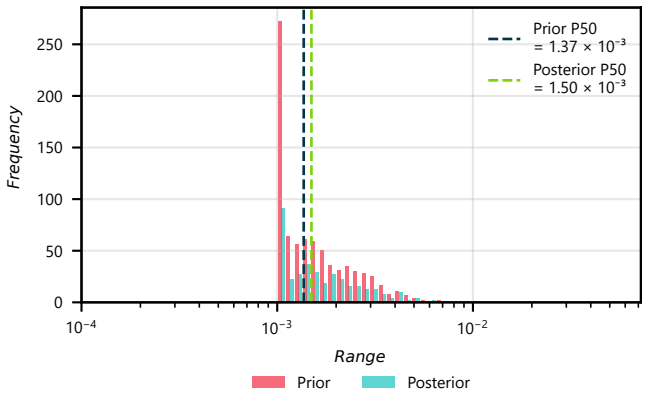
Kh:CondamineAlv



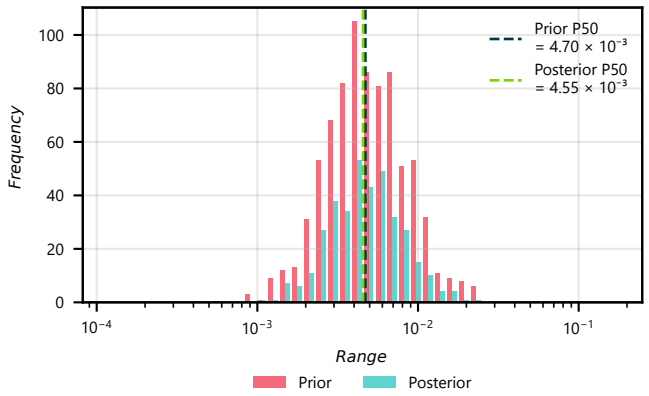
Kh:Gubb.Sst



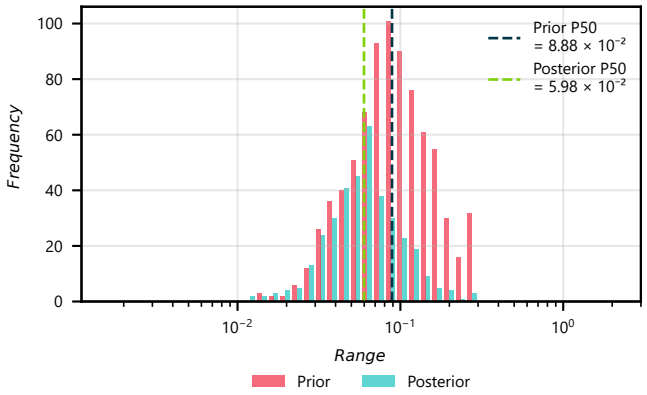
Kh:WestbourneFm



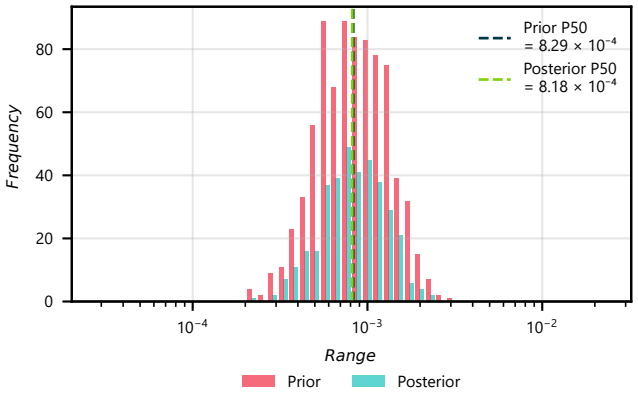
Kh:SpringbokSst



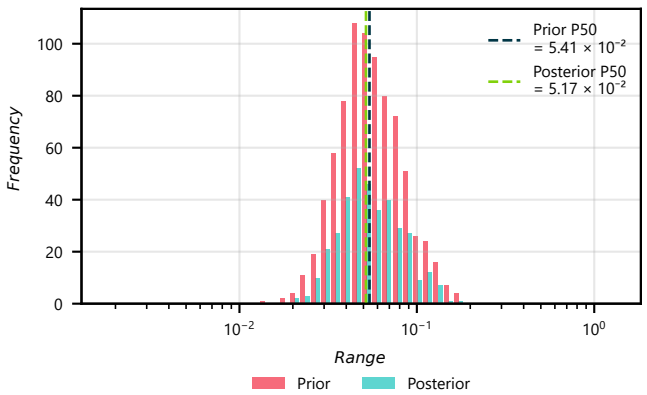
Kh:KoganC



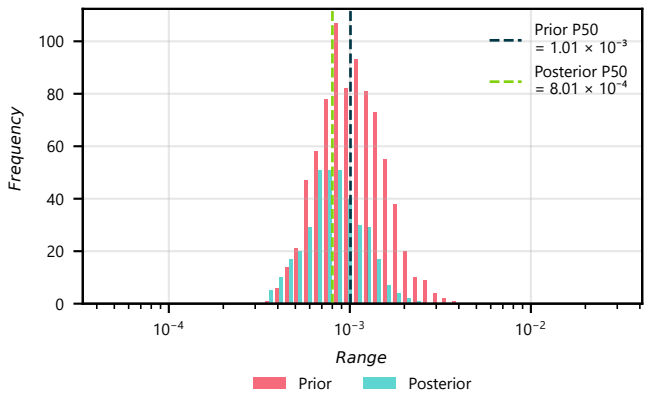
Kh:KoganIB

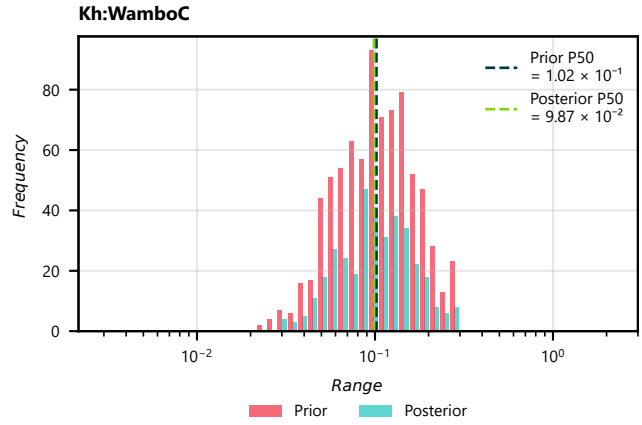


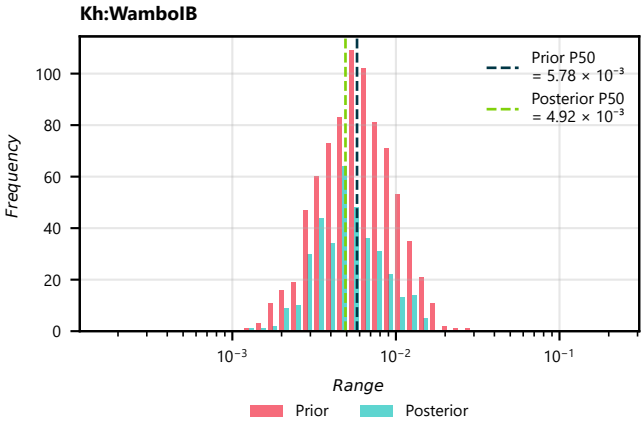
Kh:MacalisterC

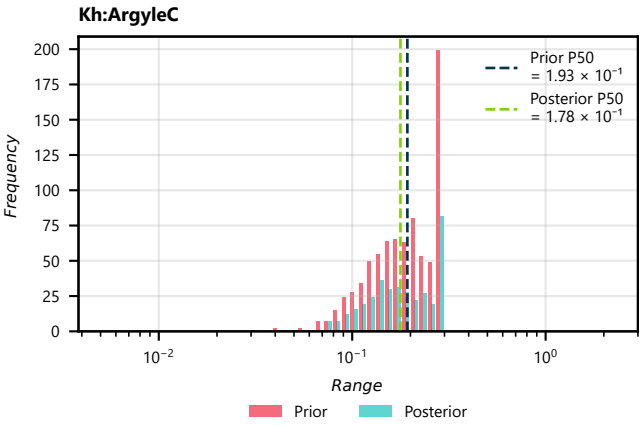


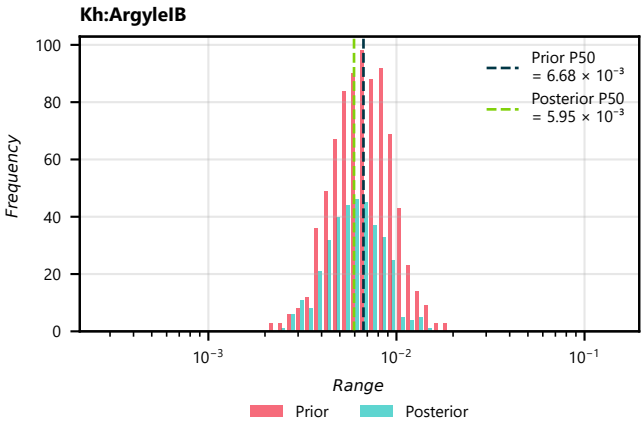
Kh:MacalisterIB

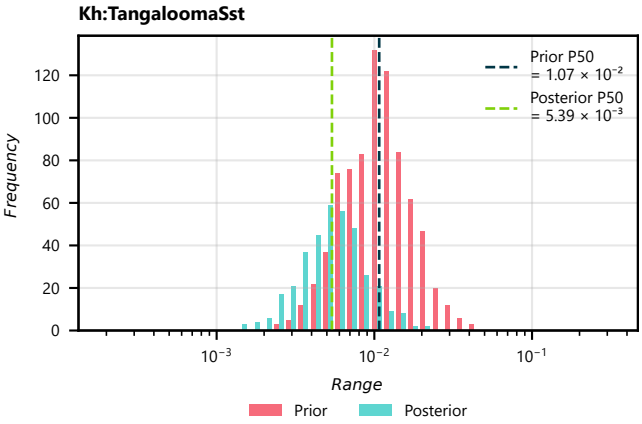


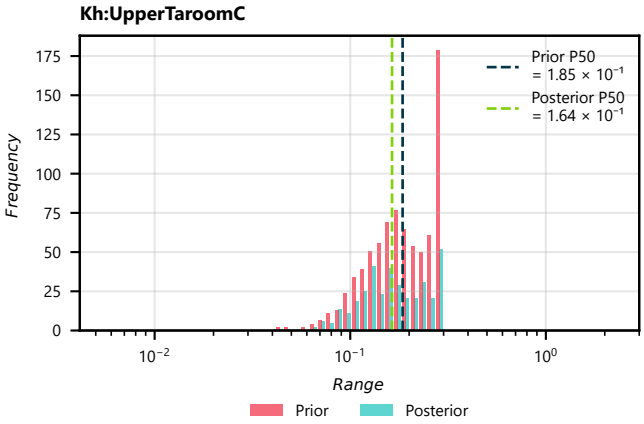

Kh:WamboC
Prior P50
= 1.02 × 10⁻¹
Posterior P50
= 9.87 × 10⁻²
Frequency
Range
Prior
Posterior

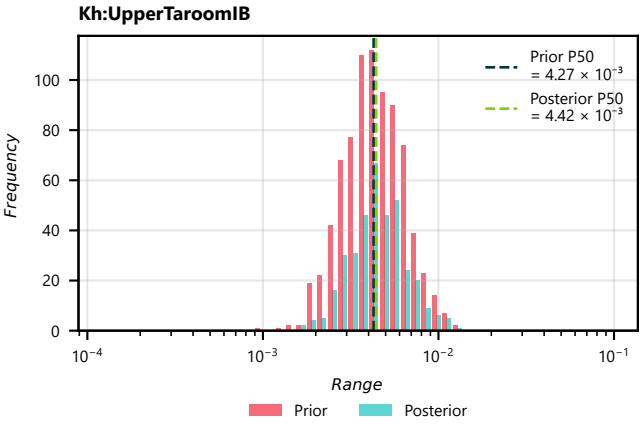

Kh:WamboIB
Prior P50
= 5.78 × 10⁻³
Posterior P50
= 4.92 × 10⁻³
Frequency
Range
Prior
Posterior

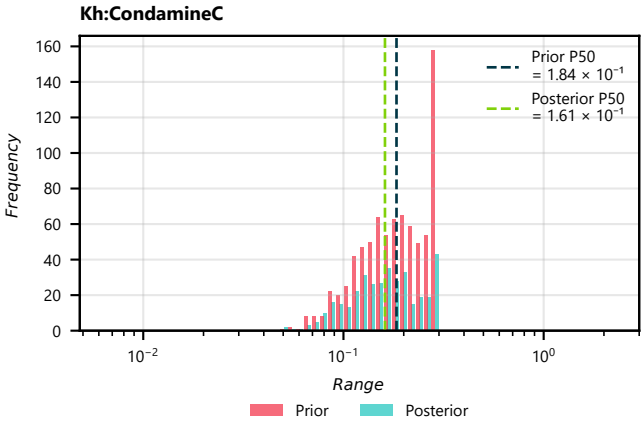

Kh:ArgyleC
Prior P50
= 1.93 × 10⁻¹
Posterior P50
= 1.78 × 10⁻¹
Frequency
Range
Prior
Posterior

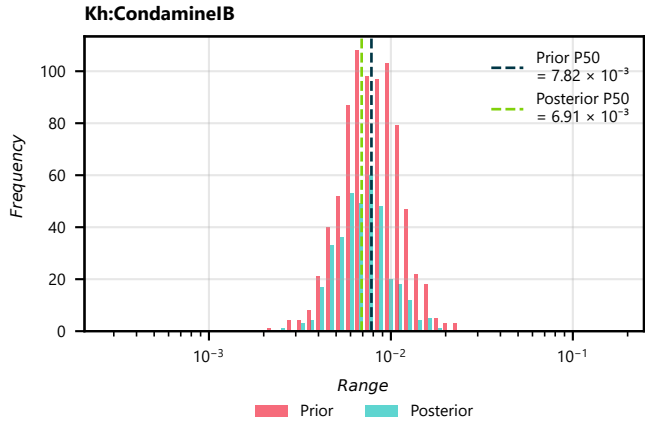

Kh:ArgyleIB
Prior P50
= 6.68 × 10⁻³
Posterior P50
= 5.95 × 10⁻³
Frequency
Range
Prior
Posterior

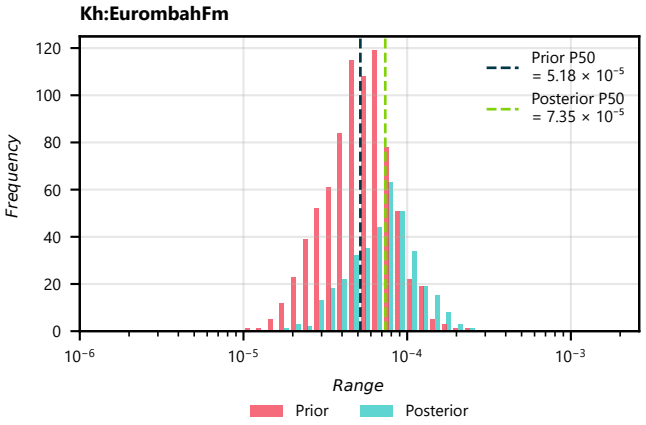

Kh:TangaloomaSst
Prior P50
= 1.07 × 10⁻²
Posterior P50
= 5.39 × 10⁻³
Frequency
Range
Prior
Posterior

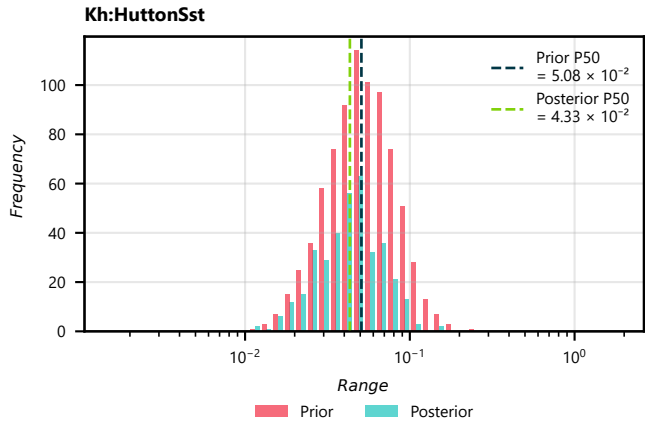

Kh:UpperTaroomC
Prior P50
= 1.85 × 10⁻¹
Posterior P50
= 1.64 × 10⁻¹
Frequency
Range
Prior
Posterior

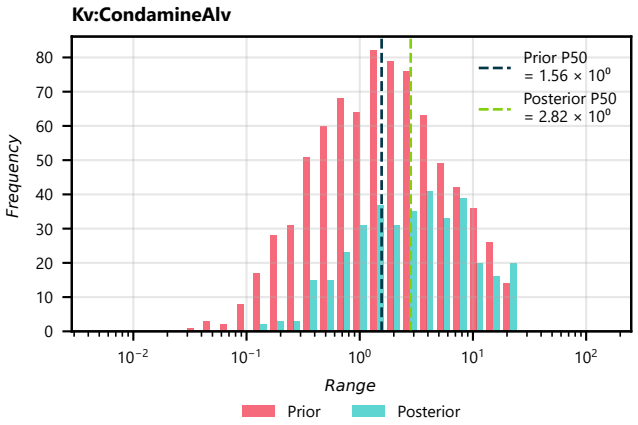

Kh:UpperTaroomIB
Prior P50
= 4.27 × 10⁻³
Posterior P50
= 4.42 × 10⁻³
Frequency
Range
Prior
Posterior

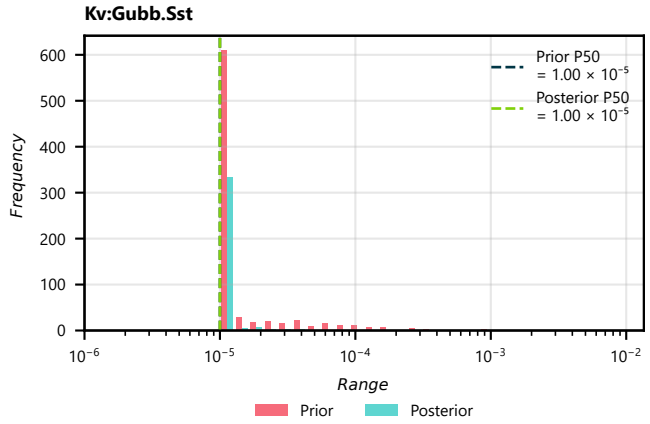

Kh:CondamineC
Prior P50
= 1.84 × 10⁻¹
Posterior P50
= 1.61 × 10⁻¹
Frequency
Range
Prior
Posterior

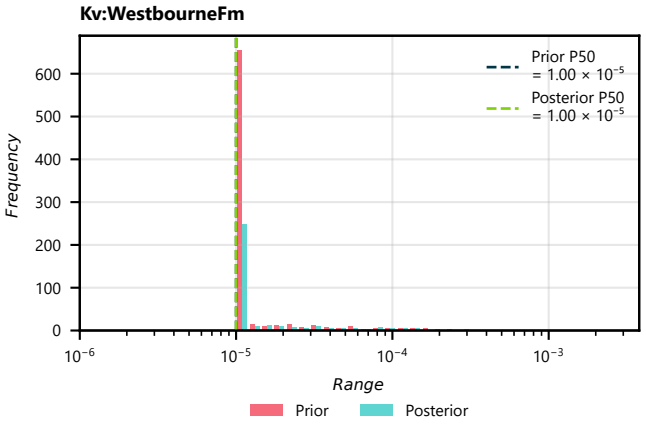

Kh:CondamineIB
Prior P50
= 7.82 × 10⁻³
Posterior P50
= 6.91 × 10⁻³
Frequency
Range
Prior
Posterior

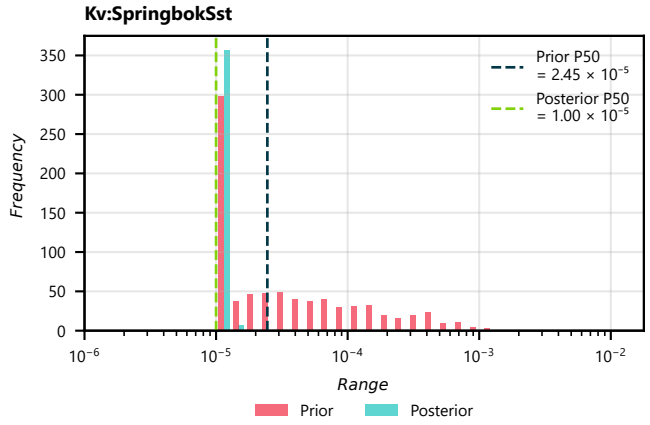

Kh:EurombahFm
Prior P50
= 5.18 × 10⁻⁵
Posterior P50
= 7.35 × 10⁻⁵
Frequency
Range
Prior
Posterior

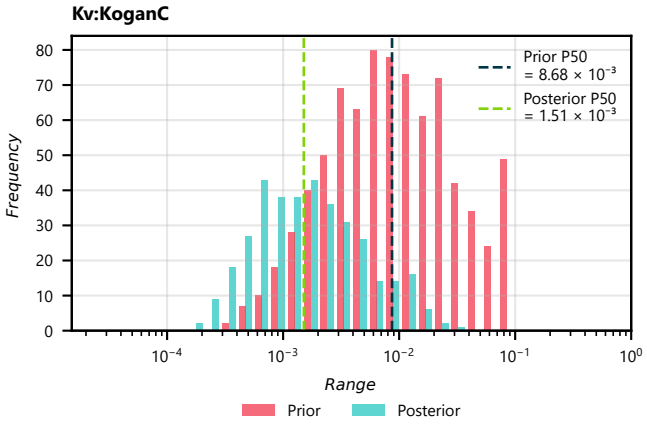

Kh:HuttonSst
Prior P50
= 5.08 × 10⁻²
Posterior P50
= 4.33 × 10⁻²
Frequency
Range
Prior
Posterior


Kv:CondamineAlv
Prior P50
= 1.56 × 10⁰
Posterior P50
= 2.82 × 10⁰
Frequency
Range
Prior
Posterior

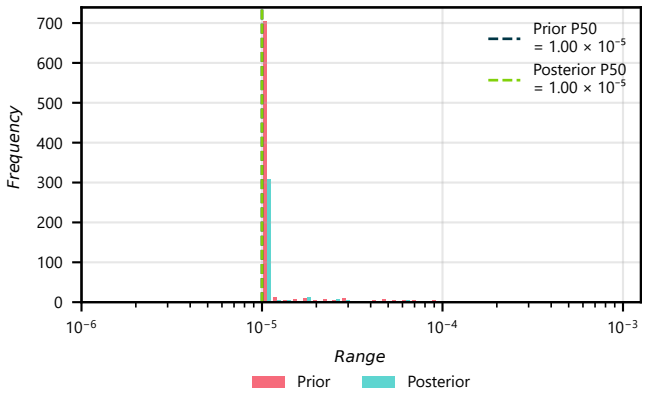

Kv:Gubb.Sst
Prior P50
= 1.00 × 10⁻⁵
Posterior P50
= 1.00 × 10⁻⁵
Frequency
Range
Prior
Posterior


Kv:WestbourneFm
Prior P50
= 1.00 × 10⁻⁵
Posterior P50
= 1.00 × 10⁻⁵
Frequency
Range
Prior
Posterior

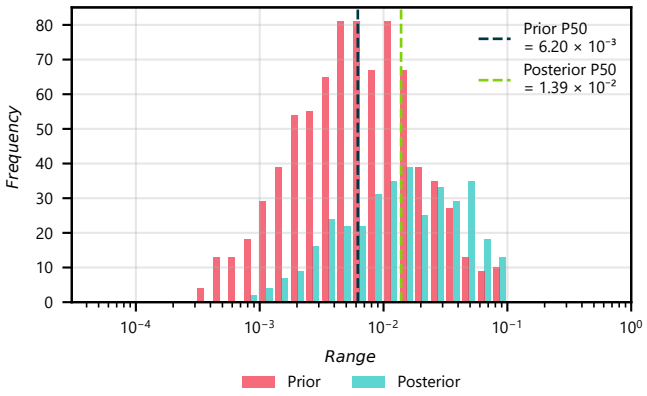

Kv:SpringbokSst
Prior P50
= 2.45 × 10⁻⁵
Posterior P50
= 1.00 × 10⁻⁵
Frequency
Range
Prior
Posterior


Kv:KoganC
Prior P50
= 8.68 × 10⁻³
Posterior P50
= 1.51 × 10⁻³
Frequency
Range
Prior
Posterior

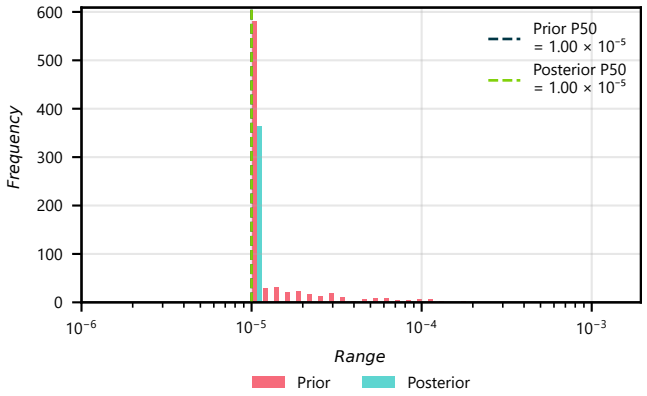
Kv:KoganIB



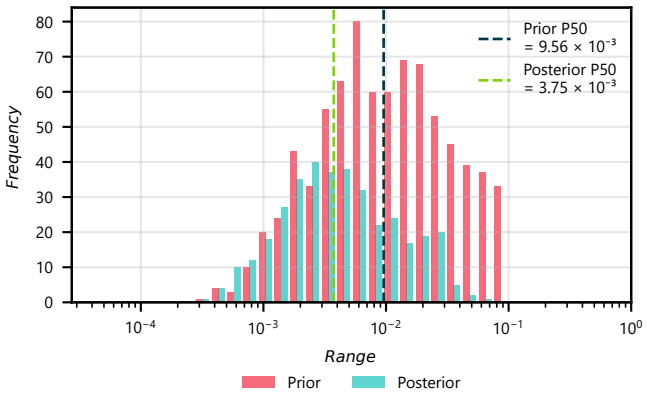
Kv:MacalisterC



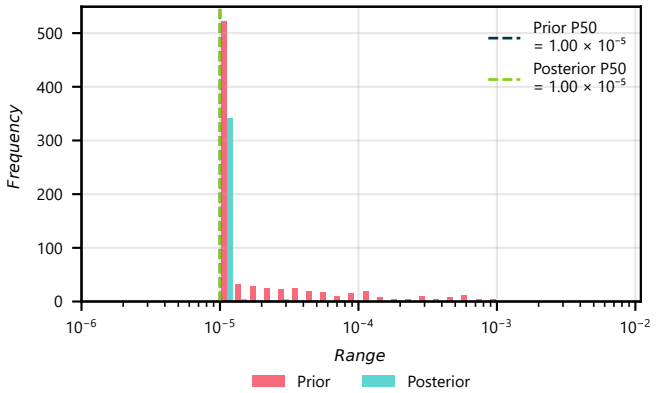
Kv:MacalisterIB



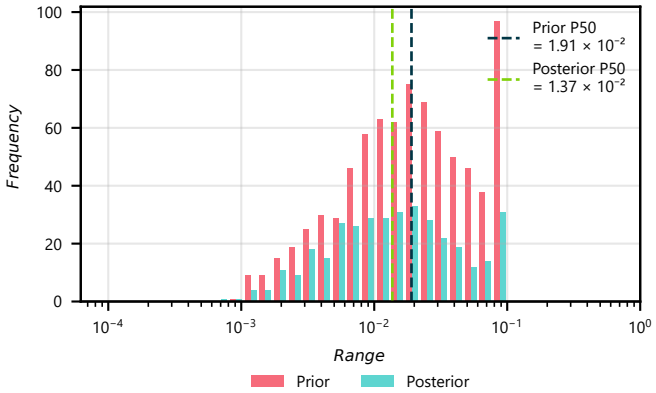
Kv:WamboC



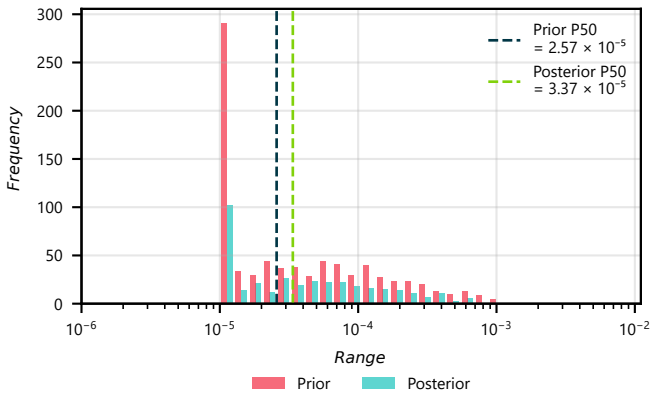
Kv:WamboIB



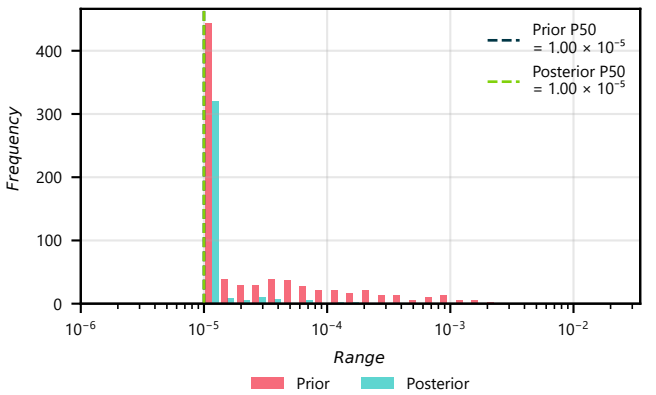
Kv:ArgyleC

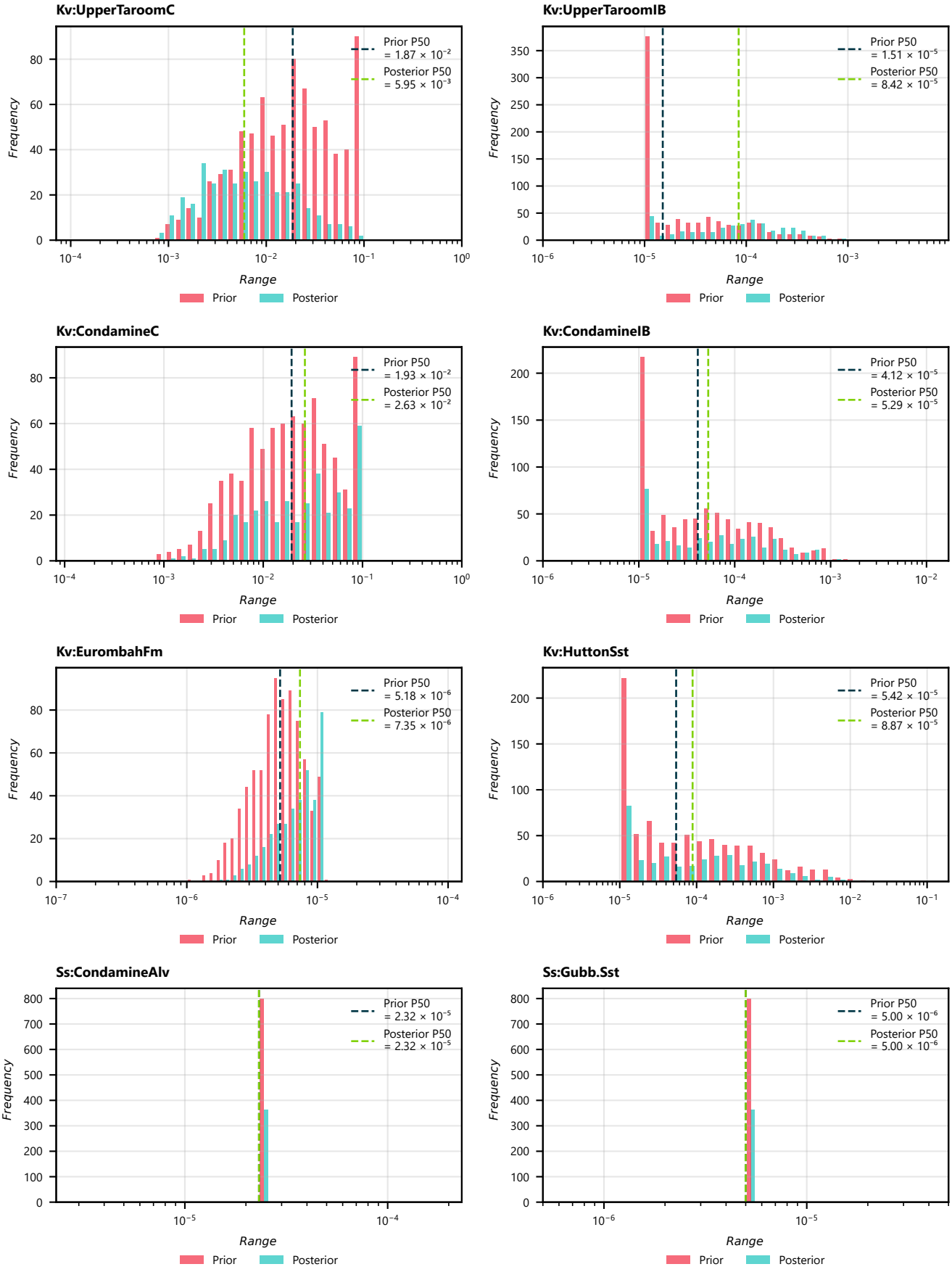


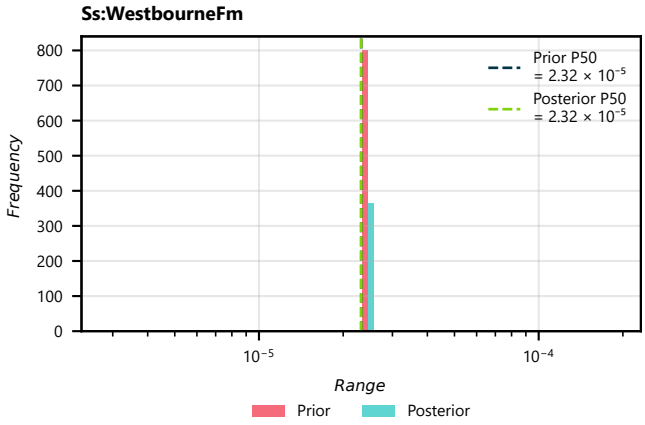
Kv:ArgyleIB

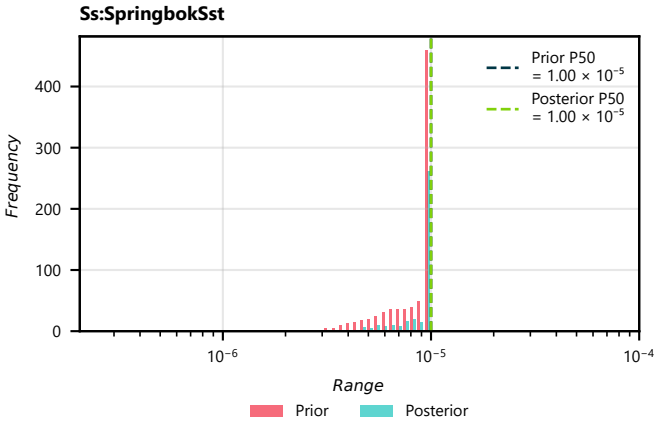


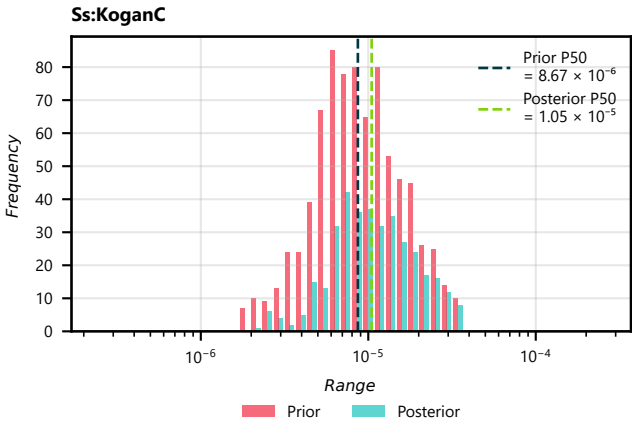
Kv:TangaloomaSst

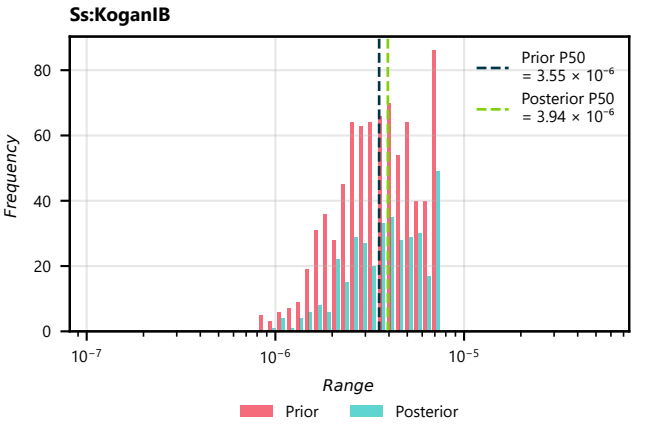


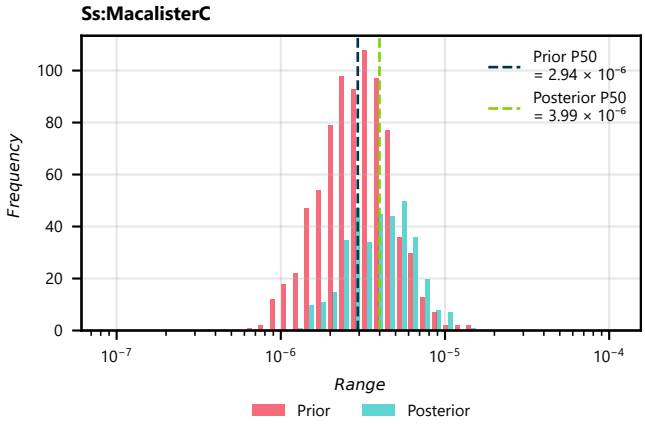

Kv:UpperTaroomC
Prior P50 = 1.87 × 10⁻²
Posterior P50 = 5.95 × 10⁻³
Kv:UpperTaroomIB
Prior P50 = 1.51 × 10⁻⁵
Posterior P50 = 8.42 × 10⁻⁵
Kv:CondamineC
Prior P50 = 1.93 × 10⁻²
Posterior P50 = 2.63 × 10⁻²
Kv:CondamineIB
Prior P50 = 4.12 × 10⁻⁵
Posterior P50 = 5.29 × 10⁻⁵
Kv:EurombahFm
Prior P50 = 5.18 × 10⁻⁶
Posterior P50 = 7.35 × 10⁻⁶
Kv:HuttonSst
Prior P50 = 5.42 × 10⁻⁵
Posterior P50 = 8.87 × 10⁻⁵
Ss:CondamineAlv
Prior P50 = 2.32 × 10⁻⁵
Posterior P50 = 2.32 × 10⁻⁵
Ss:Gubb.Sst
Prior P50 = 5.00 × 10⁻⁶
Posterior P50 = 5.00 × 10⁻⁶
Frequency
Range
Prior
Posterior

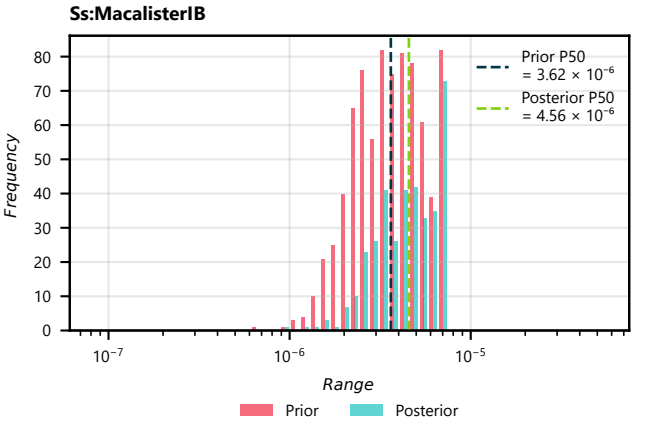

Ss:WestbourneFm
Prior P50
= 2.32 × 10⁻⁵
Posterior P50
= 2.32 × 10⁻⁵
Frequency
Range
Prior
Posterior

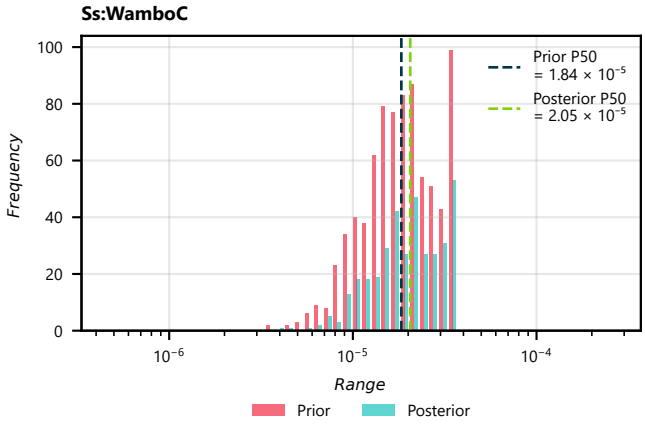

Ss:SpringbokSst
Prior P50
= 1.00 × 10⁻⁵
Posterior P50
= 1.00 × 10⁻⁵
Frequency
Range
Prior
Posterior

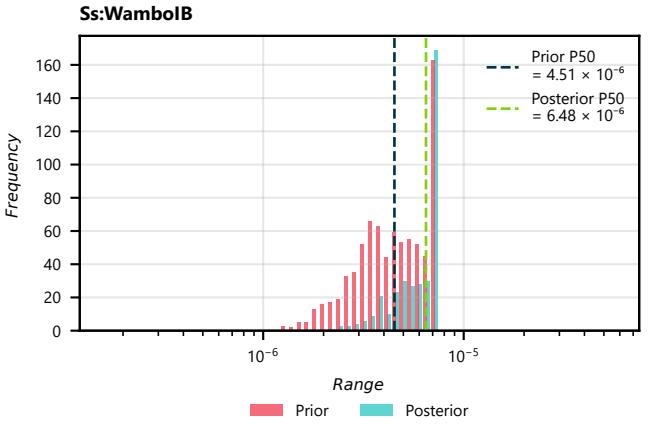

Ss:KoganC
Prior P50
= 8.67 × 10⁻⁶
Posterior P50
= 1.05 × 10⁻⁵
Frequency
Range
Prior
Posterior


Ss:KoganIB
Prior P50
= 3.55 × 10⁻⁶
Posterior P50
= 3.94 × 10⁻⁶
Frequency
Range
Prior
Posterior

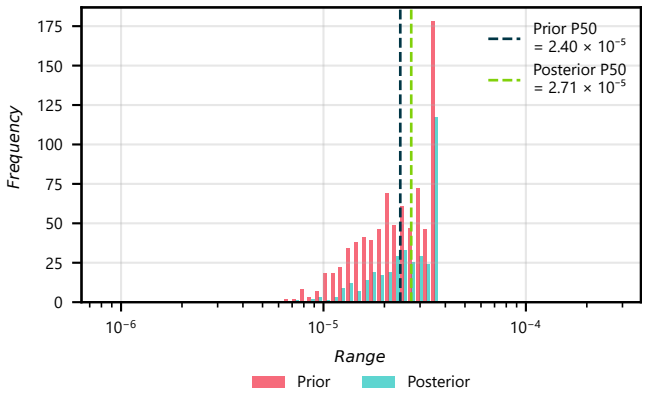

Ss:MacalisterC
Prior P50
= 2.94 × 10⁻⁶
Posterior P50
= 3.99 × 10⁻⁶
Frequency
Range
Prior
Posterior


Ss:MacalisterIB
Prior P50
= 3.62 × 10⁻⁶
Posterior P50
= 4.56 × 10⁻⁶
Frequency
Range
Prior
Posterior

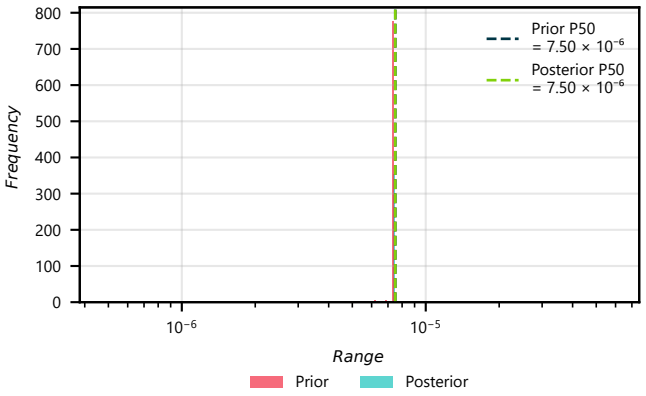

Ss:WamboC
Prior P50
= 1.84 × 10⁻⁵
Posterior P50
= 2.05 × 10⁻⁵
Frequency
Range
Prior
Posterior


Ss:WamboIB
Prior P50
= 4.51 × 10⁻⁶
Posterior P50
= 6.48 × 10⁻⁶
Frequency
Range
Prior
Posterior

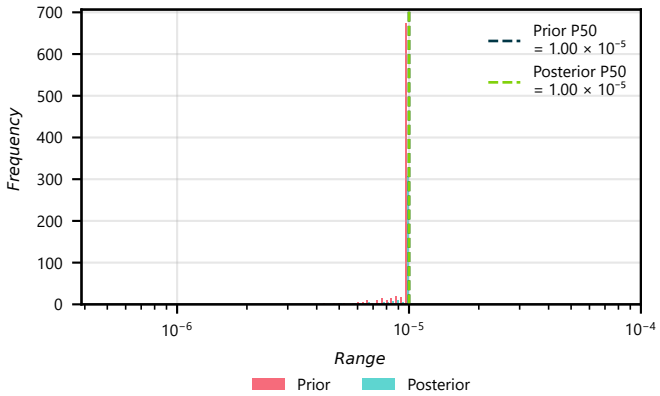
Ss:ArgyleC



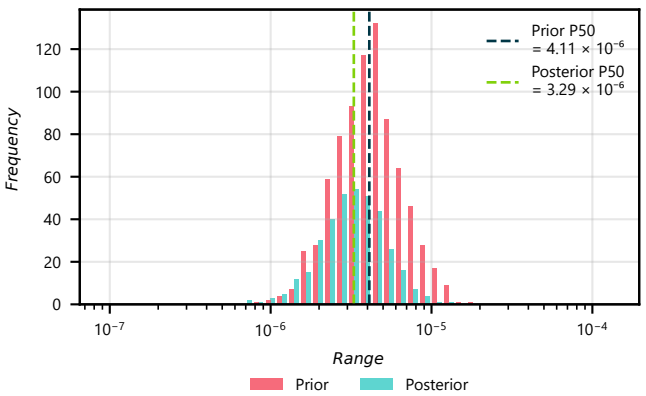
Ss:ArgyleIB



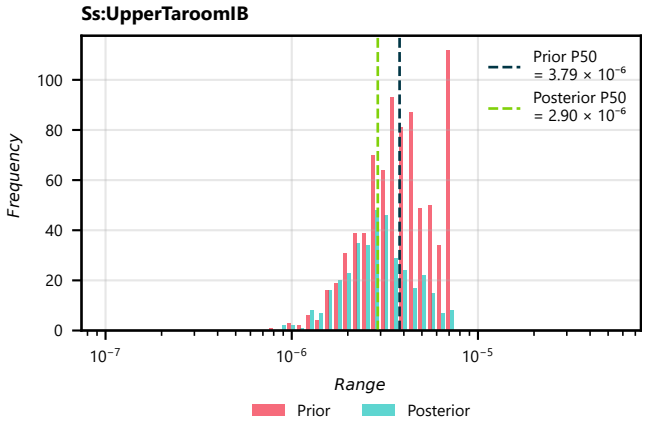
Ss:TangaloomaSst



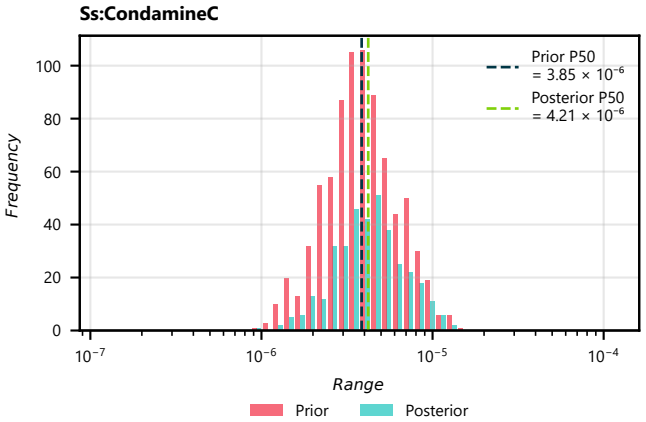
Ss:UpperTaroomC



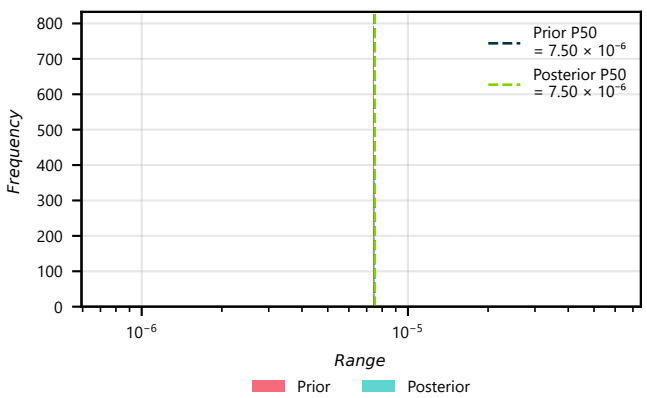
Ss:UpperTaroomIB



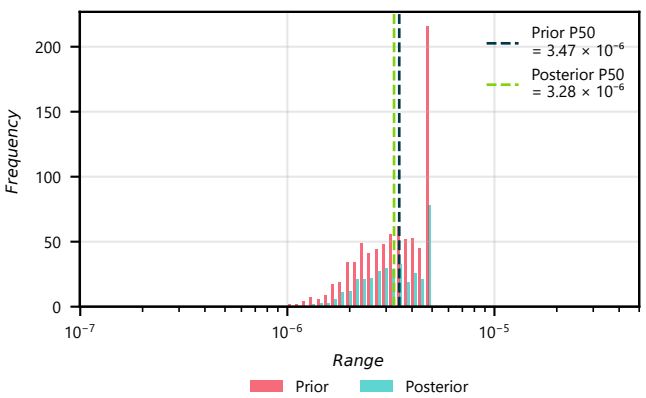
Ss:CondamineC

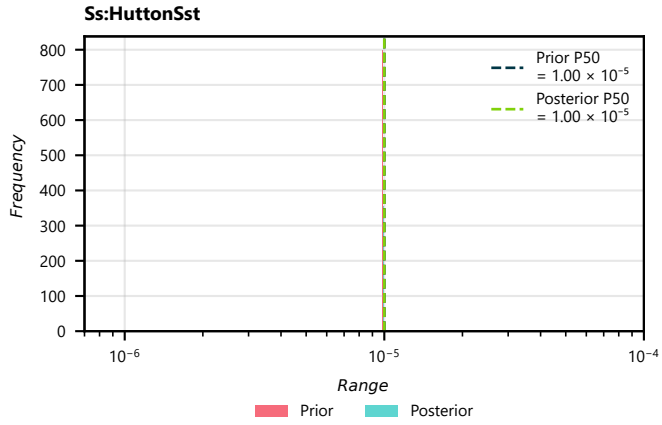


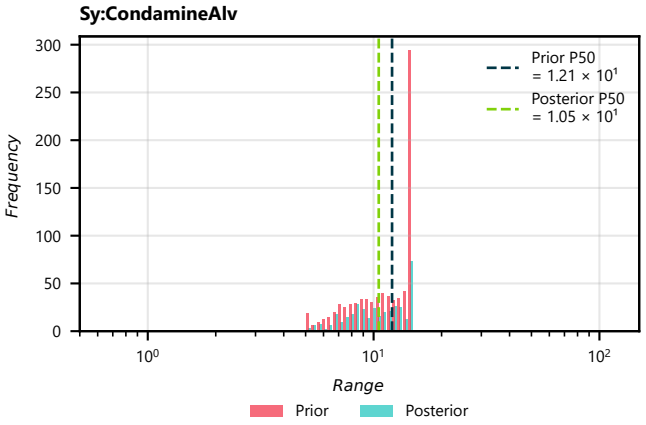
Ss:CondamineIB

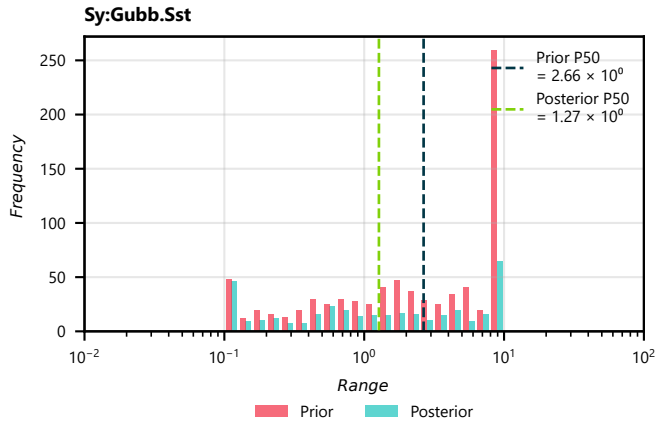


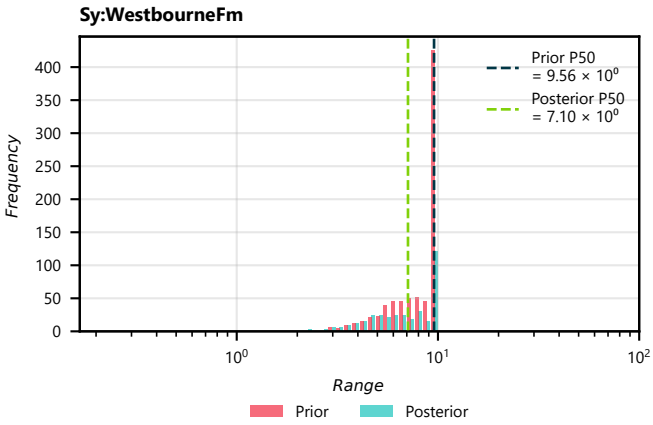
Ss:EurombahFm

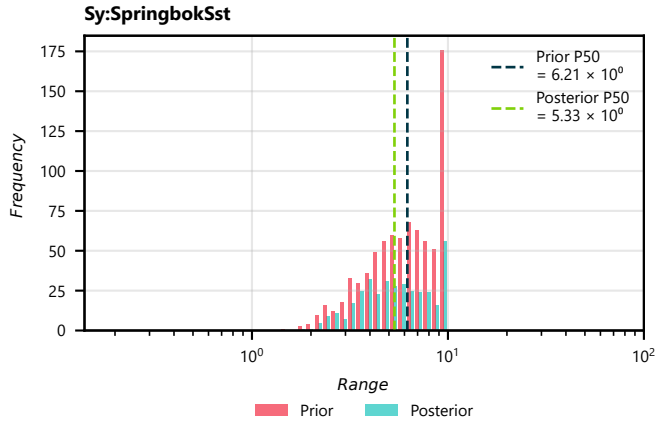


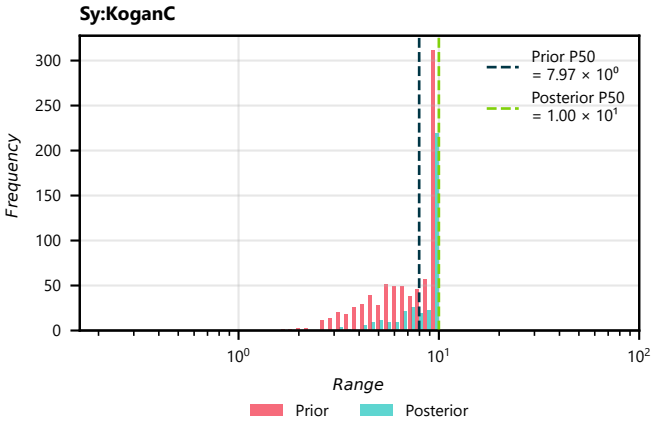

Ss:HuttonSst
Prior P50
= 1.00 × 10⁻⁵
Posterior P50
= 1.00 × 10⁻⁵
Frequency
Range
Prior
Posterior

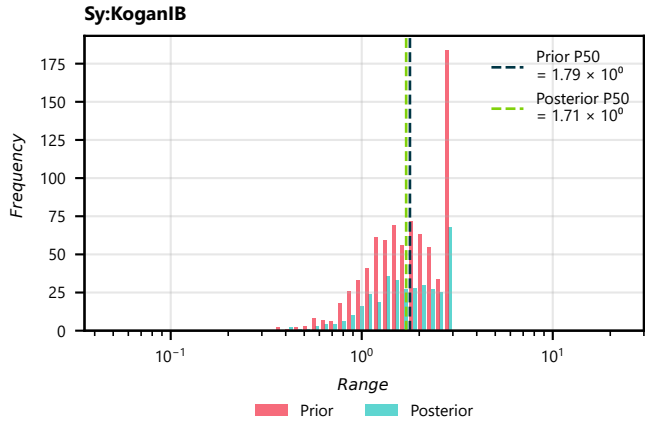

Sy:CondamineAlv
Prior P50
= 1.21 × 10¹
Posterior P50
= 1.05 × 10¹
Frequency
Range
Prior
Posterior

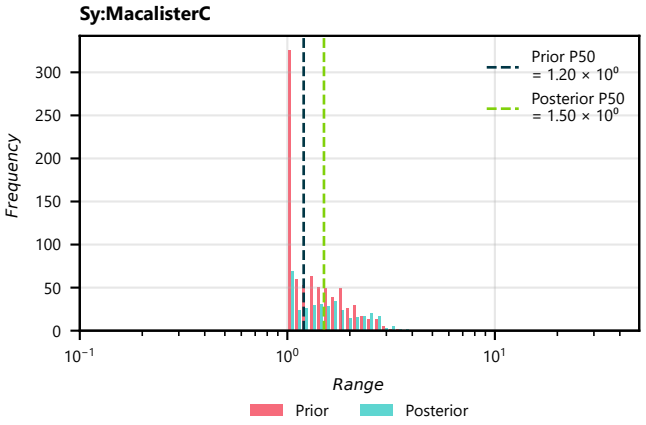

Sy:Gubb.Sst
Prior P50
= 2.66 × 10⁰
Posterior P50
= 1.27 × 10⁰
Frequency
Range
Prior
Posterior


Sy:WestbourneFm
Prior P50
= 9.56 × 10⁰
Posterior P50
= 7.10 × 10⁰
Frequency
Range
Prior
Posterior

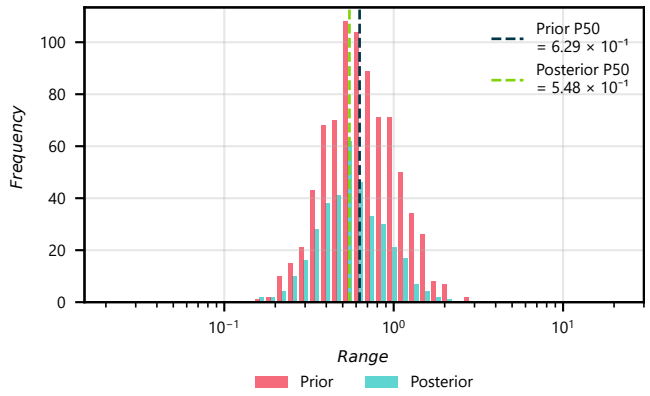

Sy:SpringbokSst
Prior P50
= 6.21 × 10⁰
Posterior P50
= 5.33 × 10⁰
Frequency
Range
Prior
Posterior


Sy:KoganC
Prior P50
= 7.97 × 10⁰
Posterior P50
= 1.00 × 10¹
Frequency
Range
Prior
Posterior

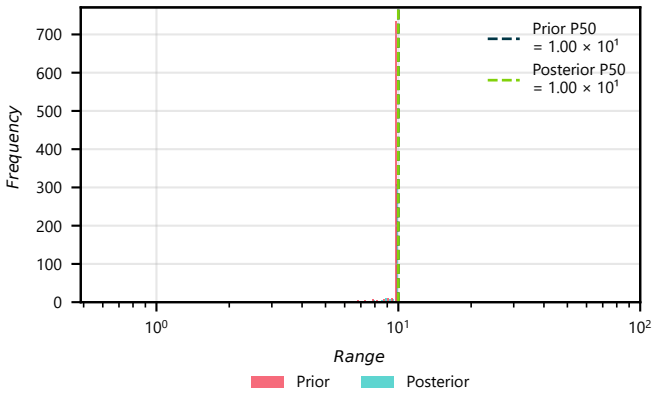

Sy:KoganIB
Prior P50
= 1.79 × 10⁰
Posterior P50
= 1.71 × 10⁰
Frequency
Range
Prior
Posterior


Sy:MacalisterC
Prior P50
= 1.20 × 10⁰
Posterior P50
= 1.50 × 10⁰
Frequency
Range
Prior
Posterior

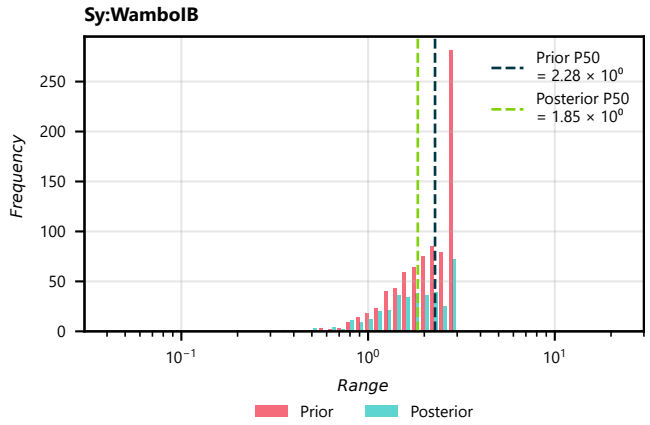
Sy:MacalisterIB



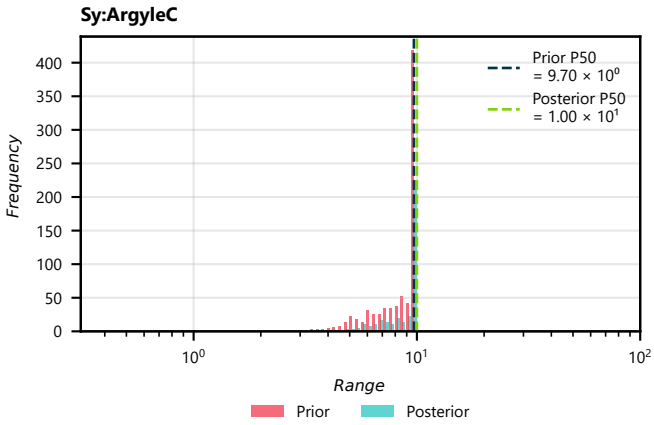
Sy:WamboC



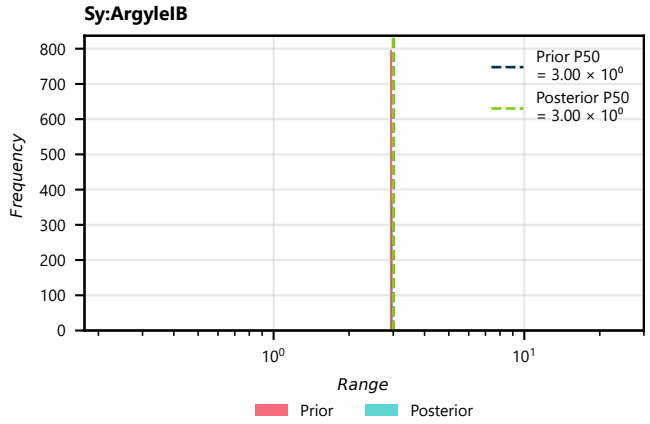
Sy:WamboIB



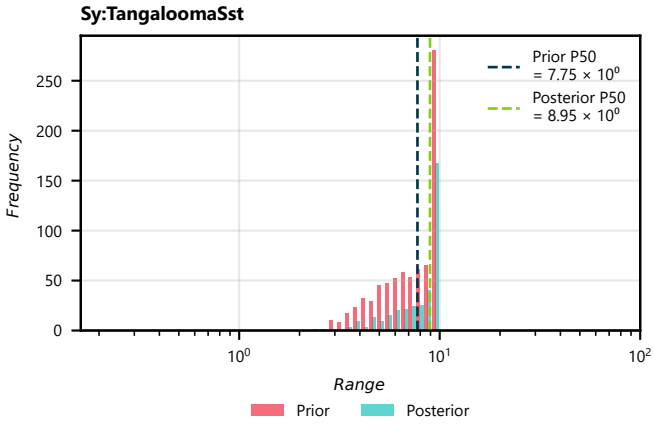
Sy:ArgyleC



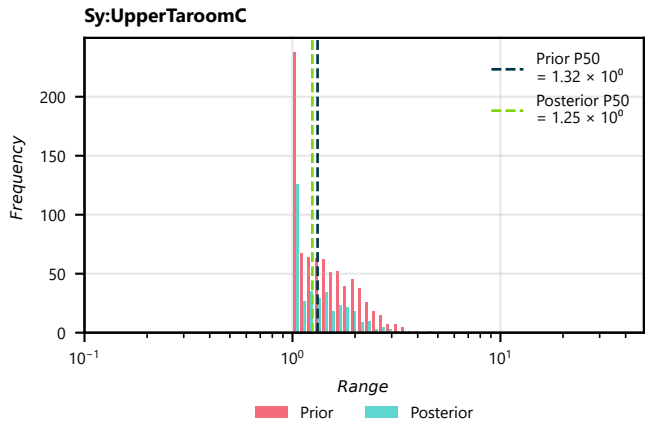
Sy:ArgyleIB



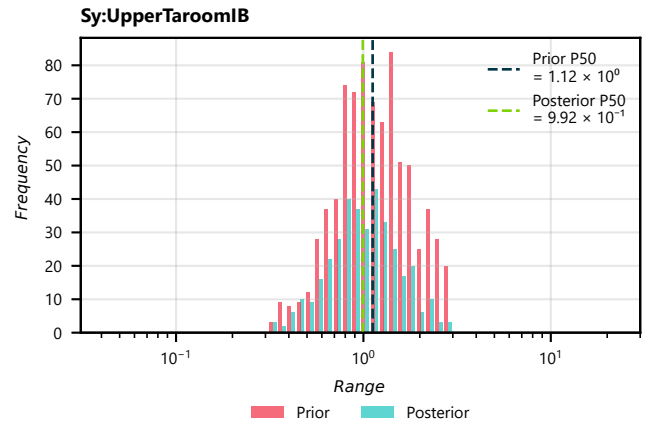
Sy:TangaloomaSst



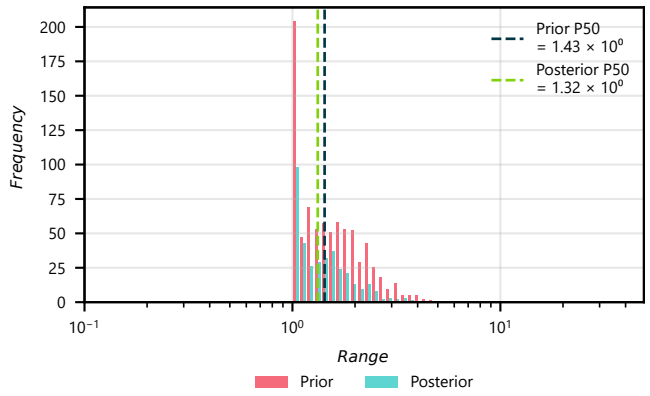
Sy:UpperTaroomC



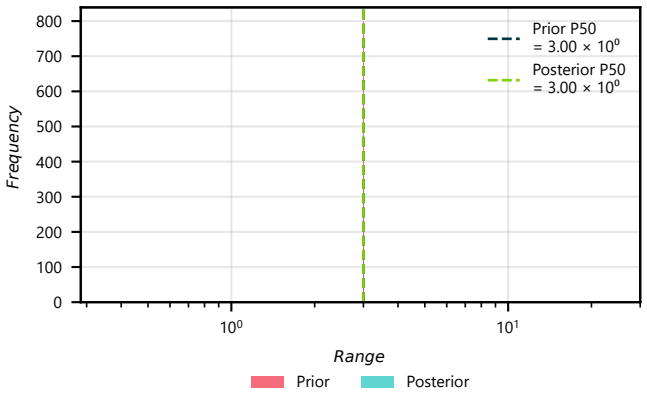
Sy:UpperTaroomIB



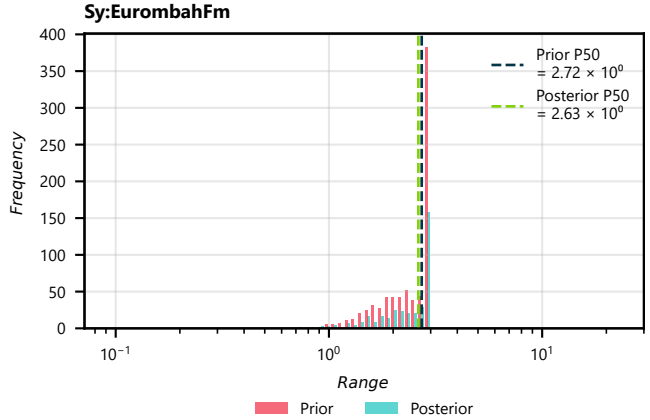
Sy:CondamineC



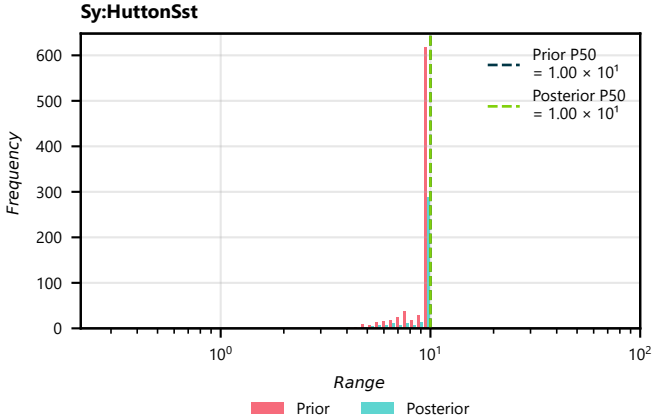
Sy:CondamineIB

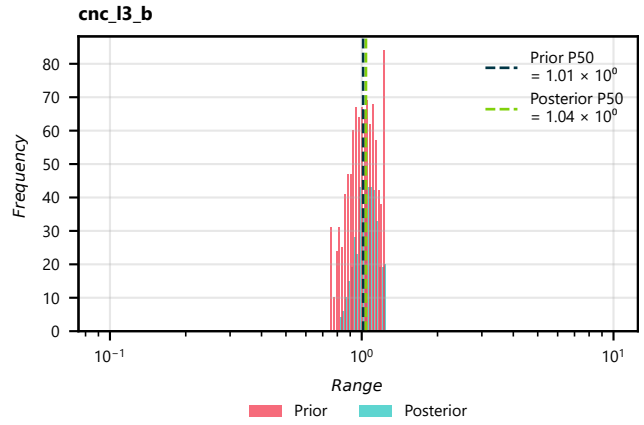


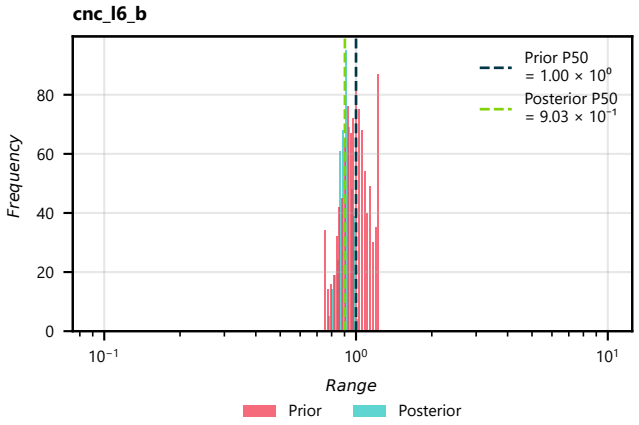
Sy:EurombahFm

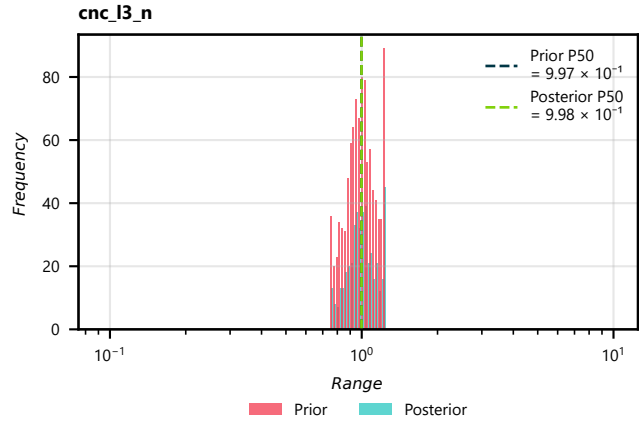


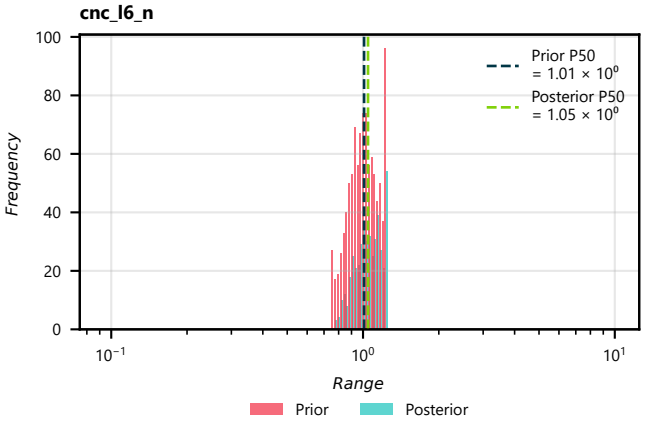
Sy:HuttonSst

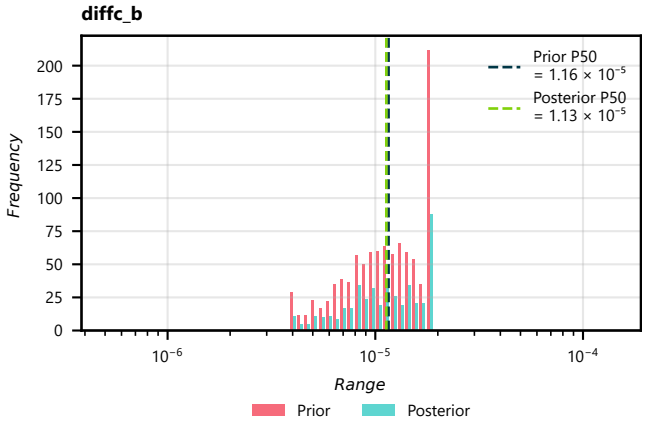


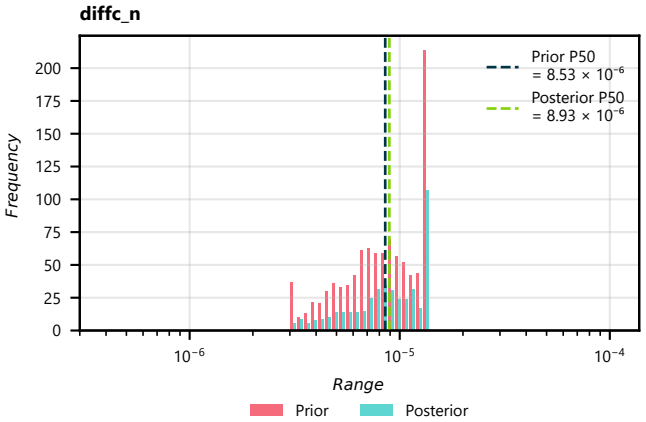

cnc_l3_b
Prior P50
= 1.01 × 10⁰
Posterior P50
= 1.04 × 10⁰
Frequency
Range
Prior
Posterior

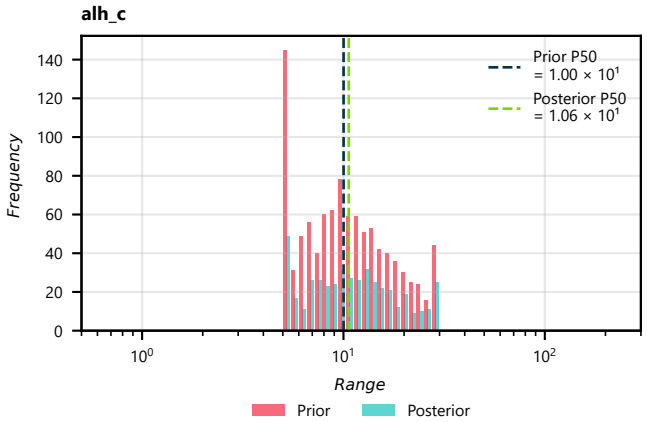

cnc_l6_b
Prior P50
= 1.00 × 10⁰
Posterior P50
= 9.03 × 10⁻¹
Frequency
Range
Prior
Posterior

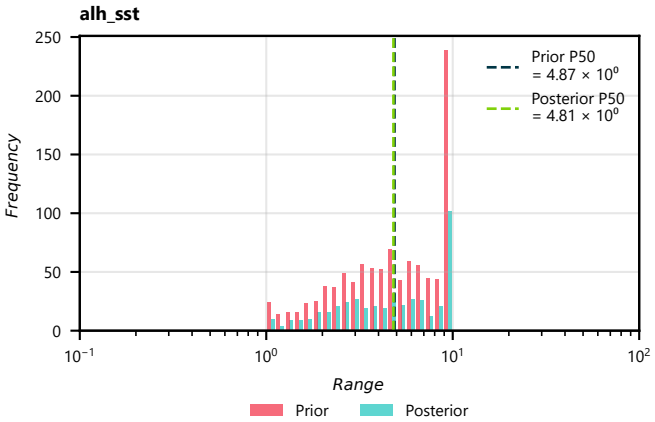

cnc_l3_n
Prior P50
= 9.97 × 10⁻¹
Posterior P50
= 9.98 × 10⁻¹
Frequency
Range
Prior
Posterior

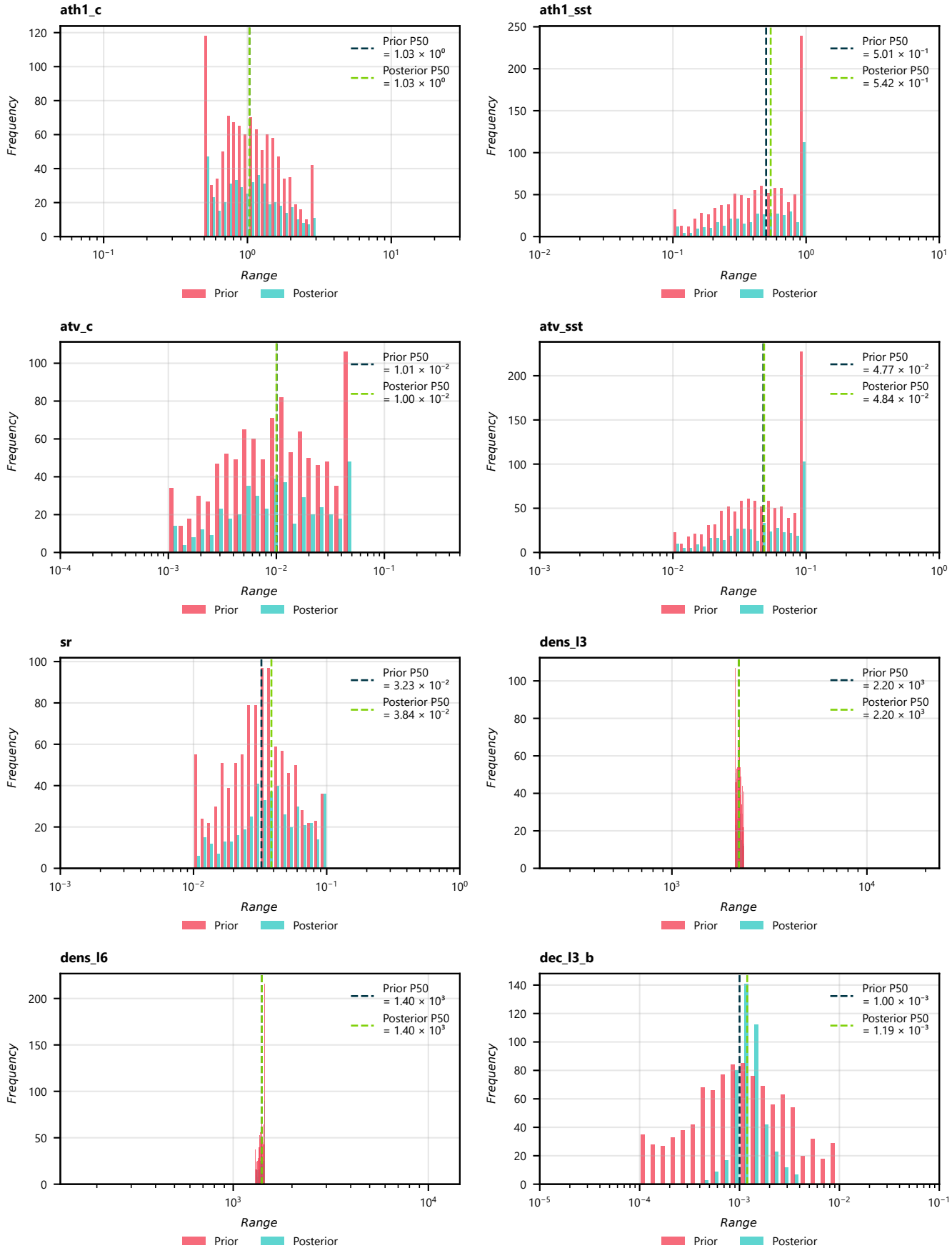

cnc_l6_n
Prior P50
= 1.01 × 10⁰
Posterior P50
= 1.05 × 10⁰
Frequency
Range
Prior
Posterior

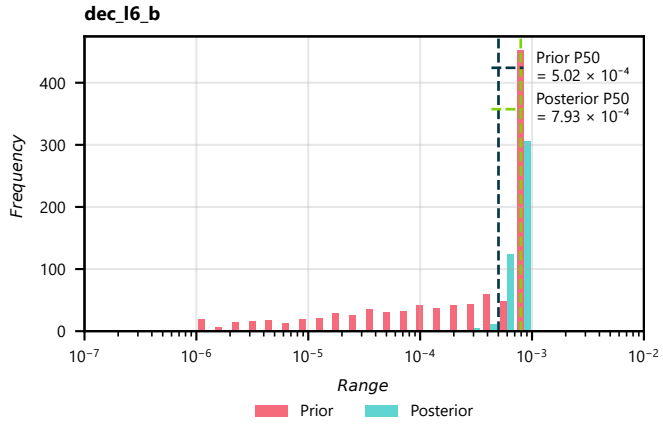

diffc_b
Prior P50
= 1.16 × 10⁻⁵
Posterior P50
= 1.13 × 10⁻⁵
Frequency
Range
Prior
Posterior

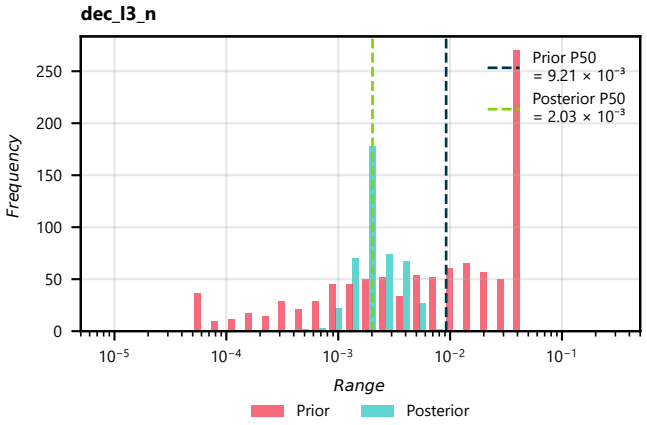

diffc_n
Prior P50
= 8.53 × 10⁻⁶
Posterior P50
= 8.93 × 10⁻⁶
Frequency
Range
Prior
Posterior

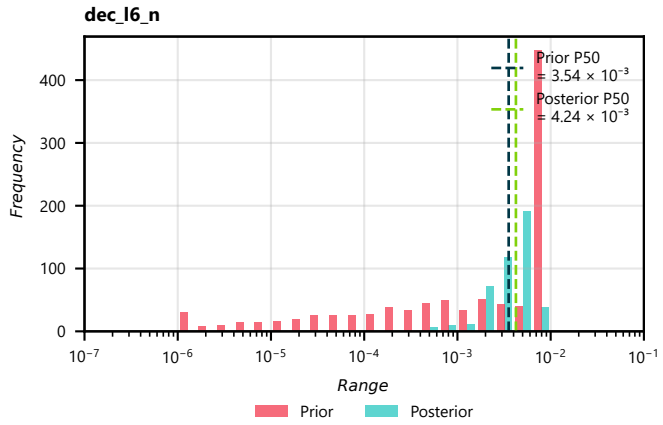

alh_c
Prior P50
= 1.00 × 10¹
Posterior P50
= 1.06 × 10¹
Frequency
Range
Prior
Posterior

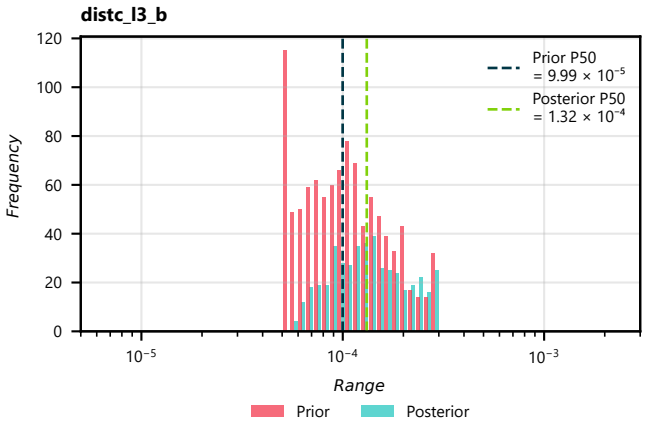

alh_sst
Prior P50
= 4.87 × 10⁰
Posterior P50
= 4.81 × 10⁰
Frequency
Range
Prior
Posterior

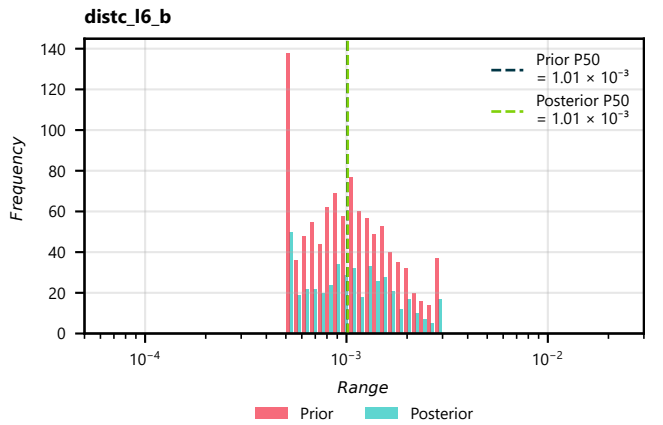

ath1_c
Prior P50 = 1.03 × 10⁰
Posterior P50 = 1.03 × 10⁰
ath1_sst
Prior P50 = 5.01 × 10⁻¹
Posterior P50 = 5.42 × 10⁻¹
atv_c
Prior P50 = 1.01 × 10⁻²
Posterior P50 = 1.00 × 10⁻²
atv_sst
Prior P50 = 4.77 × 10⁻²
Posterior P50 = 4.84 × 10⁻²
sr
Prior P50 = 3.23 × 10⁻²
Posterior P50 = 3.84 × 10⁻²
dens_l3
Prior P50 = 2.20 × 10³
Posterior P50 = 2.20 × 10³
dens_l6
Prior P50 = 1.40 × 10³
Posterior P50 = 1.40 × 10³
dec_l3_b
Prior P50 = 1.00 × 10⁻³
Posterior P50 = 1.19 × 10⁻³
Frequency
Range
Prior
Posterior

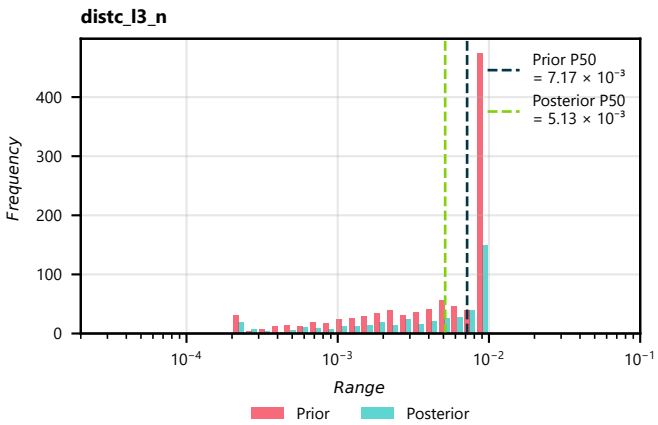

dec_l6_b
Prior P50
= 5.02 × 10⁻⁴
Posterior P50
= 7.93 × 10⁻⁴
Frequency
Range
Prior
Posterior

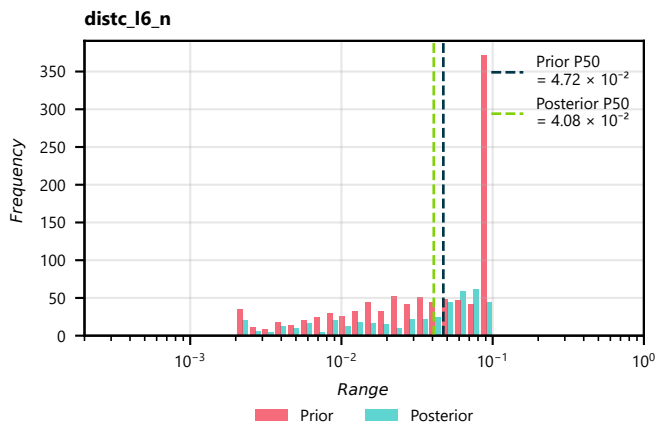

dec_l3_n
Prior P50
= 9.21 × 10⁻³
Posterior P50
= 2.03 × 10⁻³
Frequency
Range
Prior
Posterior

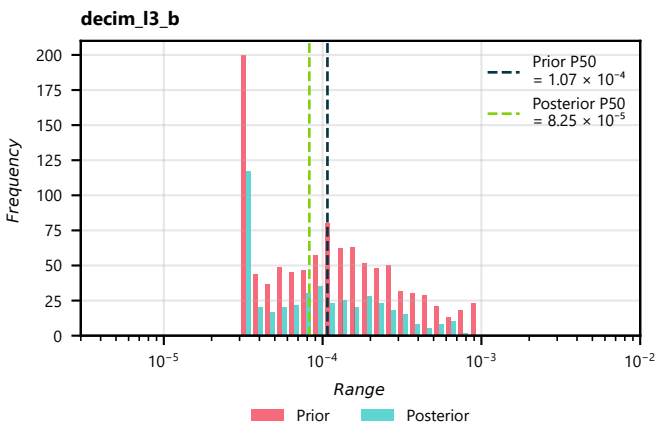

dec_l6_n
Prior P50
= 3.54 × 10⁻³
Posterior P50
= 4.24 × 10⁻³
Frequency
Range
Prior
Posterior

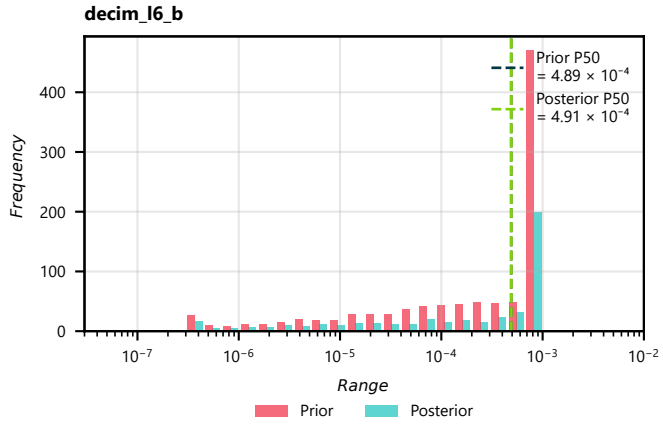

distc_l3_b
Prior P50
= 9.99 × 10⁻⁵
Posterior P50
= 1.32 × 10⁻⁴
Frequency
Range
Prior
Posterior

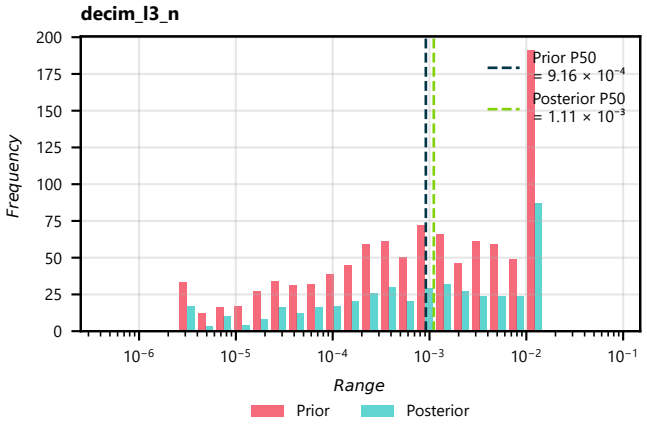

distc_l6_b
Prior P50
= 1.01 × 10⁻³
Posterior P50
= 1.01 × 10⁻³
Frequency
Range
Prior
Posterior

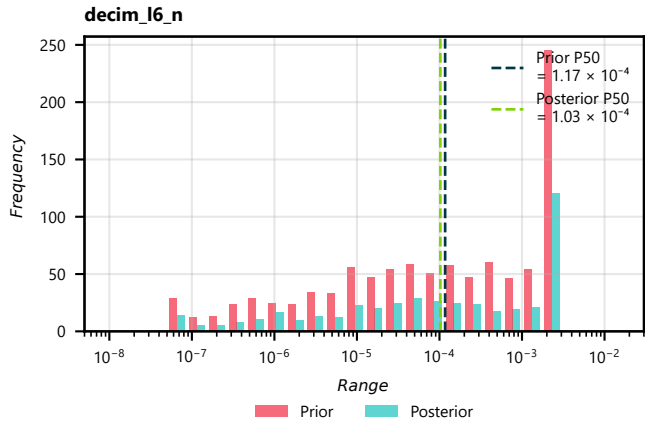

distc_l3_n
Prior P50
= 7.17 × 10⁻³
Posterior P50
= 5.13 × 10⁻³
Frequency
Range
Prior
Posterior

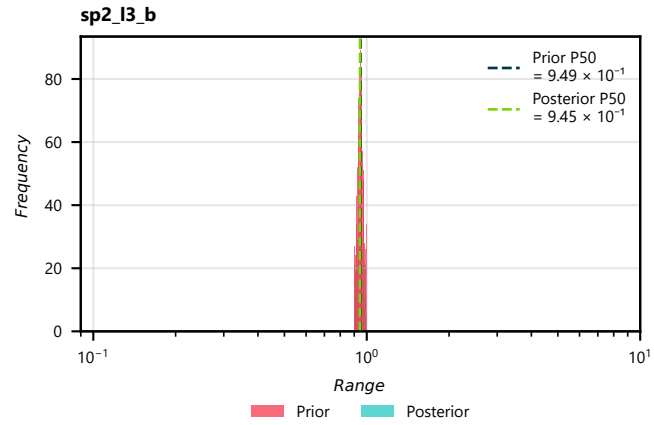

distc_l6_n
Prior P50
= 4.72 × 10⁻²
Posterior P50
= 4.08 × 10⁻²
Frequency
Range
Prior
Posterior

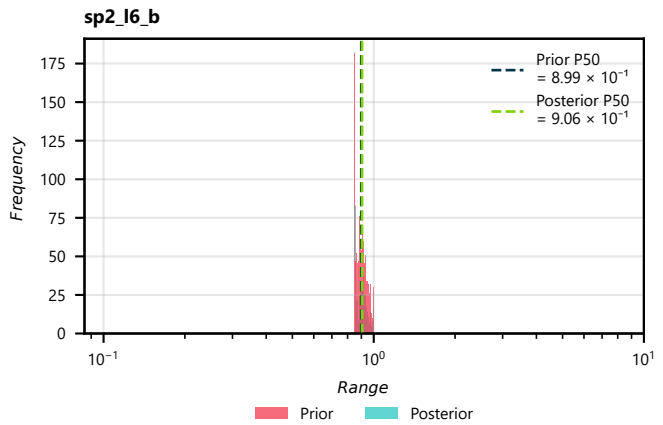

decim_l3_b
Prior P50
= 1.07 × 10⁻⁴
Posterior P50
= 8.25 × 10⁻⁵
Frequency
Range
Prior
Posterior

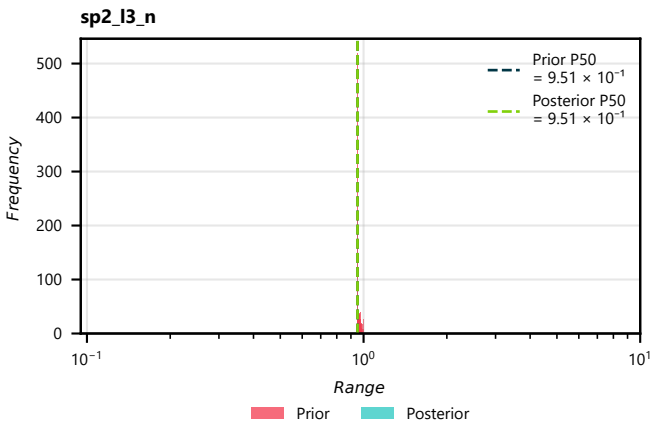

decim_l6_b
Prior P50
= 4.89 × 10⁻⁴
Posterior P50
= 4.91 × 10⁻⁴
Frequency
Range
Prior
Posterior

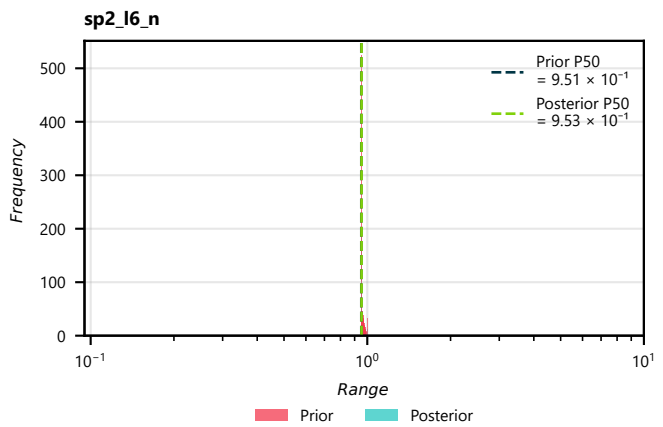

decim_l3_n
Prior P50
= 9.16 × 10⁻⁴
Posterior P50
= 1.11 × 10⁻³
Frequency
Range
Prior
Posterior

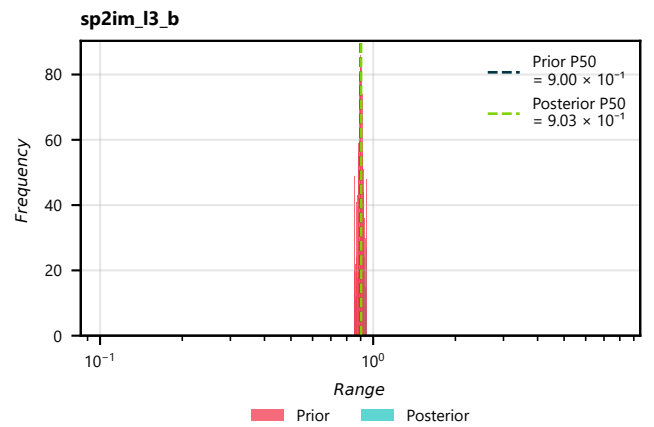

decim_l6_n
Prior P50
= 1.17 × 10⁻⁴
Posterior P50
= 1.03 × 10⁻⁴
Frequency
Range
Prior
Posterior


sp2_l3_b
Prior P50
= 9.49 × 10⁻¹
Posterior P50
= 9.45 × 10⁻¹
Frequency
Range
Prior
Posterior

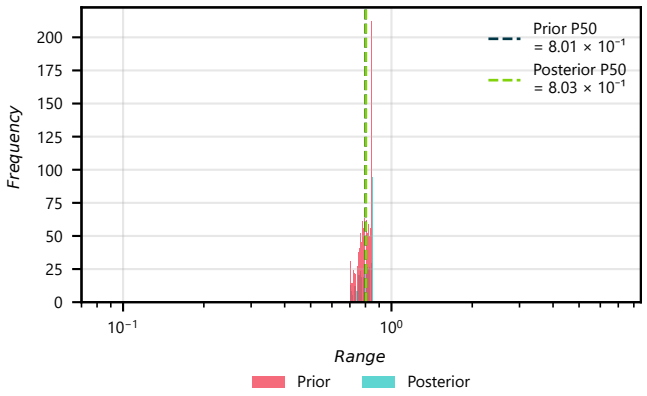

sp2_l6_b
Prior P50
= 8.99 × 10⁻¹
Posterior P50
= 9.06 × 10⁻¹
Frequency
Range
Prior
Posterior


sp2_l3_n
Prior P50
= 9.51 × 10⁻¹
Posterior P50
= 9.51 × 10⁻¹
Frequency
Range
Prior
Posterior

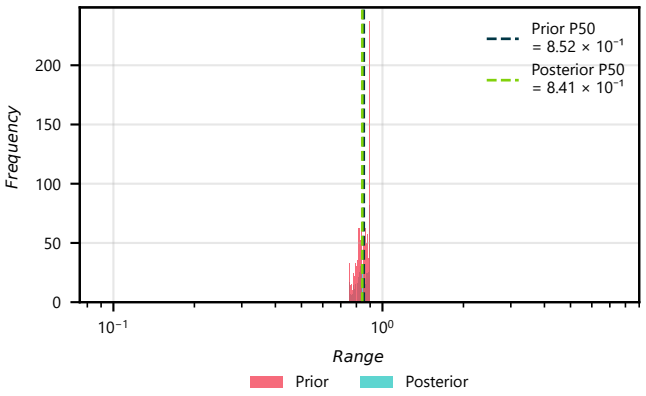

sp2_l6_n
Prior P50
= 9.51 × 10⁻¹
Posterior P50
= 9.53 × 10⁻¹
Frequency
Range
Prior
Posterior


sp2im_l3_b
Prior P50
= 9.00 × 10⁻¹
Posterior P50
= 9.03 × 10⁻¹
Frequency
Range
Prior
Posterior

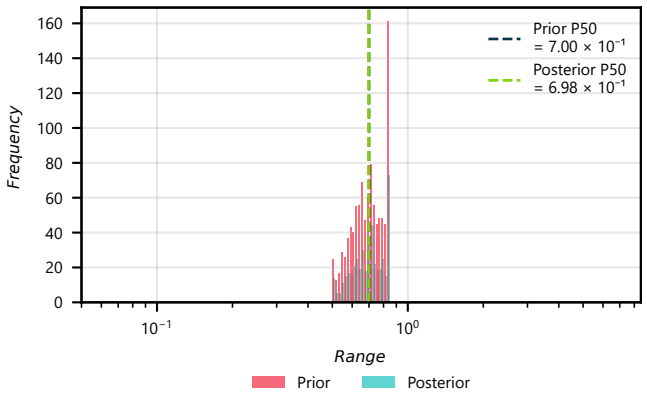
sp2im_l6_b



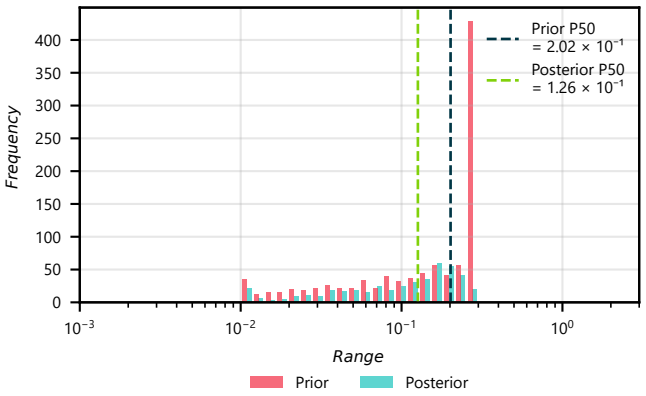
sp2im_l3_n



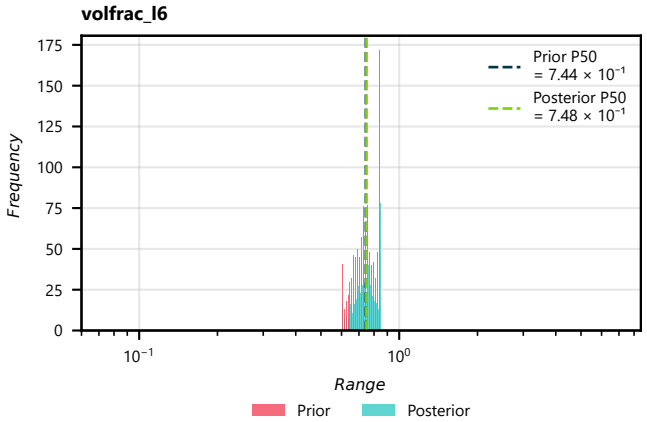
sp2im_l6_n



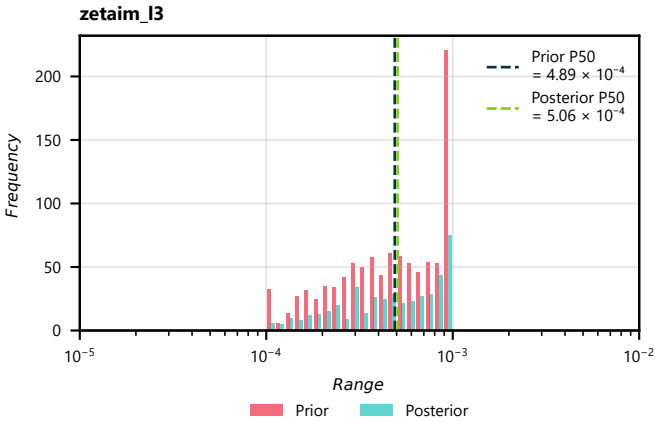
volfrac_l3



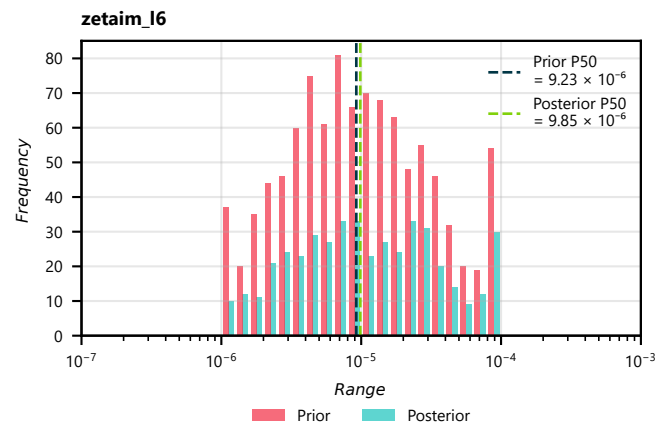
volfrac_l6



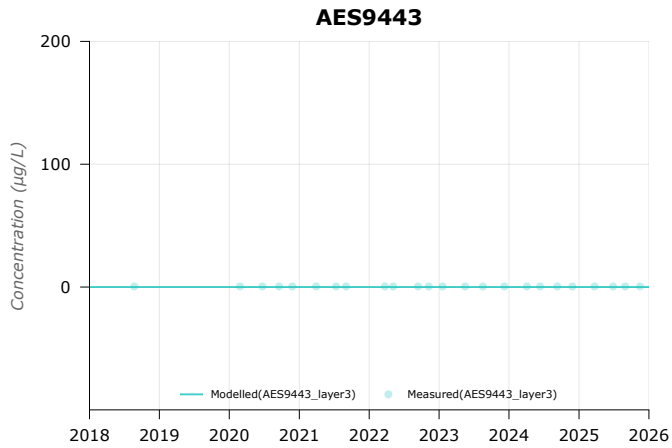
zetaim_l3

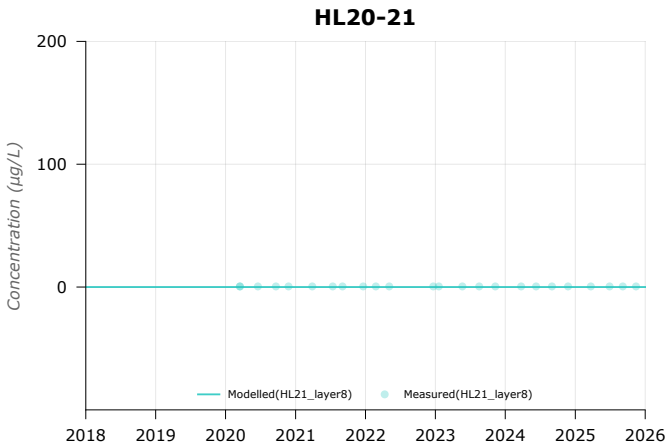


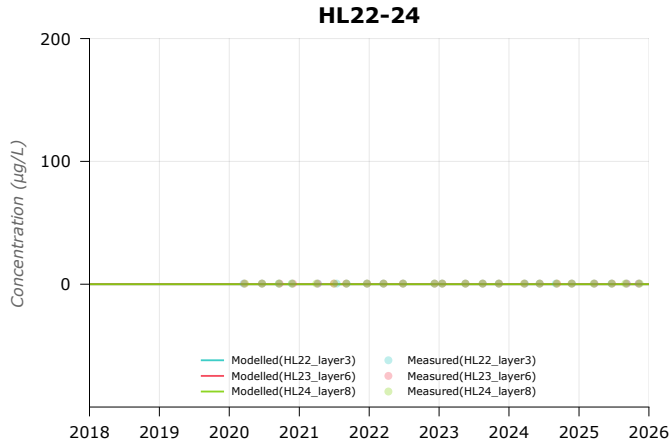
zetaim_l6

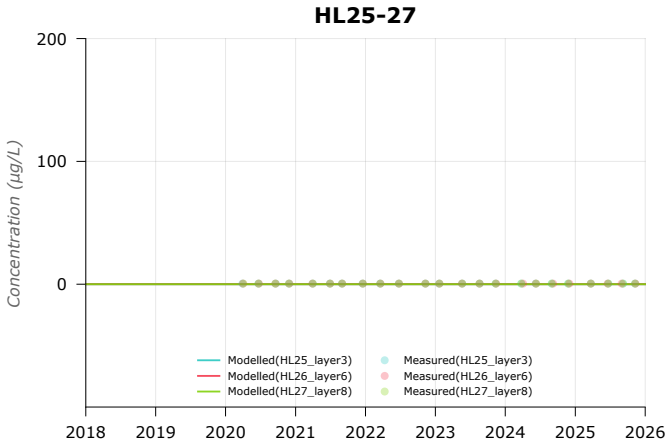


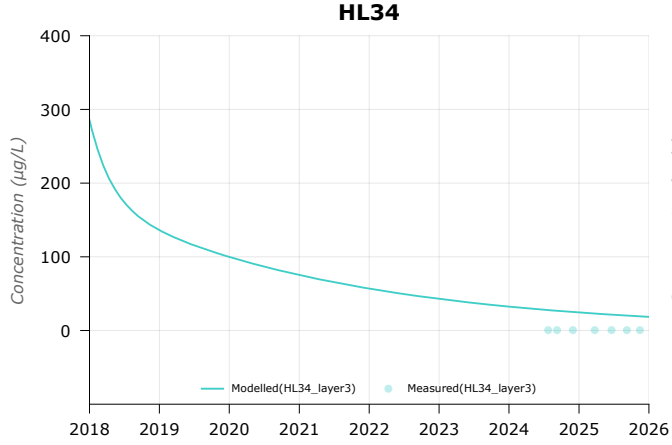
Appendix C. Modelled versus observed concentration time series plots – Benzene

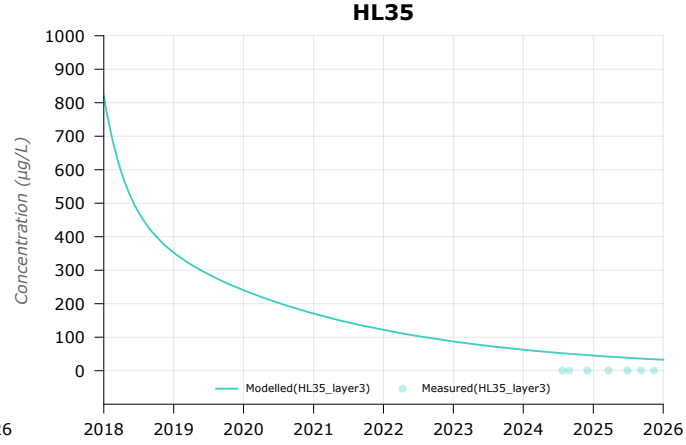

AES9443
Concentration (µg/L)
200
100
0
Modelled(AES9443_layer3)
Measured(AES9443_layer3)
2018
2019
2020
2021
2022
2023
2024
2025
2026

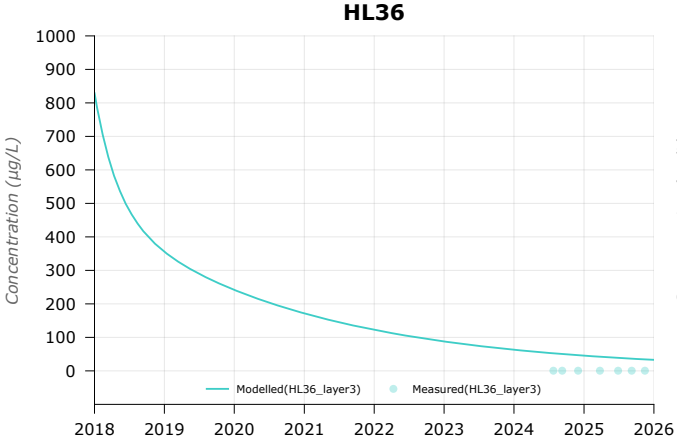

HL20-21
Concentration (µg/L)
200
100
0
Modelled(HL21_layer8)
Measured(HL21_layer8)
2018
2019
2020
2021
2022
2023
2024
2025
2026

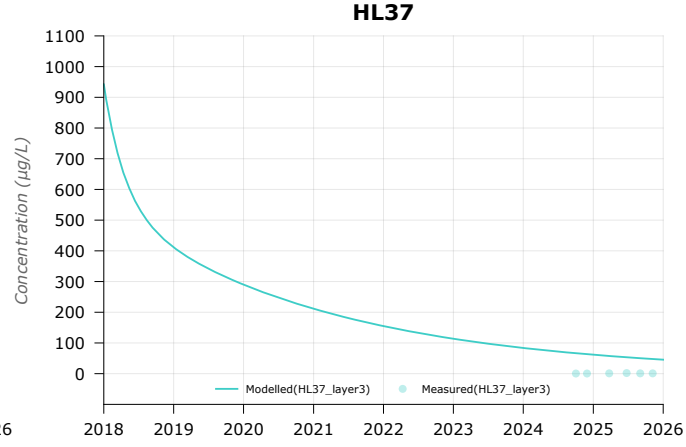

HL22-24
Concentration (µg/L)
200
100
0
Modelled(HL22_layer3)
Modelled(HL23_layer6)
Modelled(HL24_layer8)
Measured(HL22_layer3)
Measured(HL23_layer6)
Measured(HL24_layer8)
2018
2019
2020
2021
2022
2023
2024
2025
2026

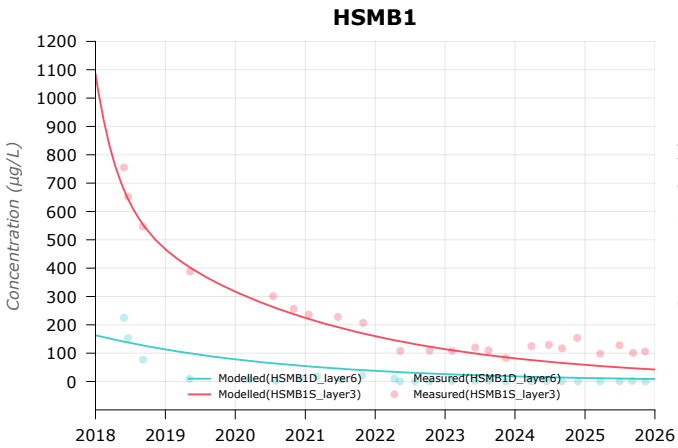

HL25-27
Concentration (µg/L)
200
100
0
Modelled(HL25_layer3)
Modelled(HL26_layer6)
Modelled(HL27_layer8)
Measured(HL25_layer3)
Measured(HL26_layer6)
Measured(HL27_layer8)
2018
2019
2020
2021
2022
2023
2024
2025
2026

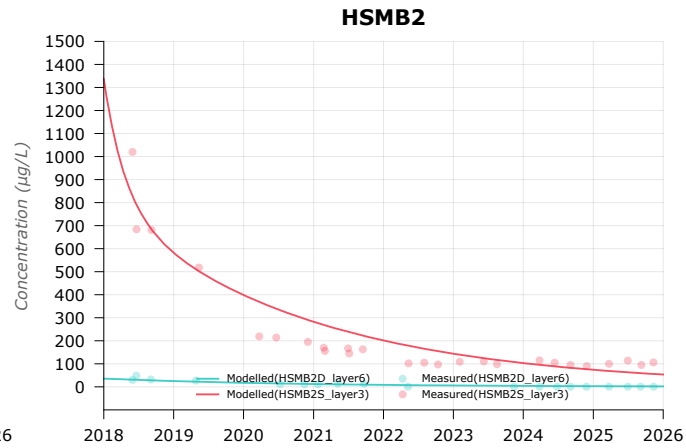

HL34
Concentration (µg/L)
400
300
200
100
0
Modelled(HL34_layer3)
Measured(HL34_layer3)
2018
2019
2020
2021
2022
2023
2024
2025
2026

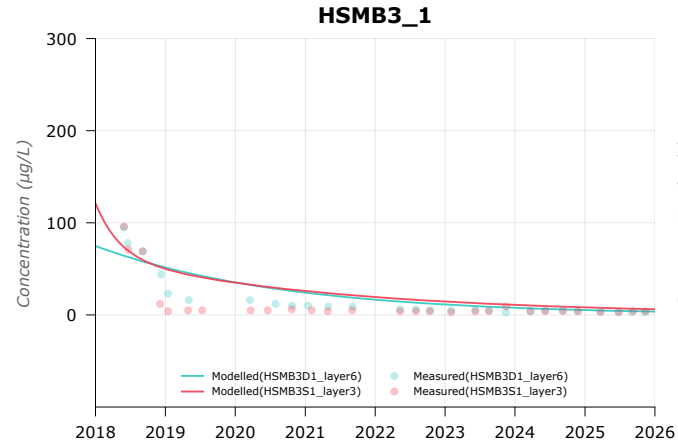

HL35
Concentration (µg/L)
1000
900
800
700
600
500
400
300
200
100
0
Modelled(HL35_layer3)
Measured(HL35_layer3)
2018
2019
2020
2021
2022
2023
2024
2025
2026

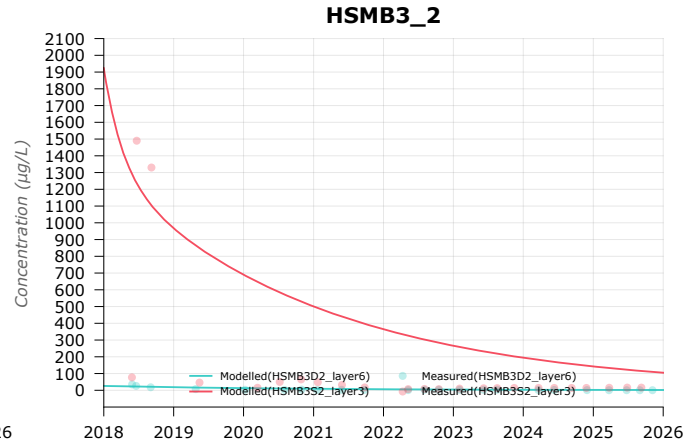

HL36
Concentration (µg/L)
1000
900
800
700
600
500
400
300
200
100
0
Modelled(HL36_layer3)
Measured(HL36_layer3)
2018
2019
2020
2021
2022
2023
2024
2025
2026

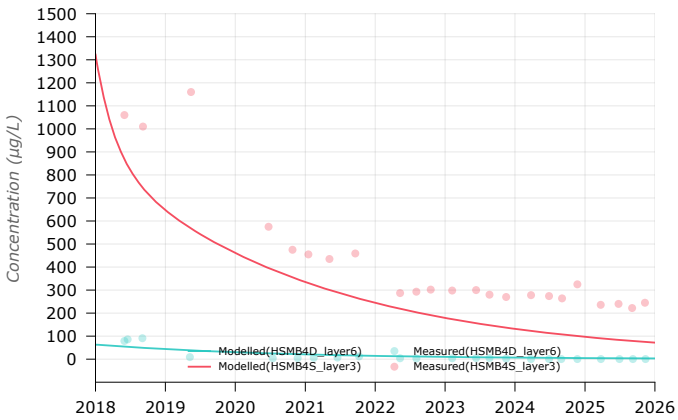

HL37
Concentration (µg/L)
1100
1000
900
800
700
600
500
400
300
200
100
0
Modelled(HL37_layer3)
Measured(HL37_layer3)
2018
2019
2020
2021
2022
2023
2024
2025
2026

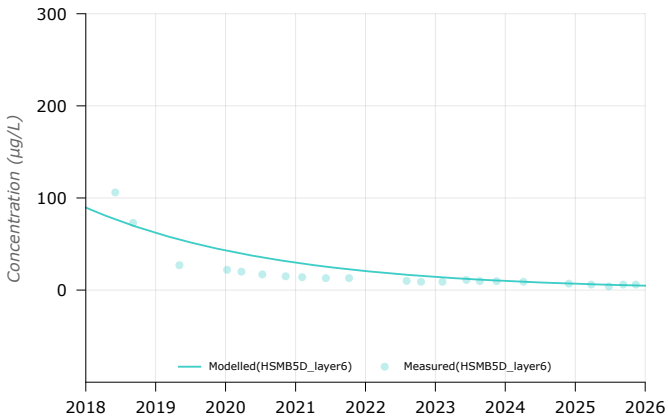

HSMB1
Concentration (µg/L)
Modelled(HSMB1D_layer6)
Modelled(HSMB1S_layer3)
Measured(HSMB1D_layer6)
Measured(HSMB1S_layer3)

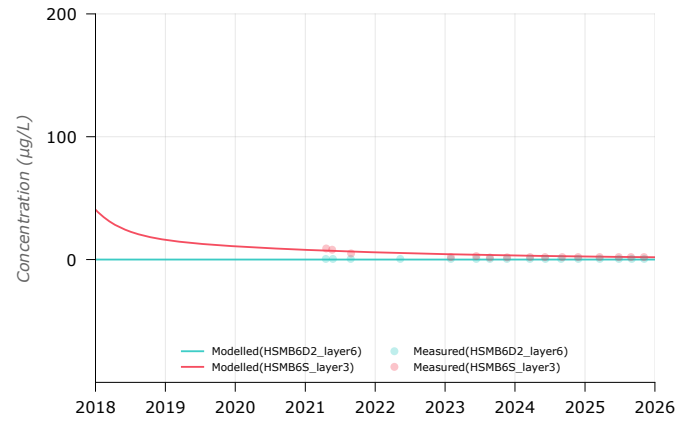

HSMB2
Concentration (µg/L)
Modelled(HSMB2D_layer6)
Modelled(HSMB2S_layer3)
Measured(HSMB2D_layer6)
Measured(HSMB2S_layer3)

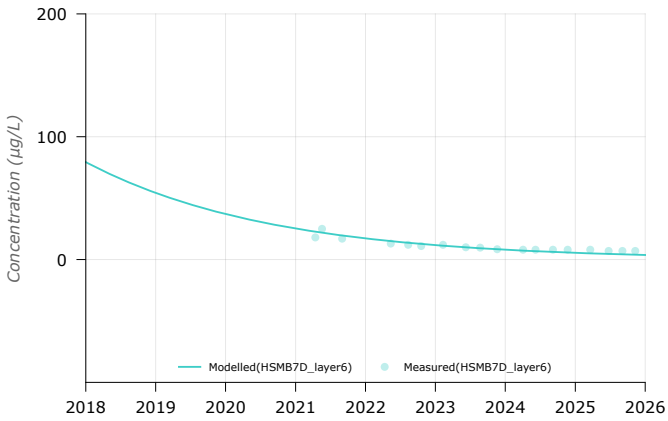

HSMB3_1
Concentration (µg/L)
Modelled(HSMB3D1_layer6)
Modelled(HSMB3S1_layer3)
Measured(HSMB3D1_layer6)
Measured(HSMB3S1_layer3)

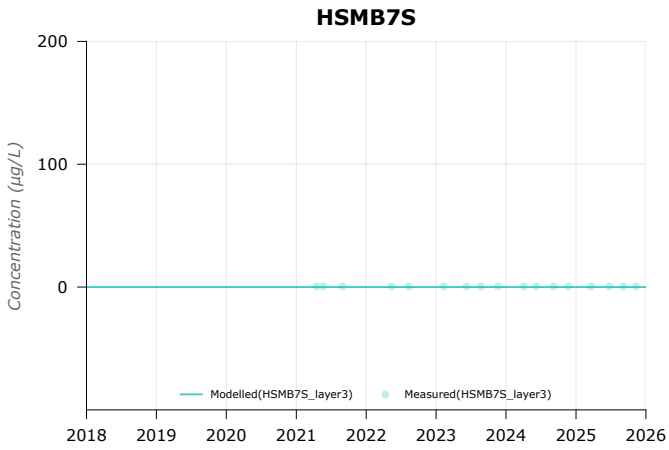

HSMB3_2
Concentration (µg/L)
Modelled(HSMB3D2_layer6)
Modelled(HSMB3S2_layer3)
Measured(HSMB3D2_layer6)
Measured(HSMB3S2_layer3)

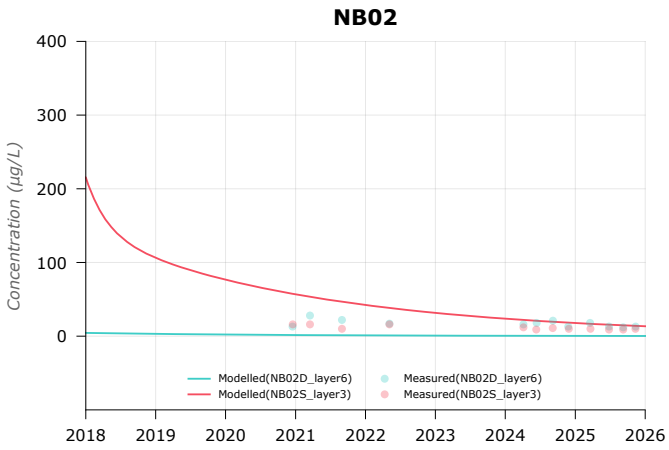

HSMB4
Concentration (µg/L)
Modelled(HSMB4D_layer6)
Modelled(HSMB4S_layer3)
Measured(HSMB4D_layer6)
Measured(HSMB4S_layer3)

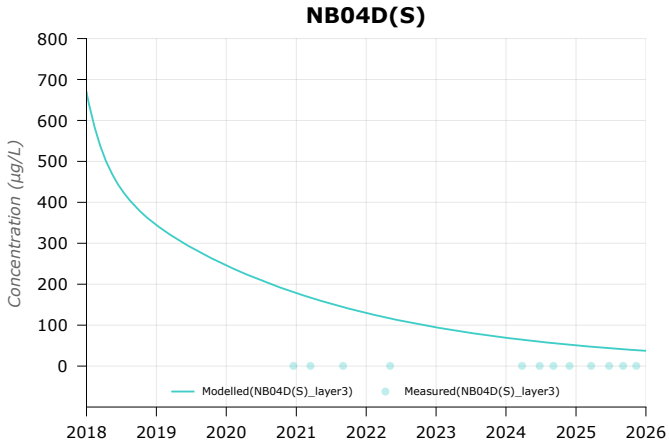

HSMB5D
Concentration (µg/L)
Modelled(HSMB5D_layer6)
Measured(HSMB5D_layer6)

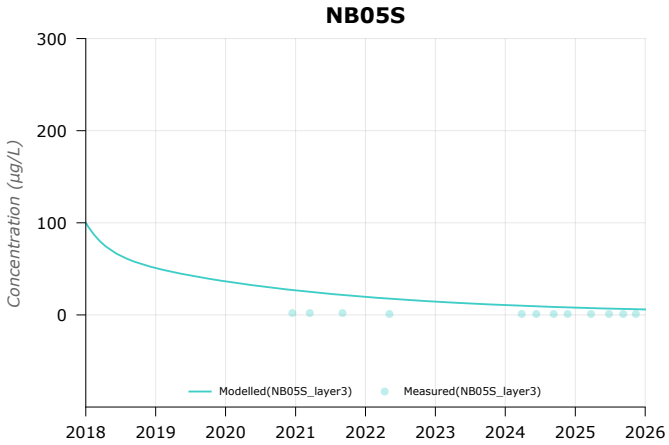

HSMB6
Concentration (µg/L)
Modelled(HSMB6D2_layer6)
Modelled(HSMB6S_layer3)
Measured(HSMB6D2_layer6)
Measured(HSMB6S_layer3)

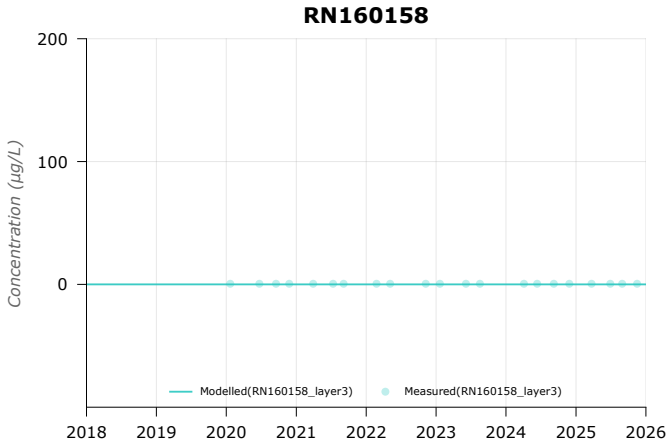

HSMB7D
Concentration (µg/L)
Modelled(HSMB7D_layer6)
Measured(HSMB7D_layer6)


HSMB7S
Concentration (µg/L)
200
100
0
Modelled(HSMB7S_layer3)
Measured(HSMB7S_layer3)
2018
2019
2020
2021
2022
2023
2024
2025
2026

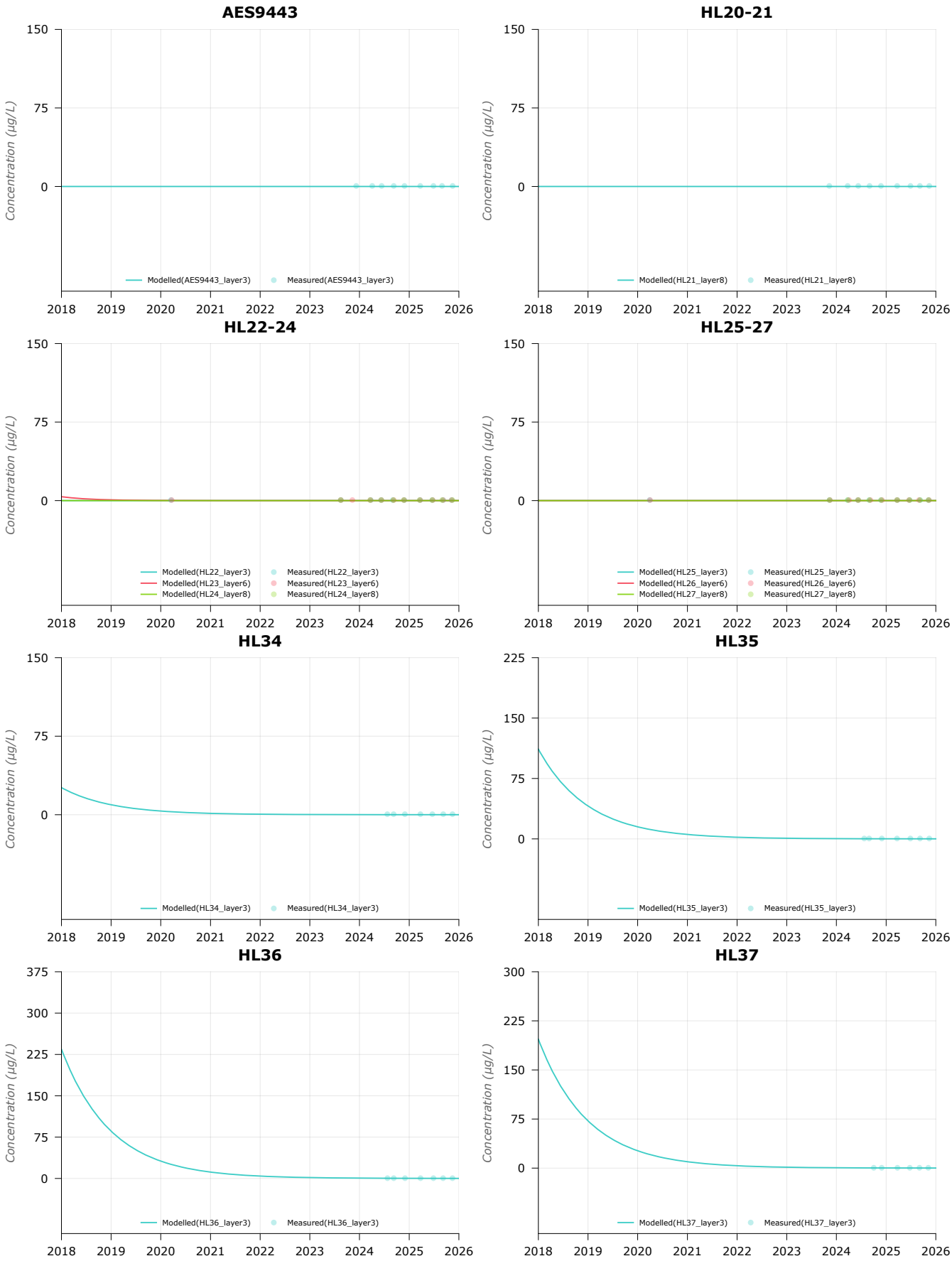

NB02
Concentration (µg/L)
400
300
200
100
0
Modelled(NB02D_layer6)
Measured(NB02D_layer6)
Modelled(NB02S_layer3)
Measured(NB02S_layer3)
2018
2019
2020
2021
2022
2023
2024
2025
2026

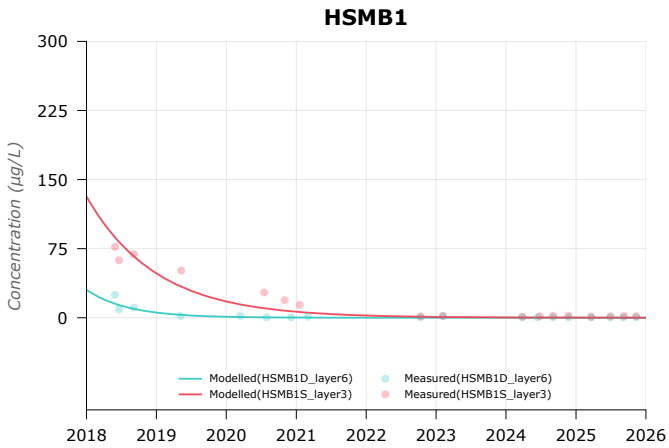

NB04D(S)
Concentration (µg/L)
800
700
600
500
400
300
200
100
0
Modelled(NB04D(S)_layer3)
Measured(NB04D(S)_layer3)
2018
2019
2020
2021
2022
2023
2024
2025
2026

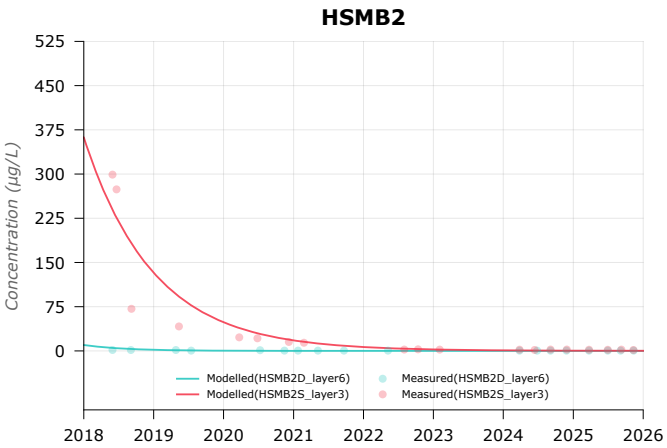

NB05S
Concentration (µg/L)
300
200
100
0
Modelled(NB05S_layer3)
Measured(NB05S_layer3)
2018
2019
2020
2021
2022
2023
2024
2025
2026

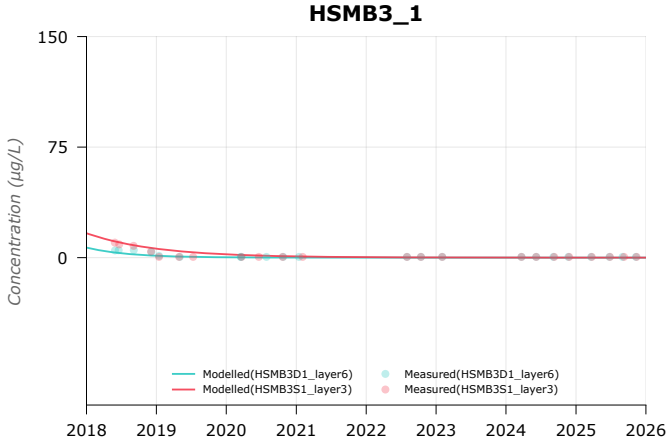

RN160158
Concentration (µg/L)
200
100
0
Modelled(RN160158_layer3)
Measured(RN160158_layer3)
2018
2019
2020
2021
2022
2023
2024
2025
2026

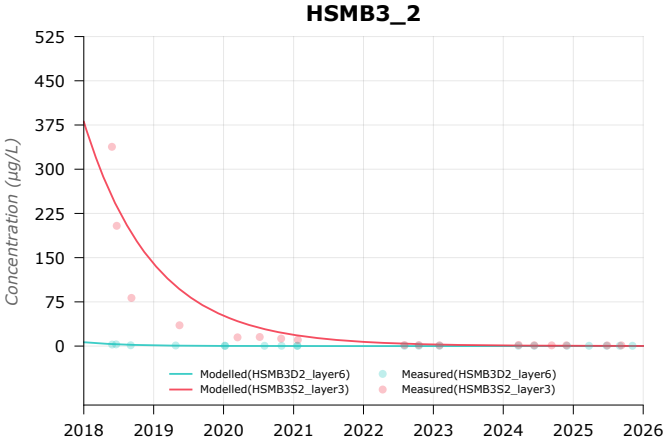
Appendix D. Modelled versus observed concentration time series plots - Naphthalene

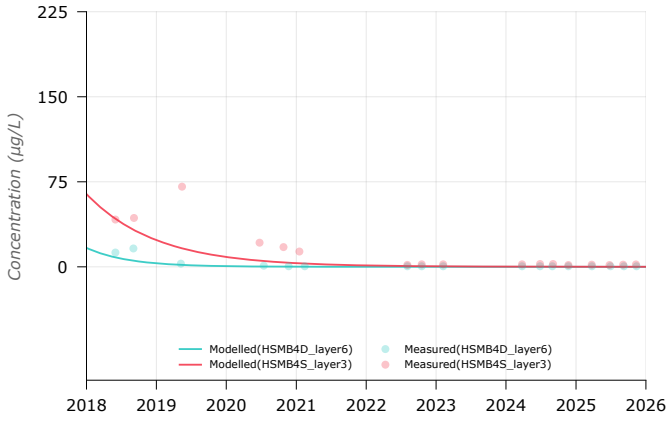

AES9443
Concentration (µg/L)
150
75
0
Modelled(AES9443_layer3)
Measured(AES9443_layer3)
2018
2019
2020
2021
2022
2023
2024
2025
2026
HL20-21
Concentration (µg/L)
150
75
0
Modelled(HL21_layer8)
Measured(HL21_layer8)
2018
2019
2020
2021
2022
2023
2024
2025
2026
HL22-24
Concentration (µg/L)
150
75
0
Modelled(HL22_layer3)
Modelled(HL23_layer6)
Modelled(HL24_layer8)
Measured(HL22_layer3)
Measured(HL23_layer6)
Measured(HL24_layer8)
2018
2019
2020
2021
2022
2023
2024
2025
2026
HL25-27
Concentration (µg/L)
150
75
0
Modelled(HL25_layer3)
Modelled(HL26_layer6)
Modelled(HL27_layer8)
Measured(HL25_layer3)
Measured(HL26_layer6)
Measured(HL27_layer8)
2018
2019
2020
2021
2022
2023
2024
2025
2026
HL34
Concentration (µg/L)
150
75
0
Modelled(HL34_layer3)
Measured(HL34_layer3)
2018
2019
2020
2021
2022
2023
2024
2025
2026
HL35
Concentration (µg/L)
225
150
75
0
Modelled(HL35_layer3)
Measured(HL35_layer3)
2018
2019
2020
2021
2022
2023
2024
2025
2026
HL36
Concentration (µg/L)
375
300
225
150
75
0
Modelled(HL36_layer3)
Measured(HL36_layer3)
2018
2019
2020
2021
2022
2023
2024
2025
2026
HL37
Concentration (µg/L)
300
225
150
75
0
Modelled(HL37_layer3)
Measured(HL37_layer3)
2018
2019
2020
2021
2022
2023
2024
2025
2026

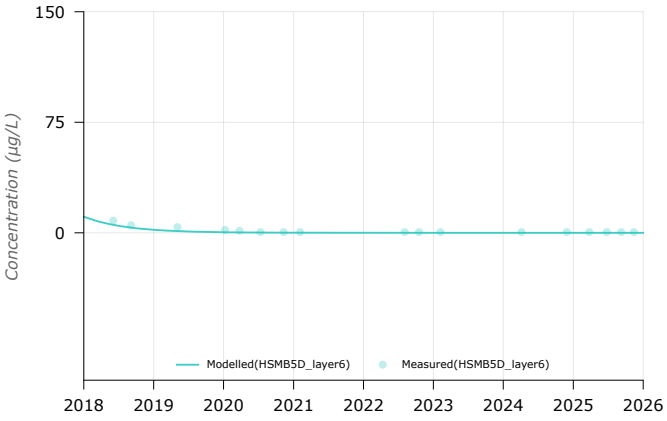

HSMB1
Concentration (µg/L)
300
225
150
75
0
2018
2019
2020
2021
2022
2023
2024
2025
2026
Modelled(HSMB1D_layer6)
Modelled(HSMB1S_layer3)
Measured(HSMB1D_layer6)
Measured(HSMB1S_layer3)

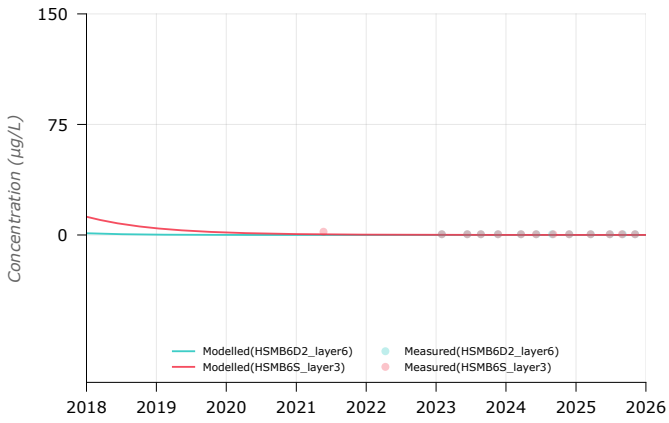

HSMB2
Concentration (µg/L)
525
450
375
300
225
150
75
0
2018
2019
2020
2021
2022
2023
2024
2025
2026
Modelled(HSMB2D_layer6)
Modelled(HSMB2S_layer3)
Measured(HSMB2D_layer6)
Measured(HSMB2S_layer3)

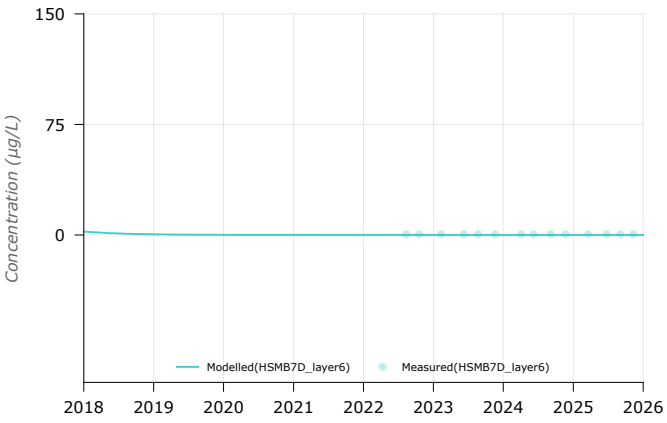

HSMB3_1
Concentration (µg/L)
150
75
0
2018
2019
2020
2021
2022
2023
2024
2025
2026
Modelled(HSMB3D1_layer6)
Modelled(HSMB3S1_layer3)
Measured(HSMB3D1_layer6)
Measured(HSMB3S1_layer3)

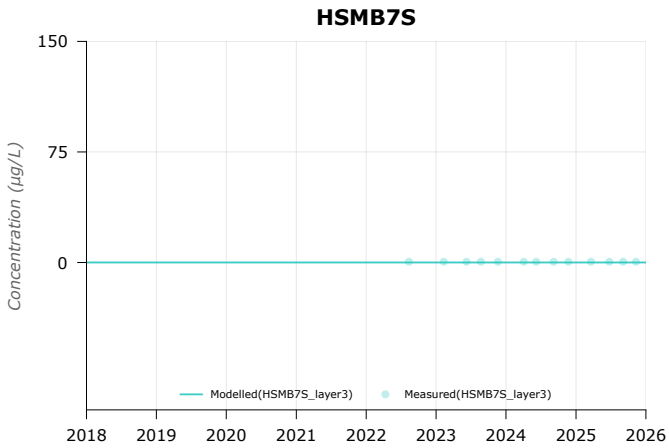

HSMB3_2
Concentration (µg/L)
525
450
375
300
225
150
75
0
2018
2019
2020
2021
2022
2023
2024
2025
2026
Modelled(HSMB3D2_layer6)
Modelled(HSMB3S2_layer3)
Measured(HSMB3D2_layer6)
Measured(HSMB3S2_layer3)

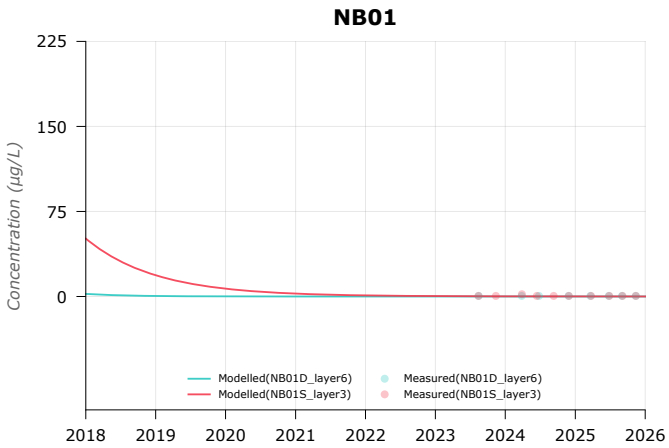

HSMB4
Concentration (µg/L)
225
150
75
0
2018
2019
2020
2021
2022
2023
2024
2025
2026
Modelled(HSMB4D_layer6)
Modelled(HSMB4S_layer3)
Measured(HSMB4D_layer6)
Measured(HSMB4S_layer3)

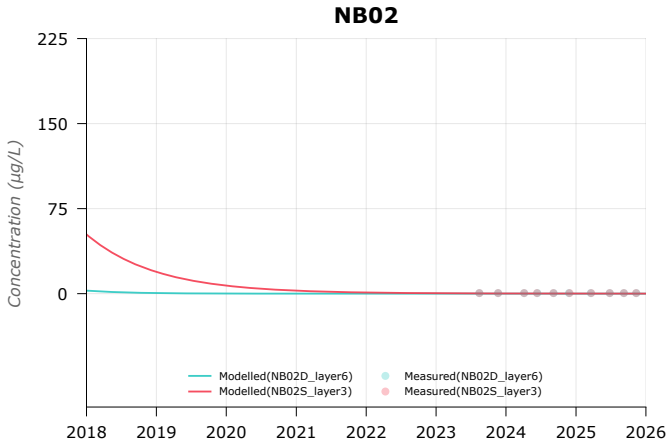

HSMB5D
Concentration (µg/L)
150
75
0
2018
2019
2020
2021
2022
2023
2024
2025
2026
Modelled(HSMB5D_layer6)
Measured(HSMB5D_layer6)

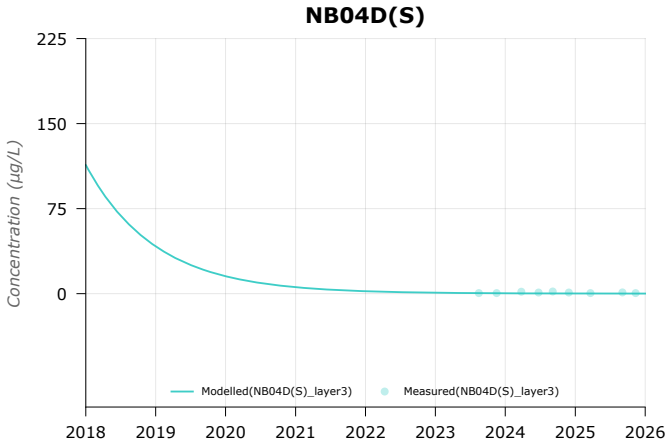

HSMB6
Concentration (µg/L)
150
75
0
2018
2019
2020
2021
2022
2023
2024
2025
2026
Modelled(HSMB6D2_layer6)
Modelled(HSMB6S_layer3)
Measured(HSMB6D2_layer6)
Measured(HSMB6S_layer3)

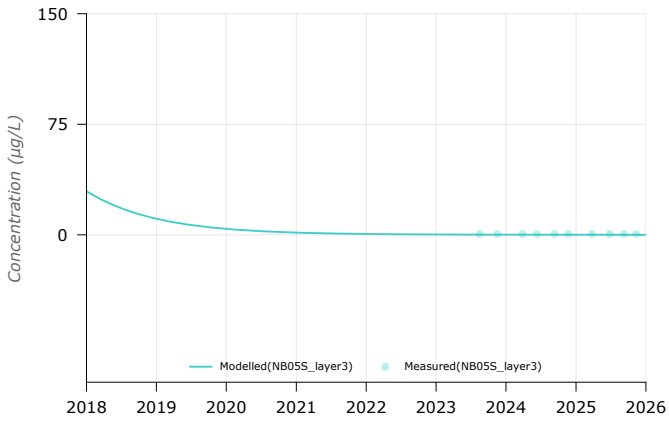

HSMB7D
Concentration (µg/L)
150
75
0
2018
2019
2020
2021
2022
2023
2024
2025
2026
Modelled(HSMB7D_layer6)
Measured(HSMB7D_layer6)

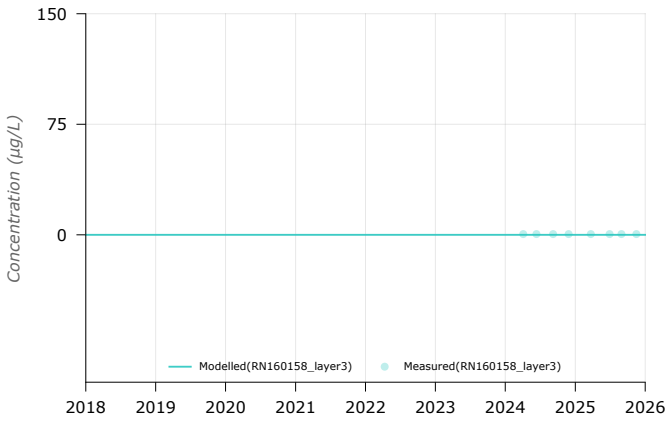

HSMB7S
Concentration (µg/L)
150
75
0
2018
2019
2020
2021
2022
2023
2024
2025
2026
Modelled(HSMB7S_layer3)
Measured(HSMB7S_layer3)


NB01
Concentration (µg/L)
225
150
75
0
2018
2019
2020
2021
2022
2023
2024
2025
2026
Modelled(NB01D_layer6)
Measured(NB01D_layer6)
Modelled(NB01S_layer3)
Measured(NB01S_layer3)

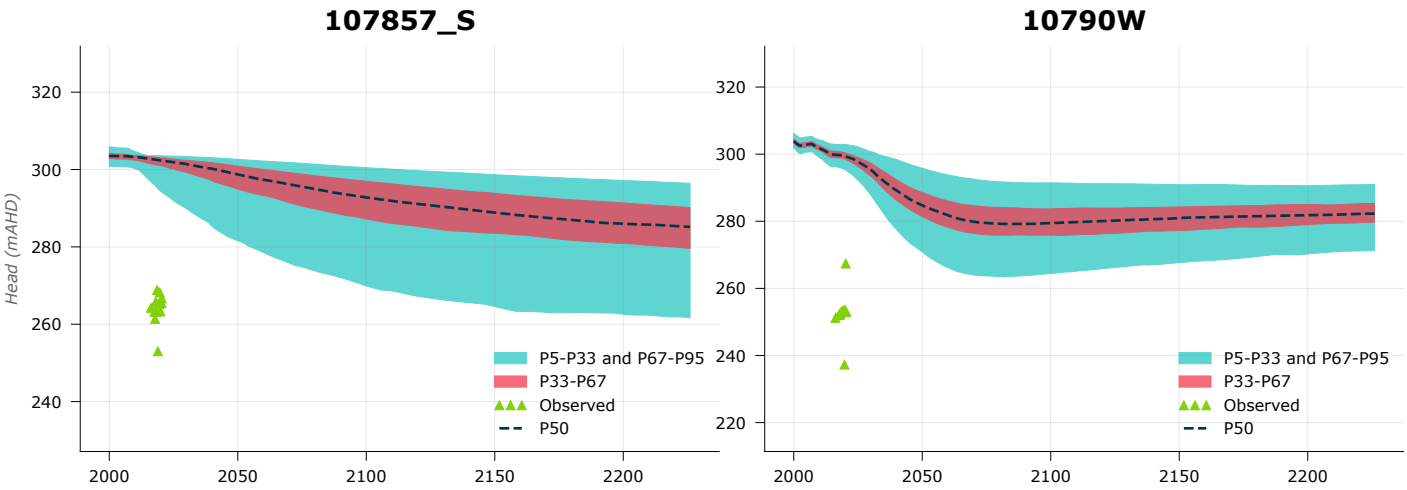

NB02
Concentration (µg/L)
225
150
75
0
2018
2019
2020
2021
2022
2023
2024
2025
2026
Modelled(NB02D_layer6)
Measured(NB02D_layer6)
Modelled(NB02S_layer3)
Measured(NB02S_layer3)


NB04D(S)
Concentration (µg/L)
225
150
75
0
2018
2019
2020
2021
2022
2023
2024
2025
2026
Modelled(NB04D(S)_layer3)
Measured(NB04D(S)_layer3)

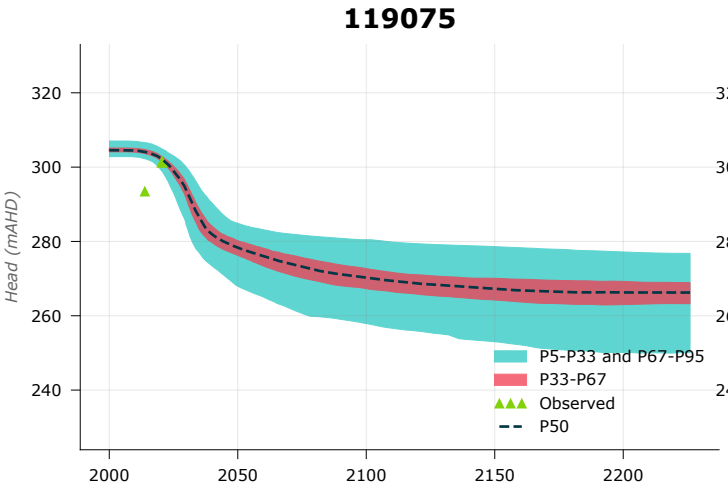

NB05S
Concentration (µg/L)
150
75
0
2018
2019
2020
2021
2022
2023
2024
2025
2026
Modelled(NB05S_layer3)
Measured(NB05S_layer3)

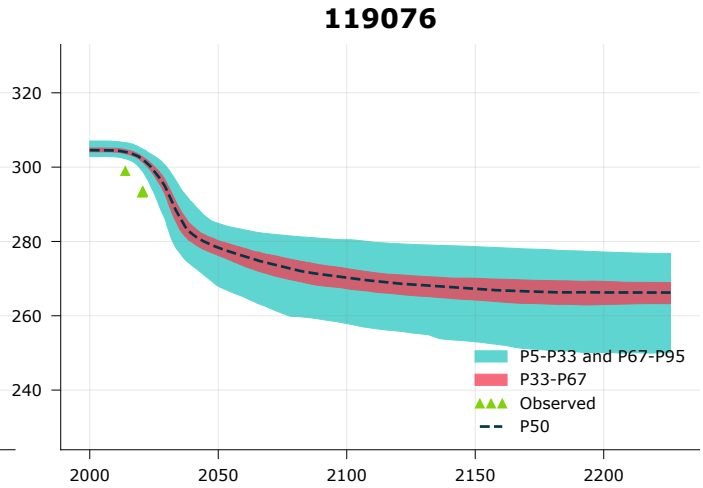

RN160158
Concentration (µg/L)
150
75
0
2018
2019
2020
2021
2022
2023
2024
2025
2026
Modelled(RN160158_layer3)
Measured(RN160158_layer3)

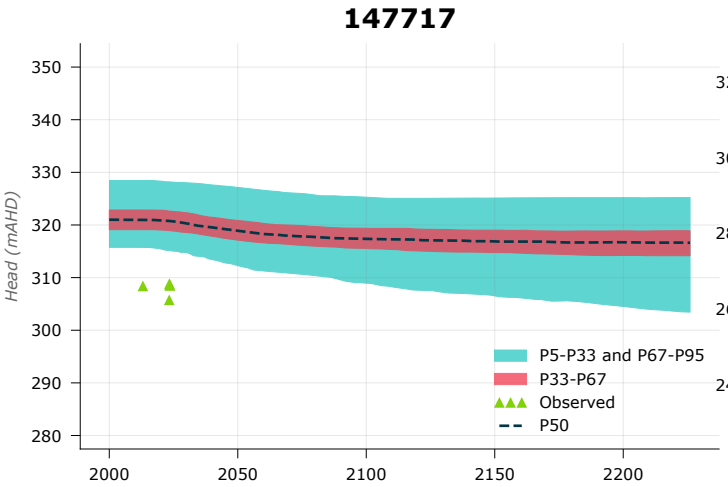
Appendix E. Predictive uncertainty - groundwater levels

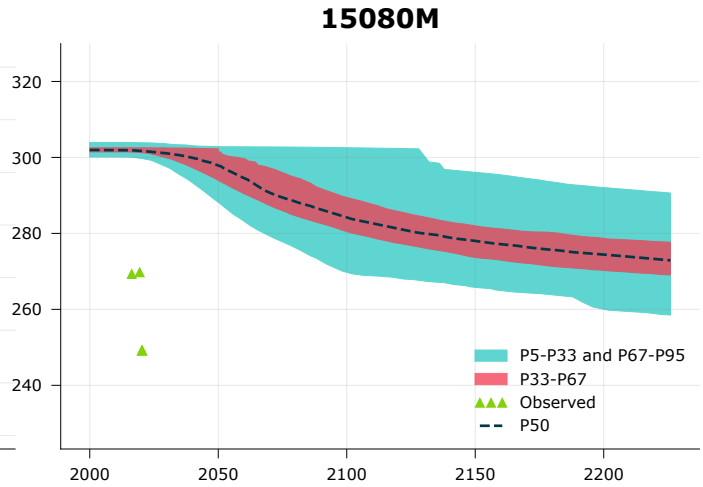

107857_S
Head (mAHD)
320
300
280
260
240
2000
2050
2100
2150
2200
P5-P33 and P67-P95
P33-P67
Observed
P50

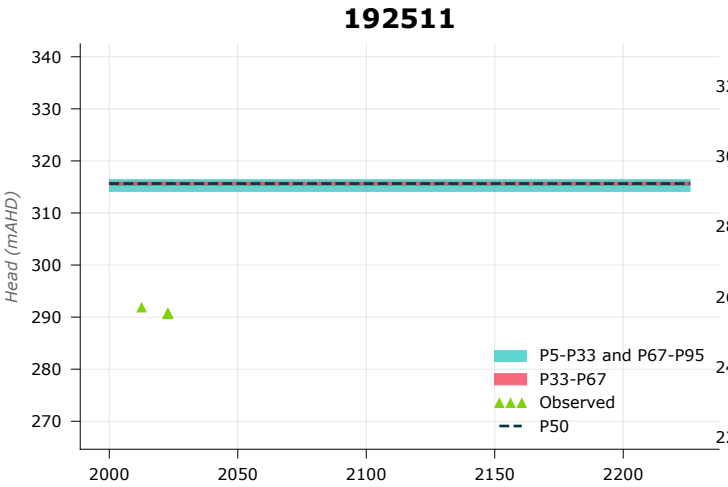
10790W
320
300
280
260
240
220
2000
2050
2100
2150
2200
P5-P33 and P67-P95
P33-P67
Observed
P50

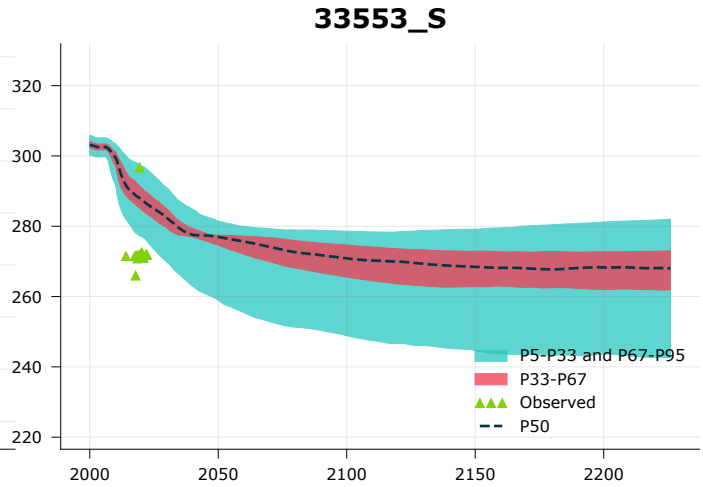

119075
Head (mAHD)
320
300
280
260
240
2000
2050
2100
2150
2200
P5-P33 and P67-P95
P33-P67
Observed
P50

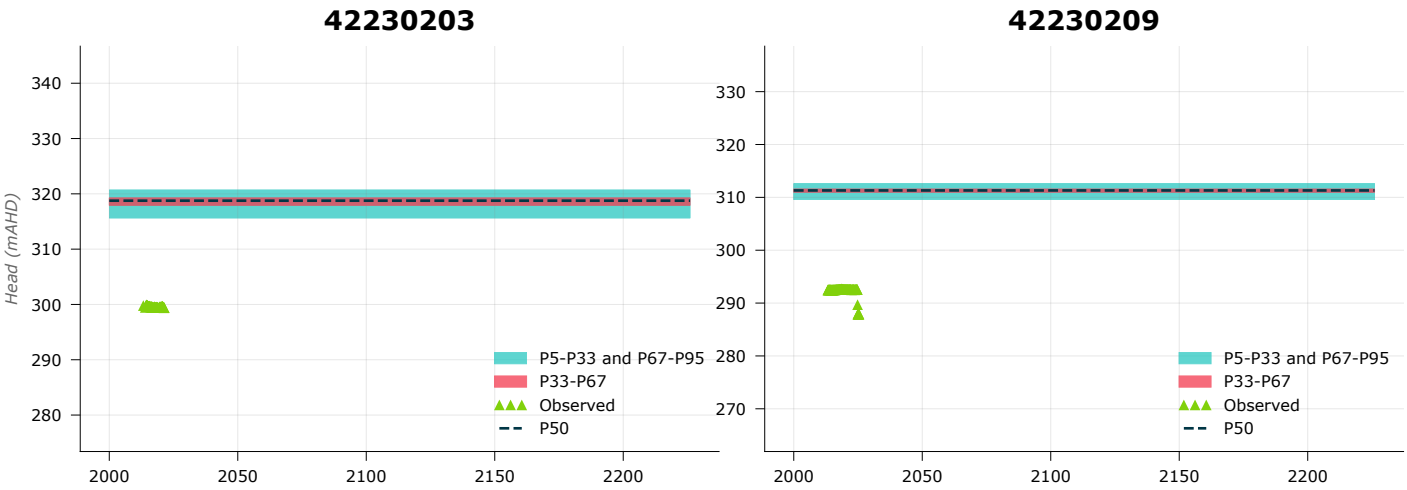

119076
320
300
280
260
240
2000
2050
2100
2150
2200
P5-P33 and P67-P95
P33-P67
Observed
P50


147717
Head (mAHD)
350
340
330
320
310
300
290
280
2000
2050
2100
2150
2200
P5-P33 and P67-P95
P33-P67
Observed
P50

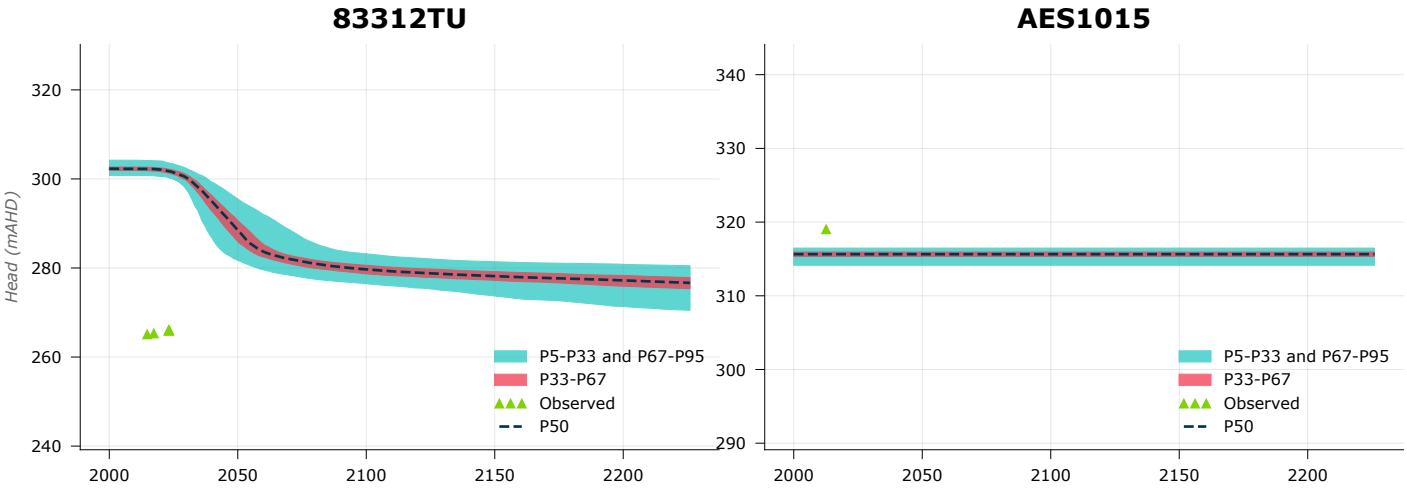

15080M
320
300
280
260
240
2000
2050
2100
2150
2200
P5-P33 and P67-P95
P33-P67
Observed
P50


192511
Head (mAHD)
340
330
320
310
300
290
280
270
2000
2050
2100
2150
2200
P5-P33 and P67-P95
P33-P67
Observed
P50

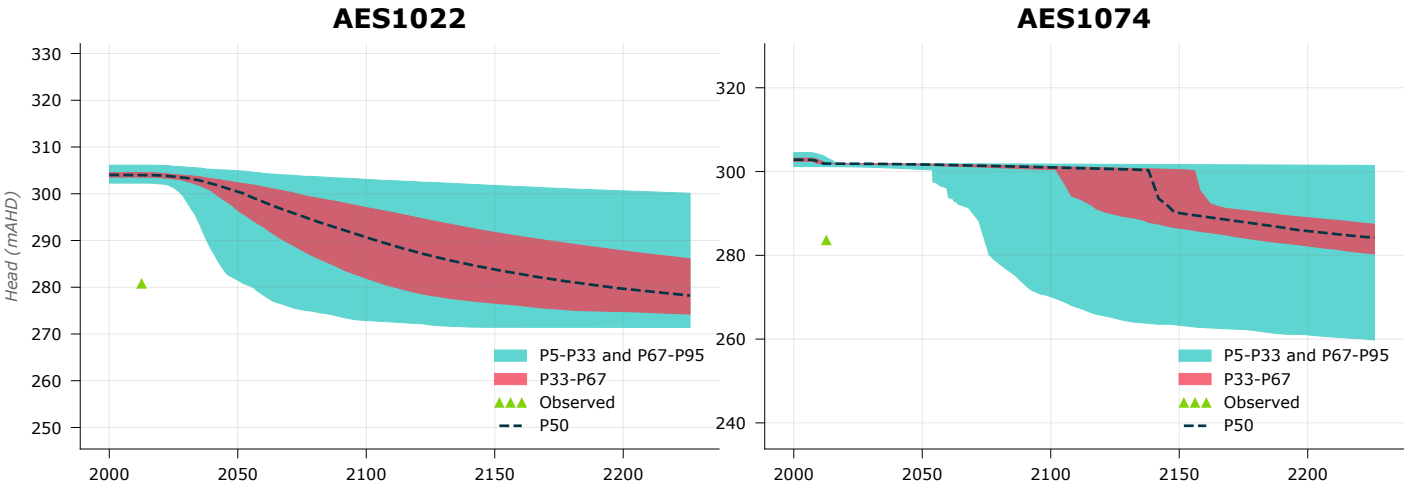

33553_S
320
300
280
260
240
220
2000
2050
2100
2150
2200
P5-P33 and P67-P95
P33-P67
Observed
P50


42230203
Head (mAHD)
340
330
320
310
300
290
280
2000
2050
2100
2150
2200
P5-P33 and P67-P95
P33-P67
Observed
P50

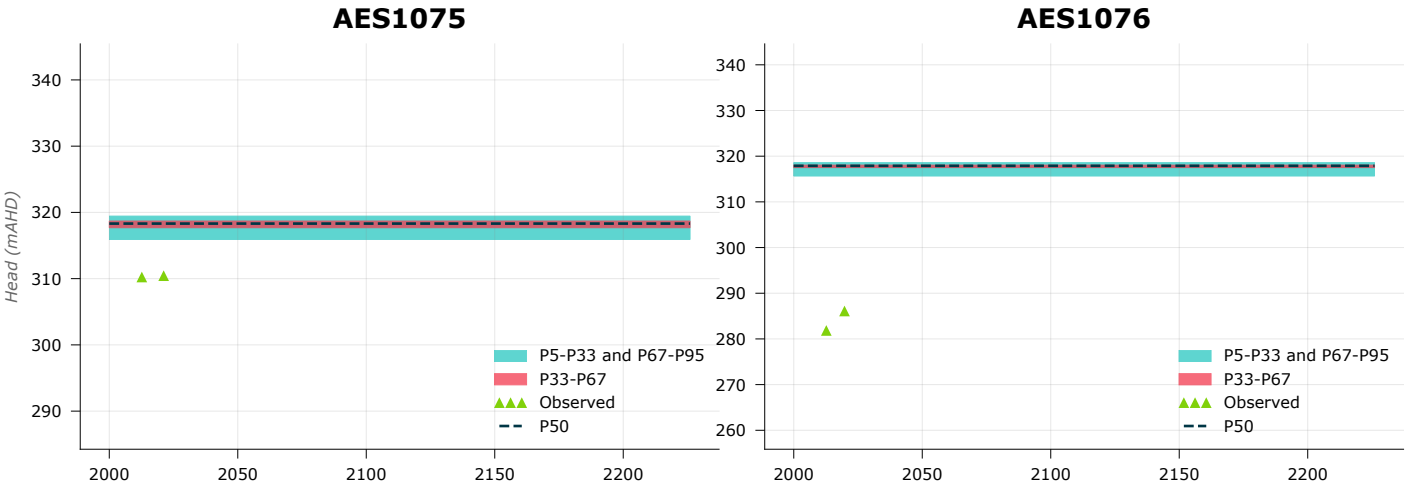
42230209
330
320
310
300
290
280
270
2000
2050
2100
2150
2200
P5-P33 and P67-P95
P33-P67
Observed
P50


83312TU
Head (mAHD)
320
300
280
260
240
2000
2050
2100
2150
2200
P5-P33 and P67-P95
P33-P67
Observed
P50

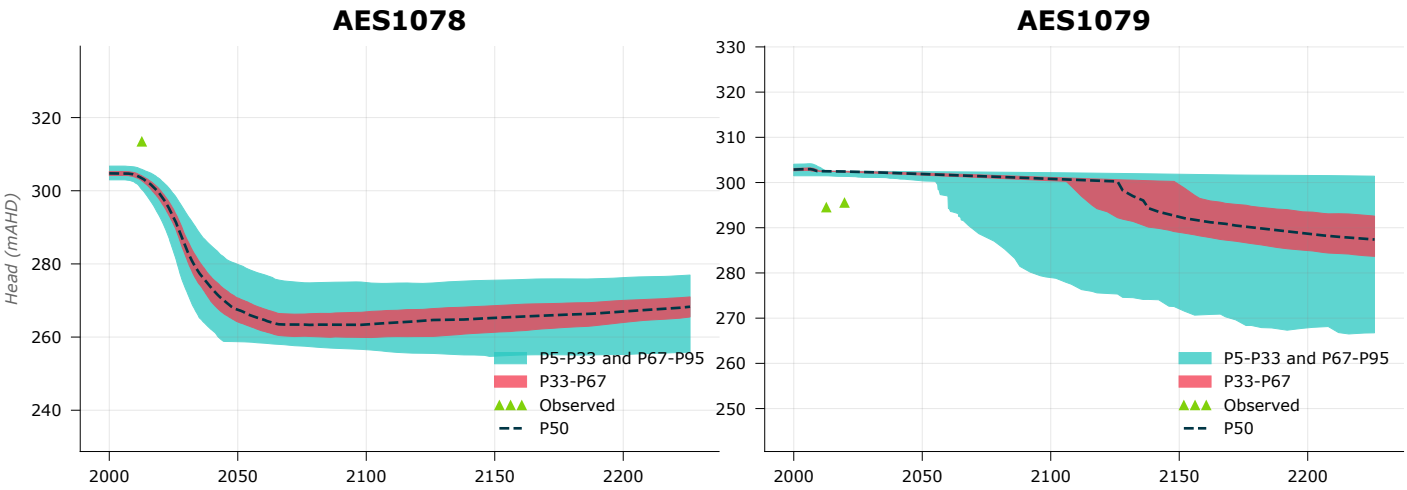
AES1015
340
330
320
310
300
290
2000
2050
2100
2150
2200
P5-P33 and P67-P95
P33-P67
Observed
P50


AES1022
Head (mAHD)
330
320
310
300
290
280
270
260
250
2000
2050
2100
2150
2200
P5-P33 and P67-P95
P33-P67
Observed
P50

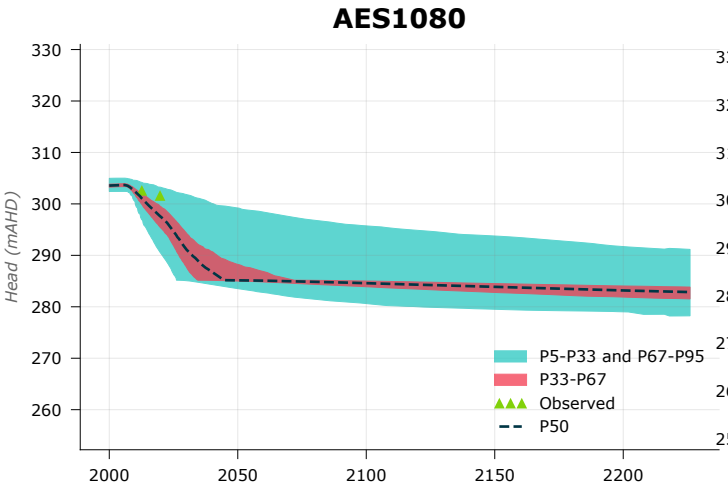
AES1074
320
300
280
260
240
2000
2050
2100
2150
2200
P5-P33 and P67-P95
P33-P67
Observed
P50

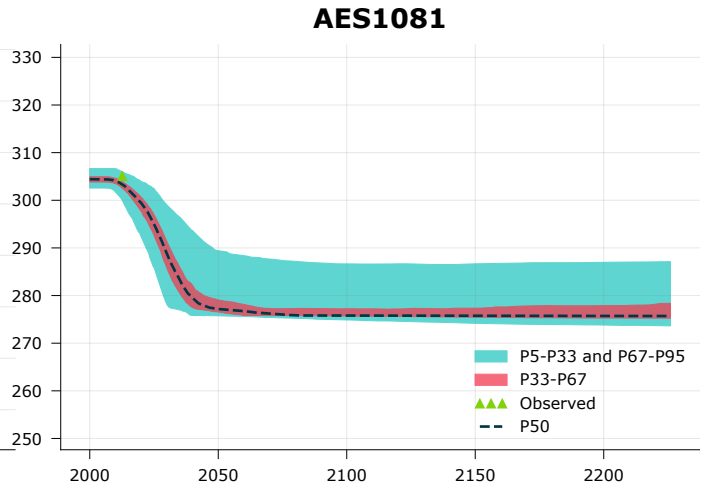

AES1075
Head (mAHD)
340
330
320
310
300
290
2000
2050
2100
2150
2200
P5-P33 and P67-P95
P33-P67
Observed
P50

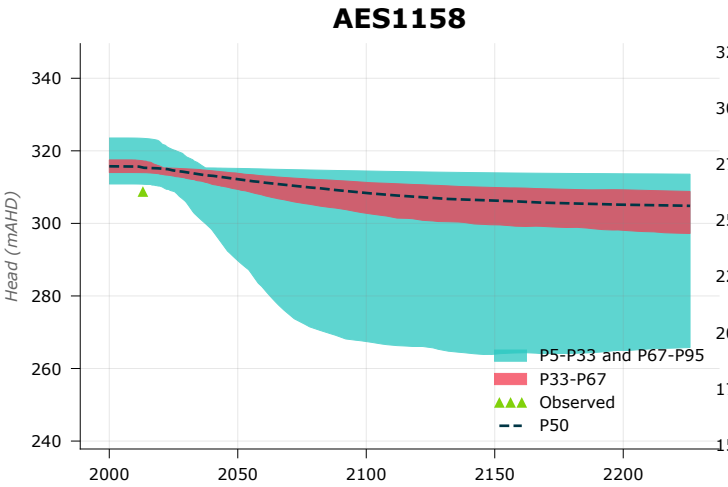
AES1076
340
330
320
310
300
290
280
270
260
2000
2050
2100
2150
2200
P5-P33 and P67-P95
P33-P67
Observed
P50

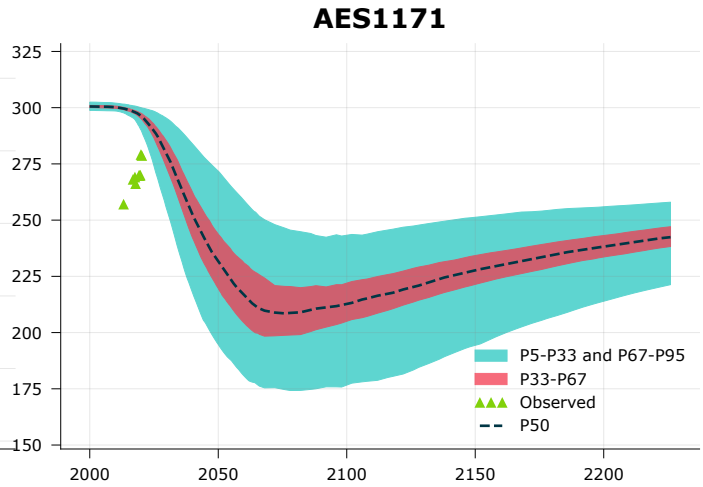

AES1078
Head (mAHD)
320
300
280
260
240
2000
2050
2100
2150
2200
P5-P33 and P67-P95
P33-P67
Observed
P50

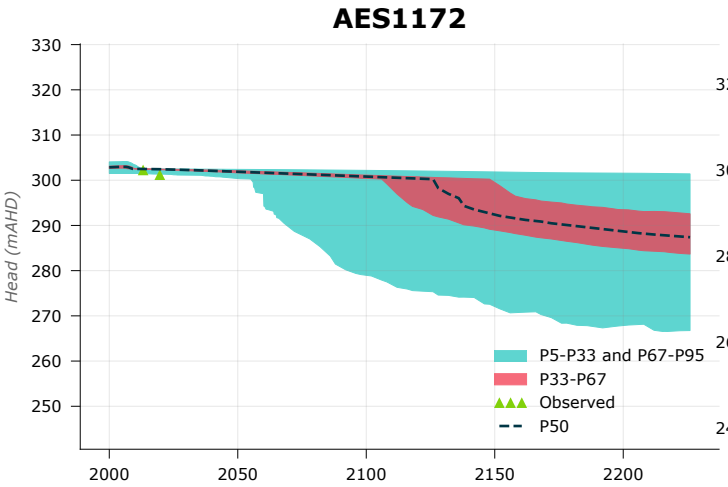
AES1079
330
320
310
300
290
280
270
260
250
2000
2050
2100
2150
2200
P5-P33 and P67-P95
P33-P67
Observed
P50

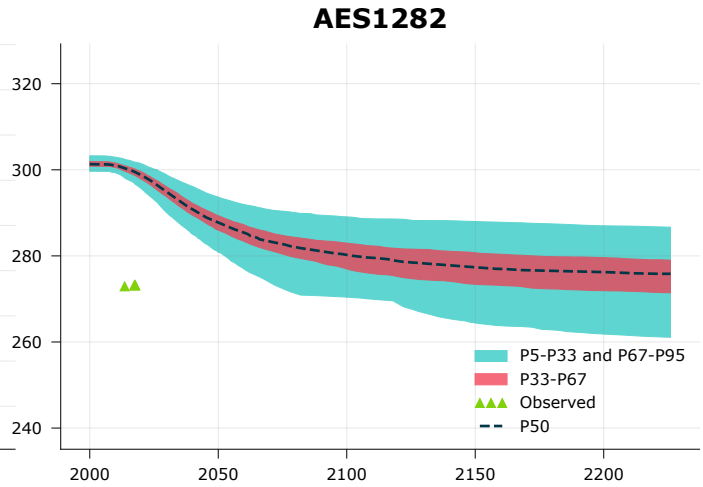

AES1080
Head (mAHD)
330
320
310
300
290
280
270
260
2000
2050
2100
2150
2200
P5-P33 and P67-P95
P33-P67
Observed
P50

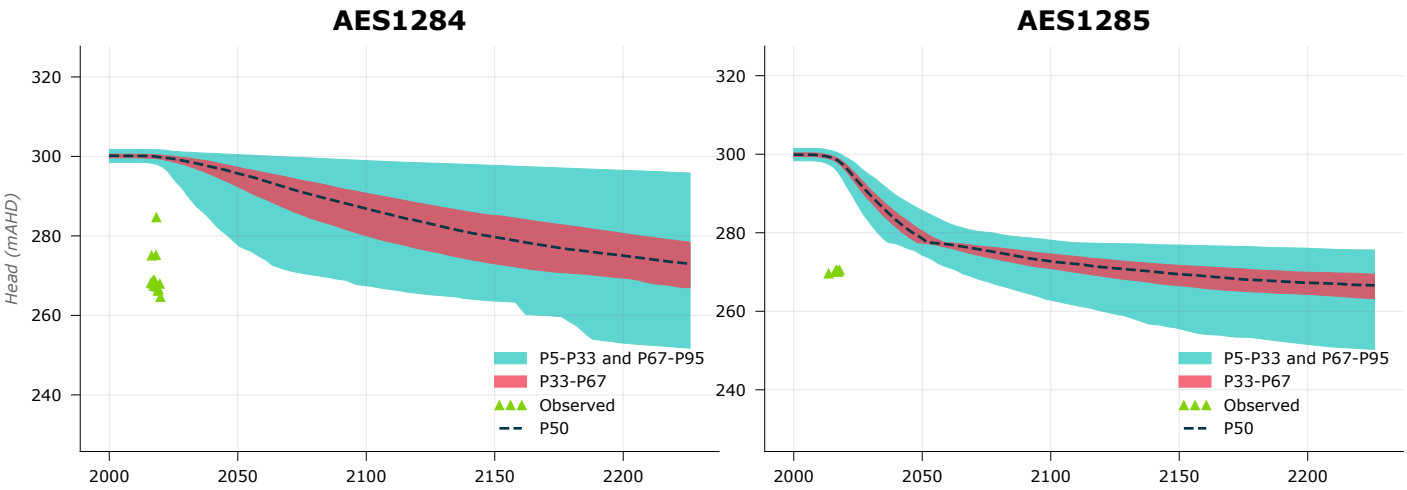

AES1081
330
320
310
300
290
280
270
260
250
2000
2050
2100
2150
2200
P5-P33 and P67-P95
P33-P67
Observed
P50


AES1158
Head (mAHD)
340
320
300
280
260
240
2000
2050
2100
2150
2200
P5-P33 and P67-P95
P33-P67
Observed
P50

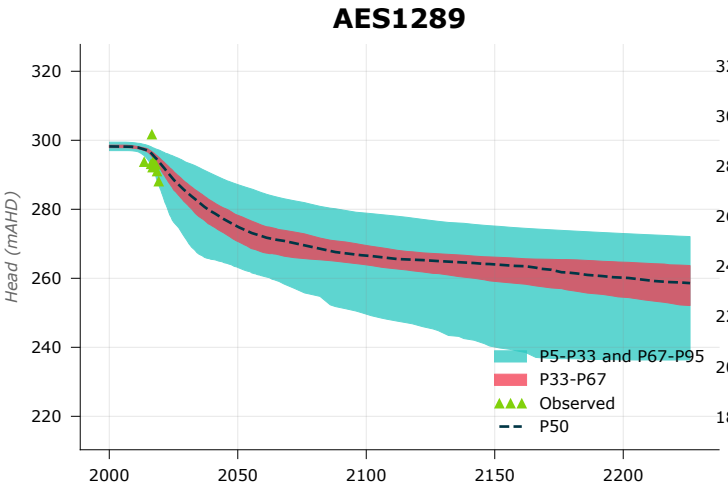

AES1171
325
300
275
250
225
200
175
150
2000
2050
2100
2150
2200
P5-P33 and P67-P95
P33-P67
Observed
P50

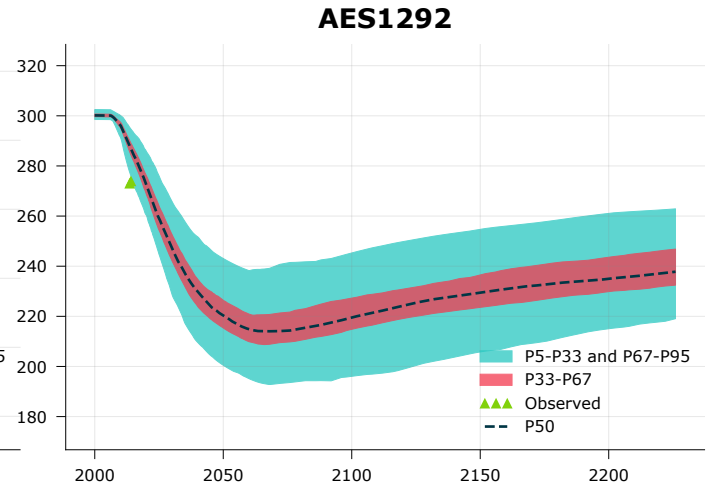

AES1172
Head (mAHD)
330
320
310
300
290
280
270
260
250
2000
2050
2100
2150
2200
P5-P33 and P67-P95
P33-P67
Observed
P50

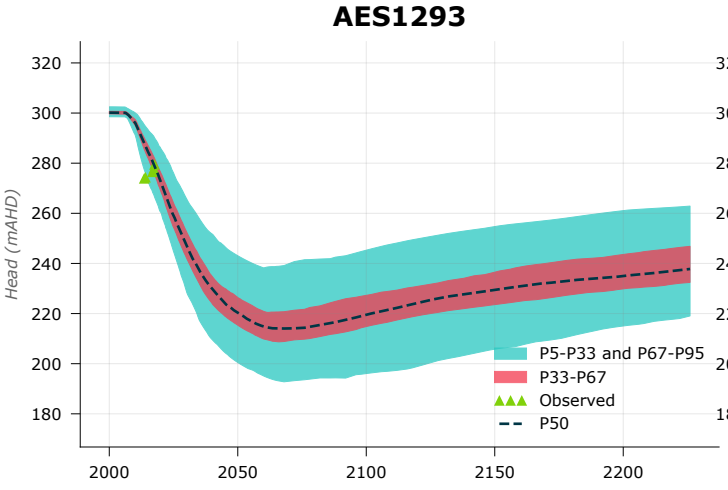

AES1282
320
300
280
260
240
2000
2050
2100
2150
2200
P5-P33 and P67-P95
P33-P67
Observed
P50

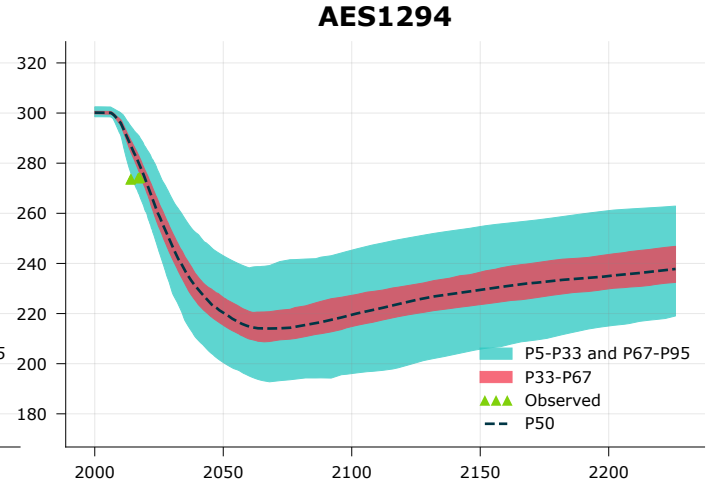

AES1284
Head (mAHD)
320
300
280
260
240
2000
2050
2100
2150
2200
P5-P33 and P67-P95
P33-P67
Observed
P50

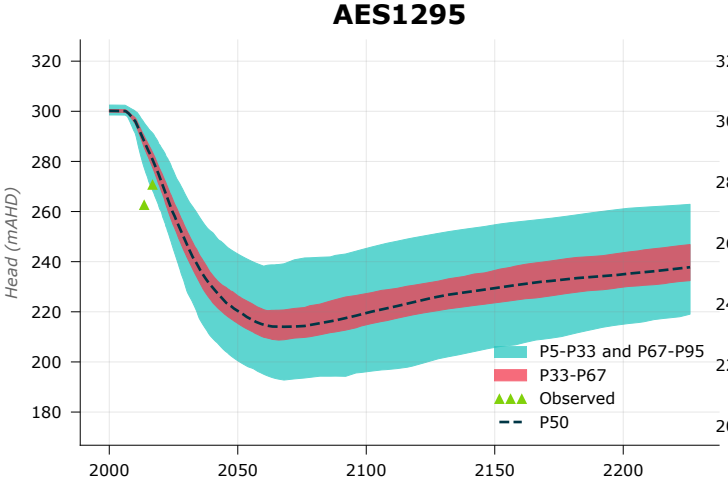
AES1285
320
300
280
260
240
2000
2050
2100
2150
2200
P5-P33 and P67-P95
P33-P67
Observed
P50

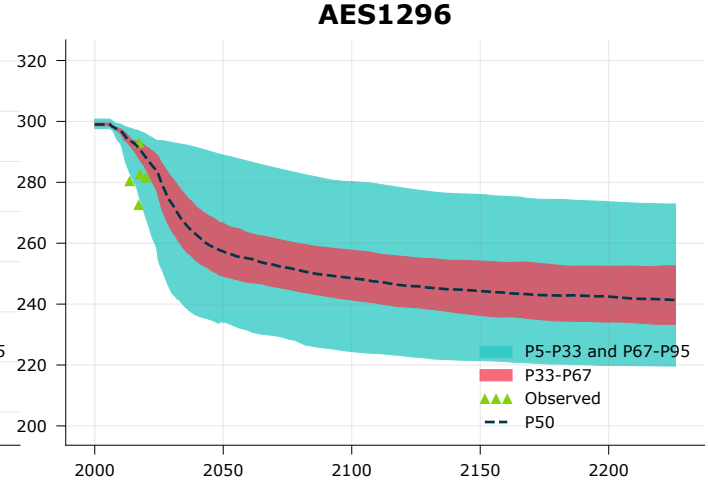

AES1289
Head (mAHD)
320
300
280
260
240
220
2000
2050
2100
2150
2200
P5-P33 and P67-P95
P33-P67
Observed
P50

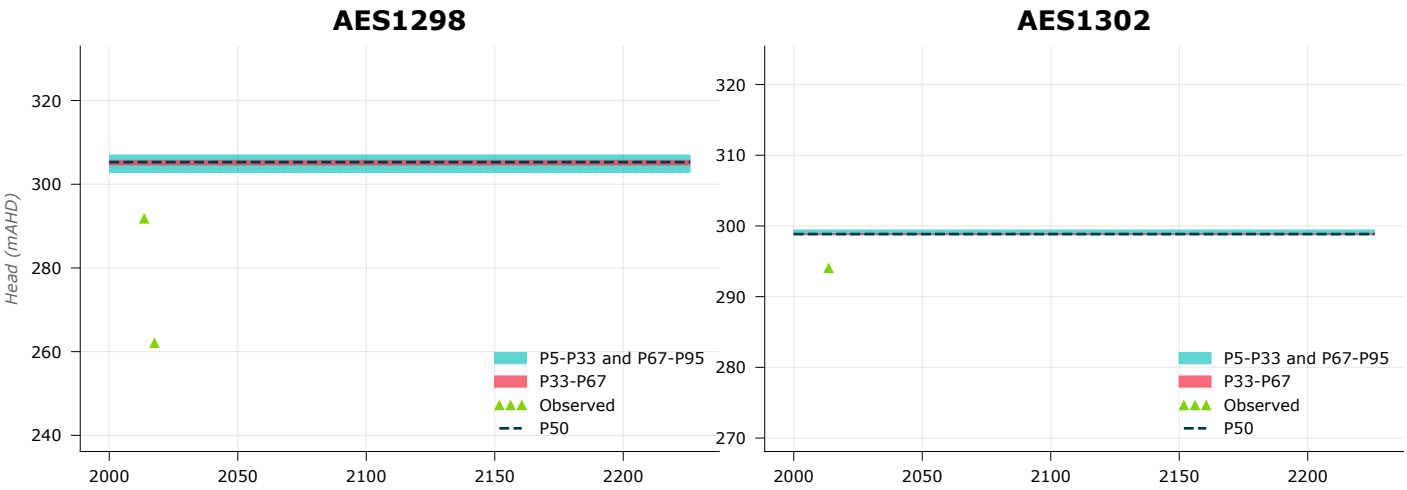

AES1292
320
300
280
260
240
220
200
180
2000
2050
2100
2150
2200
P5-P33 and P67-P95
P33-P67
Observed
P50


AES1293
Head (mAHD)
320
300
280
260
240
220
200
180
2000
2050
2100
2150
2200
P5-P33 and P67-P95
P33-P67
Observed
P50

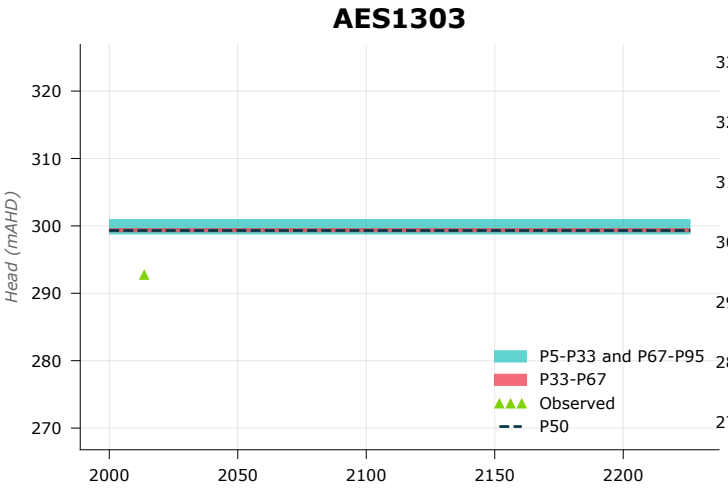

AES1294
320
300
280
260
240
220
200
180
2000
2050
2100
2150
2200
P5-P33 and P67-P95
P33-P67
Observed
P50

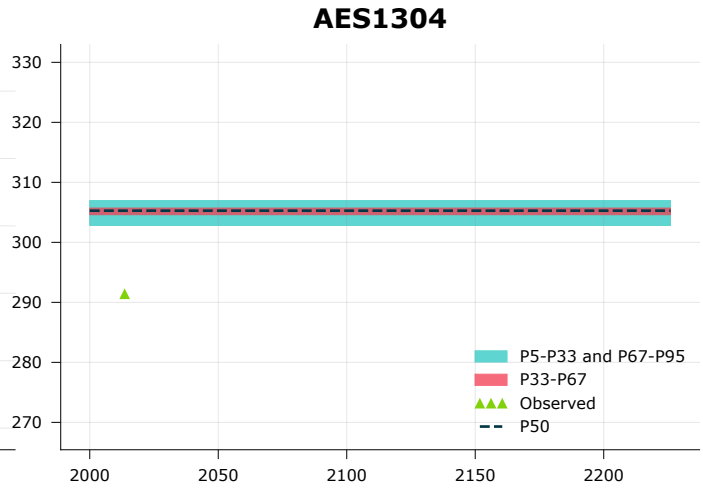

AES1295
Head (mAHD)
320
300
280
260
240
220
200
180
2000
2050
2100
2150
2200
P5-P33 and P67-P95
P33-P67
Observed
P50

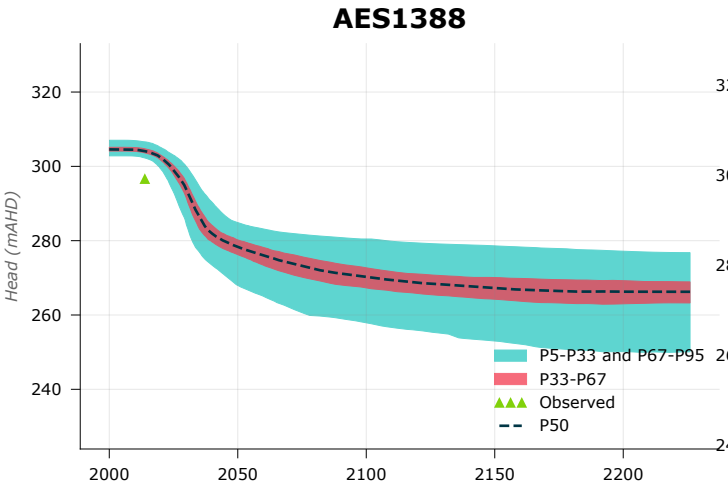

AES1296
320
300
280
260
240
220
200
2000
2050
2100
2150
2200
P5-P33 and P67-P95
P33-P67
Observed
P50

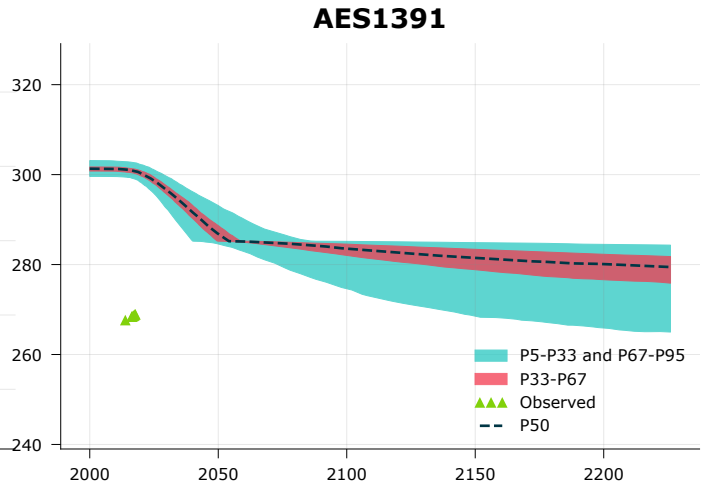

AES1298
Head (mAHD)
320
300
280
260
240
2000
2050
2100
2150
2200
P5-P33 and P67-P95
P33-P67
Observed
P50

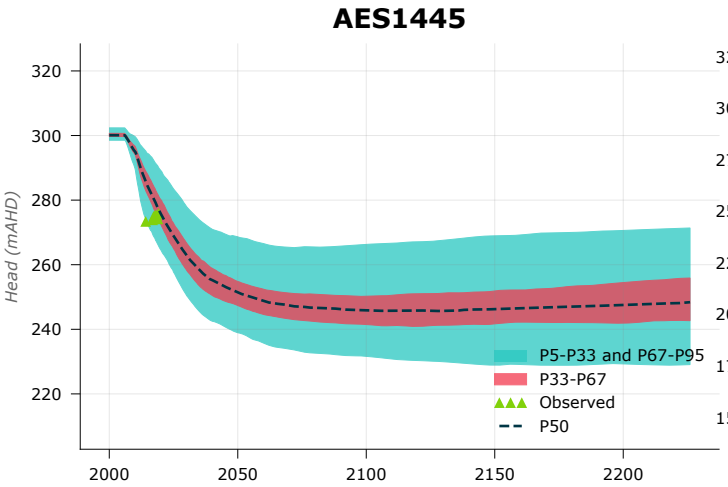
AES1302
320
310
300
290
280
270
2000
2050
2100
2150
2200
P5-P33 and P67-P95
P33-P67
Observed
P50

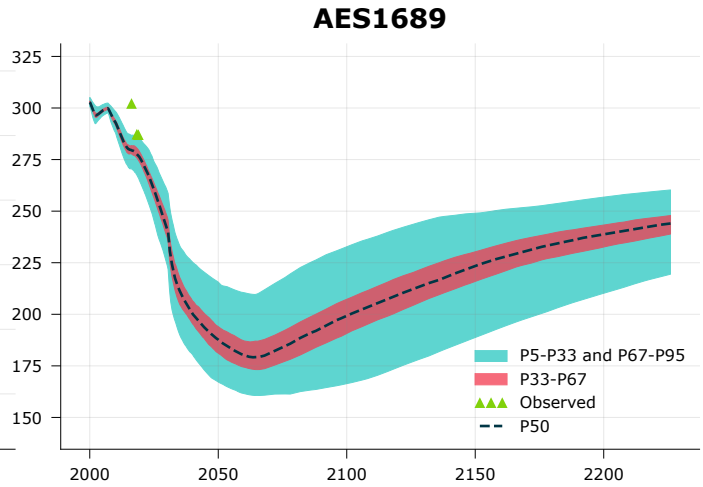

AES1303
Head (mAHD)
320
310
300
290
280
270
2000
2050
2100
2150
2200
P5-P33 and P67-P95
P33-P67
Observed
P50

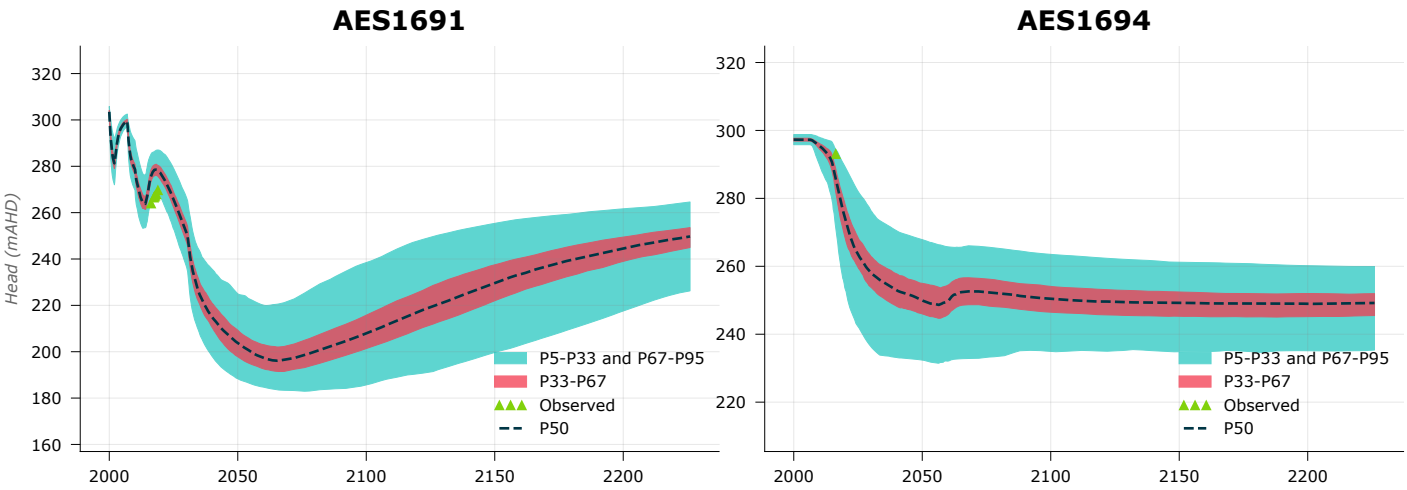

AES1304
330
320
310
300
290
280
270
2000
2050
2100
2150
2200
P5-P33 and P67-P95
P33-P67
Observed
P50


AES1388
Head (mAHD)
320
300
280
260
240
2000
2050
2100
2150
2200
P5-P33 and P67-P95
P33-P67
Observed
P50

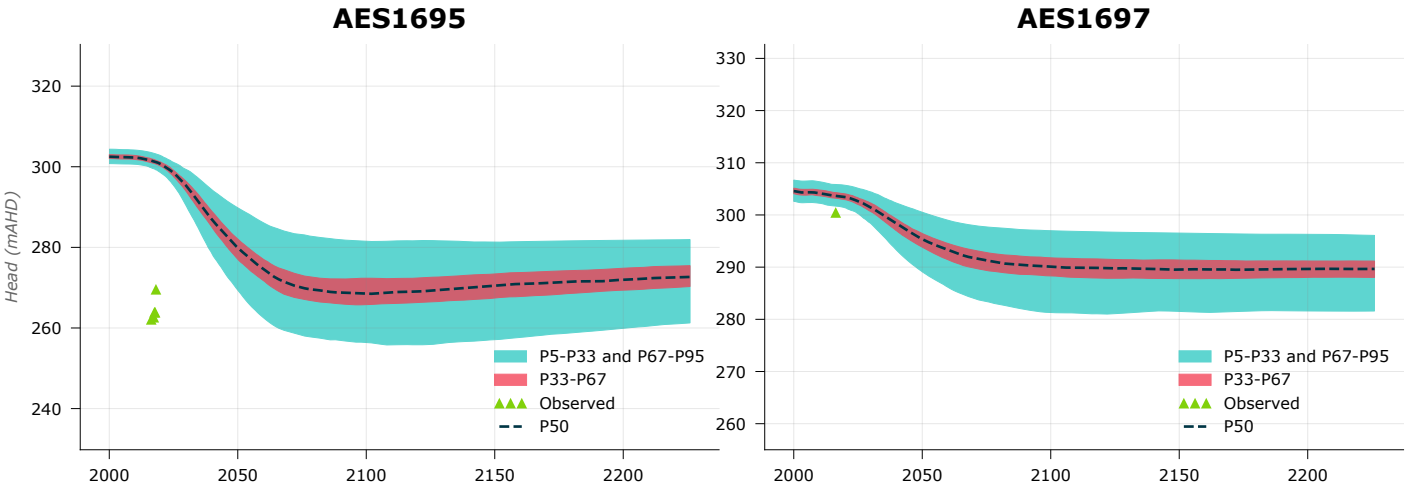

AES1391
320
300
280
260
240
2000
2050
2100
2150
2200
P5-P33 and P67-P95
P33-P67
Observed
P50


AES1445
Head (mAHD)
320
300
280
260
240
220
2000
2050
2100
2150
2200
P5-P33 and P67-P95
P33-P67
Observed
P50

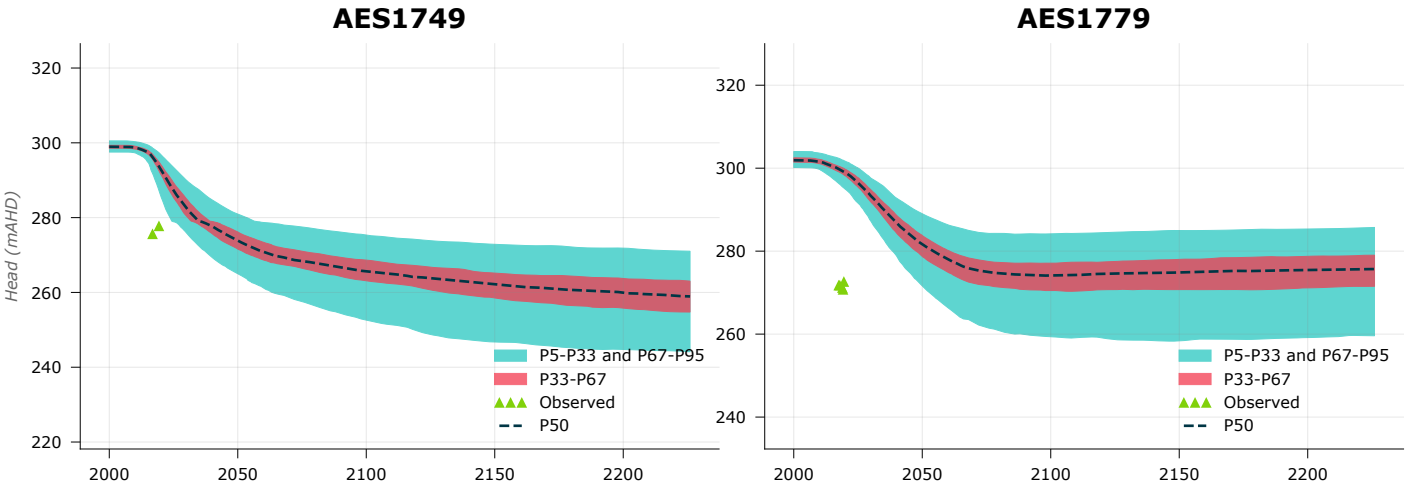

AES1689
325
300
275
250
225
200
175
150
2000
2050
2100
2150
2200
P5-P33 and P67-P95
P33-P67
Observed
P50


AES1691
Head (mAHD)
320
300
280
260
240
220
200
180
160
2000
2050
2100
2150
2200
P5-P33 and P67-P95
P33-P67
Observed
P50

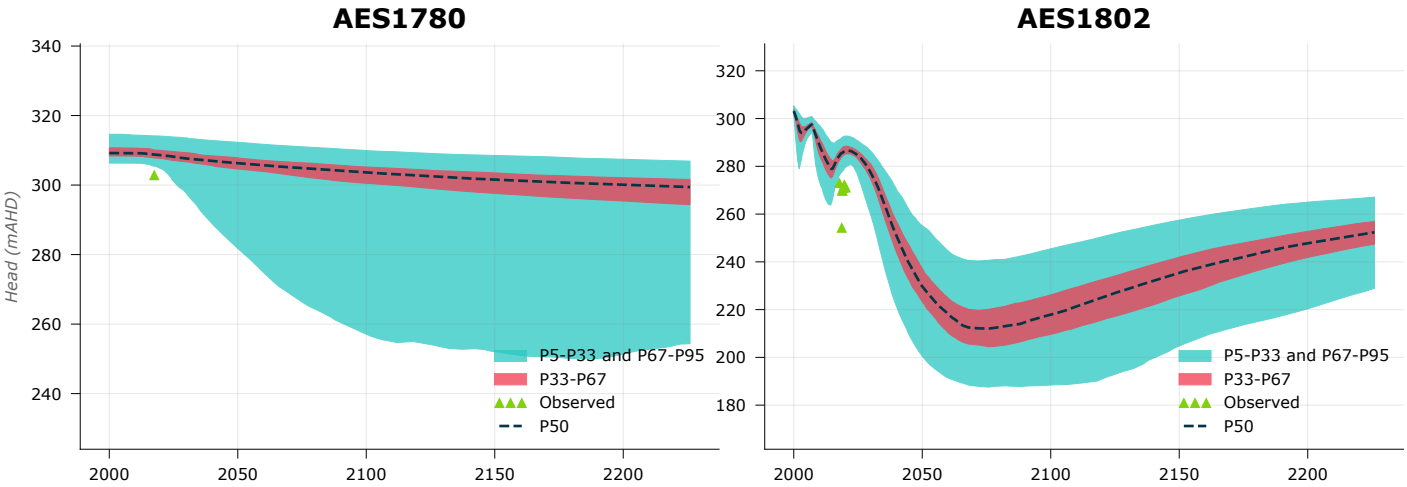
AES1694
320
300
280
260
240
220
2000
2050
2100
2150
2200
P5-P33 and P67-P95
P33-P67
Observed
P50


AES1695
Head (mAHD)
320
300
280
260
240
2000
2050
2100
2150
2200
P5-P33 and P67-P95
P33-P67
Observed
P50

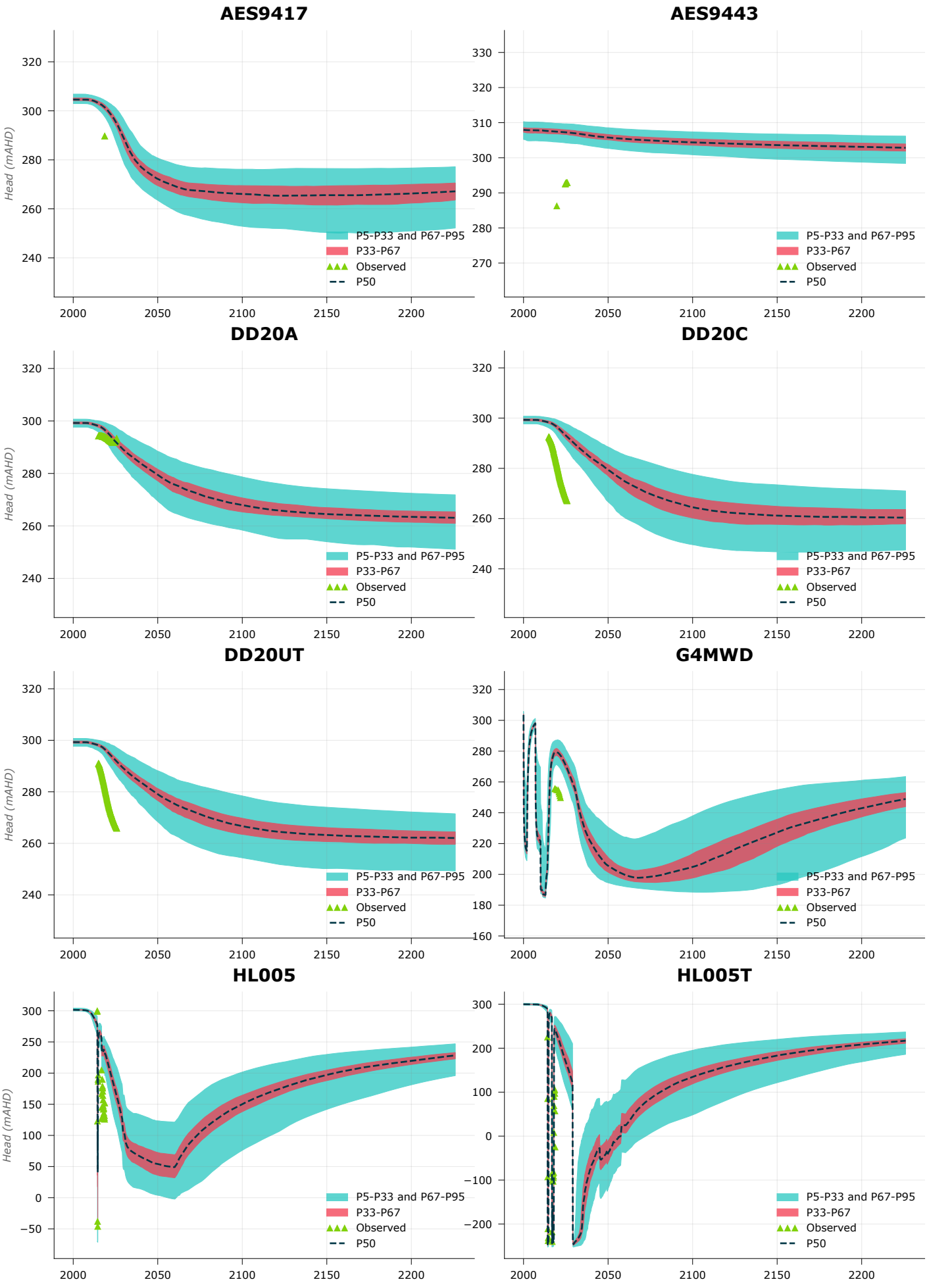
AES1697
330
320
310
300
290
280
270
260
2000
2050
2100
2150
2200
P5-P33 and P67-P95
P33-P67
Observed
P50

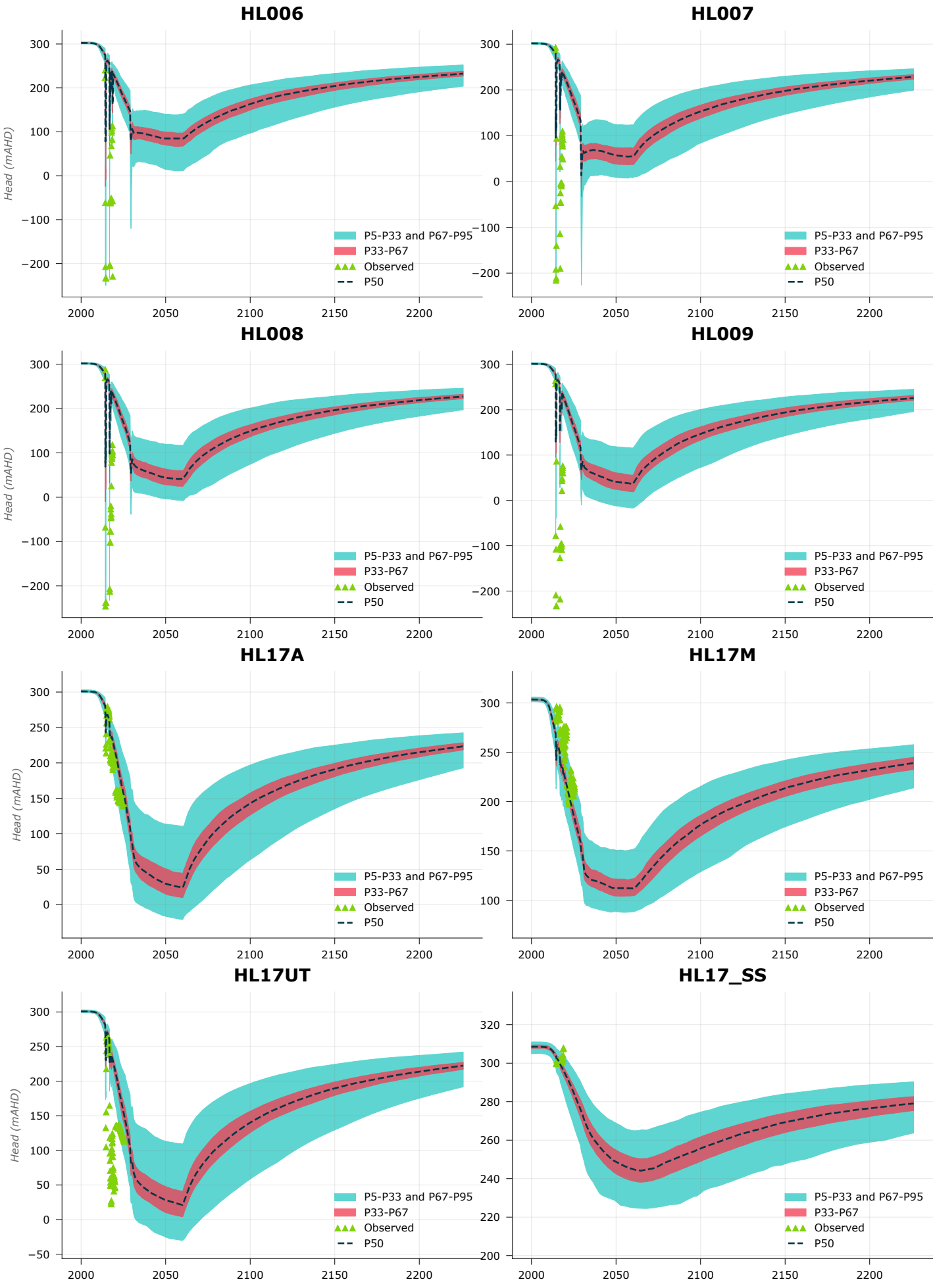

AES1749
Head (mAHD)
320
300
280
260
240
220
2000
2050
2100
2150
2200
P5-P33 and P67-P95
P33-P67
Observed
P50

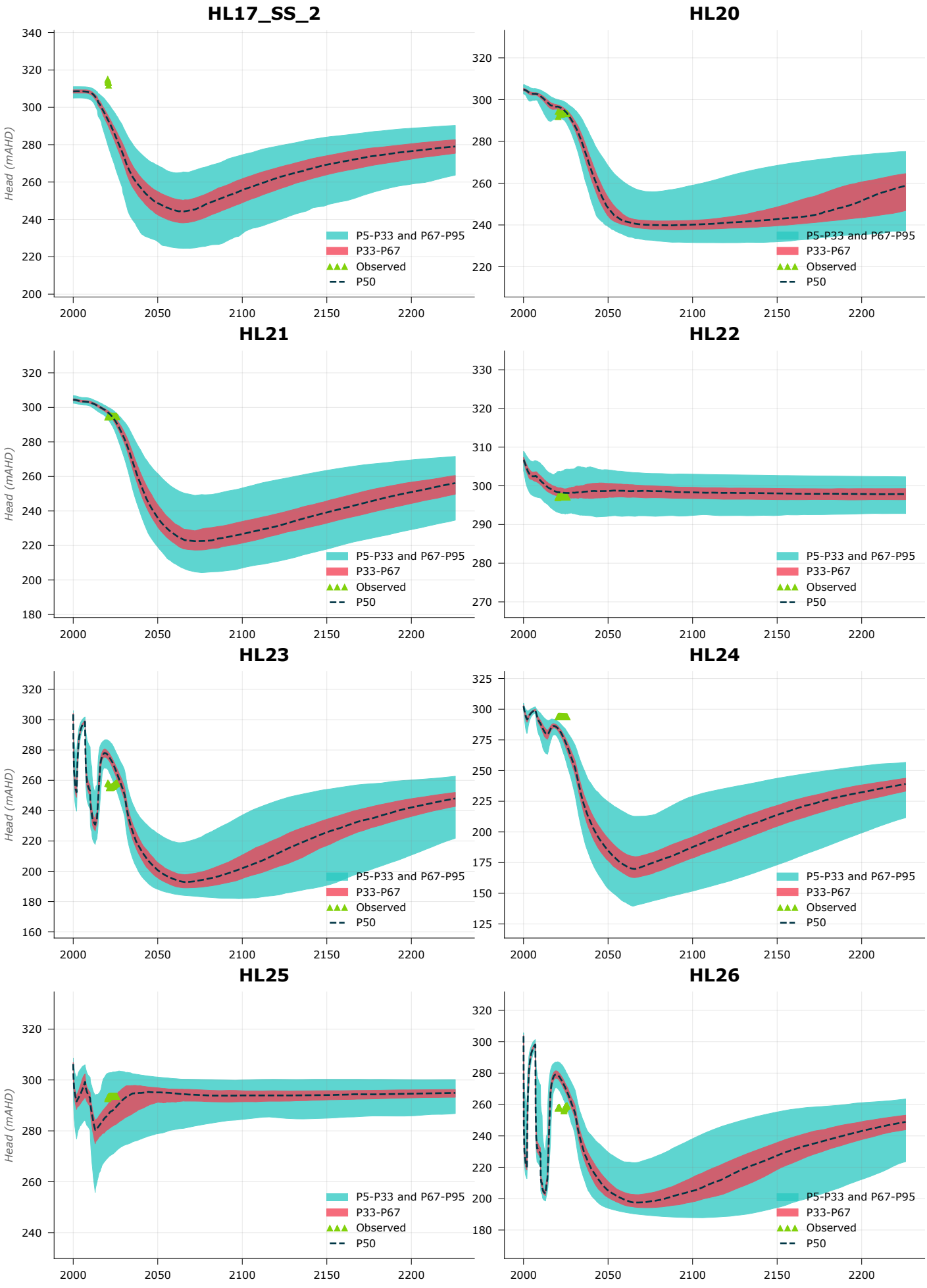
AES1779
320
300
280
260
240
2000
2050
2100
2150
2200
P5-P33 and P67-P95
P33-P67
Observed
P50

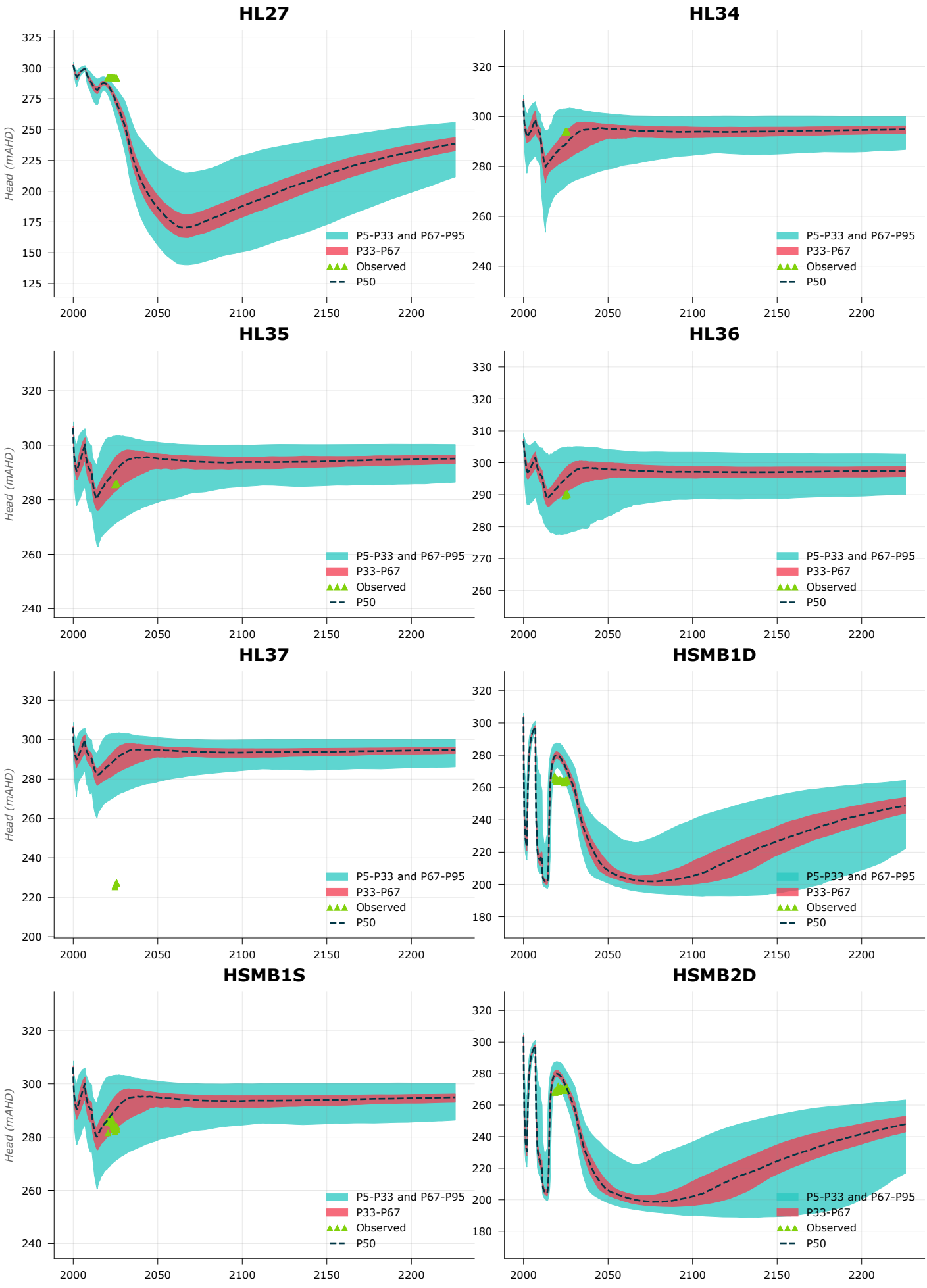

AES1780
Head (mAHD)
340
320
300
280
260
240
2000
2050
2100
2150
2200
P5-P33 and P67-P95
P33-P67
Observed
P50

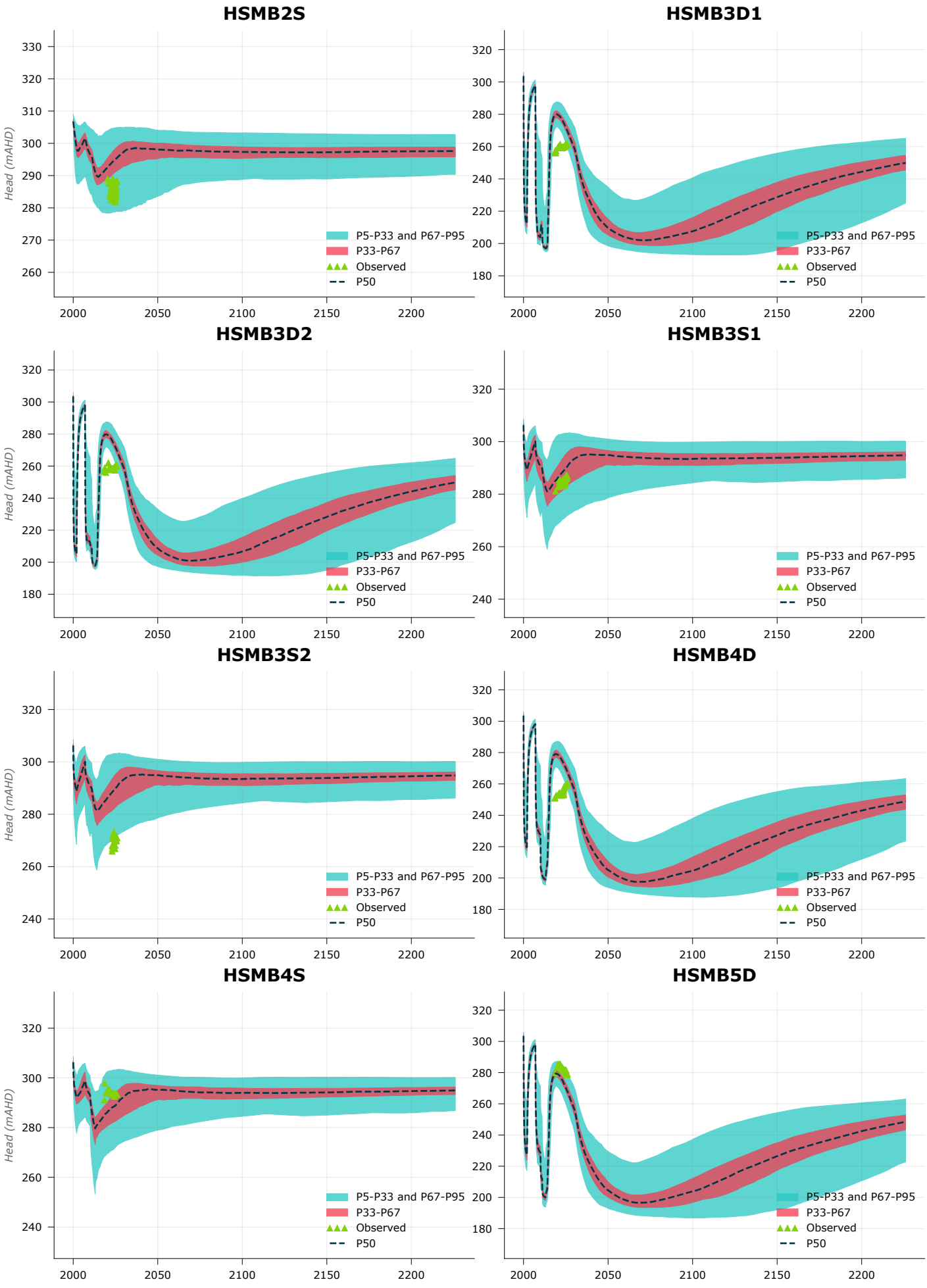
AES1802
320
300
280
260
240
220
200
180
2000
2050
2100
2150
2200
P5-P33 and P67-P95
P33-P67
Observed
P50

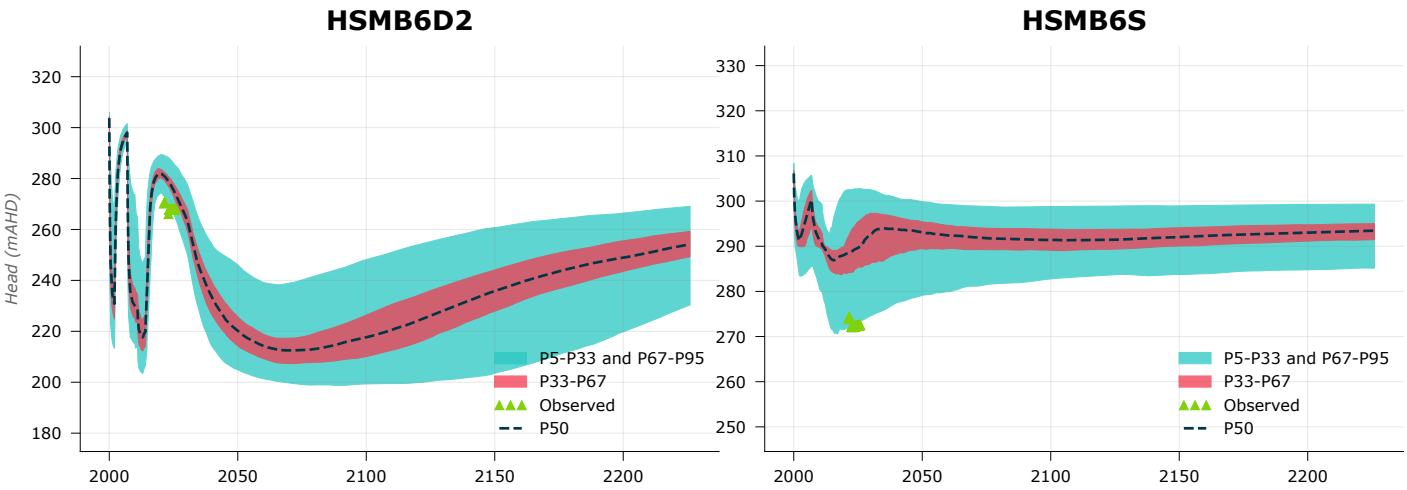

AES9417
AES9443
DD20A
DD20C
DD20UT
G4MWD
HL005
HL005T
Head (mAHD)
P5-P33 and P67-P95
P33-P67
Observed
P50


HL006
HL007
HL008
HL009
HL17A
HL17M
HL17UT
HL17_SS
Head (mAHD)
P5-P33 and P67-P95
P33-P67
Observed
P50

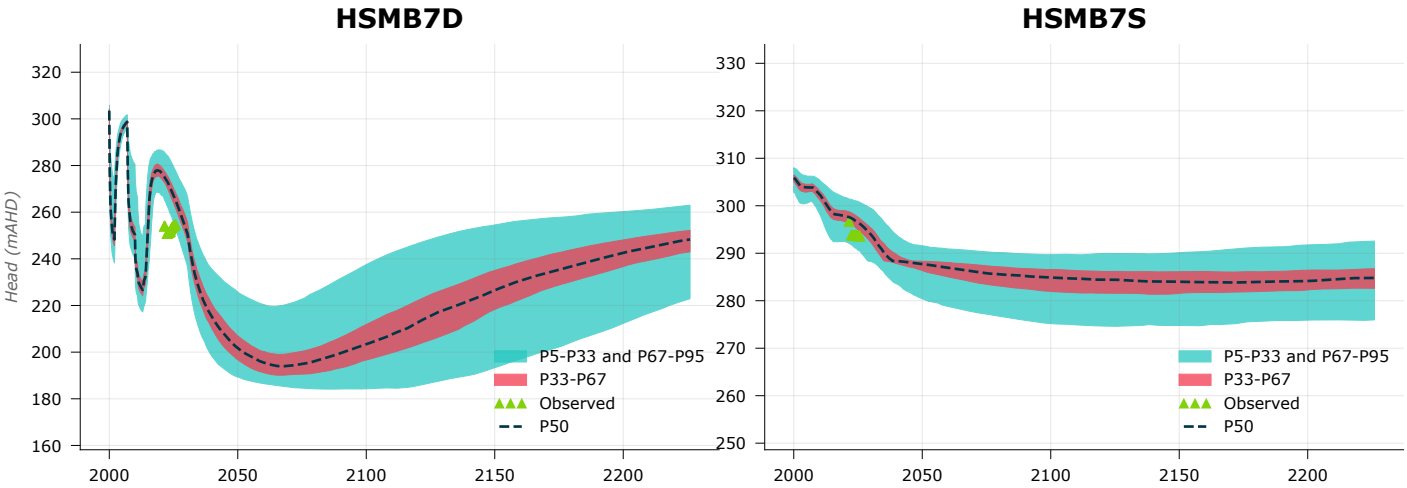

HL17_SS_2
HL20
HL21
HL22
HL23
HL24
HL25
HL26
Head (mAHD)
P5-P33 and P67-P95
P33-P67
Observed
P50


HL27
HL34
HL35
HL36
HL37
HSMB1D
HSMB1S
HSMB2D
Head (mAHD)
P5-P33 and P67-P95
P33-P67
Observed
P50
2000
2050
2100
2150
2200

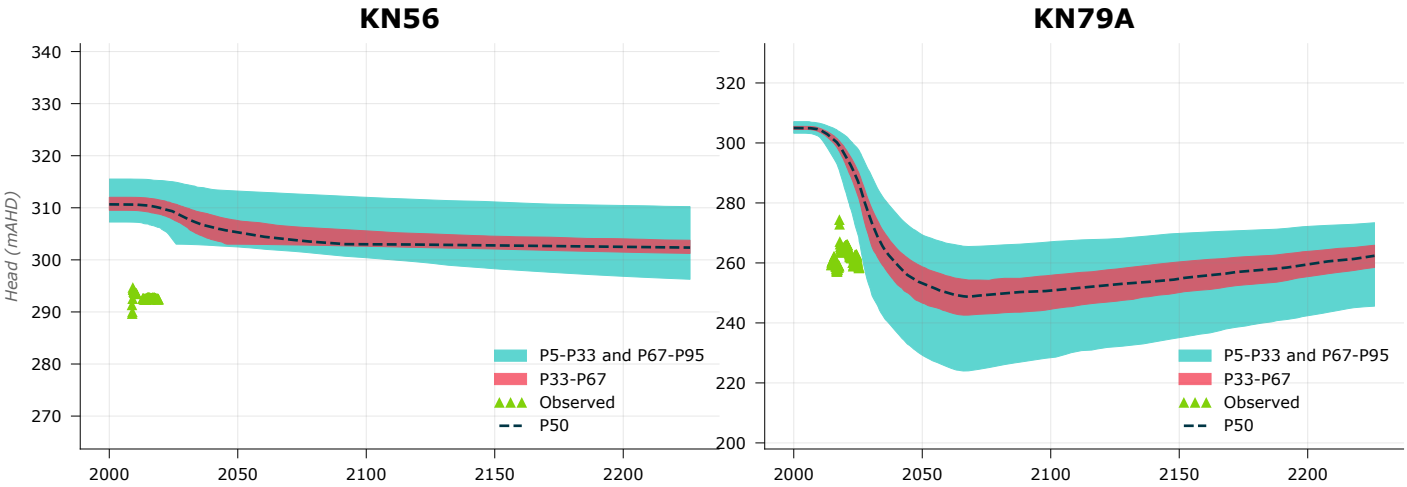

HSMB2S
HSMB3D1
HSMB3D2
HSMB3S1
HSMB3S2
HSMB4D
HSMB4S
HSMB5D
Head (mAHD)
P5-P33 and P67-P95
P33-P67
Observed
P50
2000
2050
2100
2150
2200


HSMB6D2
Head (mAHD)
320
300
280
260
240
220
200
180
2000
2050
2100
2150
2200
P5-P33 and P67-P95
P33-P67
Observed
P50

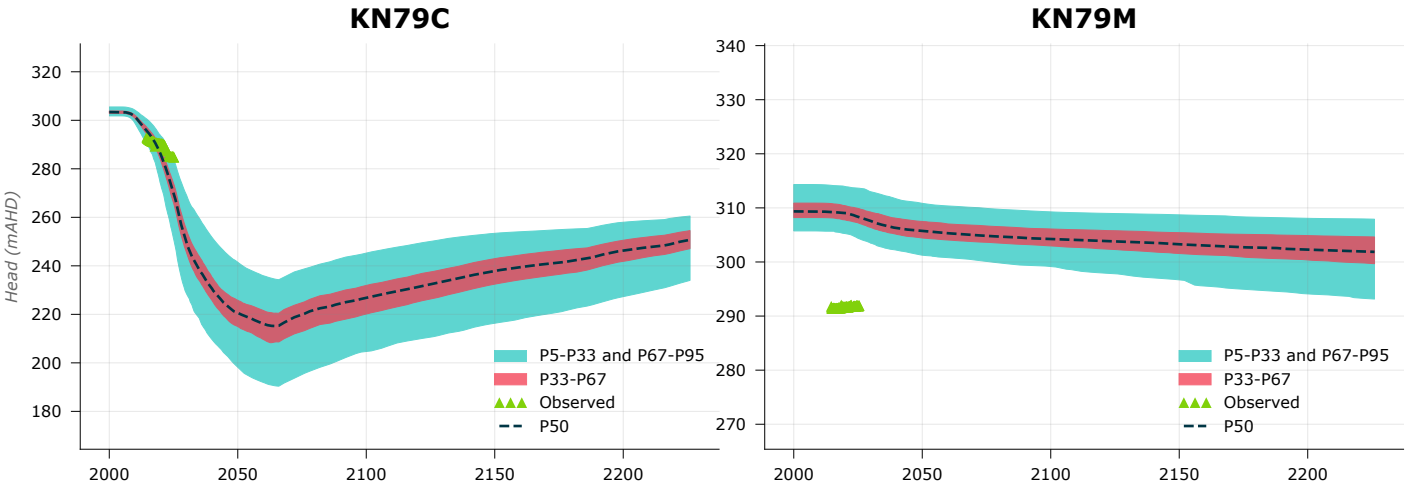
HSMB6S
330
320
310
300
290
280
270
260
250
2000
2050
2100
2150
2200
P5-P33 and P67-P95
P33-P67
Observed
P50


HSMB7D
Head (mAHD)
320
300
280
260
240
220
200
180
160
2000
2050
2100
2150
2200
P5-P33 and P67-P95
P33-P67
Observed
P50

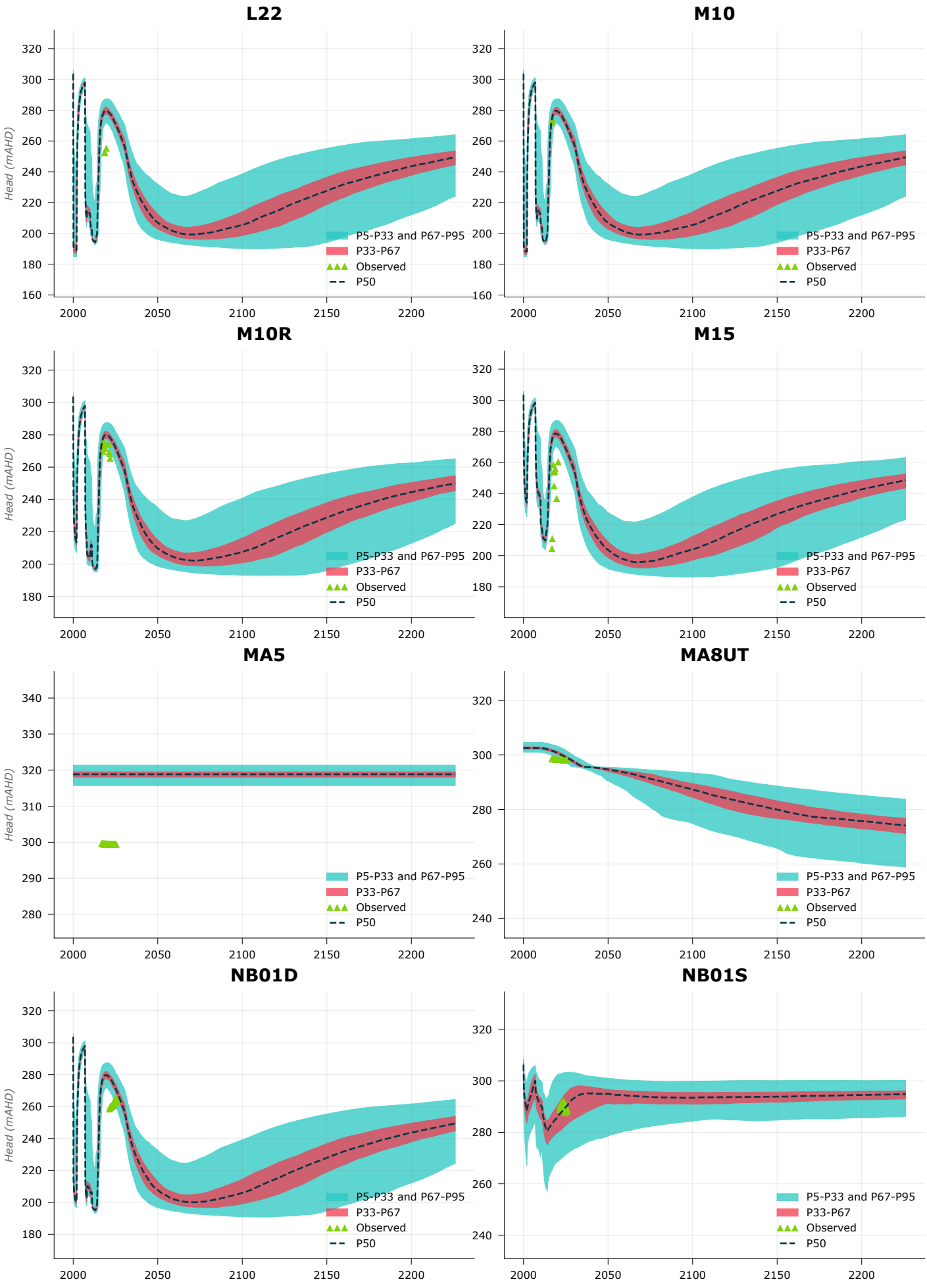
HSMB7S
330
320
310
300
290
280
270
260
250
2000
2050
2100
2150
2200
P5-P33 and P67-P95
P33-P67
Observed
P50

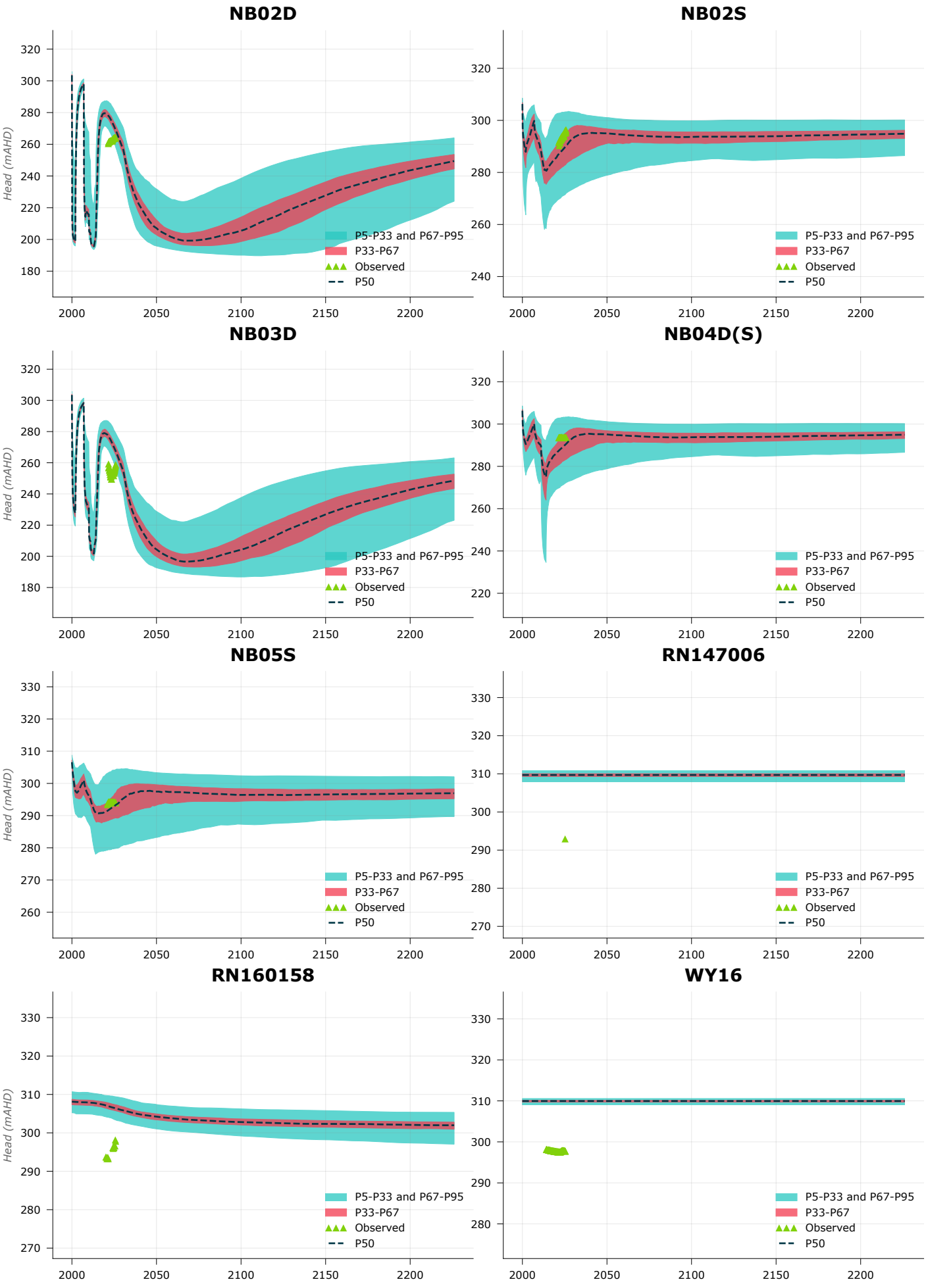

KN56
Head (mAHD)
340
330
320
310
300
290
280
270
2000
2050
2100
2150
2200
P5-P33 and P67-P95
P33-P67
Observed
P50

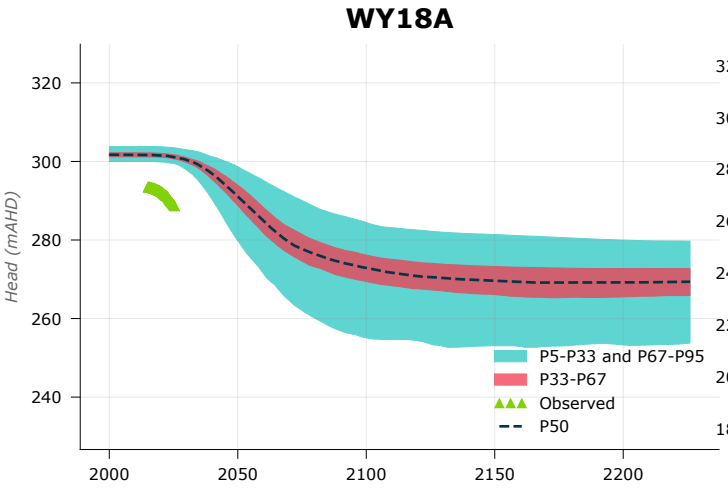
KN79A
320
300
280
260
240
220
200
2000
2050
2100
2150
2200
P5-P33 and P67-P95
P33-P67
Observed
P50

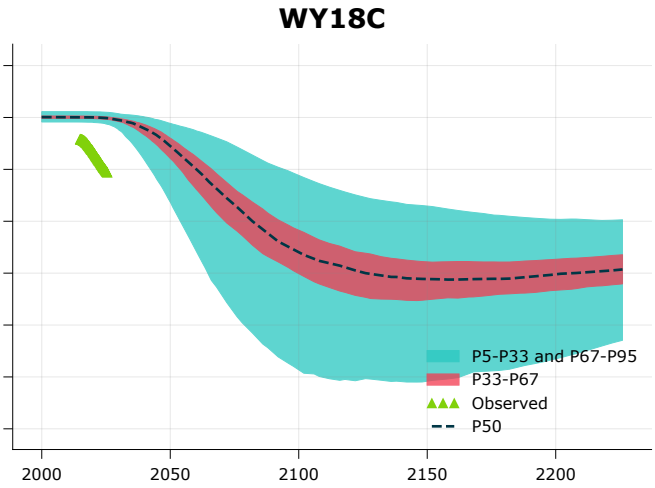

KN79C
Head (mAHD)
320
300
280
260
240
220
200
180
2000
2050
2100
2150
2200
P5-P33 and P67-P95
P33-P67
Observed
P50

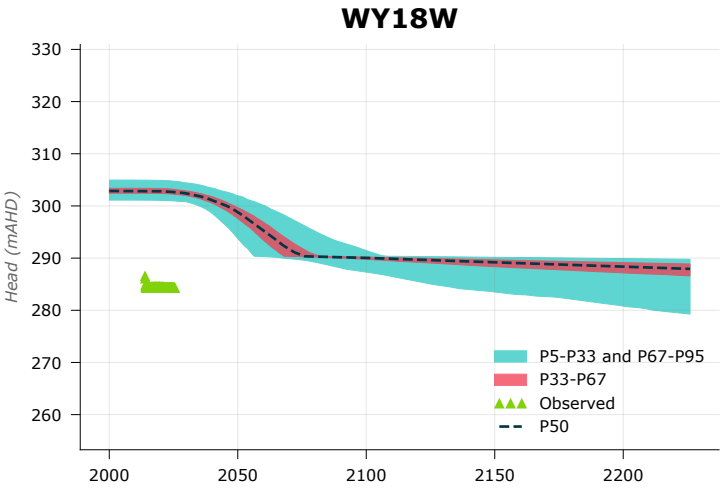
KN79M
340
330
320
310
300
290
280
270
2000
2050
2100
2150
2200
P5-P33 and P67-P95
P33-P67
Observed
P50


L22
M10
M10R
M15
MA5
MA8UT
NB01D
NB01S
Head (mAHD)
P5-P33 and P67-P95
P33-P67
Observed
P50
2000
2050
2100
2150
2200

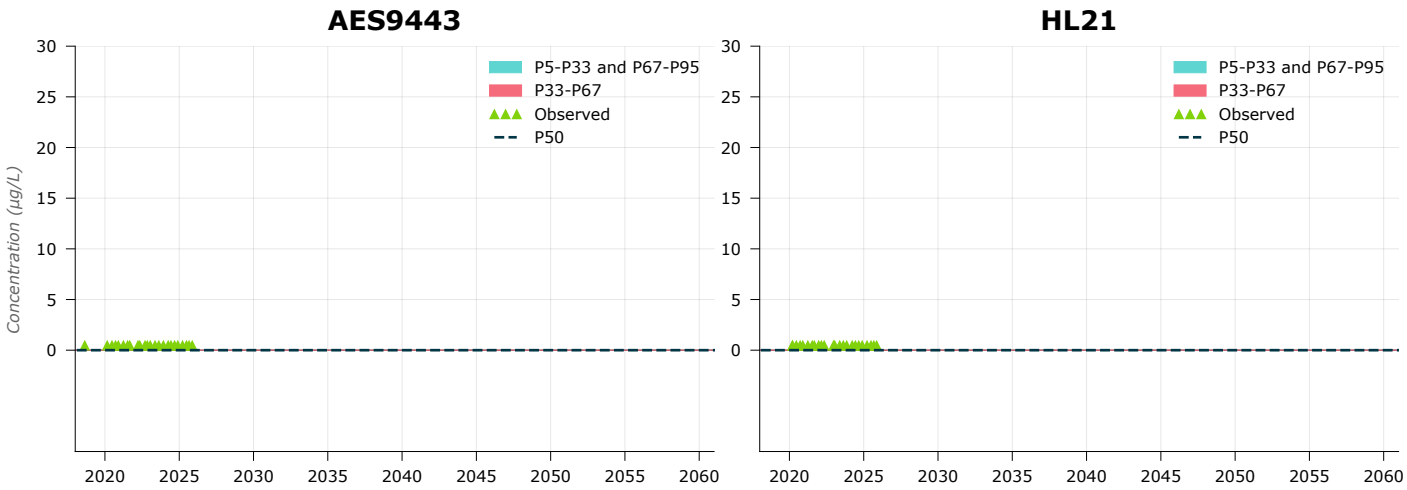

NB02D
NB02S
NB03D
NB04D(S)
NB05S
RN147006
RN160158
WY16
Head (mAHD)
P5-P33 and P67-P95
P33-P67
Observed
P50
2000
2050
2100
2150
2200

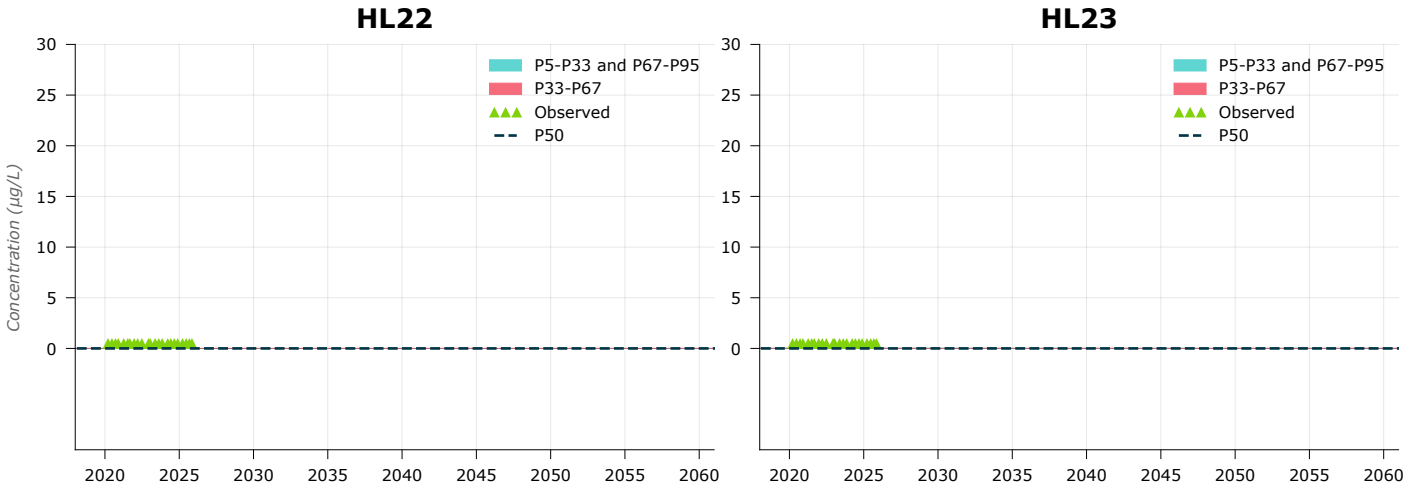

WY18A
Head (mAHD)
320
300
280
260
240
2000
2050
2100
2150
2200
P5-P33 and P67-P95
P33-P67
Observed
P50

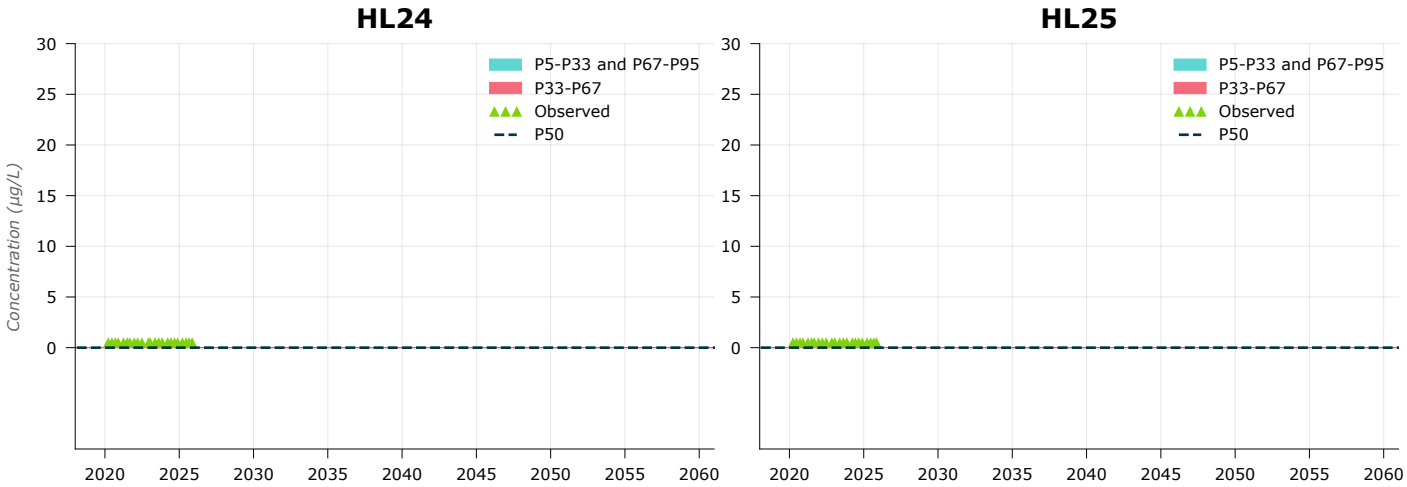

WY18C
320
300
280
260
240
220
200
180
2000
2050
2100
2150
2200
P5-P33 and P67-P95
P33-P67
Observed
P50

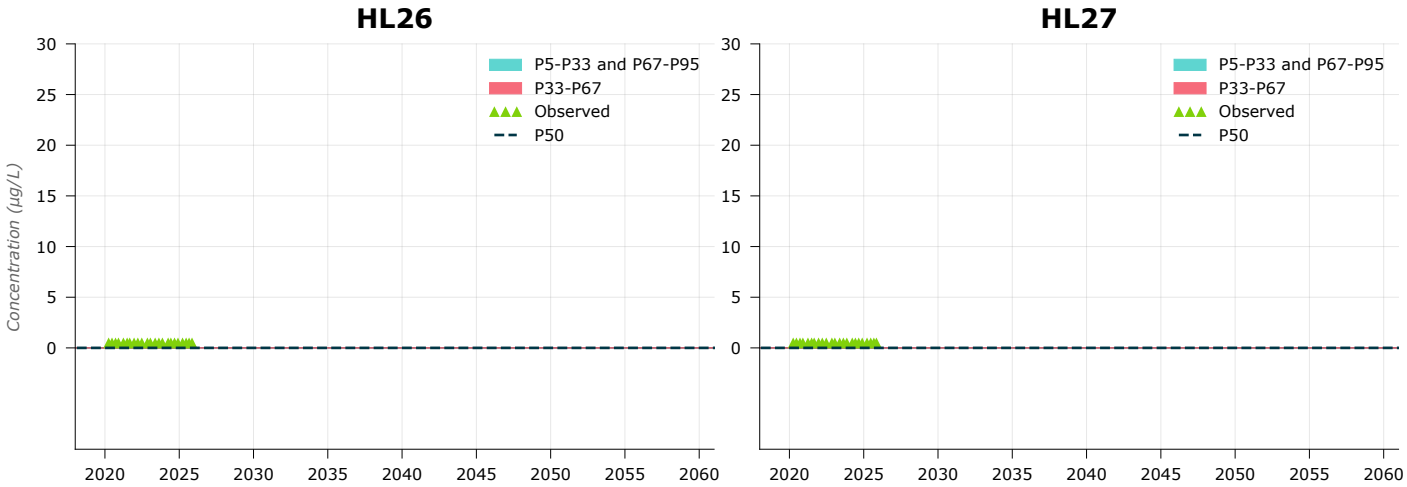

WY18W
Head (mAHD)
330
320
310
300
290
280
270
260
2000
2050
2100
2150
2200
P5-P33 and P67-P95
P33-P67
Observed
P50

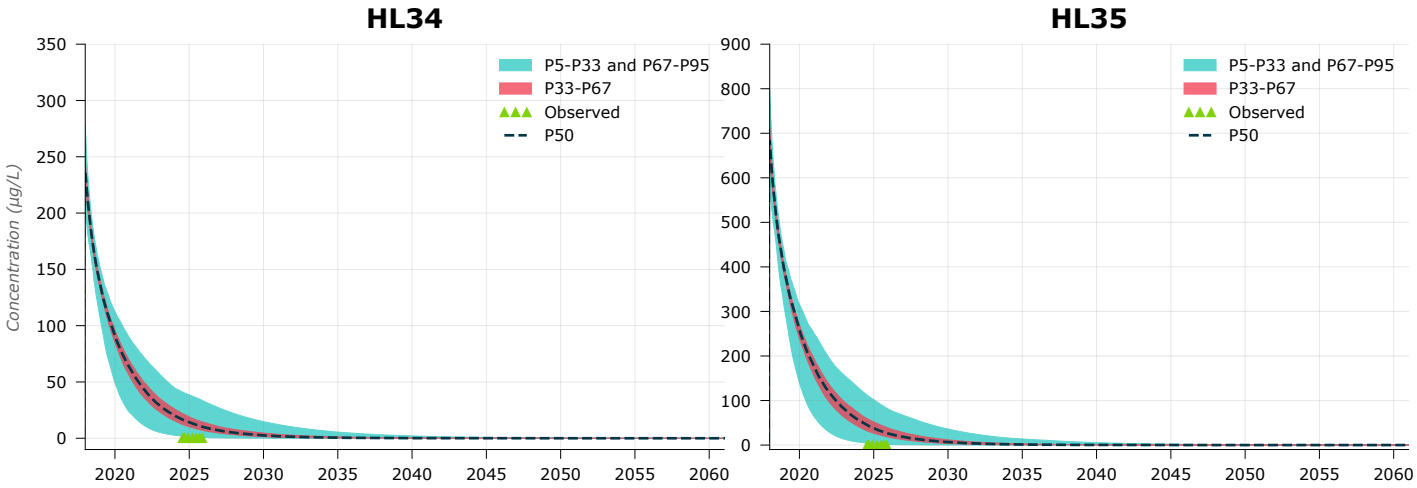
Appendix F. Predictive uncertainty – Benzene concentrations


AES9443
HL21
P5-P33 and P67-P95
P33-P67
Observed
P50
Concentration (µg/L)
0
5
10
15
20
25
30
2020
2025
2030
2035
2040
2045
2050
2055
2060

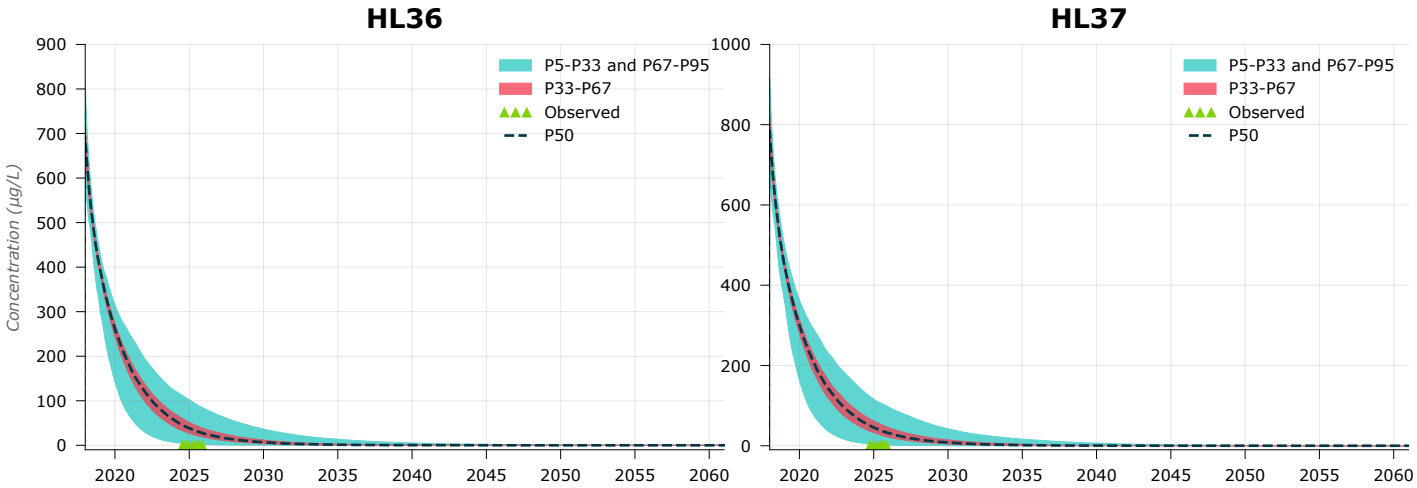

HL22
HL23
P5-P33 and P67-P95
P33-P67
Observed
P50
Concentration (µg/L)
0
5
10
15
20
25
30
2020
2025
2030
2035
2040
2045
2050
2055
2060


HL24
HL25
P5-P33 and P67-P95
P33-P67
Observed
P50
Concentration (µg/L)
0
5
10
15
20
25
30
2020
2025
2030
2035
2040
2045
2050
2055
2060

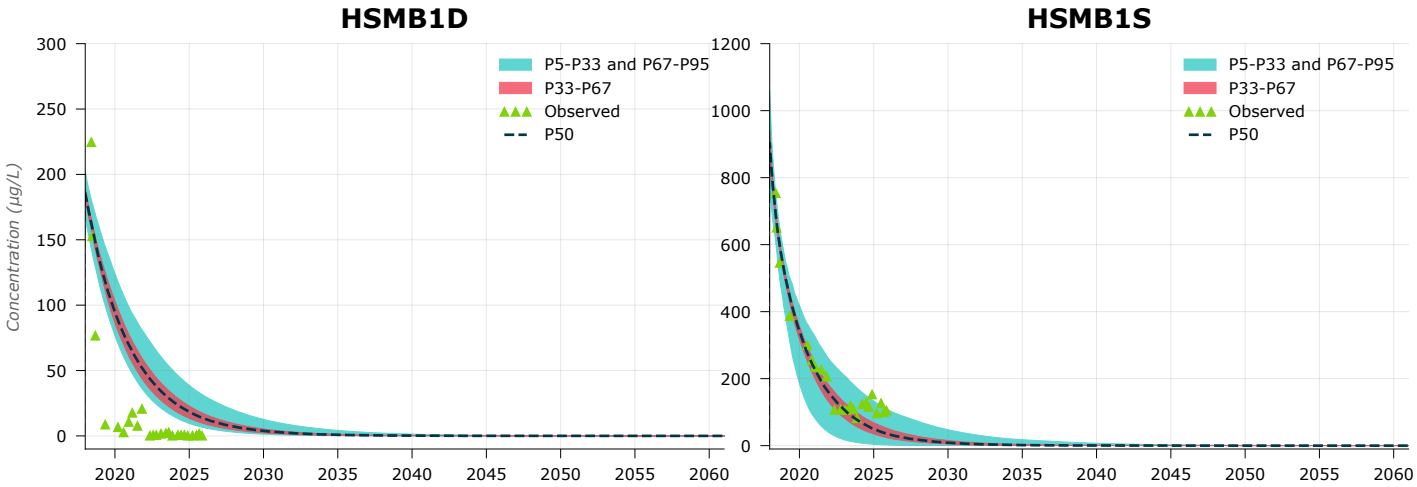

HL26
HL27
P5-P33 and P67-P95
P33-P67
Observed
P50
Concentration (µg/L)
0
5
10
15
20
25
30
2020
2025
2030
2035
2040
2045
2050
2055
2060


HL34
Concentration (µg/L)
P5-P33 and P67-P95
P33-P67
Observed
P50
0
50
100
150
200
250
300
350
2020
2025
2030
2035
2040
2045
2050
2055
2060

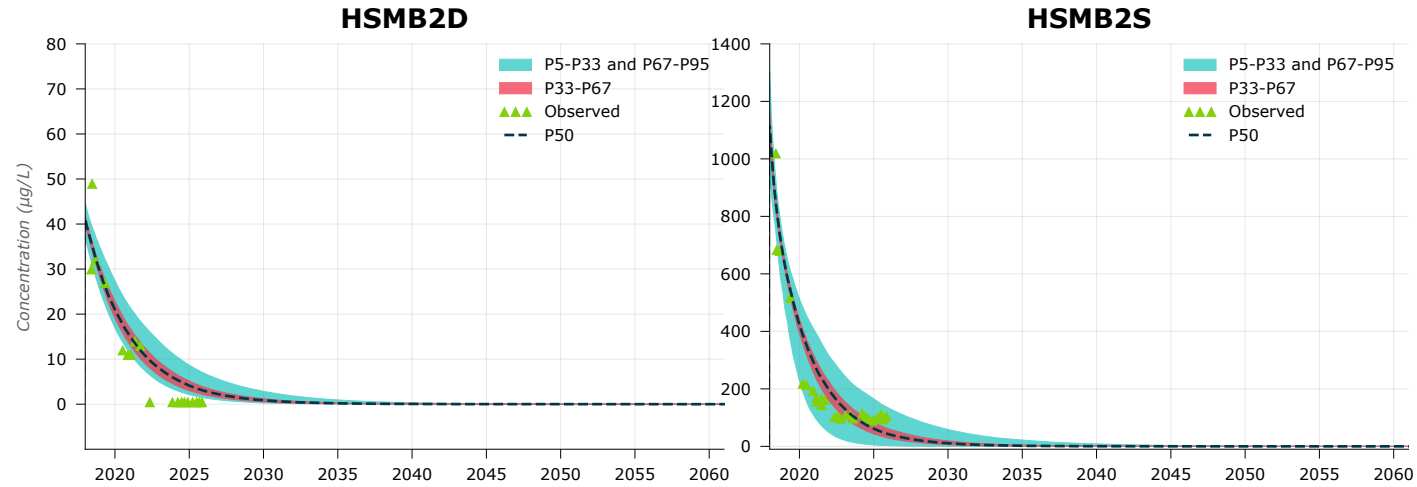
HL35
P5-P33 and P67-P95
P33-P67
Observed
P50
0
100
200
300
400
500
600
700
800
900
2020
2025
2030
2035
2040
2045
2050
2055
2060


HL36
Concentration (µg/L)
P5-P33 and P67-P95
P33-P67
Observed
P50
0
100
200
300
400
500
600
700
800
900
2020
2025
2030
2035
2040
2045
2050
2055
2060

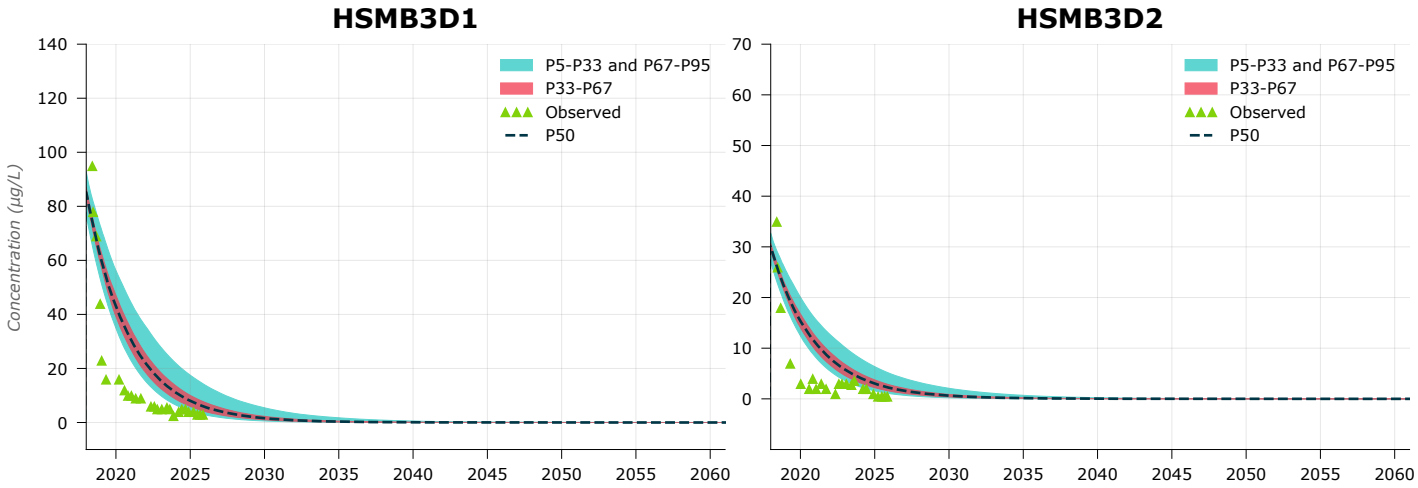
HL37
P5-P33 and P67-P95
P33-P67
Observed
P50
0
200
400
600
800
1000
2020
2025
2030
2035
2040
2045
2050
2055
2060


HSMB1D
Concentration (µg/L)
P5-P33 and P67-P95
P33-P67
Observed
P50
0
50
100
150
200
250
300
2020
2025
2030
2035
2040
2045
2050
2055
2060

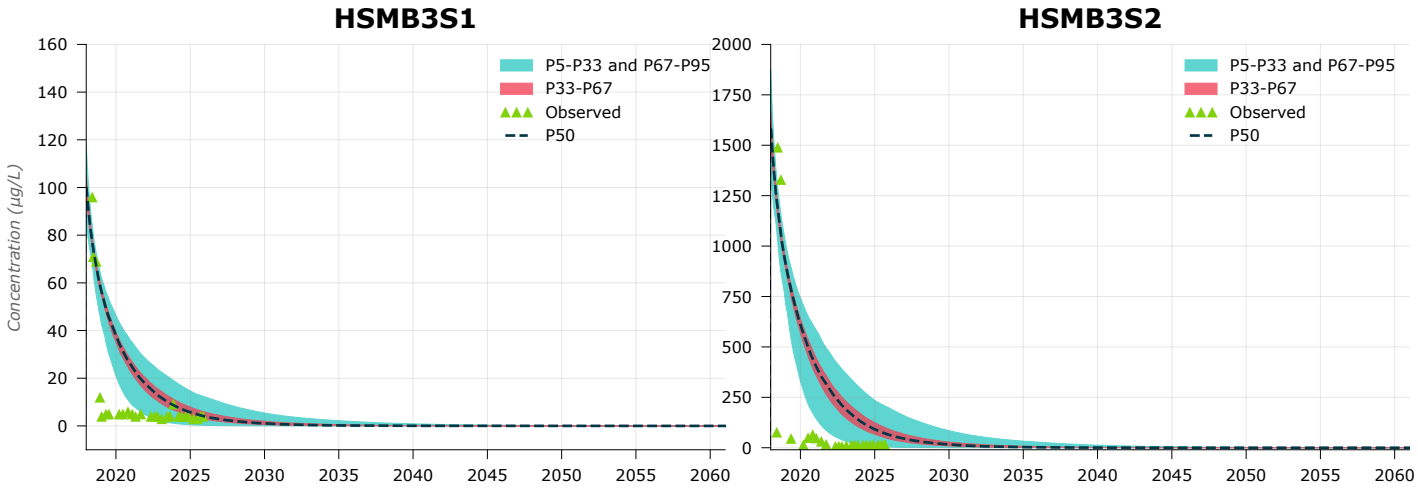
HSMB1S
P5-P33 and P67-P95
P33-P67
Observed
P50
0
200
400
600
800
1000
1200
2020
2025
2030
2035
2040
2045
2050
2055
2060


HSMB2D
Concentration (µg/L)
P5-P33 and P67-P95
P33-P67
Observed
P50
0
10
20
30
40
50
60
70
80
2020
2025
2030
2035
2040
2045
2050
2055
2060

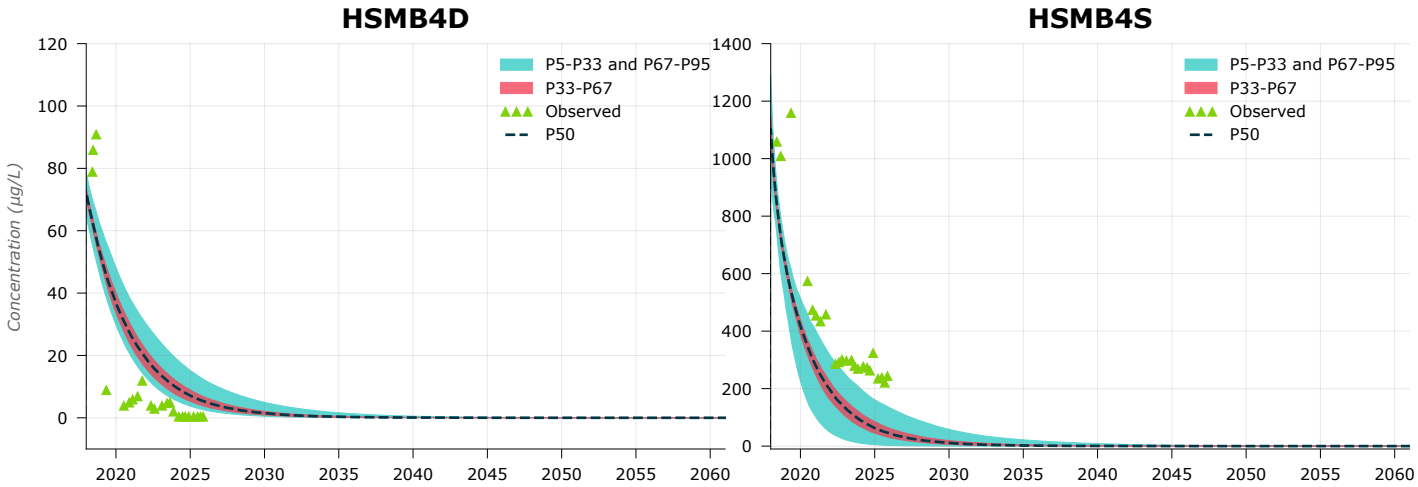
HSMB2S
P5-P33 and P67-P95
P33-P67
Observed
P50
0
200
400
600
800
1000
1200
1400
2020
2025
2030
2035
2040
2045
2050
2055
2060


HSMB3D1
Concentration (µg/L)
P5-P33 and P67-P95
P33-P67
Observed
P50
0
20
40
60
80
100
120
140
2020
2025
2030
2035
2040
2045
2050
2055
2060

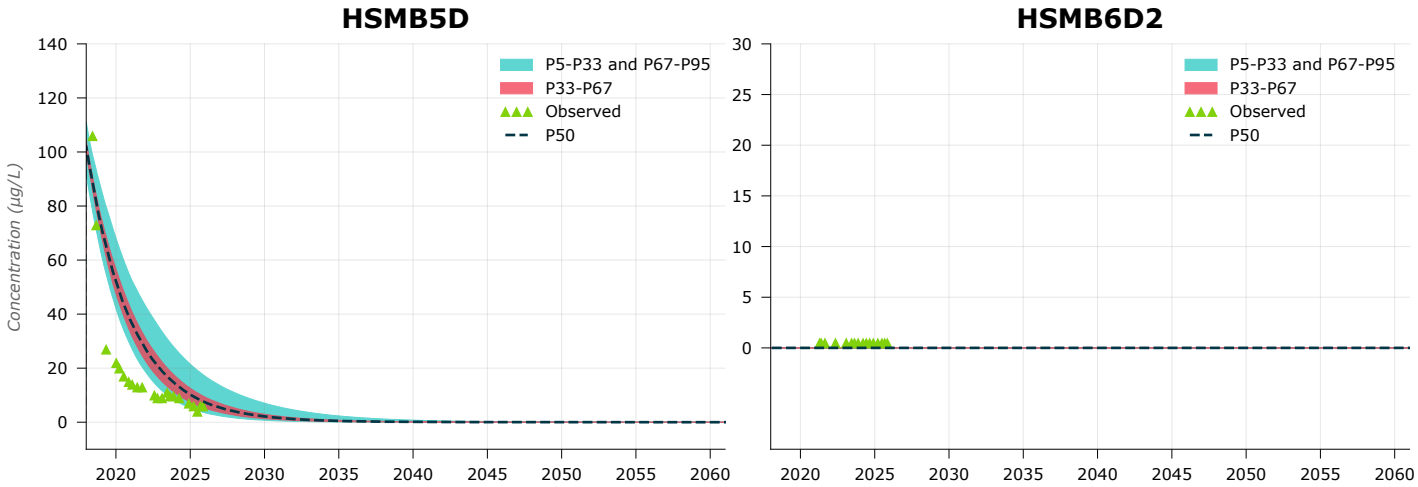
HSMB3D2
P5-P33 and P67-P95
P33-P67
Observed
P50
0
10
20
30
40
50
60
70
2020
2025
2030
2035
2040
2045
2050
2055
2060


HSMB3S1
Concentration (µg/L)
P5-P33 and P67-P95
P33-P67
Observed
P50
0
20
40
60
80
100
120
140
160
2020
2025
2030
2035
2040
2045
2050
2055
2060

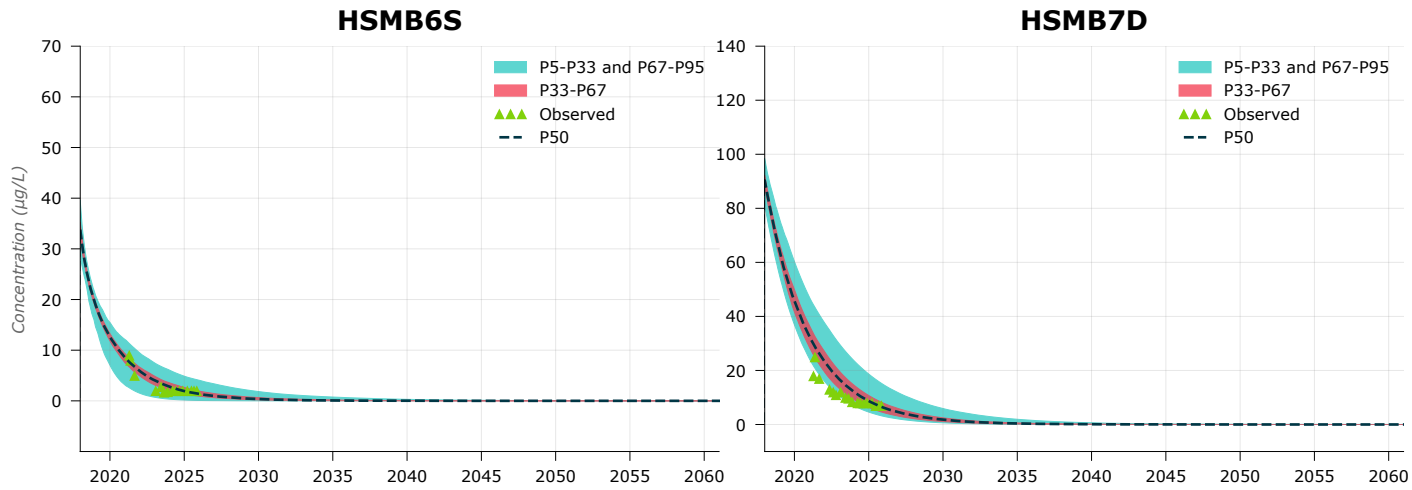
HSMB3S2
P5-P33 and P67-P95
P33-P67
Observed
P50
0
250
500
750
1000
1250
1500
1750
2000
2020
2025
2030
2035
2040
2045
2050
2055
2060

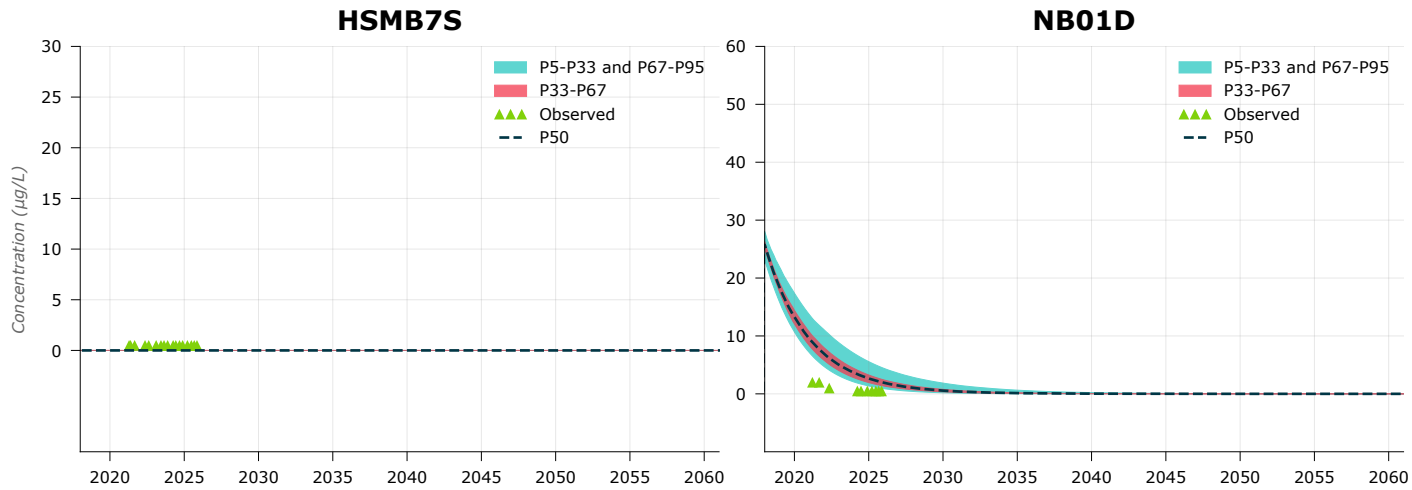

HSMB4D
Concentration (µg/L)
P5-P33 and P67-P95
P33-P67
Observed
P50
0
20
40
60
80
100
120
2020
2025
2030
2035
2040
2045
2050
2055
2060

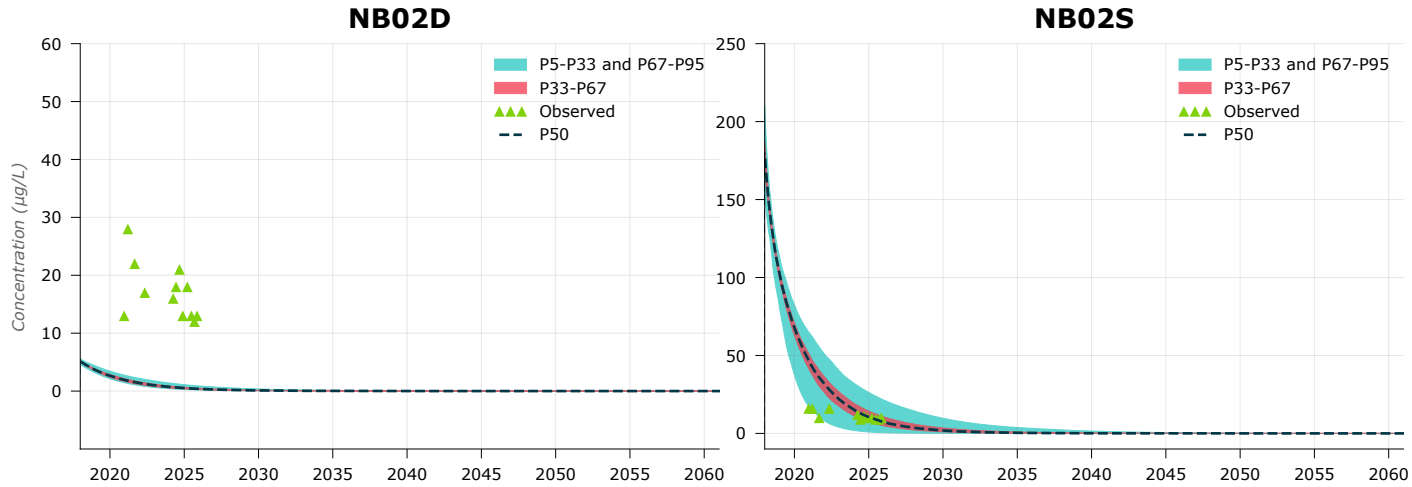
HSMB4S
P5-P33 and P67-P95
P33-P67
Observed
P50
0
200
400
600
800
1000
1200
1400
2020
2025
2030
2035
2040
2045
2050
2055
2060

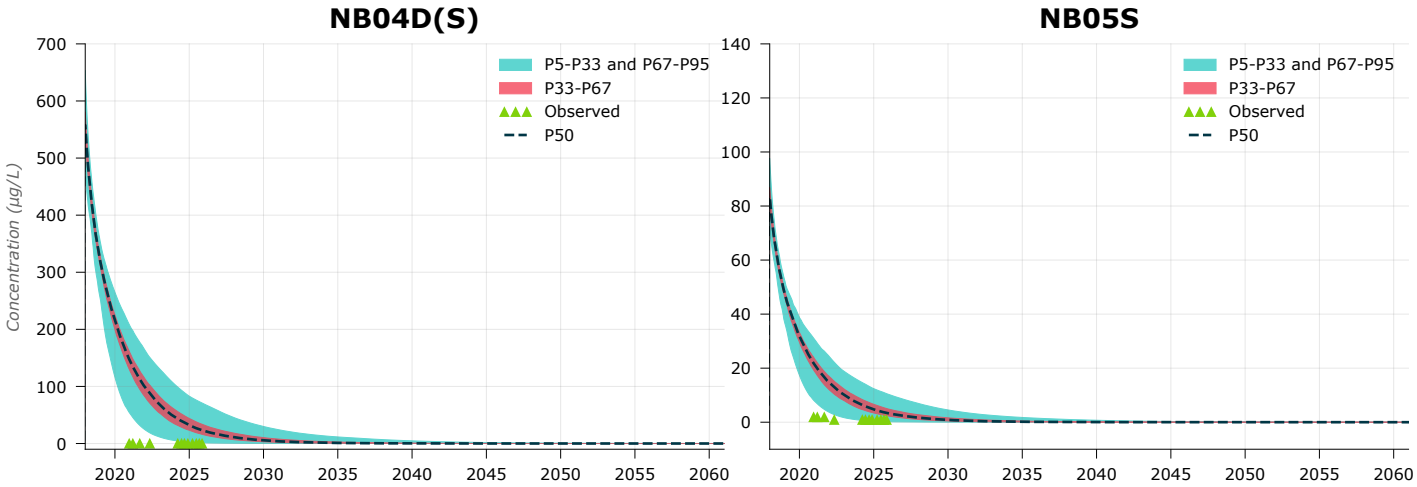

HSMB5D
Concentration (µg/L)
P5-P33 and P67-P95
P33-P67
Observed
P50
0
20
40
60
80
100
120
140
2020
2025
2030
2035
2040
2045
2050
2055
2060

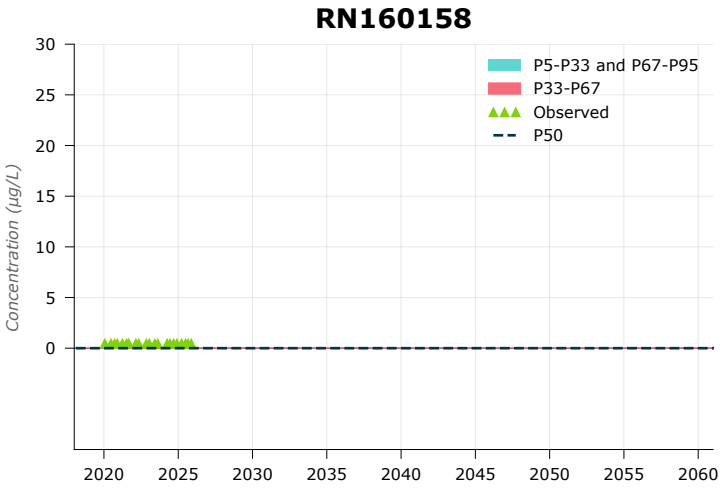
HSMB6D2
P5-P33 and P67-P95
P33-P67
Observed
P50
0
5
10
15
20
25
30
2020
2025
2030
2035
2040
2045
2050
2055
2060


HSMB6S
HSMB7D
P5-P33 and P67-P95
P33-P67
Observed
P50
Concentration (µg/L)

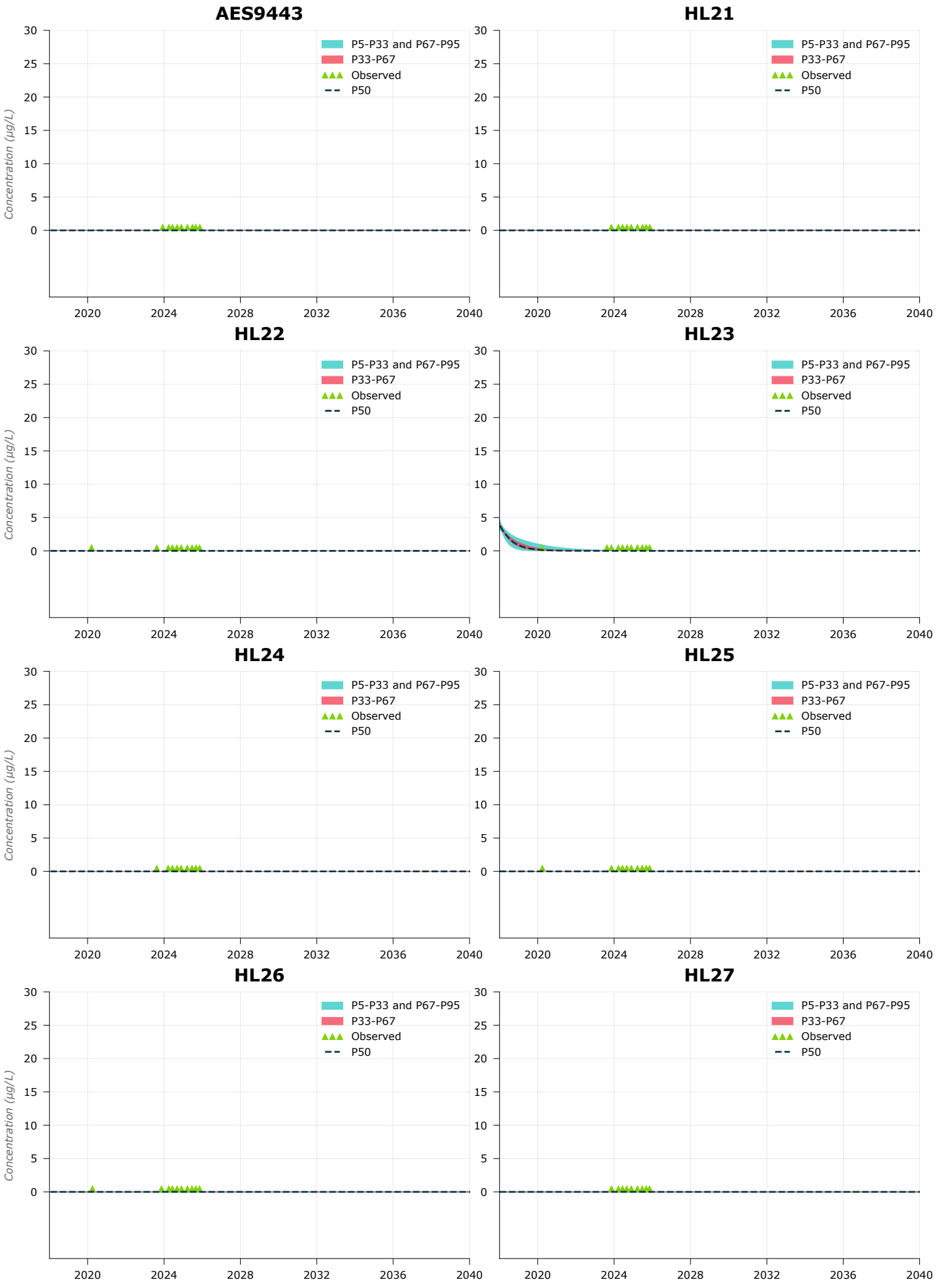

HSMB7S
NB01D
P5-P33 and P67-P95
P33-P67
Observed
P50
Concentration (µg/L)

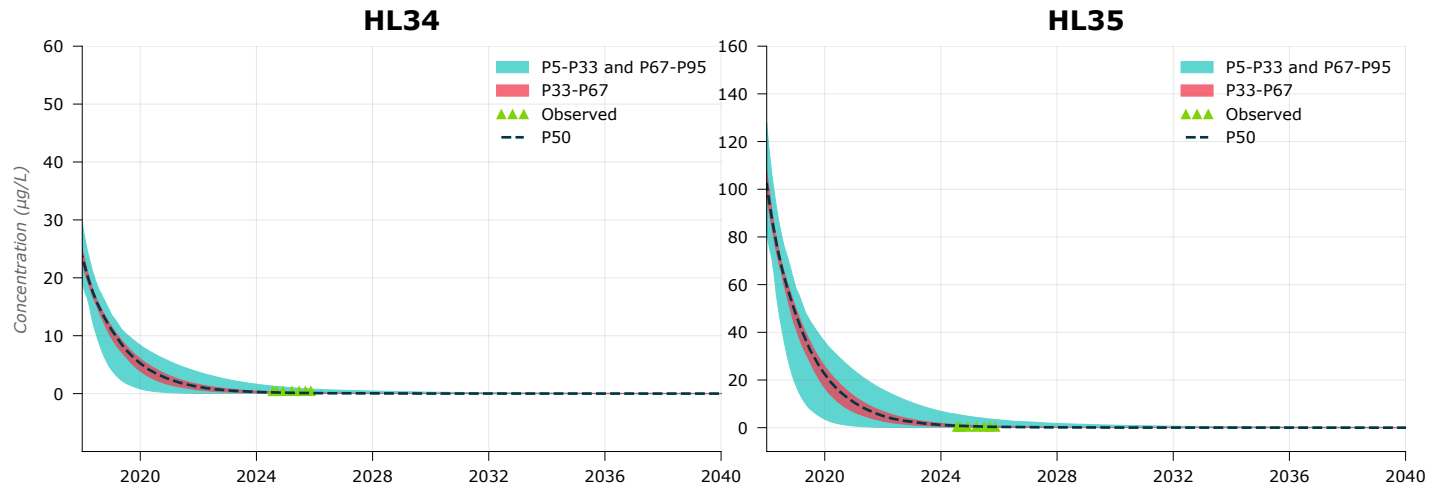

NB02D
NB02S
P5-P33 and P67-P95
P33-P67
Observed
P50
Concentration (µg/L)


NB04D(S)
NB05S
P5-P33 and P67-P95
P33-P67
Observed
P50
Concentration (µg/L)

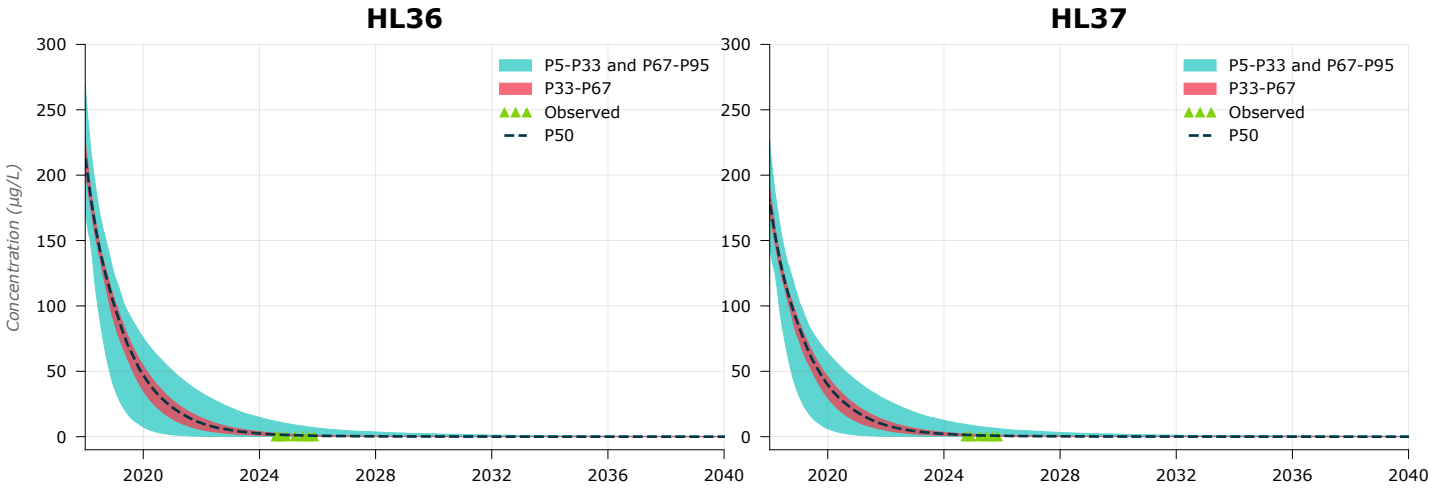

RN160158
P5-P33 and P67-P95
P33-P67
Observed
P50
Concentration (µg/L)
30
25
20
15
10
5
0
2020
2025
2030
2035
2040
2045
2050
2055
2060

Appendix G. Predictive uncertainty – Naphthalene concentrations

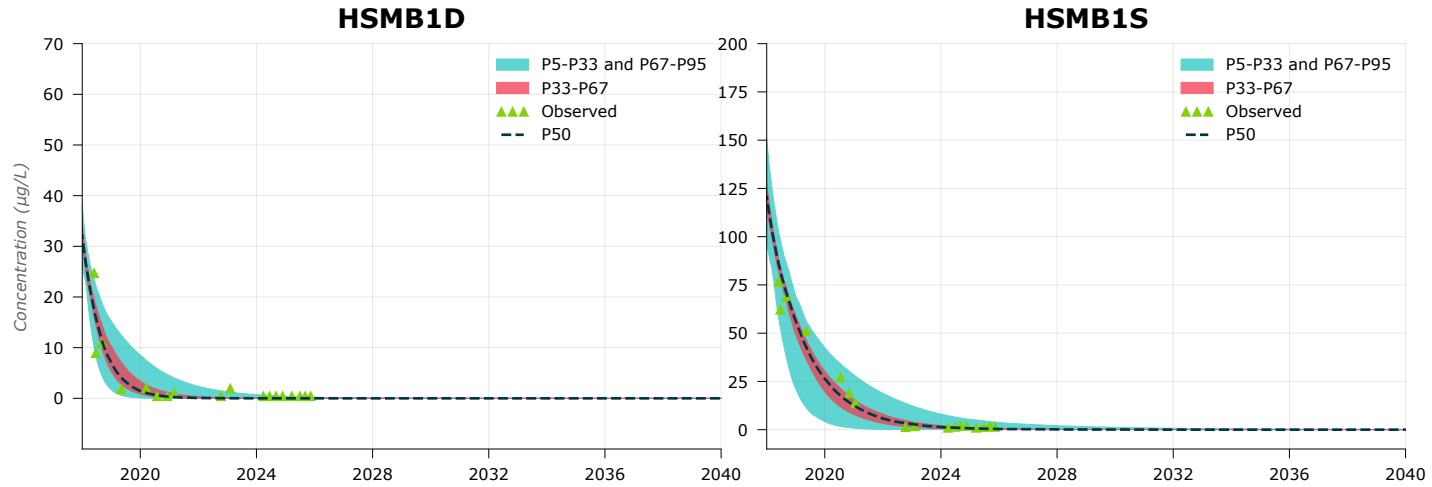

AES9443
HL21
HL22
HL23
HL24
HL25
HL26
HL27
P5-P33 and P67-P95
P33-P67
Observed
P50
Concentration (µg/L)
0
5
10
15
20
25
30
2020
2024
2028
2032
2036
2040


HL34
P5-P33 and P67-P95
P33-P67
Observed
P50
Concentration (µg/L)
0
10
20
30
40
50
60
2020
2024
2028
2032
2036
2040

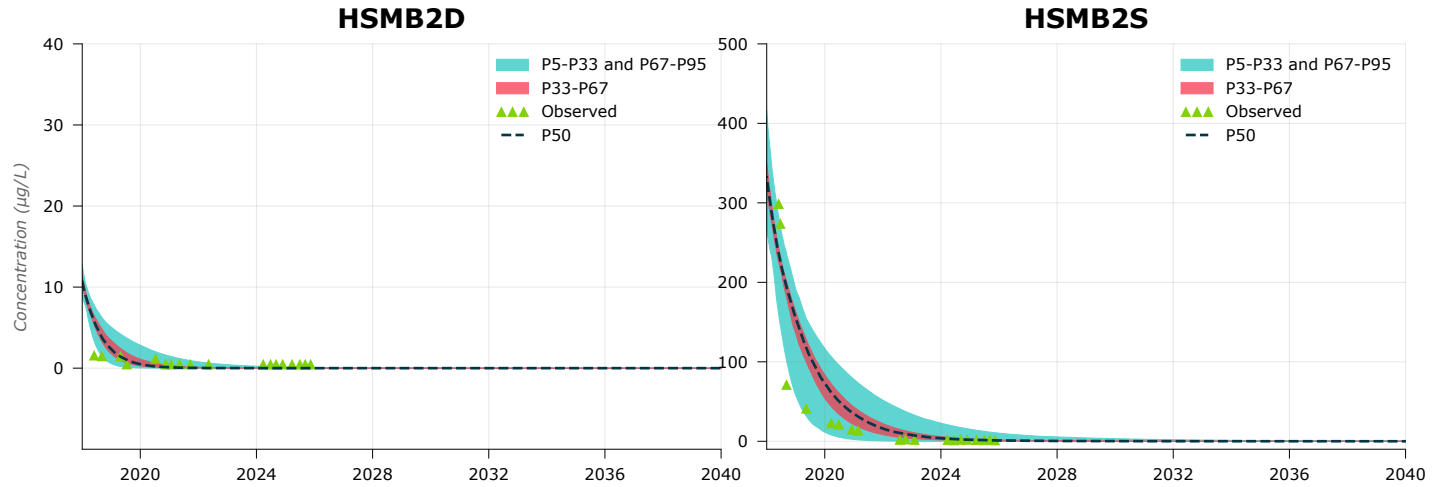
HL35
P5-P33 and P67-P95
P33-P67
Observed
P50
0
20
40
60
80
100
120
140
160
2020
2024
2028
2032
2036
2040


HL36
P5-P33 and P67-P95
P33-P67
Observed
P50
Concentration (µg/L)
0
50
100
150
200
250
300
2020
2024
2028
2032
2036
2040

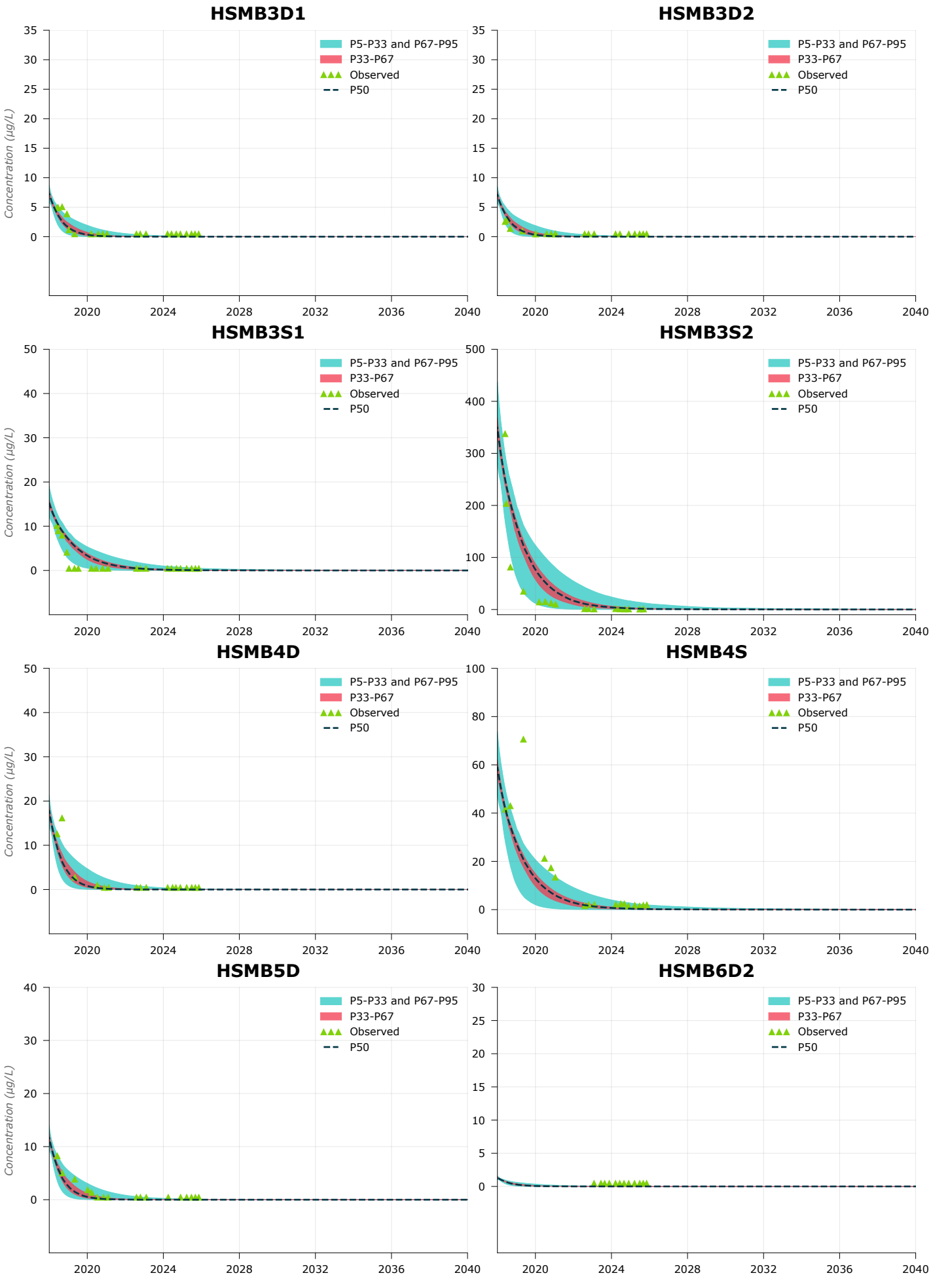
HL37
P5-P33 and P67-P95
P33-P67
Observed
P50
0
50
100
150
200
250
300
2020
2024
2028
2032
2036
2040

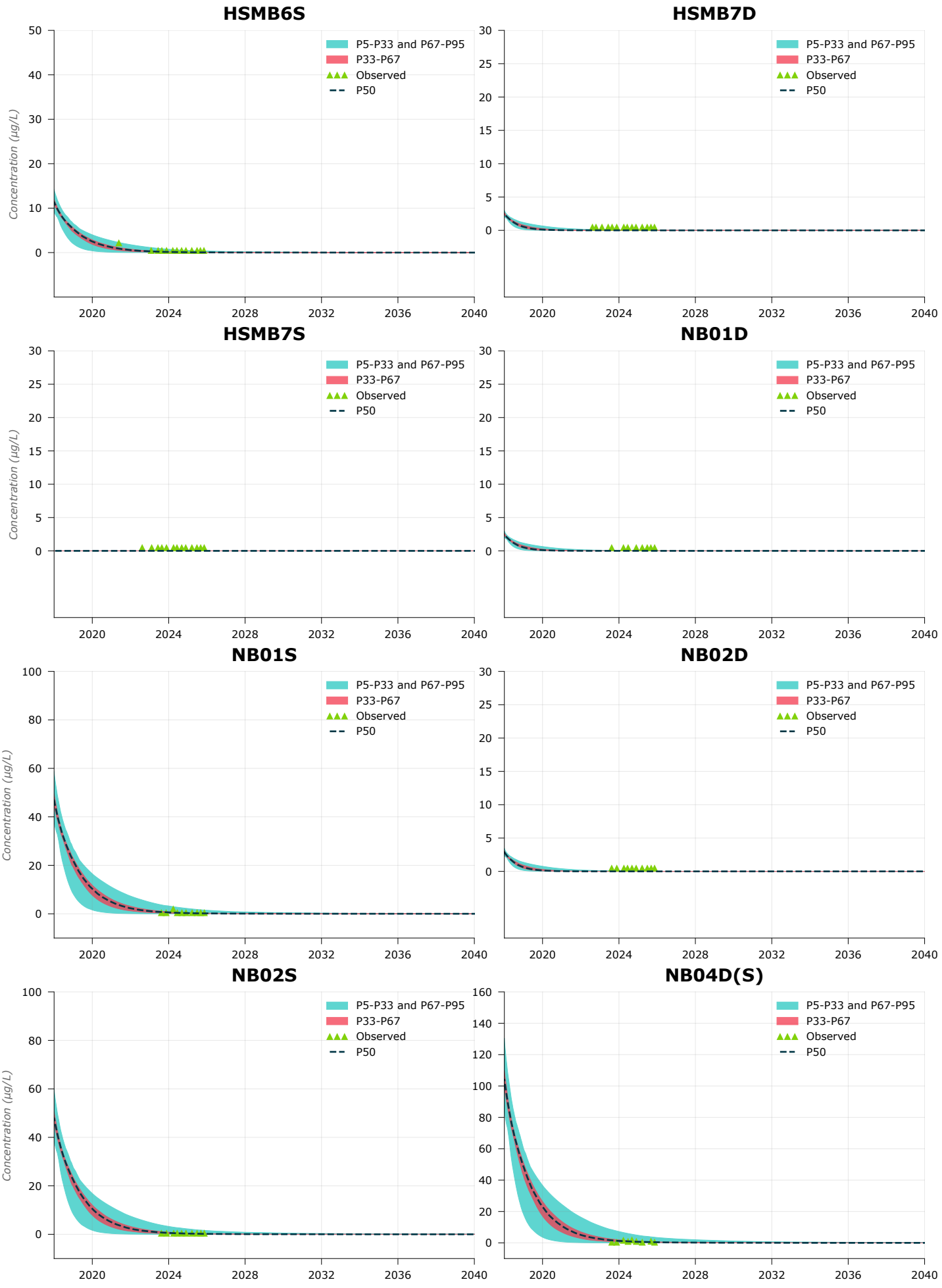

HSMB1D
P5-P33 and P67-P95
P33-P67
Observed
P50
Concentration (µg/L)
0
10
20
30
40
50
60
70
2020
2024
2028
2032
2036
2040

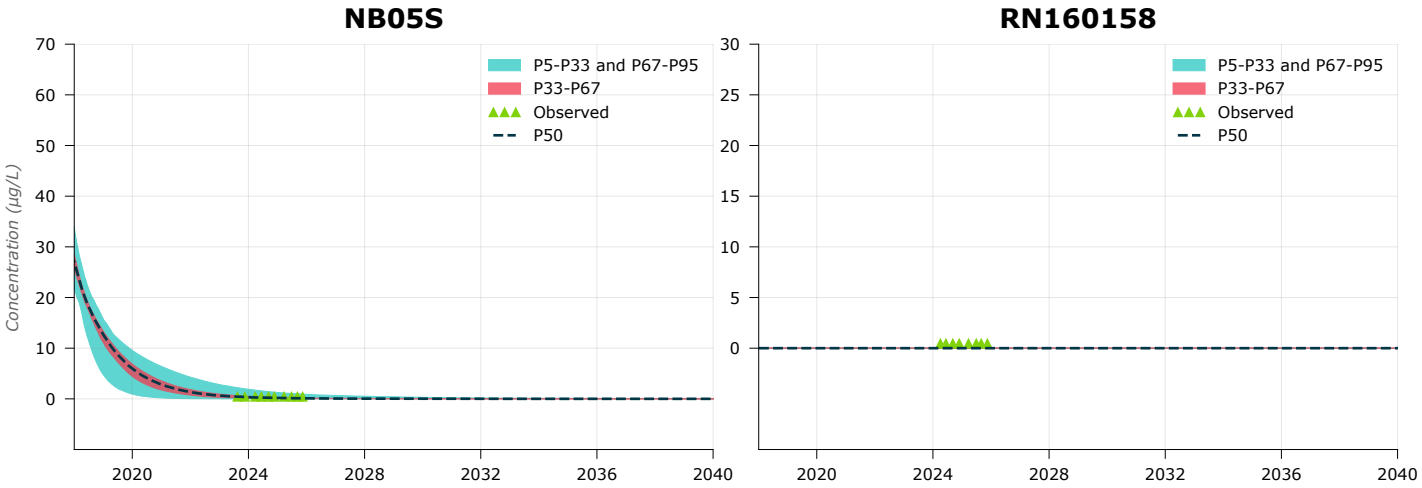
HSMB1S
P5-P33 and P67-P95
P33-P67
Observed
P50
0
25
50
75
100
125
150
175
200
2020
2024
2028
2032
2036
2040


HSMB2D
P5-P33 and P67-P95
P33-P67
Observed
P50
Concentration (µg/L)
0
10
20
30
40
2020
2024
2028
2032
2036
2040

HSMB2S
P5-P33 and P67-P95
P33-P67
Observed
P50
0
100
200
300
400
500
2020
2024
2028
2032
2036
2040


HSMB3D1
HSMB3D2
HSMB3S1
HSMB3S2
HSMB4D
HSMB4S
HSMB5D
HSMB6D2
P5-P33 and P67-P95
P33-P67
Observed
P50
Concentration (µg/L)
2020
2024
2028
2032
2036
2040


HSMB6S
HSMB7D
HSMB7S
NB01D
NB01S
NB02D
NB02S
NB04D(S)
P5-P33 and P67-P95
P33-P67
Observed
P50
Concentration (µg/L)
2020
2024
2028
2032
2036
2040


NB05S
RN160158
P5-P33 and P67-P95
P33-P67
Observed
P50
Concentration (µg/L)
70
60
50
40
30
20
10
0
30
25
20
15
10
5
0
2020
2024
2028
2032
2036
2040